NISTIR 8251

Applied and Computational Mathematics Division

Summary of Activities for Fiscal Year 2018

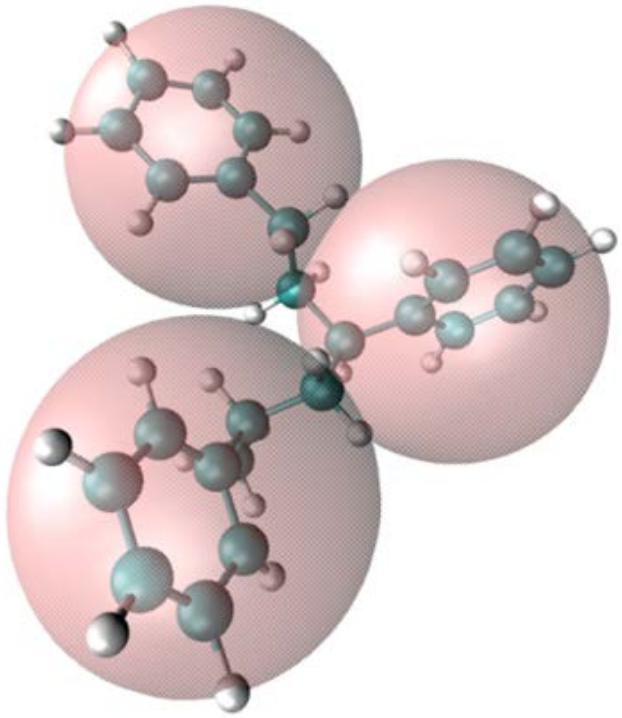

This publication is available free of charge from:
https://doi.org/10.6028/NIST.IR.8251

National Institute of Standards and Technology
U.S. Department of Commerce

NISTIR 8251

Applied and Computational Mathematics Division

Summary of Activities for Fiscal Year 2018

Ronald F. Boisvert, Editor
Applied and Computational Mathematics Division
Information Technology Laboratory

This publication is available free of charge from:
https://doi.org/10.6028/NIST.IR.8251

May 2019

U.S. Department of Commerce
Wilbur L. Ross, Jr., Secretary

National Institute of Standards and Technology
Walter Copan, NIST Director and Under Secretary of Commerce for Standards and Technology

National Institute of Standards and Technology Interagency or Internal Report 8251
Natl. Inst. Stand. Technol. Interag. Intern. Rep. 8251, 157 pages (May 2019)

This publication is available free of charge from:
https://doi.org/10.6028/NIST.IR.8251

Abstract

This report summarizes recent technical work of the Applied and Computational Sciences Division of the Information Technology Laboratory at the National Institute of Standards and Technology (NIST). Part I (Overview) provides a high-level overview of the Division's activities, including highlights of technical accomplishments during the previous year. Part II (Features) provides further details on three projects of particular note this year. This is followed in Part III (Project Summaries) by brief synopses of all technical projects active during the past year. Part IV (Activity Data) provides listings of publications, technical talks, and other professional activities in which Division staff members have participated. The reporting period covered by this document is October 2017 through December 2018.

For further information, contact Ronald F. Boisvert, 100 Bureau Drive, Mail Stop 8910, NIST, Gaithersburg, MD 20899-8910, phone 301-975-3812, email boisvert@nist.gov, or see the Division's Web site at https://www.nist.gov/itl/math/.

Keywords: applied mathematics; computational science and engineering; high-performance computing; materials modeling and simulation; mathematical knowledge management; mathematical modeling; mathematics of metrology; network science; scientific visualization; quantum information science.

Cover Visualization: Coarse-graining, i.e., the task of systematically reducing degrees of freedom to speed up computations, is becoming an increasingly important tool for reaching larger length-scales in materials modeling and simulation. Coarse-graining in molecular dynamics often amounts to projecting molecules or parts thereof onto effective particles, e.g. the light pink spheres in this image. For details, see page 15.

Section Visualizations: The "word cloud," which is found at the start of each Part of this document was created using Wordle, http://www.wordle.net/, and the text of this document as input.

Acknowledgements: Thanks to Lochi Orr for assisting in the compilation of Parts III and IV of this document. Thanks also to Justyna Zwolak and Brian Cloteaux who each carefully read the manuscript and offered many corrections and suggestions for improvement.

Disclaimer: Certain commercial entities, equipment, and materials are identified in this document in order to describe an experimental procedure or concept adequately. Such identification is not intended to imply recommendation or endorsement by the National Institute of Standards and Technology, nor is it intended to imply that the entities, materials, and equipment are necessarily the best available for the purpose.

Contents

Part I

Overview

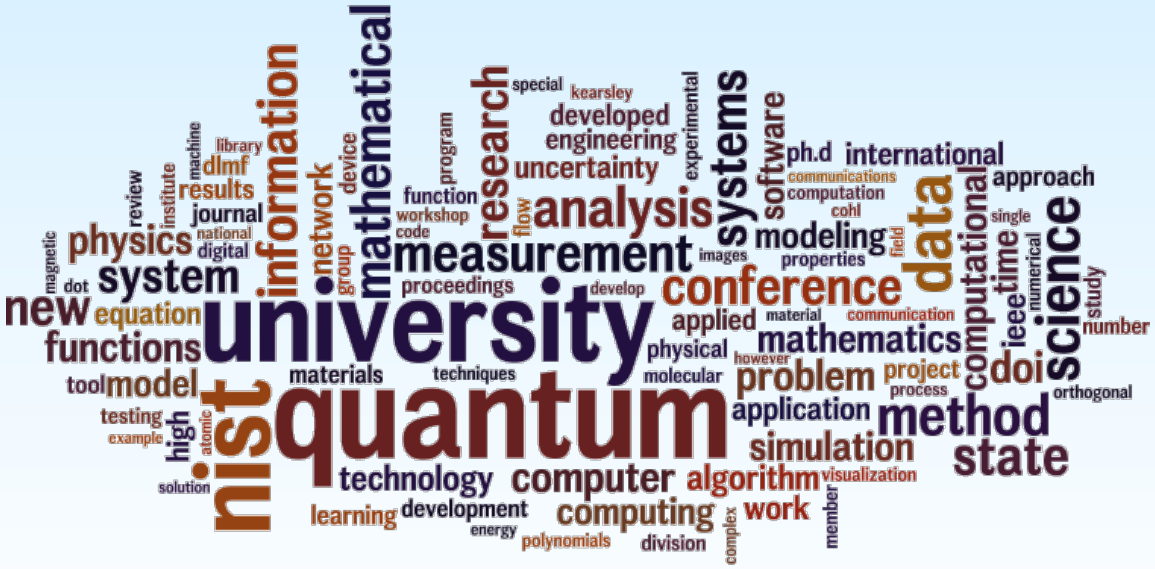

Introduction

Founded in 1901, the National Institute of Standards and Technology (NIST) is a non-regulatory federal agency within the U.S. Department of Commerce. NIST's mission is to promote U.S. innovation and industrial competitiveness by advancing measurement science, standards, and technology in ways that enhance economic security and improve our quality of life. The NIST Laboratory program is broad ranging, with research efforts encompassing physics, electrical engineering, nanotechnology, materials science, chemistry, bioscience, engineering, fire research, and information technology.

The Information Technology Laboratory (ITL) is one of six major laboratories and user facilities at NIST. ITL's overarching purpose is to cultivate trust in information technology and metrology. This is accomplished primarily through the development of measurements, tests, and guidance to support innovation in and deployment of information technology by industry and government, as well as through the application of advanced mathematics, statistics, and computer science to help ensure the quality of measurement science.

The Applied and Computational Mathematics Division (ACMD) is one of seven technical Divisions in ITL. At its core, ACMD purpose is to nurture trust in metrology and scientific computing. To do so, ACMD provides leadership within NIST in the use of applied and computational mathematics to solve technical problems arising in measurement science and related applications. In that role staff members

- perform research and development in applied mathematics and computational science and engineering, including analytical and numerical methods, high-performance computing, and visualization;
- engage in peer-to-peer collaborations to apply such techniques and tools to NIST problems;
- develop and disseminate mathematical reference data, software, and related tools; and
- work with internal and external groups to develop standards, tests, reference implementations, and other measurement technologies for scientific computation on current and future architectures.

Division staff is organized into four groups:

- Mathematical Analysis and Modeling Group (*Timothy Burns, Leader*)

  Performs research and maintains expertise in applied mathematics, mathematical modeling, and numerical analysis for application to measurement science.

- Mathematical Software Group (*Michael Donahue, Leader*)

  Performs research and maintains expertise in the methodology and application of mathematical algorithms and software in support of computational science within NIST as well as in industry and academia.

- High Performance Computing and Visualization Group (*Judith Terrill, Leader*)

  Performs research and maintains expertise in the methodologies and tools of high-performance scientific computing and visualization for use in measurement science.

- Computing and Communications Theory Group (*Ronald Boisvert, Acting Leader; Oliver Slattery, Project Leader*)

  Performs research and maintains expertise in the fundamental mathematics, physics, and measurement science necessary to enable the development and analysis of current and future computing and communications systems.

The technical work of the Division is organized into six thematic areas; these are described in the sidebar. Project descriptions in Part III of this document are organized according to these broad themes.

Division Thematic Areas

Broad Areas

Mathematics of Metrology. Mathematics plays an important role in measurement science. Mathematical models are needed to understand how to design effective measurement systems and to analyze the results they produce. Mathematical techniques are used to develop and analyze idealized models of physical phenomena to be measured, and mathematical algorithms are necessary to find optimal system parameters. Mathematical and statistical techniques are needed to transform measured data into useful information. The goal of this work is to develop fundamental mathematical methods and tools necessary for NIST to remain a world-class metrology institute, and to apply these methods and tools to problems in measurement science.

High Performance Computing and Visualization. Computational capability continues to advance rapidly, enabling modeling and simulation to be done with greatly increased fidelity (e.g., higher resolution and more complex physics). However, doing so often requires computing resources well beyond what is available on the desktop. Developing software that make effective use of such high-performance computing platforms remains very challenging, requiring expertise that application scientists rarely have. And, as the hardware landscape continues to evolve, new algorithmic techniques must constantly be developed. We maintain such expertise for application to NIST problems. Such computations, as well as modern laboratory experiments, typically produce large volumes of data, which cannot be readily comprehended without some form of analysis. We are developing the infrastructure necessary for advanced interactive, quantitative visualization and analysis of scientific data, including the use of 3D immersive environments, and applying the resulting tools to NIST problems. One of our goals is to develop the 3D immersive environment into an interactive measurement laboratory.

Current Focus Areas

Advanced Materials. Delivering technical support to the nation's manufacturing industries as they strive to out-innovate and out-perform the international competition has always been a top priority at NIST. Mathematical modeling, computational simulation, and data analytics are key enablers of emerging manufacturing technologies. The Materials Genome Initiative (MGI), an interagency program with the goal of significantly reducing the time from discovery to commercial deployment of new materials using modeling, simulation, and informatics, is a case in point. To support the NIST role in the MGI, ACMD develops and assesses modeling and simulation techniques and tools, with emphasis on uncertainty quantification, and collaborates with other NIST Laboratories in their efforts to develop the measurement science infrastructure needed by the materials science and engineering community.

Quantum Information. An emerging discipline at the intersection of physics and computer science, quantum information science is likely to revolutionize 21st century science and technology in the same way that lasers, electronics, and computers did in the 20th century. By encoding information into quantum states of matter, one can, in theory, enable phenomenal increases in information storage and processing capability. At the same time, such computers would threaten the public-key infrastructure that secures all of electronic commerce. Although many of the necessary physical manipulations of quantum states have been demonstrated experimentally, scaling these up to enable fully capable quantum computers remains a grand challenge. We engage in (a) theoretical studies to understand the power of quantum computing, (b) collaborative efforts with the multi-laboratory experimental quantum science program at NIST to characterize and benchmark specific physical realizations of quantum information processing, and (c) demonstration and assessment of technologies for quantum communication.

Foundations of Measurement Science for Information Systems. ITL assumes primary responsibility within NIST for the development of measurement science infrastructure and related standards for IT and its applications. ACMD develops the mathematical foundations for such work. This can be very challenging. For example, many large-scale information-centric systems can be characterized as an interconnection of many independently operating components (e.g., software systems, communication networks, the power grid, transportation systems, financial systems). A looming new example of importance to NIST is the Internet of Things. Exactly how the structure of such large-scale interconnected systems and the local dynamics of its components leads to system-level behavior is only weakly understood. This inability to predict the systemic risk inherent in system design leaves us open to unrealized potential to improve systems or to avoid potentially devastating failures. Characterizing complex systems and their security and reliability properties remains a challenging measurement science problem for ITL.

Mathematical Knowledge Management. We work with researchers in academia and industry to develop technologies, tools, and standards for representation, exchange, and use of mathematical data. Of particular concern are semantic-based representations which can provide the basis for interoperability of mathematical information processing systems. We apply these representations to the development and dissemination of reference data for applied mathematics. The centerpiece of this effort is the Digital Library of Mathematical Functions, a freely available interactive and richly linked online resource, providing essential information on the properties of the special functions of applied mathematics, the foundation of mathematical modeling in all of science and engineering.

Highlights

In this section we identify some of the major accomplishments of the Division during the past year. We also provide news related to ACMD staff.

Recent Technical Accomplishments

ACMD has made significant technical progress on many fronts during the past year. Here we highlight a few notable technical accomplishments. Further details are provided in Part II (Features) and Part III (Project Summaries).

ACMD staff members are applying their expertise to make wide ranging contributions to the NIST metrology program. Among these are the following.

- Microfluidics are expected to enable rapid and simultaneous screening of hundreds of diseases with only a few drops of blood. Accurately monitoring the flow rate of such devices is an important prerequisite. However, flow rates at the necessary scales have heretofore been impossible to assess. Innovative mathematical analysis by ACMD staff in collaboration with the NIST Fluidics Group has led to the realization of a *highly accurate optofluidic flow meter* usable at the nanoliter per minute scale. These techniques are the subject of a current NIST patent application. See page 37.
- The current opioid crisis is being fueled by propagation of designer drugs and chemical derivatives that differ from well-known compounds, like Fentanyl, by small inert structural components. Law enforcement need tools to be able to quickly identify such compounds. In collaboration with the NIST Biomolecular Measurements Division we have developed a novel *spectral library search algorithm* that can identify such close analogues. See page 40.
- Our collaboration with researchers from NIST's Applied Physics Division to extend SI *traceability for magnetic resonance imaging* (MRI) technology attained an important milestone this year with the inauguration of the NIST Magnetic Resonance Imaging Biomarker Calibration Service for Proton Spin Relaxation Times. Proton relaxation times are being considered as biomarkers for a wide range of pathologies including traumatic brain injury, multiple sclerosis, and liver disease. ACMD staff contributed to the modeling and uncertainty quantification necessary to develop this service. See page 45.
- Equations of state (EOS) provide quantitative relationships between thermodynamic variables of fluid mixtures, such as temperature, pressure, volume, and internal energy, that enable determination of key fluid properties by exploiting statistical physics to interpolate or extrapolate beyond where laboratory measurements are economical or feasible. The NIST data facilities REFPROP (Reference Fluid Thermodynamic and Transport Properties Database) and TDE (ThermoData Engine), which are widely accessed by the chemical engineering community, are developed from critically evaluated laboratory data in combination with EOS. The need to develop reliable algorithms for root finding from equations of state for these services has led to the development of Chebtools, a highly optimized C++11 library for *computing with Chebyshev expansions*, in collaboration with the NIST Applied Chemicals and Materials Division. See page 56.
- A computational model of the flow of dense suspensions, developed jointly by ACMD and the NIST Engineering Lab, has played a critical role in the development of the understanding of the flow of concrete. This work has led to the first ever NIST standard reference materials (for mortar and concrete) which were developed with the use of supercomputers. We have recently extended the underlying model with new physics to incorporate elastic features, such as torsion and bending, so that it is applicable to the study of biological structures. The code now has the capability of *modeling of proteins or polymeric systems* such as themonoclonal antibodies currently under study at NIST. See pages 67 and 69.

Being part of the Information Technology Laboratory, ACMD has a special focus on the development of the measurement and standards infrastructure for emerging computing and communications technologies. Examples of recent contributions in this domain follow.

- As part of a long-term program on the Internet of Things for health care applications, we have been using mathematical modeling to answer critical questions associated with the deployment of body area networks. Most recently we have been working on the development of *statistical channel models for ultra-wide band implant communications*. We have been working with experimentalists who are making measurements of signal propagation in physical phantoms in order to characterize the uncertainty induced by the placement of measurement points. See page 22.

- Many critical systems (e.g., smart grids, manufacturing systems, transportation systems) are comprised of multiple *heterogeneous component systems* (CSs) which depend on and support each other. For instance, a modern power system not only includes an electrical grid/network, but also utilizes an information and communication network to monitor the state of the electrical network and to take appropriate control actions. Intricate dependence among CSs makes the analysis of such complex systems challenging. Moreover, in many cases, a local failure of even a small number of CSs can cause widespread failures in the system, affecting many CSs. We have used the concept of probability of cascading failure to identify vulnerable nodes. See page 91.

- The NIST Randomness Beacon[1] serves as a trusted and reliable source of randomness, a critical resource for a variety of computing protocols. This year we demonstrated the use of quantum measurements to generate random bits whose security is certified by the impossibility of superluminal signaling, an accomplishment which was reported in *Nature*[2]. Quantum correlations such as those exhibited in Bell tests imply the presence of fundamental randomness and can be exploited for certified public or private randomness without requiring trust in the underlying quantum devices or their manufacturer. However, the protocols for *extracting randomness from Bell tests* have required extraordinary experimental resources before any randomness could be obtained. Our work has reduced the resources required by orders of magnitude, reducing the experimental effort for producing 512 very high-quality random bits from hours to less than 5 minutes. This was enabled by our development of a general framework for randomness generation based on quantum randomness estimation. See page 80.

- This year we gave the first construction for *pseudorandom quantum states* – quantum states that look "random" to an observer that is computationally bounded. Such states can be used to implement private-key quantum money, a natural cryptographic functionality which cannot be achieved using classical resources alone. Furthermore, in quantum statistical mechanics, pseudorandom states provide a simple example of how probabilistic ensembles on subsystems can emerge from a highly-entangled pure state of the universe. See page 83.

- *Quantum memory* is an essential requirement for quantum computing and quantum communication. Fidelity is one of its most important performance parameters and noise greatly reduces fidelity. Many research groups, including ours, have developed noise reduction techniques which we detailed in an invited review article published in *Modern Physics Letters B.* See page 86.

Engaging in fundamental research to develop techniques and tools for the future is very important for the health of the Division. Examples of recent advances in such efforts follow.

- *Coarse-graining*, i.e., the task of systematically reducing degrees of freedom to speed up computations, is becoming an increasingly important tool for reaching larger length scales in atomistic simulations of materials. However, in most cases such procedures employ ad hoc schemes whose limitations are not well characterized, thus preventing rigorous uncertainty quantification. We have

[1] https://beacon.nist.gov/home

[2] https://doi.org/10.1038/s41586-018-0019-0

developed a multipole method that connects a system of interacting molecules to its coarse-grained (CG) representation via a sequence of geometric approximations. Critically, we can recover atomistic dynamics as an appropriate limit of the CG model, thus providing a basis for a priori uncertainty quantification. We anticipate that this work will address many unresolved questions about best-practices for coarse-graining and facilitate adoption by industrial stake-holders. See page 15.

- *Time-reversed, multidimensional, nonlinear dissipative evolution equations* are of great current interest in environmental forensics, geophysics, image deblurring, and in the numerous deconvolution problems that pervade measurement science. Unfortunately, such problems are inherently ill-posed, and hence naïve approaches to their solution inevitably fail. We have developed stabilized explicit schemes for the numerical solution of such problems that are surprisingly effective and efficient and have recently demonstrated these for backward recovery in 2D viscous Burgers equation and in incompressible Navier Stokes equations. See page 27.

This year NIST began a focused effort to develop deeper expertise in techniques of artificial intelligence, with an emphasis on machine learning, in order to enhance the analysis capabilities of the NIST metrology program. In response, ACMD has started up new efforts such as the following.

- Electrons confined in arrays of semiconductor nanostructures, called quantum dots (QDs), are gaining popularity as candidate building blocks for solid-state quantum devices. In semiconductor quantum computing, devices now have tens of individual electrostatic and dynamical gate voltages that must be carefully set to isolate the system to the single electron regime and to realize good qubit performance. Configuring these manually quickly becomes infeasible as the number of qubits grows. We are using machine learning to develop a fully automated approach to *automatically tuning quantum dots for computing applications*. See page 18.

- Many researchers are now using automated techniques to mine the rapidly growing technical literature. Success in doing this relies on being able to determine the meaning, i.e., semantics, of the literature in an automated way. While much progress has been made in natural language processing, much less so has been made in deriving meaning from mathematical formulae. We are using the fast-evolving deep learning paradigm to develop techniques for extracting and *disambiguating semantics in math and science documents*. We are also creating "labeled" (i.e., annotated) datasets, which are essential for training deep learning models. See page 110.

- The simulations that we now work on are large, complex, and run for long periods of time. To make the best use of limited high-performance computing resources, we need to *monitor and analyze simulation results* while the simulation is in process. Ideally, the results of such analysis can allow intervention to improve outcomes. Unfortunately, for simulations at this scale, it is not feasible to write out detailed data to analyze during the runs. The only way to do needed analysis is to do it as part of the runs. We are using machine learning to help with this analysis. See page 71.

Finally, it is important that we explain what ACMD does to a broader audience, not only of scientists, but the general public. This year, for example, ACMD staff contributed an article on the Digital Library of Mathematical Functions to *Physics Today*[3], the member magazine of the American Physical Society. Several ACMD staff members contributed to the NIST *Talking Measure* blog, producing inspiring pieces entitled "It's All Right to Be Wrong in Science" by Paulina Kuo,[4] "Local Realism, Bell's Inequality, and T-Shirts: An Entangled Tale" by Scott Glancy,[5] and "It All Adds Up: Being a NIST NRC Postdoc in Applied Mathematics" by Ryan Evans.[6]

[3] https://doi.org/10.1063/PT.3.3846

[4] https://www.nist.gov/blogs/taking-measure/its-all-right-be-wrong-science

[5] https://www.nist.gov/blogs/taking-measure/local-realism-bells-inequality-and-t-shirts-entangled-tale

[6] https://www.nist.gov/blogs/taking-measure/it-all-adds-being-nist-nrc-postdoc-applied-mathematics

Technology Transfer and Community Engagement

The volume of technical output of ACMD remains high. During the last 15 months, Division staff members were (co-)authors of 46 articles appearing in peer-reviewed journals, 36 papers in conference proceedings, and 18 published in other venues. 13 additional papers were accepted for publication, while 29 others are undergoing review. Division staff gave 62 invited technical talks and presented 49 others in conferences and workshops.

ACMD continues to maintain an active website with a variety of information and services, most notably the Digital Library of Mathematical Functions, though legacy services that are no longer actively developed, like the Guide to Available Mathematical Software, the Matrix Market, and the SciMark Java benchmark still see significant use. During calendar year (CY) 2018, the division Web server satisfied more than 5.6 million requests for pages during more than 829,000 user visits. Another indication of the successful transfer of our technology is references to our software in refereed journal articles. For example, our software system for nano-magnetic modeling (OOMMF) was cited in 184 such papers published in CY 2018 alone; see page 54.

Members of the Division are also active in professional circles. Staff members hold a total of 15 editorial positions in peer-reviewed journals. For example, Barry Schneider is an Associate Editor-in-Chief and Isabel Beichl is an Editorial Board Member for IEEE's *Computing in Science and Engineering.* Staff members are also active in conference organization, serving on 27 organizing/steering/program committees. Of note, ACMD played an important role as sponsor or (co-)organizer of several significant events this year, including the following:

- *Numerical Reproducibility at Exascale*, at SC17, Denver, CO, November 12, 2017. (M. Mascagni and Walid Keyrouz, Co-Organizers)

  A cornerstone of the scientific method is experimental reproducibility. As computation has grown into a powerful tool for scientific inquiry, the assumption of computational reproducibility has been at the heart of numerical analysis in support of scientific computing. With ordinary CPUs, supporting a single, serial, computation, the ability to document a numerical result has been a straightforward process. However, as computer hardware continues to develop, it is becoming harder to ensure computational reproducibility, or to even completely document a given computation. These two workshops explored the current state of computational reproducibility in high-performance computing and sought to organize solutions at different levels.

- *Computational Reproducibility at Exascale*, at SC18, Dallas, TX, November 11, 2018. (M. Mascagni and Walid Keyrouz, Co-Organizers)

  The workshop is meant to address issues of numerical reproducibility as well as approaches and best practices to sharing and running code and the reproducible dissemination of computational results. The workshop is meant to address the scope of the problems of computational reproducibility in HPC in general, and those anticipated as we scale up to Exascale machines in the next decade. The participants included government, academic, and industry stakeholders; the goals of this workshop were to understand the current state of the problems that arise, what work is being done to deal with these issues, and what the community thinks the possible approaches to these problems are.

Service within professional societies is also prevalent among our staff. For example, Geoffrey McFadden served as Member-at-Large of the Council of the Society for Industrial and Applied Mathematics (SIAM). Faculty appointee Michael Mascagni is a Member of the Board of Directors of the International Association for Mathematics and Computers in Simulation (IMACS). Staff members are also active in a variety of working groups. For example, Ronald Boisvert and Andrew Dienstfrey serve as members of the International Federation for Information Processing (IFIP) Working Group 2.5 on Numerical Software, Donald Porter is a member of the Tcl Core Team, Bruce Miller is a member of W3C's Math Working Group, and Sandy Ressler is a member of the Web3D Consortium. Barry Schneider represents NIST on the High-End

Computing (HEC) Interagency Working Group of the Federal Networking and Information Technology Research and Development (NITRD) Program. Further details can be found in Part IV of this report.

Staff News

ACMD experienced an unusually large number of staffing changes in the past year. Among these are the following.

Arrivals

Ryan Evans joined the ACMD staff in August 2018. Most recently a NIST NRC Postdoctoral Associate, Evans received a Ph.D. in Applied Mathematics from the University of Delaware in 2016. At NIST he will continue his research in the mathematical modeling of biosystems.

Justin Kauffman began a two-year appointment at a NIST NRC Postdoctoral Associate in May 2018. He received a Ph.D. in Engineering Mechanics at Penn State University, where he worked on the simulation of large-scale hydrodynamic problems using dynamic meshes. At NIST he will be developing a fully parallel coupling algorithm between an overset mesh method and the hybridizable discontinuous Galerkin method. His NIST adviser is William George.

Lucas Brady arrived at NIST in September 2018 to begin a two-year appointment as a NIST NRC Postdoctoral Associate. Brady received a Ph.D. in Physics from the University of California at Santa Barbara, where his research was in quantum information theory. At NIST he will continue his study quantum optimization algorithms, with an emphasis on quantum adiabatic computing and classical analogues such as quantum Monte Carlo. Brady will be splitting his time between NIST and the Joint UMD/NIST Center for Quantum Information and Computer Science (QuICS) in College Park, MD. His postdoctoral advisors are Yi-Kai Liu and Alexey Gorshkov.

Departures

Stephen Jordan, a theoretical physicist in ACMD's Computing and Communications Theory Group, as well as a founding Fellow of the Joint UMD/NIST Center for Quantum Information and Computer Science (QuICS), left in January 2018 after six years at NIST to join Microsoft Research's Quantum Architectures and Computation Group in Redmond, WA. At NIST, Jordan performed groundbreaking research in quantum algorithms and complexity theory, including the development of the first quantum algorithm demonstrating exponential speedup for the simulation of quantum field theories. In 2016 he received the NIST Sigma Xi Katherine Gebbie Young Researcher Award. He maintains a connection to ACMD as a guest researcher to maintain the Quantum Algorithm Zoo[7], a database of all known quantum algorithms.

Xiao Tang, the leader of ACMD's experimental program in quantum communications, retired from NIST in June 2018 following 20 years of Federal service. At NIST, Tang did pioneering work in digital data preservation. He then moved to quantum information science, where he demonstrated the world's most capable cryptographic key distribution system secured through the principles of quantum mechanics. Along the way he oversaw the development of novel frequency upconversion systems which converted photons in the telecommunications bands (capable of low-loss transmission in fiber) to frequencies optimal for efficient detection by low-cost photon detectors. During his tenure at NIST Tang received two US Department of Commerce (DOC) Bronze Medals, a DOC Silver Medal, an R&D 100 Award, and was named a Fellow of the American Physical Society. Fortunately, he has returned to NIST as a re-employed annuitant to continue to contribute to NIST programs on a part-time basis.

Peter Bierhorst, a mathematician at the NIST Boulder Labs, left ACMD in July 2018 to join the Mathematics Department at the University of New Orleans. A NIST Fellow Postdoc working under the

[7] https://math.nist.gov/quantum/zoo/

mentorship of Manny Knill since January 2015, Bierhorst specialized in the statistical analysis of quantum experiments. He led in the analysis and certification of results for one of the world's first loophole-free Bell tests which took place at NIST in the fall of 2015. He then led a study, published in *Nature*, in which random bits certified by the impossibility of superluminal signaling were produced based on Bell experiments.

Isabel Beichl retired from NIST in July 2018 following 30 years of Federal service. An expert in the field of combinatorics, she was a leader in the ACMD effort to develop computationally efficient methods to estimate properties of very large networks. In the process she mentored six postdoctoral associates and one Ph.D. student. She was also instrumental in the success and growth of the ITL Summer Undergraduate Research Fellowship (SURF) program, which she co-led for many years. She continues to contribute to ACMD as a guest researcher.

William Mitchell, an expert in adaptive grid refinement and multigrid methods for the solution of partial differential equations (PDE), retired from NIST in September 2018. During his 25 years of Federal service Mitchell studied parallel adaptive multigrid methods and applied them to challenging problems at NIST such as the modeling of atomic interactions. In the process he developed the very successful PHAML software system for this class of problems. His related experimental studies of methods for *hp* adaptive grid refinement have been very influential. He also developed Fortran bindings for OpenGL graphics, which were adopted as a standard.

Figure 1. *FY 2018 witnessed retirements of several long-tenured and valued staff members. Top: Isabel Beichl with former NIST staff member Francis Sullivan at her celebratory retirement luncheon in July 2018. Bottom: Bill Mitchell addresses well wishers at his retirement luncheon in September 2018.*

Students

During FY 2018 ACMD supported the work of 23 student interns, including 11 graduate students, 9 undergraduates, and 3 high school students. See Table 3 in the Appendix (page 144) for a complete listing. ACMD staff members are also active in the education of graduate students, serving both as Ph.D. advisers and as members of thesis committees; see page 135.

Recognition

ACMD staff members were recognized with a variety of awards this year, including the following.

Figure 2. *Fern Hunt was named Fellow of the American Mathematical Society.*

Fern Hunt was elected a Fellow of the American Mathematical Society in November 2018 "for outstanding applications of mathematics to science and technology, exceptional service to the US government, and for outreach and mentoring." The AMS Fellows program recognizes members who have made outstanding contributions to the creation, exposition, advancement, communication, and utilization of mathematics. Hunt is the first NIST staff member to have received this honor.

Michael Donahue and **Donald Porter** received the Jacob Rainbow Applied Research Award at the NIST Awards Ceremony in December 2018. Widely considered NIST's highest award for applied science, the Rabinow award recognizes outstanding achievement in the practical application of the results of scientific or engineering research. Donahue and Porter were recognized for "enabling widespread use of nanomagnetic modeling and simulation to enhance U.S. innovation and product development." The software tool that they created, OOMMF, is the most widely used nanomagnetics modeling system in the world. More than 2,500 journal articles (11 in *Science* and *Nature*) and more than 18 U.S. patent applications reference use of their system, attesting to its impact for U.S. innovation.

ACMD staff showed well in the 2018 ITL Awards program. **Paul Patrone** and **Andrew Dienstfrey** received the Outstanding Journal Publication Award for their paper "Estimating yield-strain via deformation-recovery simulations," published in the journal *Polymer* in May 2017. **Michael Donahue** and **Donald Porter** took home the Outstanding Technology Transfer Award for their work on the nanomagnetics modeling system OOMMF. And, **Fern Hunt** received the first Outstanding Contribution to Diversity Award "for serving as a tireless advocate of diversity and inclusion of under-represented groups in science, technology, engineering and mathematics."

Several "best in show" awards were presented to Division staff members by external organizations.

Figure 3. *Gertrude Blanch (NIST 1938-54) and Francis Sullivan (NIST 1982-93) were inducted into the NIST Portrait Gallery of Distinguished Scientists, Engineers and Administrators*

Kamran Sayrafian, along with ACMD guest researcher **Katjana Krhac** and colleagues at the Polytechnic University of Valencia and the University of Zagreb, received a Best Paper Award at the IEEE Conference on Standards for Communications and Networking held in Paris in October 2018. Their paper was entitled "Impact of Measurement Points Distribution on the Parameters of UWB Implant Channel Model." **Justyna Zwolak**, an ACMD Guest Researcher, won the Information Engines Scholarship Award for her presentation "Applying Machine Learning to Quantum-Dot Experiments," at the Information Engines at the Frontiers of Nanoscale

Thermodynamics Workshop held at the Telluride Science Research Center (CO) on July 19-27, 2018. And finally, **Sandy Ressler** took Second Place in the World Standards Day Essay Contest sponsored by the Society for Standards Professionals for an essay entitled "Standards, the Glue for Innovation." The award was presented in Washington, DC on October 18, 2018.

Two former NIST mathematicians were inducted into the NIST Portrait Gallery of Distinguished Scientists, Engineers and Administrators in October 2017. **Gertrude Blanch**, who was at NIST during the period 1938-54, was cited for excellence as Technical Director of the Mathematical Tables Project, and for pioneering contributions to the field of numerical analysis for early computers. **Francis Sullivan**, a NIST staff member from 1982-93, and a NIST guest researcher 1979-82 and 1993-present, was cited for establishing and leading the NIST Computing and Applied Mathematics Laboratory, which pioneered modern computing technologies and techniques for NIST.

Part II

Features

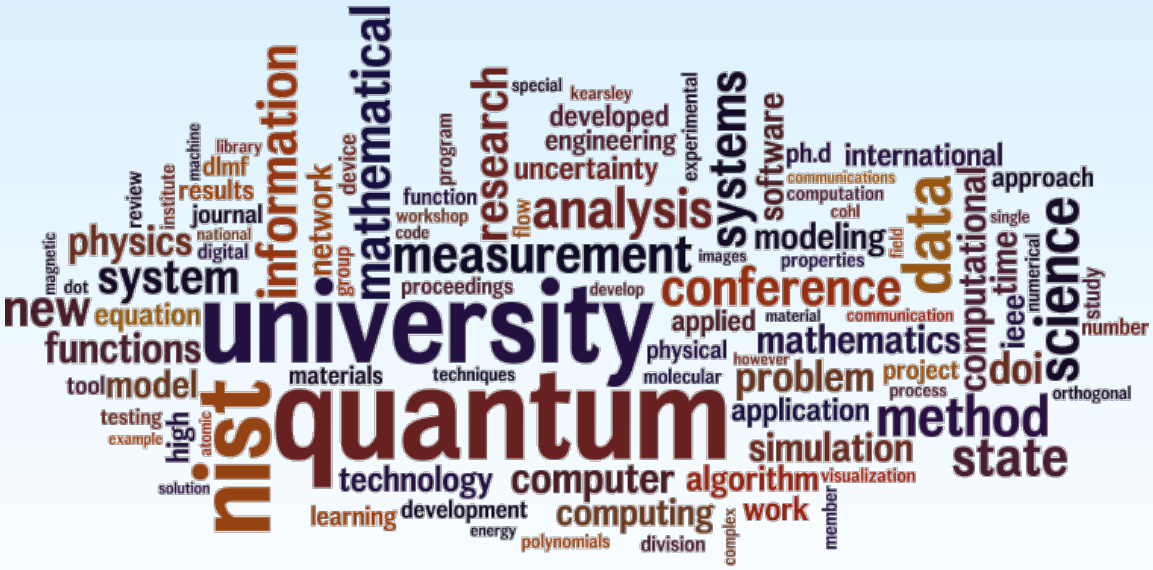

Fundamentals of Coarse-Graining: A Rigorous Approach to Reduced-order Modeling of Disordered Systems

Over the past two decades, computer simulations have become a common research and development tool in the materials science community. In this context, coarse-graining, i.e., the task of systematically reducing degrees of freedom to speed up computations, is becoming an increasingly important tool for reaching larger length-scales. However, there are many questions regarding the intrinsic limitations of such approaches. Motivated by these observations, we have developed a multipole method that connects a system of interacting molecules to its coarse-grained (CG) representation via a sequence of geometric approximations. Critically, we have shown that, for well-separated molecules, the intermolecular potentials and forces can be approximated to arbitrary accuracy depending on the order of this expansion. Thus, we can recover atomistic dynamics as an appropriate limit of the CG model. Moreover, the approach provides a basis for a priori uncertainty quantification, so that the usefulness of a CG model can be judged before simulations are ever run. We anticipate that this work will address many unresolved questions about best-practices for coarse-graining and facilitate adoption by industrial stake-holders.

Paul Patrone

Advances in computer simulations and modeling have led to a dramatic paradigm shift in how new materials are designed and manufactured [1]. As a result, a variety of industries are now integrating computational tools such as molecular dynamics (MD) into their product development cycles. From an economic perspective, the motivations for this are clear: every dollar spent on simulations yields as much as a nine-fold return-on-investment by informing decision-making, reducing excess testing, and therefore decreasing development times and costs [1, 2]. Indeed, the ability to model complicated systems at the *atomistic* scale has led to new insights into how molecular interactions and structure impact our everyday lives, with implications ranging from drug development to aerospace applications [3-5].

Despite these successes, a fundamental problem remains: for the foreseeable future, computers will lack the power to fully resolve macroscopic systems with atomistic detail. As a result, coarse-graining, i.e., the task of systematically reducing degrees of freedom to simplify and speed up modeling, is being recognized as critical for computational science. From an intuitive standpoint, everyday experiences suggest the rationale for why such approaches should work: the world appears as a relatively simple continuum of objects

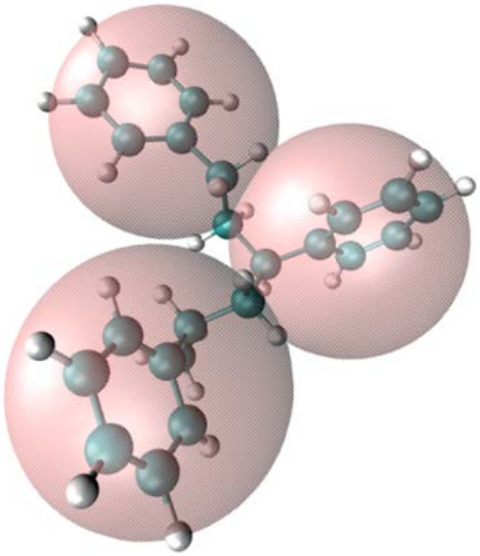

Figure 4. *Coarse-graining in molecular dynamics often amounts to projecting molecules or parts thereof onto effective particles, e.g. the light pink spheres in this image.*

characterized by a few properties, e.g., length, mass, strength, etc. Indeed, it has become a fundamental tenet of physics that much simpler macroscopic behavior of materials emerges from the complicated and often chaotic motion of many-body systems.

While this intuition has been a core principle of fundamental physics since before the advent of statistical mechanics, a deeper understanding of how to make it rigorous has remained a challenging, and in some cases, an elusive problem. Developments in the kinetic theory of gasses of the 1800's led to an atomistic basis for the famous pressure-volume-temperature relationships (e.g., the ideal gas law) first proposed in the late 1600's, providing an interpretation of temperature in terms of average kinetic energy. More recently in the 1900's, the recognition that many solids have an underlying crystalline structure led to macroscopic theories of elasticity and defects. Nonetheless, an understanding of how to extend these results to *disordered* systems, such as polymer networks and advanced composites, has had mixed success, based largely on empirical comparison. Moreover, there are few works that have treated coarse-graining of such systems in a rigorous fashion commensurate with, for example, kinetic theory.

What distinguishes these earlier successes from attempts to coarse-grain disordered systems is that the latter have not sought to connect the atomistic and CG models through a careful limiting process. Kinetic theory, for example, is based on the observation that the temperature (or pressure) of a gas is only meaningful

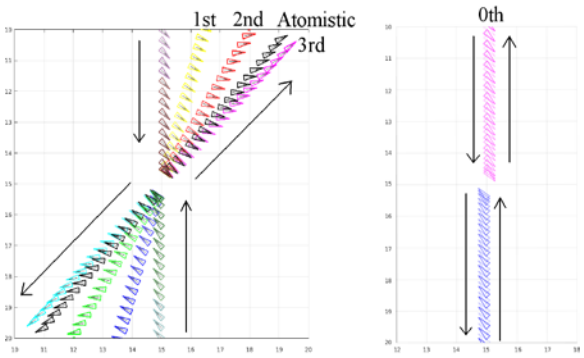

Figure 5. *Left: Collision between triangular particles using first, second, and third order truncations of Eq. (1). The trajectory of incoming particles is parallel to the vertical axis. After closest approach, the particles are deflected into the horizontal direction. Note that keeping more terms yields better agreement with the atomistic trajectory. Right: The zeroth-order (i.e. radially symmetric potential) predicts no deflection in the horizontal direction. Thus, the incoming and outgoing particles are all on the same line.*

when the number of particles goes to infinity, which is certainly reasonable given the large number of molecules in macroscopic limit ($N \approx O(10^{23})$. Coarse-graining of disordered systems, however, has tended to "project" atomistic descriptions onto a few (conjectured) "molecular" degrees of freedom at the mesoscale, see Figure 4. While such reduced-order descriptions are extremely amenable to large-scale simulations, detailed understanding of the relationship to their atomistic counterparts remains unclear as the bridge between the two scales was introduced through intuition

Invariably this perspective has led to a situation in which coarse-graining of disordered systems is treated as an exercise in empirical modeling. One postulates an *ad hoc* "molecular" (reduced-order) description of an atomistic system along with a self-consistency criterion that defines the interactions between CG particles, e.g., both representations must have the same average energy. This effective system is then evolved according to Newton's laws. While not invalid *per se*, such approaches have largely been implemented with convenience in mind. Thus, one of the most common assumptions has been that intermolecular potentials are well described by radially symmetric functions, with orientational degrees of freedom "averaging out." Ultimately, inaccurate predictions associated with such *choices* have led to much confusion about the true limitations of coarse-graining. Moreover, lack of rigor has hindered *a priori* uncertainty quantification (UQ), meaning that modelers cannot assess the accuracy of a CG model before implementing it. Given that initial development costs can be high, such issues have therefore slowed adoption by risk-averse industry stake-holders.

Multipole Coarse-Graining. Coarse graining typically invokes separation of scales to motivate a limiting process that carries one from the microscopic to the macroscopic domain. The ratio of interparticle spacing to the meter is a common choice, since this quantity is typically quite small. However, in constructing mesoscale representations of an atomistic system, this limit no longer makes sense.

In such cases, electrostatics provides an alternate approach. It is well known that the interactions between non-uniform charge distributions can be well characterized in terms of multipole expansions in the far-field regime. Such conditions hold when the characteristic sizes of the charge distributions δ are small relative to their characteristic separation R; i.e., $\delta/R \ll 1$. By analogy, we expect that a representation of molecular interactions in terms of a few geometric moments is sufficient to characterize their interactions under similar conditions. In this sense, we propose a generalized multipole theory for this task.

To make this observation more precise, we approximate molecules as rigid bodies and express the interaction potential as

$$U_{j,j'} = \sum_{k,k'} u\left(\mathbf{x}_j - \mathbf{x}_{j'} + \boldsymbol{\Theta}_j \boldsymbol{\delta}_k - \boldsymbol{\Theta}_{j'} \boldsymbol{\delta}_{k'}\right)$$

where $\mathbf{x}_j$ is a center-of-mass coordinate of the *j*th molecule, $\boldsymbol{\Theta}_j$ is a rotation matrix specifying its orientation, $\boldsymbol{\delta}_k$ is the position of the *k*th atom in a body-frame of reference, and u is the interatomic potential. Assuming that

$$\epsilon = \max_k |\boldsymbol{\delta}_k| / |\mathbf{x}_j - \mathbf{x}_{j'}| \ll 1$$

allows us to expand the potential in a Taylor series, yielding

$$U_{j,j'} = u(\mathbf{x}) + \textstyle\sum_n \epsilon^n U_n(\mathbf{x}, \boldsymbol{\Theta}_j, \boldsymbol{\Theta}_{j'}, \mathcal{K}^{(1)}, \ldots, \mathcal{K}^{(n)}) \quad (1)$$

where $\mathbf{x} = \mathbf{x}_j - \mathbf{x}_{j'}$ is the intermolecular separation and $\mathcal{K}^{(n)}$ is an nth order geometric moment associated with the internal structure of the molecules. Critically, Eq. (1) only depends on the CG variables $\mathbf{x}_j$ and $\boldsymbol{\Theta}_j$, not the atomic coordinates $\boldsymbol{\delta}_k$. Moreover, ,we have shown that our generalized multiple expansion: (i) yields controllable agreement relative to the exact intermolecular potential and atomistic dynamics, depending on truncation order of the series; and (ii) converges to the exact intermolecular potential in the limit that $n \to \infty$. To the best of our knowledge, this represents the first example of a coarse-graining strategy applied to disordered systems that connects the reduced-order representation to the exact model via an exact limiting process.

A primary benefit of this analysis is that it allows us to examine the impacts of choices associated with other coarse-graining strategies. For example, approaches that assume intermolecular potentials to be radially symmetric amount to a truncation of Eq. (1) at leading order

and/or averaging over all orientation degrees of freedom. Thus, such approaches cannot in general converge to or even well approximate the dynamics of molecular systems. Moreover, this observation has clarified a key point of confusion in the CG community. Specifically, it has long been assumed that CG potentials are inaccurate because they disregard many-body interactions. However, our work suggests that fault actually lies with omission of angular degrees of freedom and their effects on dynamics. Importantly, this observation only becomes apparent in the context of our analysis because the exact dynamics emerge as a limit of our CG analysis; see Figure 5. These results have been communicated in several manuscripts that are published and/or in preparation [6-7].

Motivated by these initial successes, we have now turned our attention to several open questions. For one, Eq. 1 suggests routes for *a priori* UQ in terms of the small parameter ϵ. Addressing this task is critical to ensuring widespread commercial adoption of coarse-graining strategies, since industry is not willing to adopt computational tools with unknown uncertainties. Moreover, more realistic models of materials permit internal vibrations within molecules. Thus, current research focuses on extending these results to systems that are of interest to a wide community of users.

References

[1] G. Goldbeck, *The Economic Impact of Molecular Modelling: Impact of the Field on Research, Industry, and Economic Development.* Goldbeck Consulting Ltd., St. John's Innovation Centre, Cambridge, United Kingdom, 2012.

[2] E. C. Joseph, C. Ingle, C. Meunier, S. Conway, G. Cattaneo, and N. Martinez. A Strategic Agenda for European Leadership in Supercomputing: HPC 2020 — IDC Final Report of the HPC Study for the DG Information Society of the European Commission. September 2010.

[3] G. Sliwoski, S. Kothiwale, J. Meiler, and E. W. Lowe Jr. Computational Methods in Drug Discovery. *Pharmacological Review* **66**:1 (2014), 334-395.

[4] S. Christensen and J. Senger. Distortional Matrix of Epoxy Resin and Diamine. U.S. Patent 7,745,549 B2, filed December 20, 2006, issued June 29, 2010.

[5] S. Christensen and J. Senger. Distortional Matrix of Epoxy Resin and Diamine. U.S. Patent 7,985,808 B2, filed April 23, 2010, issued July 26, 2011.

[6] P. N. Patrone, A. M. Dienstfrey, and G. B. McFadden. Towards A Priori Uncertainty Quantification in Coarse-Grained Molecular Dynamics: Generalized Multipole Potentials. In *Proceedings of the American Institute of Aeronautics and Astronautics SciTech 2019 Forum*, 1-10.

[1] P. N. Patrone, G. B. McFadden, A. M. Dienstfrey. Multipole Coarse-graining of Rigid-body Molecular Dynamics. in preparation.

Participants

Paul Patrone, Andrew Dienstfrey, and Geoffrey McFadden (ACMD)

Machine Learning for Experimental Quantum Dot Control

There are myriads of quantum computing approaches, each having its own set of challenges to understand and effectively control their operation. Electrons confined in arrays of semiconductor nanostructures, called quantum dots (QDs) are the basis of one such approach. Due to the ease of control of the relevant parameters, fast measurement of the spin and charge states, relatively long decoherence times, and their potential for scalability, QDs are gaining popularity as candidate building blocks for solid-state quantum devices. However, with an increasing number of QD qubits, the relevant parameter space grows exponentially, making heuristic control unfeasible. In semiconductor quantum computing, devices now have tens of individual electrostatic and dynamical gate voltages that must be carefully set to isolate the system to the single electron regime and to realize good qubit performance. It is thus highly desirable to have an automated protocol to achieve a target electronic state.

Focusing on QDs, this project aims to develop a fully automated approach to tuning experimental devices. In particular, we are investigating a novel paradigm that combines synthetic data from a physical model with machine learning and optimization to establish an automated closed-loop system of experimental control. We show that this approach can automatically tune the device to a desired dot configuration. These results serve as a baseline for future investigation of fine-grain device control (i.e., tuning to desired charge configuration), and to pave the way for similar approaches in a wide range of experiments in physics.

Justyna P. Zwolak

Arrays of *quantum dots* (QDs) are one of several candidate systems to realize qubits—the fundamental building blocks of quantum computers—and to provide a platform for quantum computing [1]. QDs are realized by electrostatically confining electrons using metal gates with voltages applied above a two-dimensional electron gas (2DEG) present at the interface of semiconductor heterostructures (see Figure 6 for a generic model of such a device with five gates). Realization of good qubit performance is achieved via electrostatic confinement, band-gap engineering, and dynamically adjusted voltages on nearby electrical gates. The voltages applied to barrier gates (V_{Bi}, $i = 1, 2, 3$, in Figure 6) and plunger gates (V_{Pj}, $j = 1, 2$ in Figure 6) define the potential landscape in which the QDs are formed (see Figure 6b). In particular, accumulation gates (not shown in Figure 6) are used to pattern a one-dimensional (1D) transport channel in the 2DEG; barriers define the dot positions by locally depleting carriers within the 1D

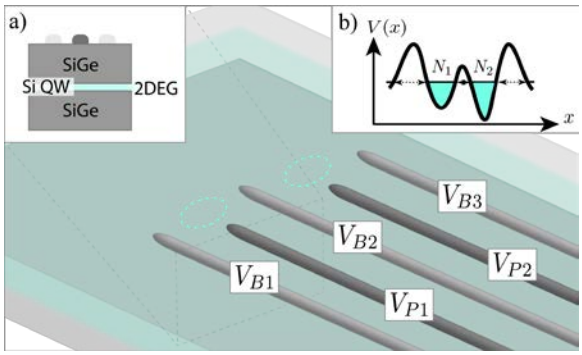

Figure 6. *A schematic of a gate-based quantum dot device with dashed ovals indicating islands where the quantum dots form. Insert (a) shows a cross-section of the device and insert (b) shows a potential profile along a one-dimensional channel patterned in the 2DEG for a double dot system, with N_1 and N_2 denoting the number of electrons on each dot.*

channel, thereby separating the electron density into disjoint regions, and the plungers shift the chemical potential in the dots relative to the chemical potentials of the contacts. In other words, the choice of gate voltages determines the number of dots, their position, and their coupling, as well as the number of electrons present in each dot.

The number of gates scales linearly with the number of dots and the voltage space grows exponentially. In order to reach a stable, few electron configuration, current experiments set the input voltages heuristically. However, such an approach does not scale well with the growing array sizes, is prone to random errors, and may result in only an acceptable rather than an optimal state. Given the recent progress in the physical construction of larger arrays of quantum dots, in both one and two dimensions [2, 3], it is thus imperative to have a reliable method to find a stable, desirable electron configuration in the dot array, i.e., to automate finding of a set of voltages that yield the right number of confinement regions (dots) with the right number of electrons and the right couplings.

The process of tuning QD devices involves identifying the state of the device from a series of measurements, followed by adjustment of parameters (gate voltages) based on the observed outcomes. As such, it heavily relies on a visual inspection and classification of images similar to the one presented in Figure 7. In recent years, machine learning (ML) algorithms, and specifically convolutional neural networks (CNNs), have emerged as a "go to" technique for automated image classification, giving reliable output when trained on a representative and comprehensive dataset [4]. Thus, a natural next step towards a fully automated tuning of experiments is to combine machine learning techniques

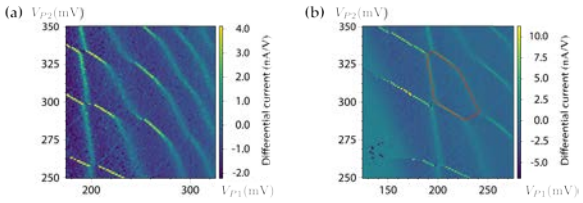

Figure 7. *Two sample measurements of the differential current as a function of voltages on plunger gates through a quantum dot device. The parallel lines (visible in (a)) suggest that the device is in a single dot regime while the hexagon-like features ("honeycombs", highlighted in (b)) suggest that the device is in a regime where two dots are formed.*

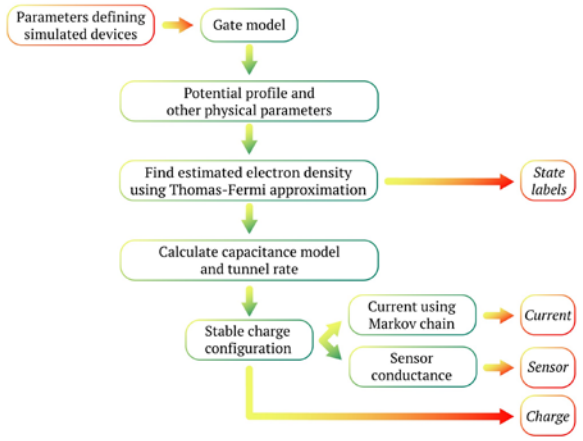

Figure 8. *Data simulation flow chart. The simulation is repeated for every point in the space of plunger gate voltages for a single device and then across an ensemble of device geometries. Details about the simulation can be found in [5] and [6].*

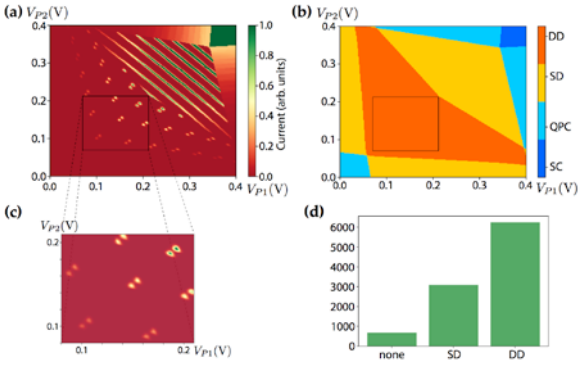

Figure 9. *(a) An example of a simulated 2D map (100 × 100 points) from the space of plunger gate voltages (V_{P1}, V_{P2}) to the current. (b) A state map corresponding to the current map presented in (a). (c) A sample sub-region showing a double dot configuration. (d) A typical distribution of states in a sample training set (N = 9009).*

with computer-supported device control to replace the heuristics developed by experimentalists.

Physical Model. As with all machine learning techniques, the availability of quality training data is essential for successful implementation. To address this issue, we developed a model for electron transport in gate-defined quantum dots that mimics the transport characteristics and the charge sensor response of an experimental device. Using a modified Thomas-Fermi approximation and treating the electronic density $n(x)$ as the main variable, we model a reference semiconductor system comprising of a quasi-1D nanowire with a series of depletion gates whose voltages determine the number of dots and the charges on each of those dots, as well as the conductance through the wire. While such an approach lacks the quantitative details of a full simulation, it reproduces the relevant qualitative features of the system and is sufficient for machine learning (as we have shown in [5]).

We generated an ensemble of 1001 gate configurations averaging over different realizations of the same type of device one might encounter in a lab. The data simulation flow is shown in Figure 8. Each sample device is stored as a 100×100-pixel map from plunger gate voltages to the specific output domains, and includes

- the current through the device at infinitesimal bias (an experimentally relevant parameter that can be measured, see Figure 9(a));
- the charge sensor readout (another experimentally relevant parameter);
- the number of charges on each dot (not directly measurable but useful for machine learning);
- the state labels (not directly measurable, used for classification, see Figure 9(b)).

The full data set was made publicly available at data.gov [7]. This will enable further study of machine learning techniques for quantum dot devices, and to provide data needed for development and study of new machine learning algorithms more broadly.

Machine Learning. The training and evaluation set is generated by taking 25 random 30×30 pixels sub-images of each full-size pixel map, resulting in 25 000 effective realizations (see Figure 9(c)). The labels for each sub-region are assigned based on the fraction of pixels within the sub-region in each of the three possible states, i.e.,

$$\boldsymbol{p} = \left[\frac{N-(\#SD+\#DD)}{N}, \frac{\#SD}{N}, \frac{\#DD}{N}\right],$$

where N is the size of the sub-image in pixels, and #SD and #DD are the numbers of pixels with *single dot* and *double dot* state label, respectively. As such, $\boldsymbol{p}$ can be thought of as a probability vector that the sub-region is in each of the possible configurations (i.e., no dot, single dot, or double dot).

To ensure reliability of the synthetic dataset in yielding data suitable for machine learning, we performed a validation test. From the full dataset, we randomly sampled 200 training sets. We then run five iterations of network training per full set, each time dividing it into two disjoint parts with 90 % of images used for training and 10 % of images used for evaluation. To

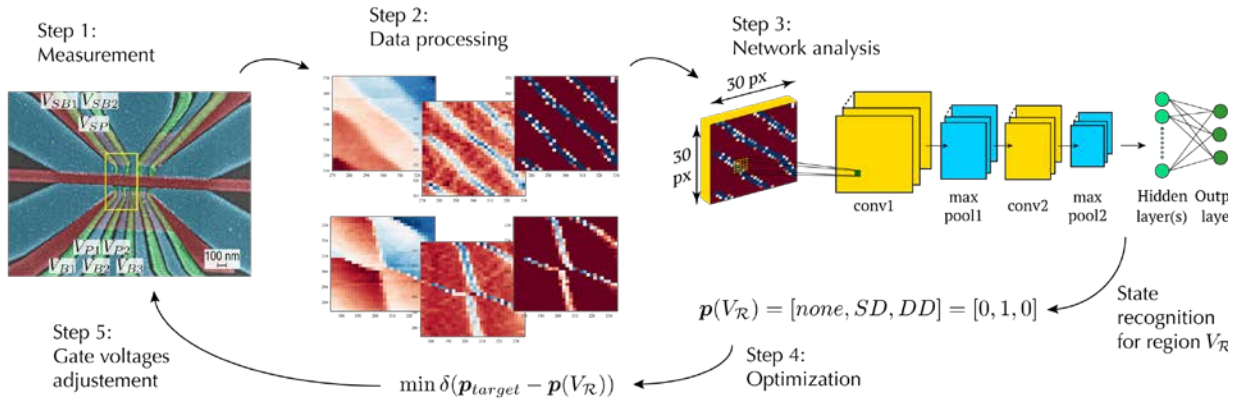

Figure 10. *Visualization of the auto-tuning loop. In Step 1, we show a false-color scanning electron micrograph of an SiGe quadruple dot device identical to the one measured. The yellow bordering shows gates used in the experiment. V_{Bi} (i=1,2,3) and V_{Pj} (j=1,2) are the barrier and plunger gates, respectively, used to form dots, while V_{SB1}, V_{SB2}, and V_{SP} are gates used to control the sensing dot. To process the data, we used the numerical derivative (central tiles in Step 2) and thresholding (right tiles in Step 2).*

account for the uneven distribution of representatives between classes in the training and evaluations sets (see Figure 9(d) for a typical distribution of the states) we used a weighted average of F1 scores of each class to determine the accuracy for each iteration [8]. We found 96.3 % accuracy in recognizing the state of a device when using current-based data, and 95.9 % accuracy for the charge-sensor-based training. The spread in accuracy over our 200 training sets is 0.5 % and 1.8 % for current- and charge-sensor-based data, respectively.

Optimization and auto-tuning. We define *auto-tuning* as the process of finding a range of gate voltages where the device is in a specific configuration (i.e., single or double dot regime). The auto-tuning process, visualized in Figure 10, compromises the following steps:

- the measurement of the current state of the device for a certain range of voltages;
- processing of the measured data: rescaling to assure compatibility with the network, filtering to remove noise (if necessary);
- the neural network analysis of the processed data to identity the state of the device;
- an optimization of the fitness function;
- an adjustment of the gate voltages as suggested by the optimizer.

The steps are then repeated until the desired state is reached. In other words, we formulate the auto-tuning as an optimization problem over the state of the device in the space of gate voltages, where the function to be optimized is a fitness function δ between probability vectors of the current and the desired sub-regions:

$$\delta(\boldsymbol{p}, \boldsymbol{p_0}) = \|\boldsymbol{p} - \boldsymbol{p_0}\|_2,$$

where $\boldsymbol{p}$ denotes the current probability vector (returned by the neural network), $\boldsymbol{p_0}$ is the probability vector of the desired state, and $\|\cdot\|_2$ is the 2-norm. The auto-tuning is considered successful if the optimizer converges to a voltage range that gives a desired dot configuration.

Performance. The proposed auto-tuning approach was tested on both simulated and experimental data. To test the synthetic dataset, for each simulated device a starting point was chosen in a uniform random fashion in the single dot region and the optimizer was set to tune to a double dot regime. We found 88.5 % accuracy in tuning, where the failure cases included tuning into the boundaries of the phase diagram and regions which mimic local minima for the optimizer.

To evaluate the auto-tuner in an experimental setup, we worked with researchers from University of Wisconsin–Madison. An SiGe quadruple quantum dot device (see Figure 10, Step 1) was pre-tuned into an operational mode, with one double quantum dot and one sensing dot active (highlighted with yellow border in Figure 5, Step 1). We first evaluated the trained network on experimental images, using 60 mV × 60 mV scans in 2 mV/pixel resolution. The neural network was able to distinguish between single dot, double dot, and no dot patterns. However, the recognition was not fully robust across all images and was subject to problems from overall scaling of the image data and choice of noise removal methods (see Figure 10, Step 2). We also performed a tuning trial run in the (V_{P1}, V_{P2}) plunger space. After adjustments of the noise filter to get pattern recognition results correctly, the tuning procedure worked as expected, shifting the voltage range from a single to a double dot state. Thus, we verified that, while further adjustments of handling the noise in experimental data and the scaling of the measured data to a range compatible with the neural network are necessary, the proposed auto-tuning approach looks promising and should be further investigated.

Summary. Working with experimental devices with high-dimensional parameter spaces poses many challenges, from performing reliable measurements to identifying the device state to tuning into a desirable configuration. By combining theoretical, computational, and experimental efforts, this interdisciplinary research sheds new light at how modern ML techniques can assist experiments. To use QD qubits in quantum computers, it is necessary to develop a reliable automated approach to control QD devices, independent of human heuristics and intervention. However, as experimental testing shows, more work is needed to improve the performance of the auto-tuner in real-life settings.

References

[1] R. Hanson, L. P. Kouwenhoven, J. R. Petta, S. Tarucha, and L. M. K. Vandersypen. Spins in Few-electron Quantum Dots. *Reviews of Modern Physics* **79:**4 (2007), 1217–1265.

[2] D. M. Zajac, T. M. Hazard, X. Mi, E. Nielsen, and J. R. Petta. Scalable Gate Architecture for a One-Dimensional Array of Semiconductor Spin Qubits. *Physical Review Applied* **6**:5 (2016), 054013.

[3] U. Mukhopadhyay, J. P. Dehollain, C. Reichl, W. Wegscheider, and L. M. K. Vandersypen. A 2 × 2 Quantum Dot Array with Controllable Inter-Dot Tunnel Couplings. *Applied Physics Letters* **112**:18 (2018), 183505.

[4] A. Krizhevsky, I. Sutskever, and G.E. Hinton. Imagenet Classification with Deep Convolutional Neural Networks. In *Advances in Neural Information Processing Systems* **25** (2012), F. Pereira, C.J.C. Burges, L. Bottou, and K.Q. Weinberger, eds., 1097–1105.

[5] S. S. Kalantre, J. P. Zwolak, S. Ragole, X. Wu, N. M. Zimmerman, M. D. Stewart, J. M. Taylor. Machine Learning Techniques for State Recognition and Auto-tuning in Quantum Dots. *npj Quantum Information* **5**:6 (2019), 1–10.

[6] J. P. Zwolak, S. S. Kalantre, X. Wu, S. Ragole, J. M. Taylor. QFlow Lite Dataset: A Machine-Learning Approach to the Charge States in Quantum Dot Experiments. *PLoS ONE* **13**:10 (2018), 1–17.

[7] National Institute of Standards and Technology. Quantum Dot Data for Machine Learning. 2018 [cited 2018 Apr 30]. Database: data.gov [Internet]. URL: https://catalog.data.gov/dataset/quantum-dot-data-for-machinelearning

[8] Chinchor N. MUC-4 Evaluation Metrics. In: *MUC4 '92: Proceedings of the 4th Conference on Message Understanding*; June 16-18, 1992, McLean, VA. Association for Computational Linguistics, 1992. 22–29.

Participants

Justyna P. Zwolak (ACMD); Jacob M. Taylor (NIST PML); Sandesh S. Kalantre, Stephen Ragole, Xingyao Wu (University of Maryland); Mark A. Eriksson, Susan Coppersmith, Tom McJunkin, J. P. Dodson (University of Wisconsin – Madison)

Uncertainty Quantification in Statistical Channel Modeling for UWB Implant Communication

Sophisticated medical implants that allow vital information delivery to/from the human body are opening the door to novel approaches in diagnosis and/or therapy of various health related issues. Ultra-Wide Band (UWB) technology is gaining the attention of researchers as a possible candidate for implant communication due to its high data rate and low power consumption capabilities. Characterization of radio frequency (RF) propagation often involves a measurement campaign (either virtual or physical) and selecting a set of sample measurement points through which numerical values of the desired signal at the receiver are collected. Statistical analysis of those data will lead to a propagation model representing the wireless communication link. Such models are required by product engineers designing RF communication modules for UWB medical implants.

Focusing on an implant using UWB technology, this project aims to highlight the potential impact of the spatial distribution of measurement points on the extracted parameters of the propagation model. This is achieved through emulating a custom-designed multi-layer liquid phantom measurement system and performing a sequence of simulations with different measurement point distributions. The results are meant to serve as a guideline for future UWB implant measurement in order to obtain more accurate propagation models.

Katjana Krhac
Kamran Sayrafian

A Wireless Body Area Network (WBAN) is a relatively new technology that has been developed to connect wearable or implantable sensors/actuators located inside or on the surface of the human body. This is a critical enabling technology for the future Internet of Things for healthcare. IEEE 802.15.6 is the first international standard that outlines the frequency bands that can be used for different use-cases in a WBAN [1]. The most common frequency bands that are used for WBAN applications are

- 402–405 MHz: Medical Implant Communication Service (MICS)
- 2.4–2.4835 GHz: Industrial, Scientific and Medical radio band (ISM), and
- 3.1 to 10.6 GHz (unlicensed Ultra-Wide Band (UWB).

At present, and as described in the IEEE 802.15.6 standard, for implant or equivalently in-body communication (i.e., communication to a node inside the human body), only the MICS frequency band has been considered. The maximum data rate that can be achieved using this band is 455 kbps [1]. However, some recent applications could require much higher data rates. One example is the need to deliver better quality images from the human gastrointestinal (GI) tract in video capsule endoscopy. For this reason, researchers are also considering UWB technology for in-body communication. An UWB signal is known to suffer from high propagation loss inside the human body. However, its high data rate capability, low transceiver complexity, as well as the possibility for miniature size antennas would still make this technology an attractive candidate for in-body applications. To enable such applications, it is important to have an accurate mathematical model for path loss, i.e., the reduction in signal power as it propagates through the human body. Such information enables engineers to design transmitters with the right power and antennas with the right sensitivity. Since *in-vivo* experimentation to determine path loss is either difficult, or in case of human subject nearly impossible, commonly used approaches to study implant UWB channels is through either computational or liquid phantom measurements.

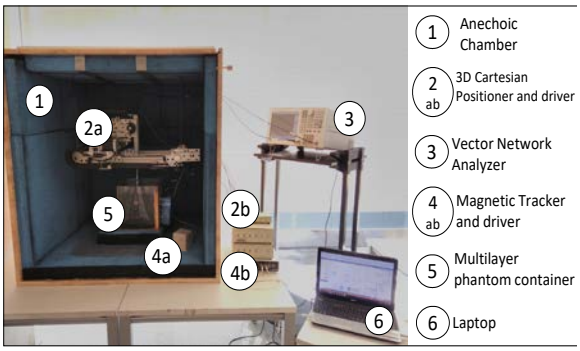

Figure 11. *Experimental setup.*

Liquid Phantoms. Liquid phantoms are aqueous solutions that precisely mimic the electromagnetic properties of the human tissue. They enable researchers to conduct physical measurements to study an implant channel in a laboratory environment. A comprehensive measurement campaign using a custom-built multi-layer phantom for UWB frequency band has been undertaken at the Universitat Politècnica de València (UPV) [2].

Figure 11 shows the main elements of their measurement setup. It consists of an anechoic chamber, a vector network analyzer (VNA), a 3D spatial positioner, a phantom container, a magnetic tracker, and a laptop. Most of the elements controlled by a specialized software on the laptop. The anechoic chamber is used to minimize the potential impact of reflections due to the surrounding environment. The chamber has an internal

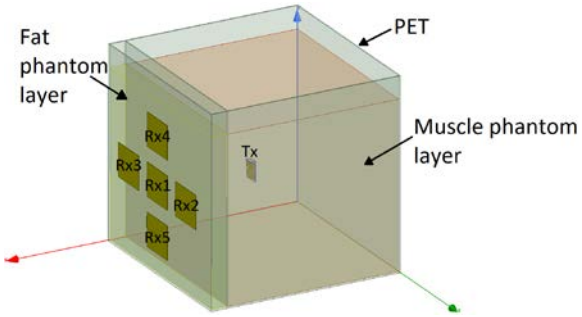

Figure 12. *Simulated phantom container.*

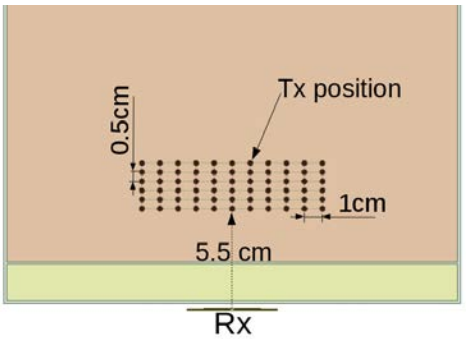

(a)

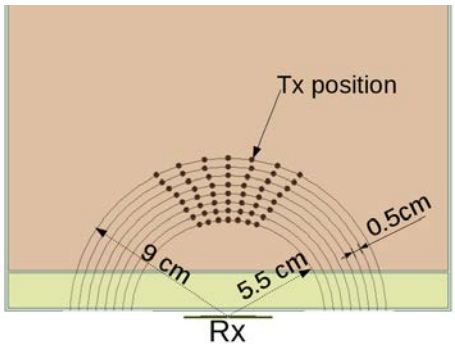

(b)

Figure 13. *(a) Sample rectangular measurement grid. (b) Sample circular measurement grid.*

volume of 1 × 1 × 1 m^3 enclosed in a wooden structure with 22 mm width.

A 3D Cartesian positioner is placed inside the anechoic chamber (Figure 11, element 2a) to allow calculation of the distances between receiver and transmitter antennas. This positioner has a 1 mm precision along the *x*, *y*, and *z* axes, and 30 × 30 × 10 cm^3 movement range. The in-body antenna is attached to the positioner in this measurement setup. In addition to the 3D positioning system, the spatial position of each antenna is calculated by a 3D magnetic tracker using sensors that are attached to the center of each antenna (Figure 11, element 4b).

The multi-layer phantom container (shown in Figure 11, element 5) is made of polyethylene terephthalate (PET) with a width of 1.5 mm and has an overall internal volume of 25 × 25 × 25 cm^3. The container consists of two layers (i.e., segments) of liquid phantoms emulating muscle and fat with dimensions of 23 × 25 × 25 and 2 × 25 × 25 cm^3 respectively. A divider sheet, also made of PET (with 1.5 mm thickness), separates the liquid phantom layers. The walls of the container are made as thin as possible in order to have minimum impact on the signal propagation inside the multi-layer phantom. The liquid phantoms used in this experiment accurately mimic the electrical properties of human muscle and fat tissue for the entire UWB frequency band [3].

Computational Model. Extensive computational time and high memory requirements often create an obstacle in performing sophisticated electromagnetic simulations to study a UWB wireless channel. However, such simulations are extremely helpful to gain understanding of the general behavior of a wireless link, or to identify appropriate scenarios to perform physical measurements.

Using a dedicated computer with 64 cores and 3 TB of memory, the core elements of the physical measurement system (i.e., the container along with the liquid phantom layers) was emulated using ANSYS HFSS (see Figure 12) by ACMD. The simulated container has identical dimensions, thickness and material properties as the one shown in Figure 11 element 5. The container also includes the divider sheet that separates the fat and muscle phantoms in the experiment. Each segment of the container is then filled with muscle and fat tissue. The corresponding frequency-dependent material properties of these tissues are programmed to be identical to the liquid phantoms used in the experiment.

Uncertainty Quantification. We use the computational model to study the sensitivity of path loss parameters measured in the experiment to the distribution of measurement points. To do this, two different grids were set up in the virtual model of the multi-layer phantom as shown in Figure 13. The rectangular grid is a uniform rectangular lattice with 0.5 cm spacing on the *x* axis and a 1 cm spacing on the *y* axis. To increase the number of sample points, two or more levels of this rectangular grid (i.e., with different elevations) can be considered for simulation purposes. Here, to minimize the impact of antenna orientation on the results, only one level of grid points (at the same elevation as the receiver) was considered. The actual distances between the grid points and the receiver location (i.e., the distance between the center of the in-body and on-body antenna) results in the histogram shown in Figure 14(a).

As an alternative, we set up a circular grid through intersection of circles (co-centered at the receiver location) with different radii as shown in Figure 14(b). The spacing between circles, as well as angular spacing among different radii, can be variable and chosen according to the requirement of the statistical model under consideration. In this study, the spacing between circles was chosen to be 0.5 cm; and, to minimize the impact of

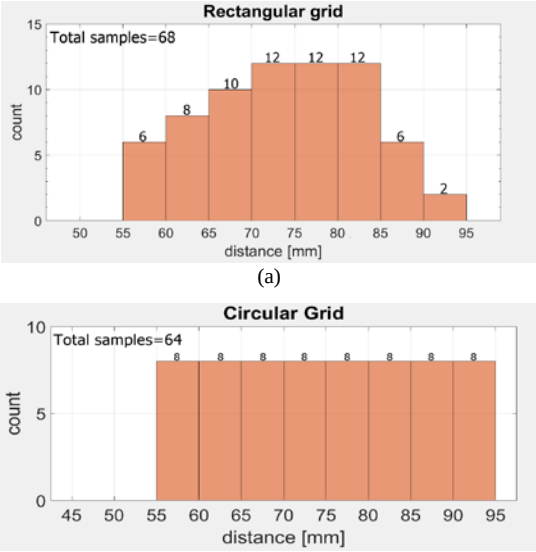

(a)

(b)

Figure 14. *Histogram of the TX-RX distances in the (a) rectangular grid, and (b) circular grid.*

antenna orientation on the extracted parameters, a small angular spread was considered. The circular grid shown in Figure 13(b) results in the transmitter-receiver distance histogram in Figure 14(b).

Simulations with the virtual model of the multilayer phantom were performed using both types of grids to obtain the $S_{21}(f)$ values for frequency range of 3.1 to 4.1 GHz. It should be noted that at each grid point the in-body antenna was facing parallel to the receiver and no antenna rotation was considered at any points. Through statistical analysis of these data, and again assuming a simple path loss model, the average path loss exponent, $\overline{n(f)}$, was obtained and presented in Table 1.

Analysis of Results. The results show the potential impact of the distribution of measurement points on the extracted path loss exponent. The circular grid leads to a more uniform distribution of sample point distances, and, therefore, all samples are fairly and equally represented during the statistical analysis process. This in turn could lead to more accurate channel model parameters. The mathematical nature of the statistical model could also provide additional input on grid point selection. For example, logarithmic based models might benefit from a logarithmic scale for circle spacing in the circular measurement layout. The characteristics of the specific implant application being considered can provide guidelines for the arrangement and selection of optimal grid points for the measurement process.

Table 1. *Average path loss exponent for different grids.*

	$\overline{n(f)}$
Rectangular grid	9.68
Circular grid	10.60

Through a joint simulation and experimentation study, this research highlights the potential impact of the location and distribution of sample measurement points on the extracted parameters of a statistical channel model such as a frequency-dependent path loss exponent. It is shown that for studying a UWB implant channel a judicious selection of measurement points could lead to a sample set that better represents the transmitter-receiver distances as well as relative antenna pattern orientation [4]. This process will result in a more accurate statistical model for the communication channel. To the best of our knowledge, there are no similar studies in the literature for UWB implant channels. Although only the impact on the path loss exponent was considered in this study, we conjecture similar impacts exist on other parameters of the statistical model obtained through the fitting process. The short communication distances and limited number of measurement points are among the reasons that differentiates implant communication with other wireless channels. In general, the specifics of the intended use-case should drive the selection of sample measurement points for such channel modeling efforts.

References

[2] IEEE Standards Association. *IEEE Standard for Local and Metropolitan Area Networks*, Part 15.6: Wireless Body Area Networks. February. 2012.

[3] S. Perez-Simbor, M. Barbi, C. Garcia-Pardo, S. Castelló-Palacios, and N. Cardona. Initial UWB In-Body Channel Characterization Using a Novel Multilayer Phantom Measurement Setup. In *Proceedings of the 2018 IEEE Wireless Communications and Networking Conference Workshops (WCNCW)*, Barcelona, Spain, 2018, 384-389.

[4] C. Andreu, C. Garcia-Pardo, A. Fornes-Leal, M. Cabedo-Fabrés, and N. Cardona. UWB In-Body Channel Performance by Using a Direct Antenna Designing Procedure. In *Proceedings of the 2017 11th European Conference on Antennas and Propagation (EUCAP)*, Paris, France, 2017, 278-282.

[5] S. Perez-Simbor, K. Krhac, C. Garcia-Pardo, K. Sayrafian, D. Simunic, and N. Cardona. Impact of Measurement Points Distribution on the Parameters of UWB Implant Channel Model. In *Proceedings of the IEEE Conference on Standards for Communications and Networking*, Paris, France, October 29-31, 2018. DOI: 10.1109/CSCN.2018.8581808

Participants

Katjana Khrac, Kamran Sayrafian (ACMD); Sofia Perez-Simbor, Concepcion Garcia-Pardo, Narcis Cardona (University Polytechnic Valencia); Dina Simunic (University of Zagreb, Croatia)

Part III

Project Summaries

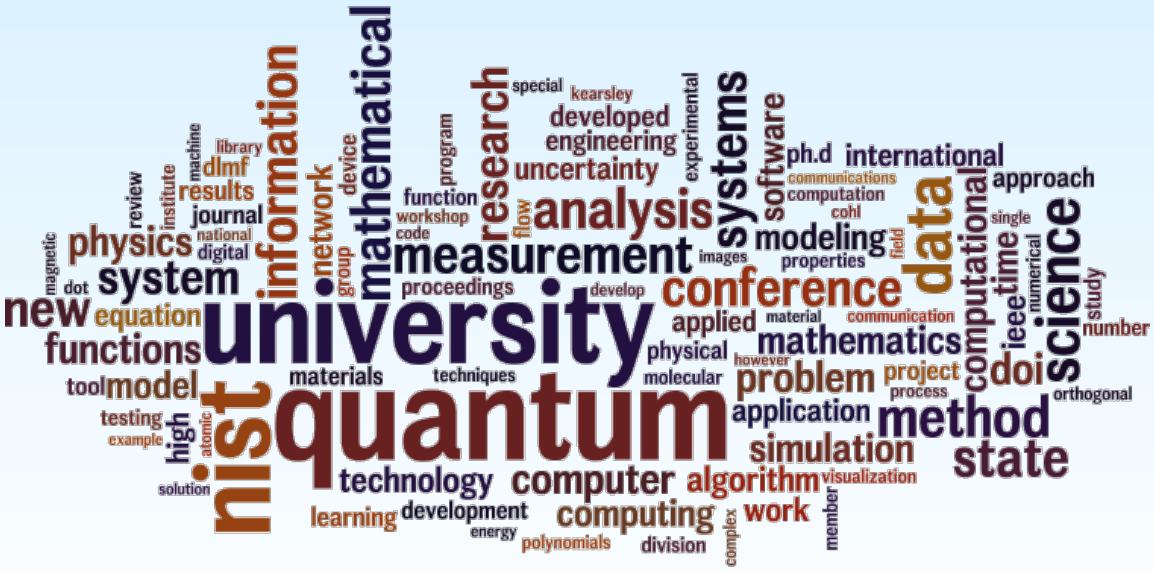

Mathematics of Metrology

Mathematics plays an important role in measurement science. Mathematical models are needed to understand how to design effective measurement systems and to analyze the results they produce. Mathematical techniques are used to develop and analyze idealized models of physical phenomena to be measured, and mathematical algorithms are necessary to find optimal system parameters. Mathematical and statistical techniques are needed to transform measured data into useful information. The goal of this work is to develop fundamental mathematical methods and tools necessary for NIST to remain a world-class metrology institute, and to apply these methods and tools to problems in measurement science.

Numerical Computation of Ill-Posed Time-Reversed Nonlinear Evolution Equations

Alfred Carasso

Recently developed stabilized explicit schemes constitute a significant ACMD intervention, one that permits effective numerical computation of ill-posed, time-reversed, multidimensional, nonlinear dissipative evolution equations. Such retrospective problems are of great current interest in environmental forensics, geophysics, image deblurring, and in the numerous deconvolution problems that pervade measurement science, [1-7]. In a series of papers [8-13], such stabilized schemes have been successfully applied to interesting classes of time-reversed initial value problems for parabolic equations, viscous wave equations, coupled sound and heat flow, thermoelastic vibrations, and 2D viscous Burgers' equations. Currently, exploratory work is in progress on the time-reversed 2D incompressible Navier-Stokes equations.

The Forgetfulness of Dissipative Equations. There is a necessary uncertainty in backward in time reconstructions from imprecise data given at some positive time T. That uncertainty is a function of how quickly the given evolution equation forgets the past as time advances. This is a deep subject that is explored in such publications as [14-17] and the references therein. Using logarithmic convexity approaches pioneered by Knops, Payne, and their students, sharp L^2 error estimates in the form $\|err(t)\|_2 \leq K\delta^{\mu(t)}, 0 \leq t \leq T$, have been obtained for many time-reversed problems. The exponent $\mu(t)$ typically tends to zero exponentially as $t \downarrow 0$, indicating rapid loss of accuracy in backward recovery from given data at time $T > 0$, known to be accurate to within $\delta > 0$ in the L^2 norm. In fluid flow problems, the constant K depends on both T and the Reynolds Number RE in such a way that with large RE, the uncertainty becomes unacceptably large as $t \downarrow 0$, unless $T \ll 1$. While these logarithmic convexity estimates are sharp, they necessarily reflect worse-case error accumulation scenarios that may be too pessimistic in practice. As demonstrated in the two examples below, useful reconstruction may sometimes be possible even at relatively large RE.

Backward Recovery in 2D Viscous Burgers' Equation. As may be seen from the Lana Turner experiment in Figure 15, the use of 8-bit gray scale face images provides visually instructive examples in backward recovery, while posing challenging ill-posed reconstruction problems due to the highly non-smooth intensity data that typically define such images. Given the exact data shown in the left column in Figure 1, together with the chosen kinematic viscosity $\nu > 0$, we have $RE = 3400$ in this experiment. A stable forward computation in the 2D Burgers' system already produces a noticeably blurred image at time $T = 2.5 \times 10^{-4}$, as shown in the middle column in Figure 1. However, successful backward recovery from the data at time T can be achieved, using the stabilized backward explicit scheme developed in [13]. Much less successful recovery would be feasible from more severely blurred data at larger values of T.

Backward Recovery in 2D Incompressible Navier-Stokes Equations. As discussed in [18], the stream function-vorticity formulation is a useful approach in the forward numerical computation of the 2D Navier-Stokes equations. A given stream function $\psi(x, y, t)$ at time t defines the velocities $u(x, y, t) = \psi_y, v(x, y, t) = -\psi_x$, and the vorticity $\omega(x, y, t) = -\Delta\psi$. An advection diffusion equation, with advection coefficients u, v, is now used to advance the vorticity ω to time $t + \Delta t$, and an advanced stream function $\psi(x, y, t + \Delta t)$ is then obtained by solving the Poisson equation $\Delta\psi = -\omega$. This leads to advanced velocities u, v at time $t + \Delta t$. A stabilized backward explicit scheme applied to the advection diffusion equation, coupled with a multigrid Poisson solver at each time step, have been found useful in running this process backward in time.

In the experiment described in Figure 16, Elizabeth Taylor's image in the left column is chosen as the stream function $\psi(x, y, 0)$, with contour plots for ψ and ω at time $t = 0$, shown immediately below. Here, the Reynolds number is $RE = 10300$. The results of a stable forward computation to time $T = 3.0 \times 10^{-3}$ are shown

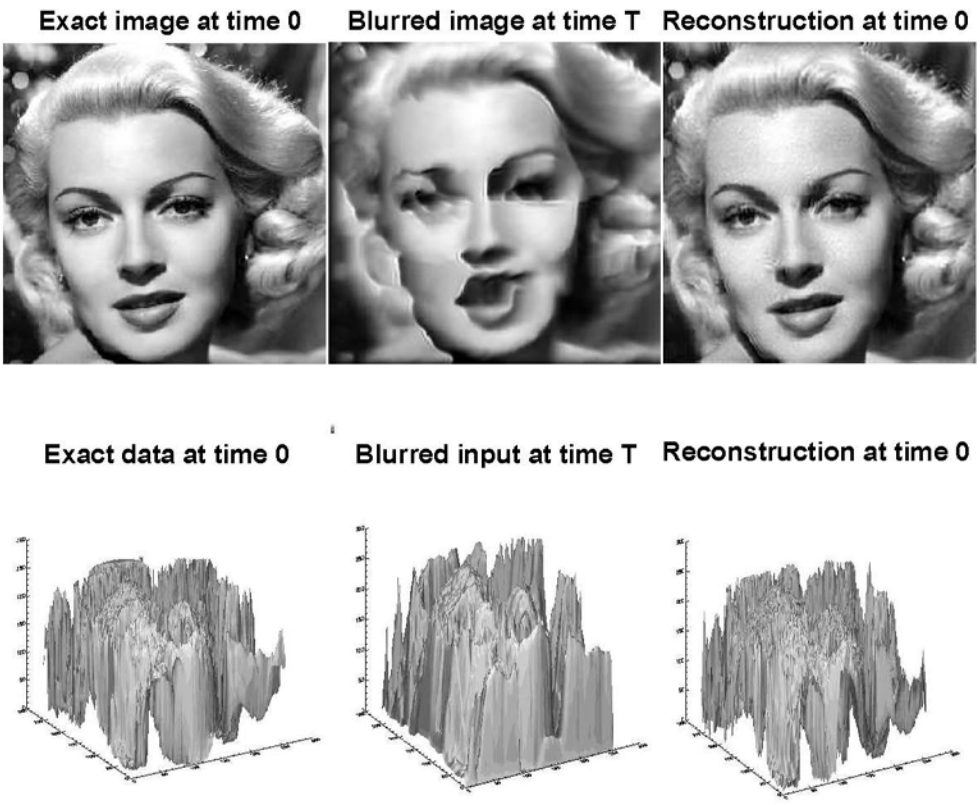

Figure 15. *Successful backward recovery in 2D Burgers' equation at high Reynolds Number when* $T = 2.5 \times 10^{-4}$*, using stabilized backward explicit scheme developed in Reference [13].*

in the middle column, with substantial blurring indicated in the image and contour plots at time T. Nevertheless, useful information can be retrieved from the data at time T.

[1] J. Atmadja and A. C. Bagtzoglou. State of the Art Report on Mathematical Methods for Groundwater Pollution Source Identification. *Environmental Forensics* **2** (2001), 205-214.

[2] R. N. Singh. Advection Diffusion Equation Models in Near-Surface Geophysical and Environmental Sciences. *Journal of the Indian Geophysical Union* **17** (2013), 117-127.

[3] A. Ismail-Zadeh, et al. Three-Dimensional Forward and Backward Numerical Modeling of Mantle Plume Evolution: Effects of Thermal Diffusion. *Journal of Geophysical Research* **111** (2006), B06401.

[4] A. Ismail-Zadeh, et al. Numerical Techniques for Solving the Inverse Retrospective Problem of Thermal Evolution of the Earth Interior. *Computers and Structures* **87** (2009), 802-811.

[5] G. Gilboa, et al. Forward-and-Backward Diffusion Processes for Adaptive Image Enhancement and Denoising. *IEEE Transactions on Image Processing* **11** (2002), 669-703.

[6] A. Carasso, D. S. Bright, and A. E. Vladar. APEX Method and Real-Time Blind Deconvolution of Scanning Electron Microscope Imagery. *Optical Engineering* **41** (2002), 2499-2514.

[7] A. S. Carasso. Bochner Subordination, Logarithmic Diffusion Equations, and Blind Deconvolution of Hubble Space Telescope Imagery and Other Scientific Data. *SIAM Journal on Imaging Sciences* **3** (2010), 954-980.

[8] A. S. Carasso. Compensating Operators and Stable Backward in Time Marching in Nonlinear Parabolic Equations. *International Journal of Geomathematics* **5** (2014), 1-16.

[9] A. S. Carasso. Stable Explicit Time-Marching in Well-Posed or Ill-Posed Nonlinear Parabolic Equations. *Inverse Problems in Science and Engineering* **24** (2016), 1364-1384.

[10] A. S. Carasso. Stable Explicit Marching Scheme in Ill-Posed Time-Reversed Viscous Wave Equations. *Inverse Problems in Science and Engineering* **24** (2016), 1454-1474.

[11] A. S. Carasso. Stabilized Richardson Leapfrog Scheme in Explicit Stepwise Computation of Forward or Backward

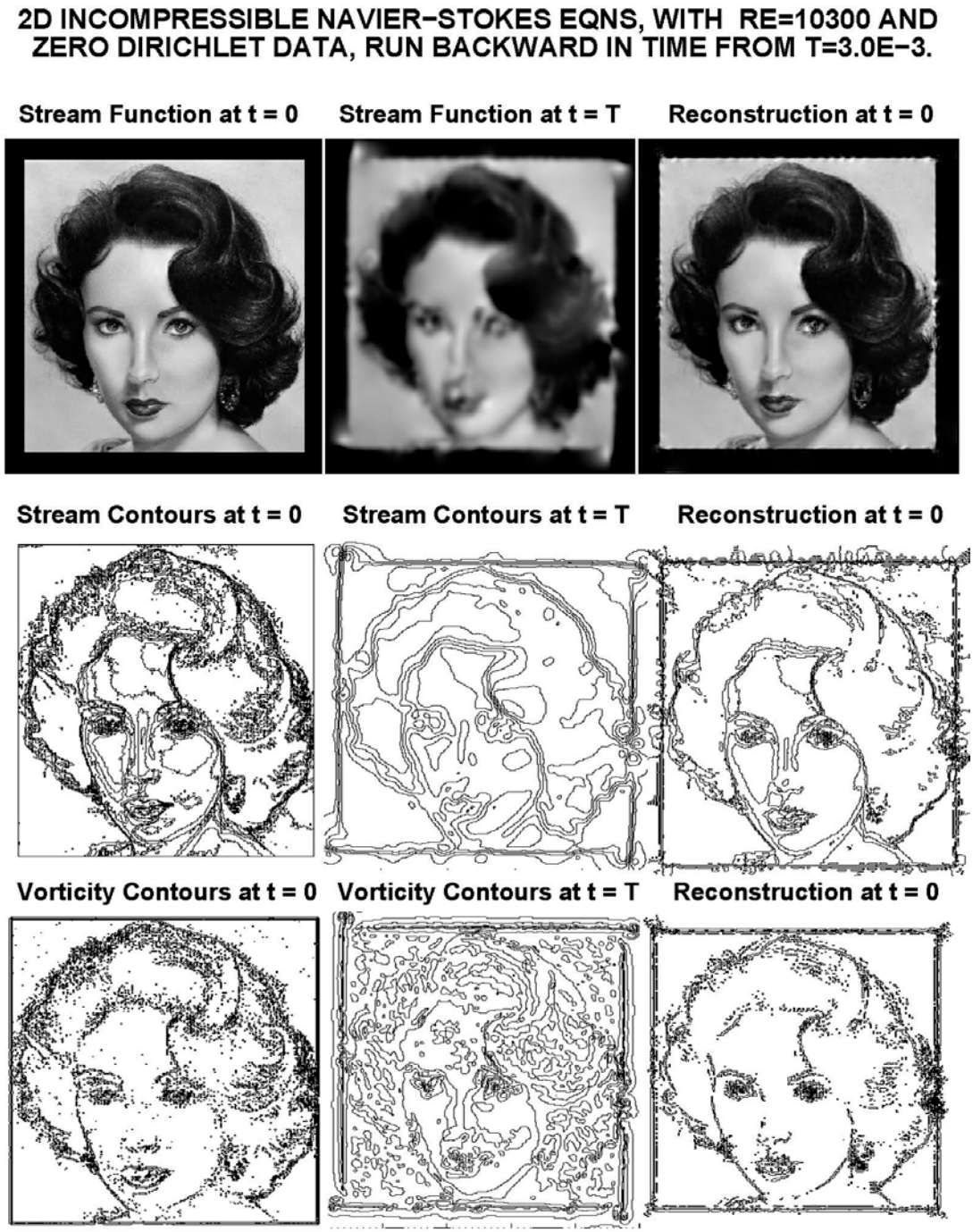

Figure 16. *Successful backward recovery in 2D incompressible Navier-Stokes equations at high Reynolds Number when* $T = 3.0 \times 10^{-3}$*, using stabilized backward explicit scheme currently being developed.*

Nonlinear Parabolic Equations. *Inverse Problems in Science and Engineering* **25** (2017), 1719-1742.

[12] A. S. Carasso. Stabilized Backward in Time Explicit Marching Schemes in the Numerical Computation of Ill-Posed Time-Reversed Hyperbolic/Parabolic Systems. *Inverse Problems in Science and Engineering* **27**:2 (2019), 134-165. DOI: 10.1080/17415977.2018.1446952

[13] A. S. Carasso. Stable Explicit Stepwise Marching Scheme in Ill-Posed Time-Reversed 2D Burgers' Equation. *Inverse Problems in Science and Engineering* (2018). DOI: 10.1080/17415977.2018.1523905

[14] A. Carasso. Computing Small Solutions of Burgers' Equation Backwards in Time. *Journal of Mathematical Analysis and Applications* **59** (1977), 169-209.

[15] A. S. Carasso. Reconstructing the Past from Imprecise Knowledge of the Present: Effective Non-Uniqueness in Solving Parabolic Equations Backward in Time. *Mathematical Methods in Applied Sciences* **36** (2012), 249-261.

[16] R. J. Knops and L. E. Payne. On the Stability of Solutions of the Navier-Stokes Equations Backward in Time. *Archives of Rational Mechanics and Analysis* **29** (1968), 331-335.

[17] K. A. Ames and B. Straughan. *Non-Standard and Improperly Posed Problems*, Academic Press, New York, 1997.

[18] H. Johnston and J. G. Liu. Finite Difference Schemes for Incompressible Flow Based on Local Pressure Boundary Conditions. *Journal of Computational Physics* **180** (2002), 120-154.

Computational Tools for Image and Shape Analysis

Günay Doğan (Theiss Research)
Javier Bernal
Charles R. Hagwood (NIST ITL)
Harbir Antil (George Mason University)
Soeren Bartels (University of Freiburg)
Marilyn Y. Vazquez (George Mason University)
Shuang Li (University of Southern California)
Hasan Hüseyin Eruslu (University of Delaware)
Eve N. Fleisig (Thomas Wootton High School)
Kevin Su (Poolesville High School)

The main goal of this project is to develop efficient and reliable computational tools to detect geometric structures, such as curves, regions and boundaries, from given direct and indirect measurements, e.g., microscope images or tomographic measurements, as well as to evaluate and compare these geometric structures or shapes in a quantitative manner. This is important in many areas of science and engineering, where the practitioners obtain their data as images, and would like to detect and analyze the objects in the data. Examples are microscopy images for cell biology or micro-CT (computed tomography) images of microstructures in material science and shoeprint images in crime scenes for footwear forensics. In fiscal year 2018, advances were made in the following two fronts of this project.

Image Segmentation. Image segmentation is the problem of finding distinct regions and their boundaries in given images. It is a necessary data analysis step for many problems in cell biology, forensics and material science, as well as other fields in science and engineering. In FY 2018, G. Doğan pursued a new approach to image segmentation with his collaborators, H. Antil from George Mason University, and S. Bartels from University of Freiburg. In this approach, the regions and their boundaries are represented implicitly with a phase field function, and the segmentations are obtained by minimizing an associated cost functional. They implemented an efficient minimization algorithm for this cost functional. The phase field is represented in the Fourier domain, and is then updated iteratively at a cost of a few Fast Fourier Transform operations per iteration. The advantage of this algorithm is that it is concise, and easily implemented for 3D image data, as well as 2D image data. Doğan, Antil, and Bartels evaluated the new model on a variety of synthetic and real image examples and found that it did very well in detecting fine geometric features around the regions, such as thin inclusions or protrusions [1].

G. Doğan worked with M. Vazquez, a Ph.D. student from George Mason University, on a segmentation algorithm based on data clustering. Vazquez had implemented a manifold-based clustering algorithm and used it for patch-based texture segmentation of images. She successfully applied this to material microstructure images, in particular, pearlite images provided by S. Yen Li from NIST MML [2]. She presented her work at ACMD Division Seminar in July 2018.

G. Doğan worked with two graduate student interns, S. Li from University of Southern California, and H. Eruslu from University of Delaware. Li developed a new segmentation algorithm using topological derivatives. Her goal was to segment images into regions of distinct statistics, modeled with parametric distributions of pixel values. This was different from Doğan's earlier work, which focused on piecewise constant segmentation. Her approach was also different in that it progressed by iteratively updating pixel labels, rather than evolving region boundaries. This initially led to noisy segmentations, but Doğan and Li developed a novel region regularization term that helped attain clean spatially-coherent region labels [3].

H. Eruslu, on the other hand, focused on volumetric image segmentation. The goal was to extract boundary surfaces of regions or objects in 3D volumetric images. For this, Eruslu implemented a surface evolution algorithm using the finite element package Dolfin. The surface was discretized as a triangulated surface, and the evolution was driven by energy minimization principles. He used a weighted surface energy, which favored surfaces fitting edges on images [4]. Eruslu achieved promising results segmenting synthetic 3D images. This work is still in progress, Eruslu is working with Doğan to improve algorithm's accuracy and speed to be able to address more realistic segmentation scenarios.

Shape Analysis. In FY 2018, G. Doğan worked on optimization algorithms for elastic shape analysis. He had previously developed a fast algorithm to compute an elastic shape distance between two given closed curves, working together with J. Bernal (ACMD) and C. Hagwood (ITL/SED). The elastic shape distance is a powerful dissimilarity metric to quantify the dissimilarity of two given closed curves [5, 6], and is widely

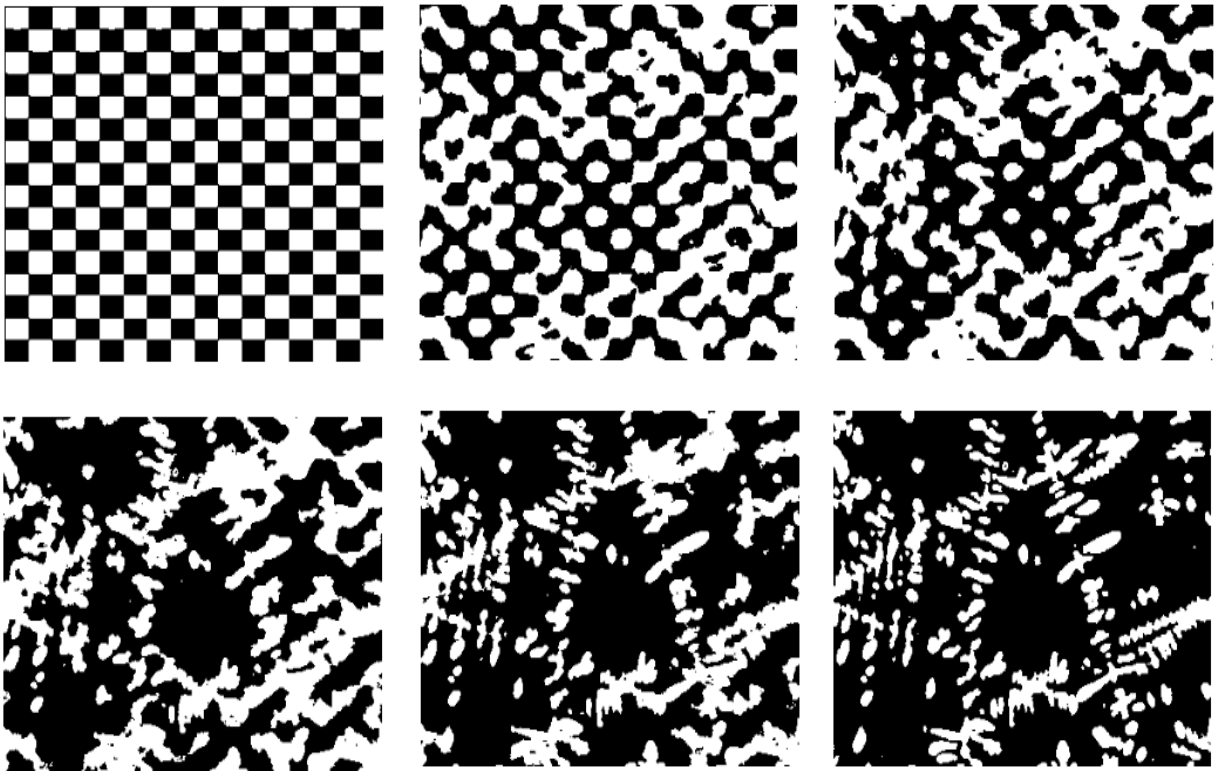

Figure 17. *Segmentation of a material microstructure image (bottom right) obtained by the phase field function evolution of a checkerboard initialization (top left).*

applicable to shape analysis problems in science and engineering. However, the computation of the elastic shape distance is expensive, as it requires solving a difficult optimization problem. Another challenge of the optimization is that the theoretical shape distance definition requires finding the global minimum of the underlying energy, which is very difficult and expensive to do in practice. To overcome these two difficulties of the problem, Doğan developed two reduced energy formulations of the model. These formulations have the advantage that the reduced variable (which becomes a hidden intermediate variable) is kept optimal at all stages of the computation. He was able to use a particular reduced form of the shape distance energy, depending only on two scalar variables, the starting point and the rotation angle, to sample the energy landscape efficiently, and to obtain good initializations for the iterative optimization algorithm. This new approach seemed to produce high quality optima with very reasonable computation times.

J. Bernal investigated the problem of computing the elastic registration of curves in n-dimensional space using dynamic programming (DP). Shape analysis of curves in higher dimensions, in particular in three dimensions, is useful for studying fiber tracts, geological terrains, protein structures, facial surfaces, color images, cylindrical helices, etc. We plan to implement the necessary code for the elastic registration of curves in n-dimensional space, and use it to compare lines of proteins, a 3D problem. Given two curves in *n*-dimensional space, the problem is to align them by optimally reparametrizing one curve with respect to the other one using dynamic programming [8], and by finding a rotation matrix [7] that minimizes an L_2 distance between two curves, which may be open or closed. In order to reparametrize optimally one curve with respect to the other, an existing efficient DP algorithm for the 1D and 2D cases must be generalized to n-dimensional curves. In order to compute an optimal rotation efficiently, an existing procedure for the 2D case based on the singular value decomposition and Fast Fourier Transform must be generalized to the *n*-dimensional case.

One undesirable aspect of the work on shape analysis is that the implementation is done in Matlab, which is a proprietary software environment. To provide a free open source alternative, G. Doğan has been working with high school volunteer K. Su (Poolesville High School) to implement an improved version of the shape distance code in Python. In FY 2018, a newer more efficient version of the dynamic programming code for elastic matching was completed. This will be followed with incorporation of starting point and rotation optimization to attain a full optimization algorithm for rotation-invariant shape distances for closed boundary curves.

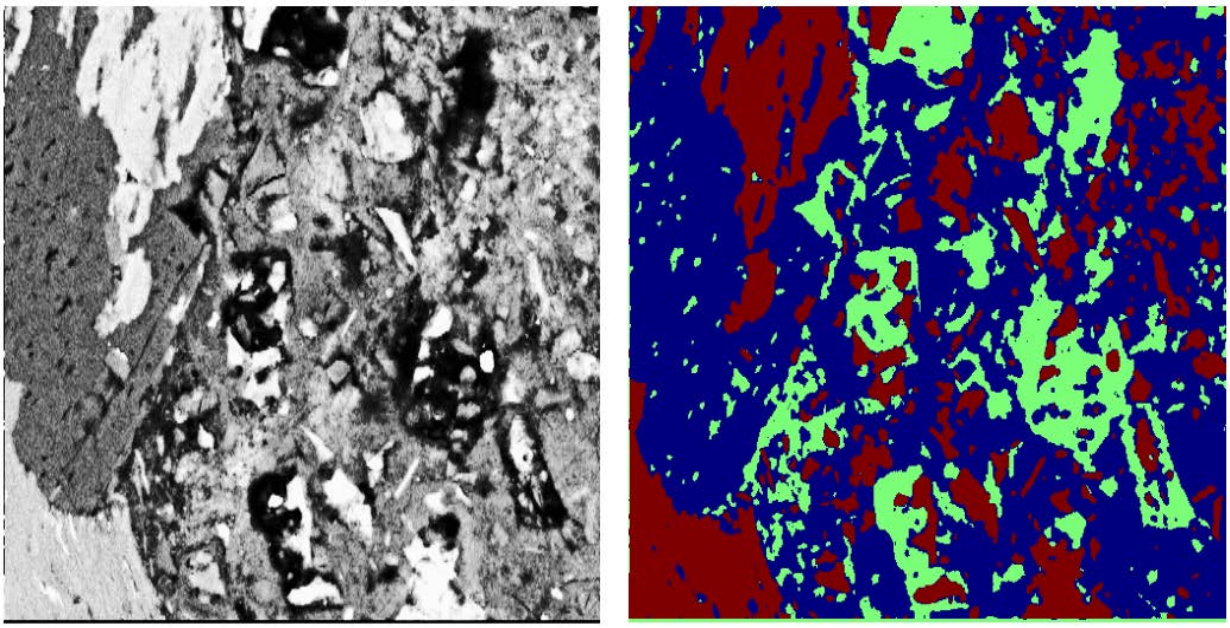

Figure 18. *Segmentation (right) of a noisy microstructure image (left) using region-regularized topology optimization.*

There are several different choices that can be made in the shape distance model and algorithms, and these result in different shape distance values for a given a pair of shapes. In general, for any dissimilarity metric between pairs of objects, multiple models or versions are available to compute dissimilarity. Thus, a critical problem is to decide which dissimilarity metric, or shape distance in this situation, is most useful for a particular application. For this, G. Doğan worked with high-school volunteer, E. Fleisig (Wootton High School) to develop a visual dissimilarity evaluation tool. This tool was completed and can be used in a versatile manner to evaluate multiple alternative dissimilarity metrics for heterogeneous data sets, which can include images, shapes, point clouds and other data types [9].

[1] H. Antil, S. Bartels, and G. Doğan. A Phase Field Segmentation Model with Improved Boundary Regularization. In preparation.

[2] M. Vazquez, G. Doğan, T. Sauer, and T. Berry. Microstructure Image Segmentation Via Density-Based Clustering. In preparation.

[3] S. Li and G. Doğan. Image Segmentation by Topology Optimization of Region Statistics. In preparation.

[4] G. Doğan. An Efficient Lagrangian Algorithm for an Anisotropic Geodesic Active Contour Model. In *Proceedings of 5th International Conference on Scale Space and Variational Methods in Computer Vision (SSVM'17)*, June 2017.

[5] A. Srivastava, E. Klassen, S. Joshi, and I. Jermyn. Shape Analysis of Elastic Curves in Euclidean Space. *IEEE Transactions on Pattern Analysis and Machine Intelligence* **33**:7 (2011), 1415-1428.

[6] G. Doğan, J. Bernal, and C. R. Hagwood. Fast Algorithms for Shape Analysis of Planar Objects. In *Proceedings of the IEEE Conference on Computer Vision and Pattern Recognition (CVPR'15)*, Boston, MA, June 2015.

[7] G. Doğan, J. Bernal, and C. R. Hagwood. FFT-based Alignment of 2D Closed Curves with Application to Elastic Shape Analysis. In *Proceedings of the 1st International Workshop on Differential Geometry in Computer Vision for Analysis of Shapes, Images and Trajectories (DiffCV'15)*, Swansea, United Kingdom, September 2015.

[8] J. Bernal, G. Doğan, and C.R. Hagwood. Fast Dynamic Programming for Elastic Registration of Curves. In *Proceedings of the 2nd International Workshop on Differential Geometry in Computer Vision and Machine Learning (DiffCVML'16)*, Las Vegas, NV, July 1, 2016.

[9] E. Fleisig and G. Doğan. VEMOS: GUI for Evaluation of Distance Metrics of Heterogeneous Data Sets. In preparation.

Parallel Adaptive Refinement and Multigrid Finite Element Methods

William F. Mitchell
Justin Kauffman
Eite Tiesinga (NIST PML)
Paul Julienne (NIST PML)
John Villarrubia (NIST PML)
Gale Holmes (NIST MML)

http://math.nist.gov/phaml

Finite element methods using adaptive refinement and multigrid techniques have been shown to be very efficient for solving partial differential equations (PDEs). Adaptive refinement reduces the number of grid points by concentrating the grid in the areas where the action is, and multigrid methods solve the resulting linear systems in an optimal number of operations. Recent research has been with *hp*-adaptive methods where adaptivity is in both the grid size and the polynomial order of approximation, resulting in exponential rates of convergence. W. Mitchell has been developing a code, PHAML, to apply these methods on parallel computers. The expertise and software developed in this project are useful for many NIST laboratory programs, including material design, semiconductor device simulation, the quantum physics of matter, and simulation of scanning electron microscopes.

Much of the work this year was related to wrapping up this project, as the principal investigator retired in September 2018. This involved cleaning up PHAML by removing temporary and dead code, dropped and ineffective approaches, and Fortran 2008 depreciated features in legacy code (mostly from Netlib). A final version of the software was released in August. We also installed PHAML and supporting software on the computers of our collaborators so that their work with PHAML can continue.

We completed the implementation of two new approaches in PHAML. One is to use nearest neighbor communication in MPI whenever possible, instead of the all-to-all communication originally implemented. The other is to use a refinement-edge based adaptive refinement instead of element-based refinement. This approach supports a directed acyclic graph (DAG) interpretation of the parallel structure of the code, which matches well with modern architectures. As shown in Figure 19, we obtain better than 50 % efficiency on a 68-core Intel Knights Landing computer with a speed-up of 37.7 on 64 cores.

Modeling Atomic Interactions. There are two major collaborative efforts with PML that apply PHAML to their physical models. First, in a collaboration with E. Tiesinga and P. Julienne, we are using PHAML to study the interaction of atoms and molecules held in an optical trap. In particular, we are using 2D and 3D models to calculate the bound states, scattering properties and dynamics of two interacting dipolar molecules. Tiesinga has recently found a near-exact solution to the dipole problem using second-order perturbation theory. We are currently working to confirm this solution using computational solutions from PHAML. This requires very high accuracy solutions while varying the dipole strength over small values, using problems with a symmetric trap and with a "pancake" trap. Using PHAML, we obtained computational eigenvalues with 10 significant digits by using a mesh with 25 million vertices and fourth-order elements. The computed eigenvalues over a neighborhood of the asymptotic expansion point provide estimates of certain parameters in the near-exact solution, and then the computed eigenvalues can be compared to the predicted eigenvalues. This work is ongoing and will be continued by Tiesinga.

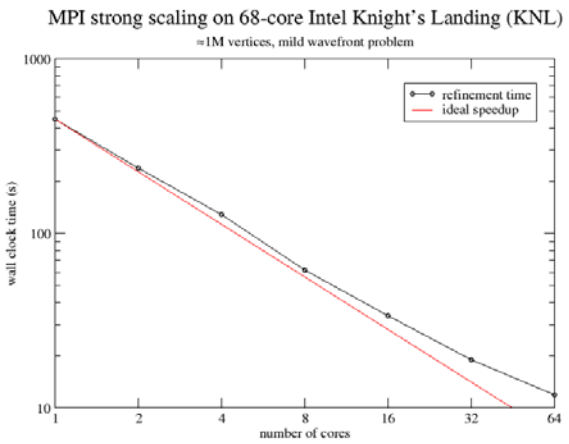

Figure 19. *Strong scaling of adaptive refinement in PHAML on a 68-core Intel Knight's Landing computer.*

SEM Modeling. We are also collaborating with J. Villarrubia to apply PHAML to the modeling of scanning electron microscope (SEM) images of samples containing a mixture of conducting and insulating regions. Villarrubia has a code, JMONSEL, that models electron scattering in materials, secondary electron production, and detection. We have coupled this code with PHAML, which performs the finite element analysis to determine the electric fields that affect the image.

We developed a new *a posteriori* error estimator suited to SEM simulations. The idea is to design an estimate that minimizes the error in the deflection of the electron path rather than minimizing some norm of the electric potential. We performed experiments [1] to compare the performance of the adaptive meshes from the new error estimator with those from a standard error estimator and with the fixed graded meshes currently used. For this experiment we used a simulation with 10 500 randomly placed point charges in a parallelepiped within a layer of conducting material below the vacuum

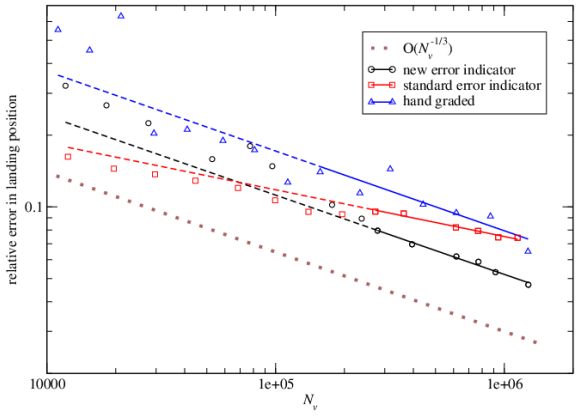

Figure 20. *Comparison of the error as a function of mesh size for adaptive refinement with the new error indicator and standard error indicator, and for the hand graded mesh.*

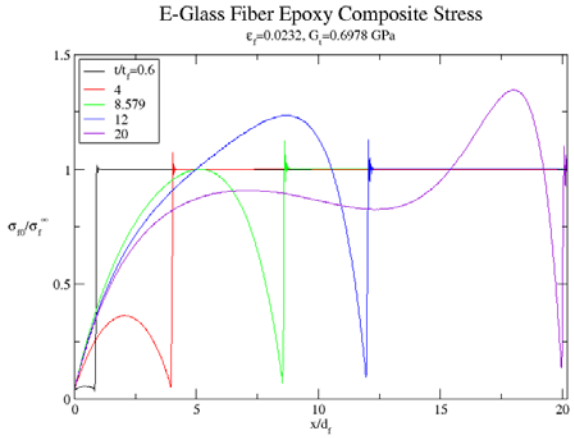

Figure 21. *Propagation of the stress down the length of a fractured fiber, shown at five points in time during the simulation.*

for which an exact solution is known. This allows us to compute an error metric based on the trajectories of a collection of electrons using the computed electric field compared to using the exact electric field. The metric is the error in the landing position of an electron that escapes into the vacuum and returns to the surface. We used a collection of 273 electrons with different random initial positions and velocities and compute the average of the errors in landing position as the error metric. The graph in Figure 20 shows the error as a function of the number of vertices, N_v, in the mesh. We expected to see $O(h)$ convergence, the slope of which is indicated by the dotted brown line. The new error estimate exhibits near-perfect $O(h)$ convergence. The hand graded mesh is also close to $O(h)$ but with a larger constant and requires 3.5 times as many vertices to achieve a given error tolerance. The standard error estimate fails to achieve $O(h)$ convergence, which is not surprising since it is designed to optimize a different error metric.

In other work on this project, we implemented a charge flow model to extend Villarrubia's simulation capabilities. When a sample becomes sufficiently charged by the electron microscope, electrons will flow due to their mutual repulsion. This is modeled by an ordinary differential equation for the charge, which is coupled with the partial differential equation for the electric field. Villarrubia will continue to use PHAML with JMONSEL for his SEM modeling research.

Modeling of Fiber Fracture in Composites. In a new effort this year, we are collaborating with G. Holmes to solve the equations of a fiber fracture model in composite materials. The model involves a hyperbolic differential equation that gives the displacement and stress of a fiber undergoing fracture due to stresses applied to the composite material. For a model of a single fiber, this is a 1D time-dependent problem giving the propagation of the displacement and stress. We determined that PDECOL from Netlib was an appropriate program to use for this equation and implemented a solution of this model using PDECOL. The computational results in Figure 21 agree very well with their experimental results [2] and confirm their theories. Future work will extend the model to 2D where the stresses are propagated through the background material of the composite to determine if those stresses cause other fibers to fracture resulting in material failure. This work will be continued by J. Kauffman.

[1] W. F. Mitchell and J. S. Villarrubia. An *A Posteriori* Error Estimate for Scanning Electron Microscope Simulation with Adaptive Mesh Refinement. Submitted.

[2] J. W. Woodcock, R. Sheridan, R. Beams, S. J. Stranick, W. F. Mitchell, L. C. Brinson, V. Gudapati, D. Hartman, A. Vaidya, J. W. Gilman, and G. A. Holmes. Damage Sensing Using a Mechanophore Crosslinked Epoxy Resin in Single-fiber Composites. Submitted.

[3] NIST Adaptive Mesh Refinement Benchmark Problems. URL: http://math.nist.gov/amr-benchmark

A Thousand-Fold Performance Leap in Ultrasensitive Cryogenic Detectors

Bradley Alpert
Joel Ullom, et al. (NIST PML)
Lawrence Hudson, et al. (NIST PML)
Terrence Jach (NIST MML)

Small arrays of cryogenic microcalorimeters developed at NIST have driven breakthroughs in x-ray materials analysis, nuclear forensics, and astrophysics. From the sharp change in resistance near their critical temperature for superconductivity, these transition-edge sensors (TES) enable exquisite energy resolution and high detection efficiency over a broad energy band. They have also played a large role in prominent international science collaborations in recent years. Despite these

successes, existing cryogenic sensor technology is inadequate for new applications such as in-line industrial materials analysis, energy resolved x-ray imaging, and next-generation astrophysics experiments, which all require faster sensors, much larger arrays, or both.

Four years ago, NIST initiated an Innovations in Measurement Science (IMS) project whose goal was a 1000-fold increase in sensor throughput, to be accomplished via a completely new sensor readout (a microwave multiplexer) enabling much larger detector arrays, and through major new, higher throughput, processing capabilities. The success of this project, especially the microwave multiplexing, has led to additional NIST funding for evaluating the feasibility of new quantum-noise-limited amplifiers and to additional interest in outside collaborations.

These collaborations include one with BAE Systems, funded by IARPA, for x-ray tomographic imaging of the internal structure of microcircuits at 20 nm resolution; with the SLAC National Accelerator Laboratory, funded by DOE, for development of a spectrometer for an upgrade of the LINAC Coherent Light Source (LCLS-II), an ultra-fast, ultra-bright free electron laser; and with the HOLMES team led at the Italian National Institute for Nuclear Physics (INFN) and University of Milan, funded by the European Research Council (ERC), for measurement of neutrino mass. Each of these efforts requires TES microcalorimeter detector arrays operated at higher photon rates than previously achieved, with the LCLS-II collaboration also stipulating better energy resolution than ever achieved with TES detectors.

A side effect of higher photon arrival rates on an array of detectors, which share multiplexed readout channels, is increased risk of crosstalk. The new microwave multiplexing technology is designed to minimize this effect but does not eliminate it entirely. This year Alpert created an initial simulation to evaluate the degradation in energy resolution due to crosstalk, particularly for LCLS-II. This source of uncertainty is projected to be more significant than previously hoped. Alpert plans to further extend this simulation capability.

Sensor nonlinearity at high photon arrival rates remains a significant data analysis challenge, despite prior and continuing analysis efforts. This year B. Alpert introduced a new method for processing data collected at rates anticipated for LCLS-II and other collaborations. Evaluation of the method on data collected with newly-acquired pulsed soft x-ray sources and new detector designs, both for the LCLS-II project, is anticipated in the next few months. In addition to detector nonlinearity at these rates, an important hurdle is the lack of visibility of the detector baseline response and the associated difficulty of characterizing system drift. Related project work on calibration curves and spectrum analysis methods have led to improved energy resolution and decreased uncertainty of positions and shapes of fluorescence lines of certain lanthanide metals and demonstration of potential for standard reference data based on microcalorimeter measurements. These capabilities will remain in focus for the near term.

[1] A. Nucciotti, B. Alpert, M. Balata, D. Becker, D. Bennett, A. Bevilacqua, M. Biasotti, V. Ceriale, G. Ceruti, D. Corsini, M. De Gerone, R. Dressler, M. Faverzani, E. Ferri, J. Fowler, G. Gallucci, J. Gard, F. Gatti, A. Giachero, J. Hays-Wehle, S. Heinitz, G. Hilton, U. Köster, M. Lusignoli, J. Mates, S. Nisi, A. Orlando, L. Parodi, G. Pessina, A. Puiu, S. Ragazzi, C. Reintsema, M. Ribeiro-Gomez, D. Schmidt, D. Schuman, F. Siccardi, D. Swetz, J. Ullom, and L. Vale. Status of the HOLMES Experiment to Directly Measure the Neutrino Mass. *Journal of Low Temperature Physics* **193**:5-6 (2018), 1137-1145. DOI:10.1007/s10909-018-2025-x

[2] D. Li, B. K. Alpert, D. T. Becker, D. A. Bennett, G. A. Carini, H.-M. Cho, W. B. Doriese, J. E. Dusatko, J. W. Fowler, J. C. Frisch, J. D. Gard, S. Guillet, G. C. Hilton, M. R. Holmes, K. D. Irwin, V. Kotsubo, S.-J. Lee, J. A. B. Mates, K. M. Morgan, K. Nakahara, C. G. Pappas, C. D. Reintsema, D. R. Schmidt, S. R. Smith, D. S. Swetz, J. B. Thayer, C. J. Titus, J. N. Ullom, L. R. Vale, D. D. Van Winkle, A. Wessels, and L. Zhang. TES X-ray Spectrometer at SLAC LCLS-II. *Journal of Low Temperature Physics* **193**:5-6 (2018), 1287-1297. DOI: 10.1007/s10909-018-2053-6

[3] W. B. Doriese, P. Abbamonte, B. K. Alpert, D. A. Bennett, E. V. Denison, Y. Fang, D. A. Fischer, C. P. Fitzgerald, J. W. Fowler, J. D. Gard, J. P. Hays-Wehle, G. C. Hilton, C. Jaye, J. L. McChesney, L. Miaja-Avila, K. M. Morgan, Y. I. Joe, G. C. O'Neil, C. D. Reintsema, F. Rodolakis, D. R. Schmidt, H. Tatsuno, J. Uhlig, L. R. Vale, J. N. Ullom, and D. S. Swetz. A Practical Superconducting-Microcalorimeter X-Ray Spectrometer for Beamline and Laboratory Science. *Review of Scientific Instruments* 88 (2017), 053108. DOI: 10.1063/1.4983316

[4] J. W. Fowler, C. G. Pappas, B. K. Alpert, W. B. Doriese, G. C. O'Neil, J. N. Ullom, and D. S. Swetz. Approaches to the Optimal Nonlinear Analysis of Microcalorimeter Pulses. *Journal of Low Temperature Physics* 193:3-4 (2018), 539-546. DOI: 10.1007/s10909-018-1892-5

[5] J. W. Fowler, B. K. Alpert, W. B. Doriese, G. C. Hilton, L. T. Hudson, T. Jach, Y.-I. Joe, K. M. Morgan, G. C. O'Neil, C. D. Reintsema, D. R. Schmidt, D. S. Swetz, C. Szabo-Foster, and J. N. Ullom. A Reassessment of Absolute X-ray Line Energies for Lanthanide Metals. *Metrologia* 54:4 (2017), 494-511. DOI: 10.1088/1681-7575/aa722f

The Role of Data Analysis in Metrology of DNA

Paul Patrone
Anthony Kearsley
Jacob Majikes (NIST PML)
Alex Liddle (NIST PML)

Despite being the building block of life, little is known about the fundamental physical properties of DNA that characterize its behavior *in vivo*. For example, its local cellular environment is essentially a thermodynamic system at constant temperature; yet it is exceedingly difficult to measure the entropy of DNA. Likewise, the kinetic rates associated with molecular binding events (e.g., which "extract information" from DNA) are difficult to probe with any accuracy.

Conceptually, these problems arise from the fact that it is virtually impossible to ensure that experimental conditions are repeatable. In more detail, large DNA samples are cost-prohibitive. As a result, reaction volumes, which involve as many as several hundred different reagents, are limited to microliters or less. Given pipetting errors associated with combining these ingredients, it is inevitable that each realization of a system will vary enough to produce appreciable differences in measurement signals; see Figure 22 (top). Thus, the biology community has come to realize that (i) *absolute* comparison between DNA experiments is often meaningless, and (ii) advanced data analysis techniques are critical for making sense of raw data. Despite this recognition, there has been little engagement with the mathematics community, and many open questions remain regarding best practices for analyzing DNA data.

To address these issues, ACMD staff have been collaborating with scientists in PML to understand fluorescence data associated with folding of DNA rings. Simplistically, the fraction F of unfolded rings should increase with temperature T, although the precise relationship between these quantities is unknown. Using fluorescent markers that only emit light when the strand is unfolded, it should be possible to measure $F(T)$. From this, many other thermodynamic properties of the DNA can be deduced. However, as illustrated in Figure 22 (top), variations in DNA concentrations between samples lead to $O(1)$ variations in fluorescence signals. By eye it is not even clear that one can average this data in a meaningful way to attain a "mean" behavior of the system.

Conceptually, however, a key simplification emerges when we recognize that the same physical processes generate the signals from each sample. This implies that differences between signals in Figure 22 (top) should arise from variations in concentration;

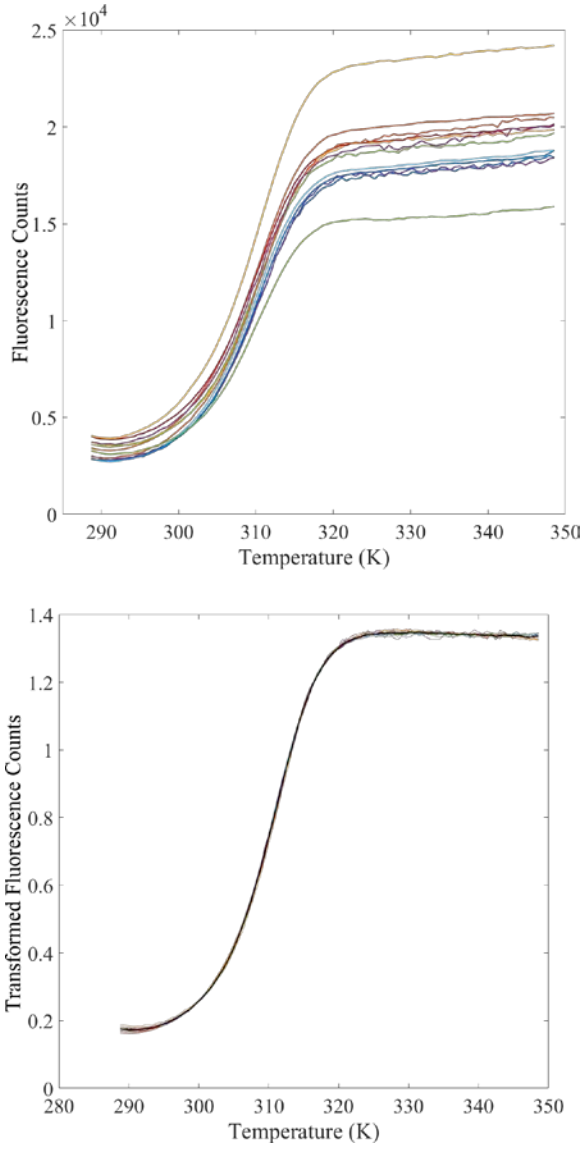

Figure 22. *(Top) Raw fluorescence counts as a function of temperature for a DNA ring sample as a function of temperature. In principle, each sample is prepared identically, although variation between the curves is O(1). (Bottom) After minimizing a regularized version of our objective function, we transform the twelve fluorescence curves on top of one another. The remarkable degree of data collapse suggests that concentration-dependent effects are solely responsible for differences between the curves in the top figure.*

mathematically each dataset should be related by an unknown affine transformation. This motivates us to postulate a model of the form

$$f_i(T) = \hat{a}_i F(T) R(T) + \hat{b}_i B(T) + \hat{c}_i$$

where $f_i(T)$ is the *measured* fluorescence signal associated with the ith sample, $F(T)$ is the true underlying fluorescence signal (proportional to unfolded DNA) normalized to unity, $R(T)$ is the fluorescence rate of the fluorophores, $B(T)$ is a background signal as a function

of temperature, and $\hat{a}_i, \hat{b}_i$, and $\hat{c}_i$ are concentration-dependent coefficients that are unknown. To determine these, assume N datasets and invert the above expression for $F(T)$ in terms of $f_i(T)$. As $F(T)$ thus expressed is (in principle) sample independent, we construct the objective function

$$L^{(F)} = \sum_{i,j,T} \left[a_i \frac{f_i(T)}{R(T)} + b_i \frac{B(T)}{R(T)} + \frac{c_i}{R(T)} - a_j \frac{f_j(T)}{R(T)} - b_j \frac{B(T)}{R(T)} - \frac{c_j}{R(T)} \right]^2$$

between all $\binom{N}{2}$ datasets, where the a_i, b_i, c_i are to be determined. Note that $L = 0$ should hold if there is a set of these parameters for which this equation holds exactly for all datasets. Regularization and constrained optimization techniques can also be invoked if more information is known about the behavior of the datasets.

The bottom of Figure 22 shows an example of such optimization applied to the datasets in the top subplot. Note that after transformation, the difference between each dataset is less than 1% relative to the maximum scale of the data. This suggests the above equation is a valid approximation of the data and allows us to perform subsequent downstream analysis on the $F(T)$ curves. This analysis and related extensions are currently being prepared in a series of manuscripts, which we anticipate submitting in FY 2019. Further work aims to extend these techniques to other fluorescence-based measurements for DNA systems.

Metrology for Microfluidics

Paul Patrone
Anthony Kearsley
Gregory Cooksey (NIST PML)

Advances in microfluidics promise to fundamentally change the way many scientific disciplines operate by enabling precise control over the motion of fluids and solutes in micron-scale systems. For example, microfluidic fabrication techniques allow chemical reaction vessels to be reduced to the size of a human hair, parallelized, and subsequently interconnected. This facilitates high-throughput experimentation and combinatorial testing; see Figure 23. Moreover, the medical community has recognized that related approaches can, *in principle*, enable rapid and simultaneous screening of hundreds of diseases with only a few drops of blood. Indeed, the lure of disrupting this $50 billion blood-testing industry has led to significant venture capital investments in high-profile startups that specialize in microfluidics for lab-on-a-chip applications. Despite the

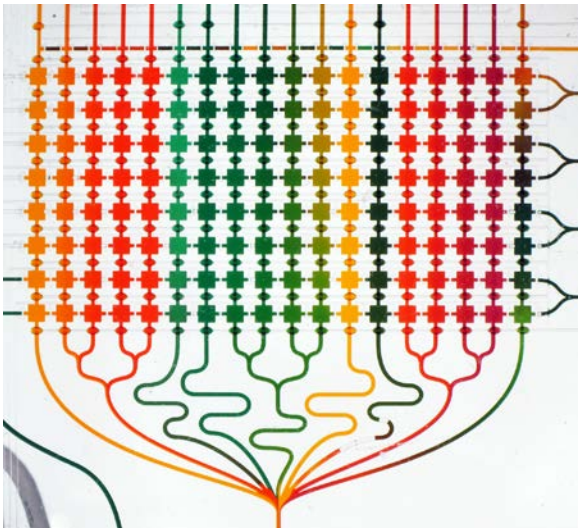

Figure 23. *Example of a microfluidic device used to establish concentration gradients. Fluid of different colors flows through the input channels (bottom) and enters the mixing chambers (squares). Because the flow is laminar, diffusion is the only mechanism responsible for mixing. In this way it is possible to precisely control concentrations of reactants in combinatorial testing assays.*

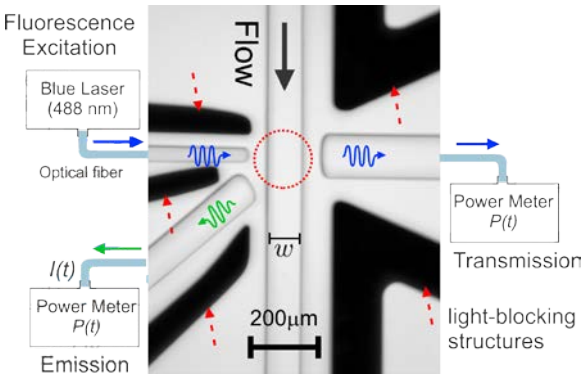

Figure 24. *Microscopic view of our device.*

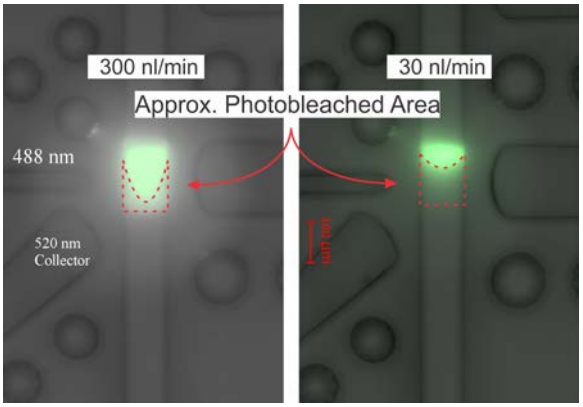

Figure 25. *Our device in operation. At lower flow rates, more of the fluorophores are destroyed. Mathematically, the fluorescence efficiency is a monotone increasing function of flow rate, which forms the basis for our measurement technique.*

promise, few commercial implementations of such devices have emerged, leading the community to reflect on the fundamental measurement challenges that have stalled progress.

Perhaps the most important quantity of interest in microfluidic systems is the volumetric flow rate v_v. The ability to fix the relative ratios of reactants, determine reaction rates, and measure other time-dependent phenomena all require control and knowledge of v_v. Despite this, there are no *in-situ* and continuous approaches for accurately measuring flow rate, especially at the nanoliter per minute scale of interest to the community. Moreover, existing techniques are not compatible with cell-based systems necessary for biomolecular applications. Thus, fundamental measurement capability enabling precise control over all microfluidic systems is needed.

To address this problem, ACMD and PML staff have developed a novel, precise technique for measuring v_v down to the scale of 1 nL/min. Our device is comprised of: (*i*) a laser beam that illuminates a small swath of a microfluidic channel; (*ii*) biocompatible fluorophores that emit light and photobleach (irreversibly decay) in the presence of the laser; and (*iii*) a collector that measures the quantity of fluorescent light emitted from the illumination region (see Figure 24.) The device is described by a system of non-linear integro-differential equations of the form

$$c_z = -g(\xi)B(c,\mathbf{r})$$
$$I = p\int d\mathbf{r}\ F(c,\mathbf{r})$$

where c is the concentration of fluorophores, z is the variable in the direction of flow, $B(c)$ is a non-linear, nonlocal function of concentration that accounts for photobleaching, I is the intensity of collected fluorescence light, and $F(c,\mathbf{r})$ is a non-linear function of c accounting for the rate of fluorescence. *Critically,* the precise functional forms of B and F, as well as the system geometry, are unknown. Thus, any measurement of v_v must rely on generic properties of c and I.

Key ideas from mathematical analysis and advanced metrology are employed to resolve this situation: a successful measurement is a bijection from a measurand (e.g., I) to the quantity of interest (v_v). Observing that B and F are positive and monotone increasing in c (i.e., fluorescence and bleaching increase with concentration), we have been able to prove that the fluorescence efficiency $I/p = \hat{I}(\xi)$ is a strictly monotone decreasing function of the dosage $\xi = f(p)/\,v_v$, where $f(p)$ is a (known) function of the laser power p, which yields the desired bijection for fixed laser power (see Figure 25).

To calibrate our device, we use an independent flowmeter to measure v_v at the lower limit of the latter's range (which is still far above our scales of interest). By varying the laser power, we map out the bijection $\hat{I}(\xi)$. All subsequent measurements are performed by decreasing the laser power and measuring $\hat{I}$ for some other (lower) flow rate. Knowledge of p and $\hat{I}$ is then sufficient to determine v_v. *Amazingly, this measurement can be performed without ever needing to know the system geometry, flow profile, or physics of bleaching a fluorescence.* We have further shown that our device preserves the *relative error* of the calibration flowmeter, yielding uncertainties on the order of 5 % or less at the 10 nL/min scale for a prototype device. This feat has yet to be matched by any other research group.

Serendipitously, the need to validate our measurement technique led to a second discovery: our device can operate in a second, independent mode to accurately measure zero flow rate. Specifically, the steady-state fluorescence intensity reaches a minimum when the flow stops because all of fluorophores photobleach. *Using this to calibrate a gravimetric-based flow controller, we can set v_v to within 0.2 nL/min down to zero flow, which has never before been achieved.* Comparison between the flow controller and our flow meter is within 5%, indicating a profound consistency between these methods. These first-of-a kind feats have been described in several publications in print and under review [1-3] and have generated a patent application that is pending.

[1] G. A. Cooksey, P. N. Patrone, J. R. Hands, S. E. Meek, and A. J. Kearsley. Dynamic Measurement of Nanoliter Per Minute Flow by Scaled Dosage of Fluorescent Solutions. In *Proceedings of the 22nd International Conference on Miniaturized Systems for Chemistry and Life Sciences (MicroTAS)*, Kaohsiung, Taiwan, November 11-15, 2018, 742-745.

[2] P. N. Patrone, G. A. Cooksey, and A. J. Kearsley. Dynamics Measurement of Nanoflows: Analysis and Theory of an Optofluidic Flowmeter. Under review.

[3] G. A. Cooksey, P. N. Patrone, J. R. Hands, S. E. Meek, and A. J. Kearsley. Dynamics and Measurement of Nanoflows: Realization of an Optofluidic Flow Meter to the Nanoliter Per Minute Scale. Under review.

Classifying Chemical Measurements for Inter-Laboratory Studies

Anthony Kearsley
Ryan M. Evans
John Marino (UMD/NIST IBBR)
Frank Delaglio (UMD/NIST IBBR)
Luke Arbogast (UMD/NIST IBBR)
Robert Brinson (UMD/NIST IBBR)
John Schiel (UMD/NIST IBBR)
Trina Mouchahoir (UMD/NIST IBBR)

Nuclear magnetic resonance (NMR) spectroscopy and mass spectrometry are foundational tools of analytical chemistry and have far-reaching applications. Mass

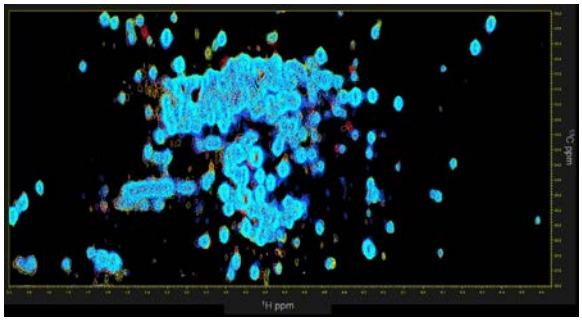

Figure 26. *Multiple overlay of NMR spectra.*

spectrometry is currently being used to identify illicit drug compounds, and two-dimensional NMR has recently emerged as a tool for characterizing monoclonal antibodies [1-3], biologically-based therapeutics derived from proteins that are used to treat a wide number of diseases ranging from rheumatoid arthritis to certain kinds of cancer. Analysis of NMR or mass spectra typically requires an expert and is commonly done through visual inspection. For example, consider a set of two-dimensional NMR spectra of monoclonal antibodies (see Figure 26). Since NMR spectra encapsulate a type of chemical *signature*, scientists are interested in comparing NMR spectra with a known reference to establish safety and efficacy. This is crucial in industrial settings to evaluate heterogeneity arising from manufacturing process modifications. Though expert feedback can be invaluable, visual inspection is ultimately subjective and error prone, especially when analyzing hundreds of spectra. Thus, quantitative analysis of NMR spectroscopy and mass spectrometry data is of fundamental importance.

The Institute for Bioscience and Biotechnology Research (IBBR) is the home to a research group, led by J. Marino, that seeks to improve accuracy and robustness of two-dimensional NMR spectroscopy for characterizing monoclonal antibodies. This project recently conducted a benchmark international inter-laboratory study in which scientists from twenty-six different laboratories in nine different countries spanning five continents. This large research group performed a variety of NMR experiments on samples derived from the NISTmAb, a monoclonal antibody developed by NIST that has become a standard reference material (SRM 8671). Hundreds of spectra were acquired under numerous experimental conditions, by varying factors such as sample type, instrument manufacturer, magnet strength, and temperature. Spectral information was concisely summarized in the form of *peak tables*, which consist of a weighted l_2 norm of significant peak locations for each spectrum. By applying principle component analysis (PCA) and the unweighted pair group method with arithmetic mean (UPGMA) to a set of peak tables, it was demonstrated that it is possible to accurately and reliably detect sample type and temperature of spectra from this study (see Figure 27). It was confirmed that differences resulting from variations in sample type and temperature are minor, and that two-dimensional NMR can characterize the NISTmAb across a wide variety of experimental conditions in a highly repeatable and reproducible manner [4]. These results move the 2D NMR method from an emerging technology to a harmonized, routine measurement that can be generally applied with great confidence to high precision assessments of the structure of a wide-array of protein therapeutics.

A second arm of this research project involved mass spectrometry, which can be used as a complementary tool for characterizing monoclonal antibodies. When using mass spectrometry to analyze these life-saving therapies, it is of critical importance to establish validity of a given method, i.e., it must be repeatable and reproducible to within high precision. This notion is also known as *system suitability*. J. Schiel and T. Mouchahoir are currently spearheading a novel inter-laboratory study at the IBBR to establish the significance of system suitability in the context of mass spectrometry experiments that involve monoclonal antibodies. This

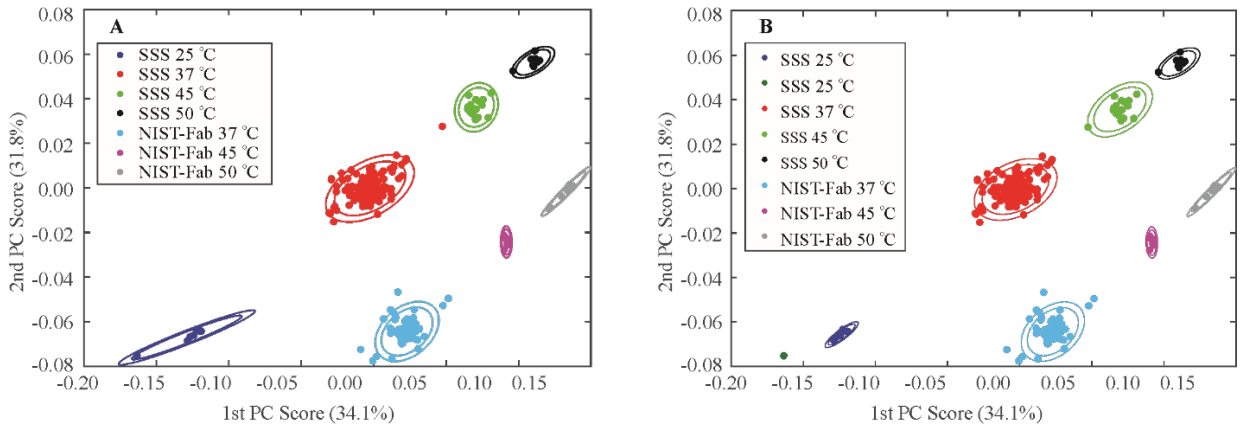

Figure 27. *Left: manual classification of peak tables of NMR spectra according to sample type and temperature in principle component space. Right: classification of NMR spectra in principle component space using UPGMA. Observe that the two figures are nearly identical.*

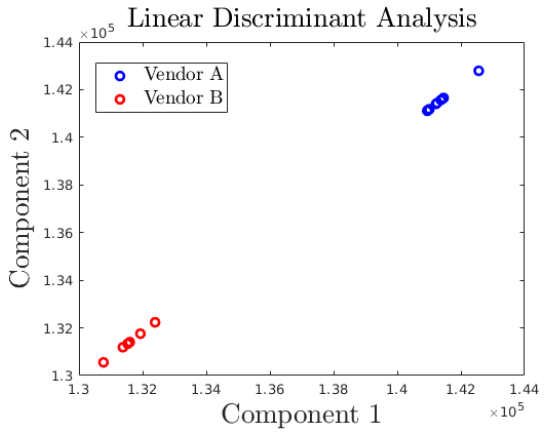

Figure 28. *Classification of mass spectra according to vendor.*

study is comprised of fifteen participants from different laboratories each of whom has performed a mass spectrometry experiment on a monoclonal antibody. Using linear discriminant analysis (LDA), we have shown that it is possible to partition each spectrum according to vendor of the instrument with which it was measured (see Figure 28). This preliminary finding shows that we can effectively classify participants according to certain attributes. Future work will investigate the classification of participants according to attributes. Of interest is the possibility of separating spectra into distinct classes: those deemed to be well-measured and reproducible, and those that are not. Quantitative analysis is expected to play an integral role in establishing the significance of system suitability of mass spectrometry experiments involving monoclonal antibodies.

[1] Y. Aubin, G. Gingras, and S. Sauvé. Assessment of the Three-Dimensional Structure of Recombinant Protein Therapeutics by NMR Fingerprinting: Demonstration on Recombinant Human Granulocyte Macrophage-Colony Stimulation Factor. *Analytical Chemistry* **80**:7 (2008), 2623-2627.

[2] L. W. Arbogast, R. G. Brinson, and J. P. Marino. Mapping Monoclonal Antibody Structure by 2D 13C NMR at Natural Abundance. *Analytical Chemistry* **87**:7 (2015), 3556-3561.

[3] R. Kiss, Á. Fizil, and C. Szántay Jr. What NMR Can Do in the Biopharmaceutical Industry. *Journal of Pharmaceutical and Biomedical Analysis* **147** (2018), 367-377.

[4] R. G. Brinson, J. P. Marino, F. Delaglio, L. W. Arbogast, R. M. Evans, A. Kearsley, G. Gingras, H. Ghasriani, Y. Aubin, G. K. Pierens, X. Jia, M. Mobli, H. G. Grant, D. W. Keizer, K. Schweimer, J. Ståhle, G. Widmalm, E. R. Zartler, C. W. Lawrence, P. N. Reardon, J. R. Cort, P. Xu, F. Ni, S. Yanaka, K. Kato, S. R. Parnham, D. Tsao, A. Blomgren, T. Rundlöf, N. Trieloff, P. Schmieder, A. Ross, K. Skidmore, K. Chen, D. Keire, D. I. Freedberg, T. Suter-Stahel, G. Wider, G. Ilc, J. Plavec, S. A. Bradley, D. M. Baldisseri, M. L. Sforça, A. Carolina de Mattos Zeri, J. Y. Wei, C. M. Szabo, C. A. Amezcua, J. B. Jordan, and M. Wikström. Enabling Adoption of 2D-NMR for the Higher Order Structure Assessment of Monoclonal Antibody Therapeutics. *mAbs* **11**:1 (2019), 94-105.

Improved Match Factors for Illicit Drug Identification and Classification

Anthony J. Kearsley
Brian Cooper (UNC Charlotte)
Gary Mallard (NIST MML)
Arun Moorthy (NIST MML)
Stephen E. Stein (NIST MML)
Dmitri Tchekhovskoi (NIST MML)
William E. Wallace (NIST MML)

The identification of illicit drugs is a problem that has posed an enormous obstacle to the forensics science community. The development of classification methods that can appropriately categorize drugs and their analogs is a pressing need. Given an unknown compound, forensic scientists will often want to search the NIST Mass Spectrometry database in hopes of class identification for the unknown compound. A few years ago, NIST developed a so-called “hybrid search” [1] for exactly this purpose. Hybrid search seeks to compute inter-spectral similarity differently than the traditional search developed many years ago when the library of compounds was significantly smaller [2, 3]. Recently an investigation of novel multi-objective schemes for agglomerative hierarchical clustering of these important compounds has yielded interesting results. These groupings, or clusters, can be employed to compute confidence and uncertainty levels of a class identification. Hybrid search considers fragment-ion and neutral-loss matches

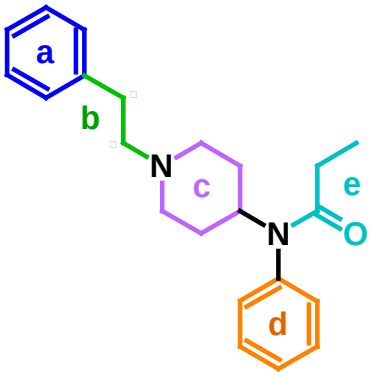

Figure 29. *Molecular structure of Fentanyl with potential sites for modification.*

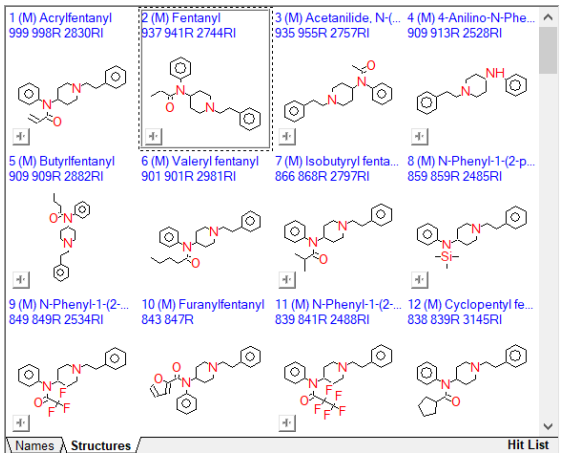

Figure 31. *Fentanyl being identified as top hit #2 using the hybrid match factor.*

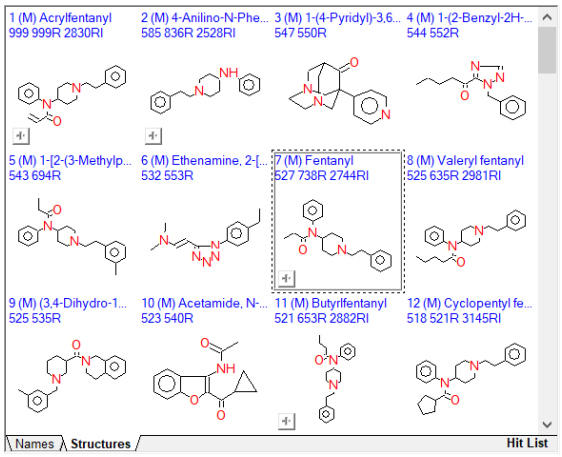

Figure 32. *Fentanyl being identified as top hit #7 using the simple match factor.*

when computing spectral similarity. An analyte compound is first searched against a library to generate a preliminary hit-list. An important example is the compound Fentanyl (Figure 29), the identification of which is a growing problem in law-enforcement. One can see that hybrid search (Figure 31) is far better at identification inside MS search than the traditional search method (Figure 32).

In addition to using MS spectra to identify unknown compounds, the underlying modified dot-product calculation can be used to generate an inter-object dissimilarity matrix from the spectra in the preliminary hit-list. This, in turn, can be clustered using our novel multi-objective agglomerative-hierarchical clustering algorithm. The result of this procedure is a dendrogram from which the likely classification of the analyte can be determined, and the uncertainty of this determination can be quantified.

To illustrate this, Figure 30 demonstrates clustering of a sub-library of 22 compounds chosen from the SWG Drug Library for assessment. It contained spectra for five analogs each of JWH-167, Fentanyl, MDMA and Cathinone, and two additional spectra of "unknown" compounds. The results of a preliminary implementation of the multi-objective classification method was able to classify the first unknown as a Fentanyl analog with a certainty of ≈56 % (uncertainty of 44 %) and as a Fentanyl or JWH-167 or cathinone analog with ≈93 % certainty. The second unknown was only classifiable as a Fentanyl or MDMA or cathinone analog, but with 99 % uncertainty. This discrepancy is due to the "spectral space" between Fentanyl analogs being tight, whereas the dissimilarity between MDMA spectra is more substantial. For comparison, the same multi-objective classification method was implemented using the traditional dot product rather than the "hybrid" dot product. The first unknown was classified as a Fentanyl or MDMA or Cathinone analog with 95 % certainty, but without further classification. These results are further evidence that the hybrid dot product better captures spectral similarity between structurally similar compounds.

[1] A. S. Moorthy, W. E. Wallace, A. J. Kearsley, D. V. Tchekhovskoi, and S. E. Stein. Combining Fragment-Ion and Neutral-Loss Matching during Mass Spectral Library Searching: A New General Purpose Algorithm Applicable to Illicit Drug Identification. *Analytical Chemistry* **89**:24 (November 20, 2017), 13261-13268.

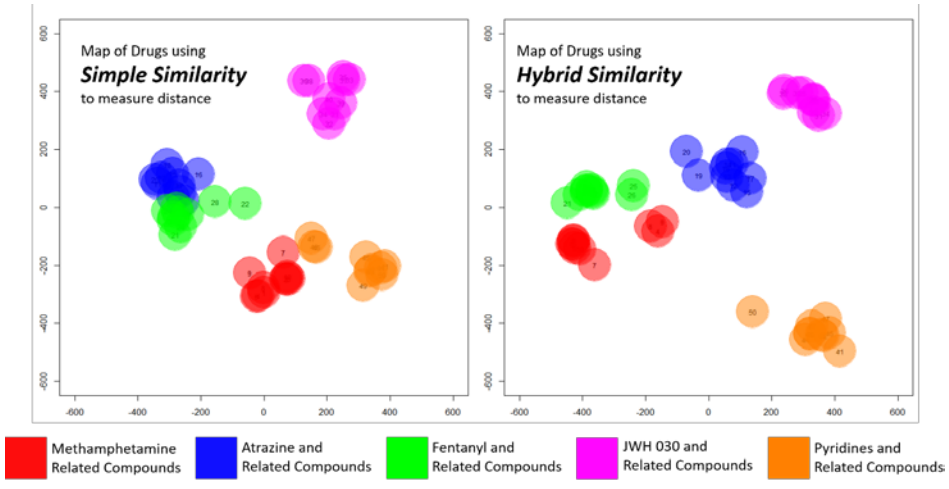

Figure 30. *Clustering of a sub-library of 22 compounds chosen from the SWG Drug Library using alternate metrics.*

[2] S. E. Stein. Estimating Probabilities of Correct Identification from Results of Mass Spectral Library Searches. *Journal of the American Society for Mass Spectrometry* **5** (1994), 316-318.

[3] S. E. Stein and D. R. Scott. Optimization and Testing of Mass Spectral Library Search Algorithms for Compound Identification. *Journal of the American Society for Mass Spectrometry* 5 (1994), 859-866.

Modeling for Biological Field Effect Transistor Measurements

Ryan M. Evans
Anthony Kearsley
Arvind Balijepalli (NIST PML)

The ability to tailor therapies to individuals or specific subsets of a population to deliver personalized care has the potential to fundamentally improve healthcare delivery. The most promising therapeutic candidates for such targeted care are new classes of biologic drugs based on naturally occurring molecules, made possible due to rapid advances in genomics and proteomics [1]. Importantly, such therapies can be safer and yield better outcomes at lower doses when treating debilitating conditions such as diabetes, Alzheimer's disease, or certain cancers [2]. Unfortunately, widespread use of personalized care is currently limited by our ability to routinely measure pathology in individuals, including biomarkers, metabolites, tissue histology, and gene expression. Moreover, existing clinical diagnostics are cumbersome, require specialized facilities, can take days to weeks to perform, and are in many cases prohibitively expensive.

This has led to the development of new portable detection tools, including antibody-based lateral flow assays [3], microelectromechanical sensor (MEMS) based resonators that can detect binding of biomarkers to the sensor surface [4], surface plasmon resonance [5], ring cavity resonators [6] and electronic measurements with biological field effect transistors (Bio-FETs) [7, 9]. The latter are particularly well-suited for biomarker measurements due their high charge sensitivity and direct signal transduction, allowing label-free measurements at physiological concentrations. Furthermore, by leveraging semiconductor processing techniques, measurements with FETs can be made massively parallel, cost-effective, and portable.

A Bio-FET is a three-terminal device as represented in Figure 33. A semiconductor channel between the source and drain terminals conducts a current that is strongly modulated by an electrostatic potential applied to the gate. Biomarkers in aqueous solution exhibit a well-defined electrostatic surface potential [10] arising from charged hydrophilic residues that interact with water. When these molecules adsorb to the Bio-FET

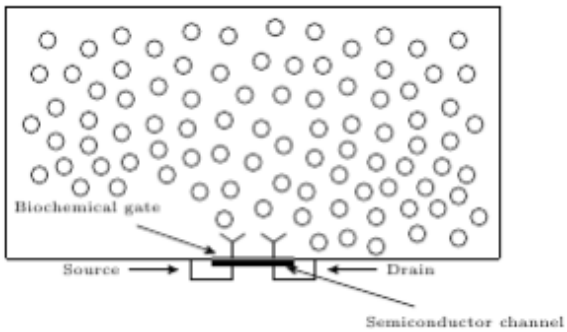

Figure 33. *Schematic of a Bio-FET experiment.*

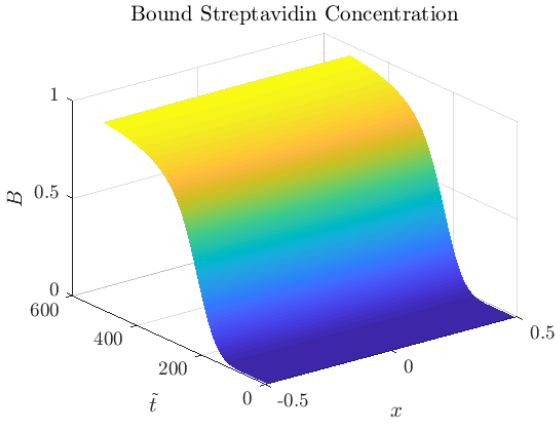

Figure 34. *Space-time curve of reacting species concentration. Here x represents space and t represents dimensional time.*

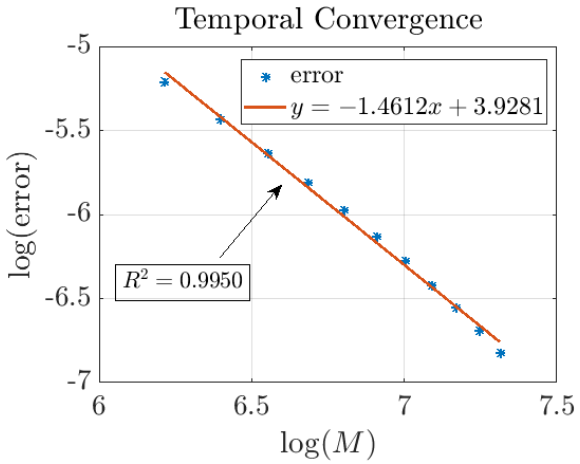

Figure 35. *Error in infinity norm as a function of the number of points in time M.*

biochemical gate, they strongly modulate the channel current proportional to the magnitude of their surface potential. This phenomenon allows Bio-FETs to be used to detect and quantify adsorbed biomarkers in solution. Furthermore, functionalizing the Bio-FET, by attaching molecules to the gate surface that have a high inherent affinity for biomarkers of interest, allows measurements

with high specificity that are tailored to one or more biomarkers of interest.

An accurate time-dependent model of receptor-ligand interactions can be used to identify key parameters associated with Bio-FET experiments, such as kinetic coefficients and diffusion constants. Although Bio-FETs measure the time-dependent change in current, and are thus dynamic experiments in nature, most previous modeling efforts assume a steady distribution of biomolecules on the biochemical gate and focus on characterizing charge transport through the semi-conductor [5, 11, 12]. Such models are useful for elucidating semiconductor physics but cannot utilize time-dependent measurements to estimate parameters associated with Bio-FET experiments. One could ostensibly use steady-state data to estimate binding affinities as Edwards discusses in [13] in the context of surface plasmon resonance biosensor experiments, but this requires multiple experiments to obtain accurate estimates and yields only the ratio of the association and dissociation rate constants. A dynamic model can utilize measured time-series data from a single experiment to estimate not only kinetic coefficients, but also other important parameters such as diffusion coefficients.

A time dependent model for Bio-FET experiments was presented in [1, 14], where the authors quantified the evolution of the reacting species concentration in presence of a continuous and uniform injection of ligand at the top boundary. Recently, Evans, Balijepalli, and Kearsley have developed a mathematical model for a sealed experiment in which a drop of ligand is injected at an instance of time. This model takes the form of a diffusion equation coupled to a nonlinear equation that describes the evolution of the reacting species concentration. Through a Laplace transform and tools from complex analysis, this coupled set of equations has been reduced to a single nonlinear integrodifferential equation (IDE) in terms of the reacting species concentration. Though this equation exhibits a singular convolution kernel that approaches infinity at a rate proportional to $1/\sqrt{t}$ as t approaches 0, a numerical solution to this equation has been developed which achieves greater than first-order accuracy. See Figure 34 for a space-time curve that depicts the numerical IDE solution, and Figure 33 for evidence of convergence at a rate of $O(\Delta t^{1.46})$ in time, despite the singular convolution kernel.

To compare the numerical solution of the IDE with experimental data, stochastic regression was employed to separate signal from noise in Bio-FET measurements [4]. This involved modeling the Bio-FET signal as a stochastic differential equation that has a deterministic term and a stochastic term:

$$X_t = (a_0(t) + a_1(t)X_t)dt + b_0(t)dW_t,$$
$$X_t(0) = 0.$$

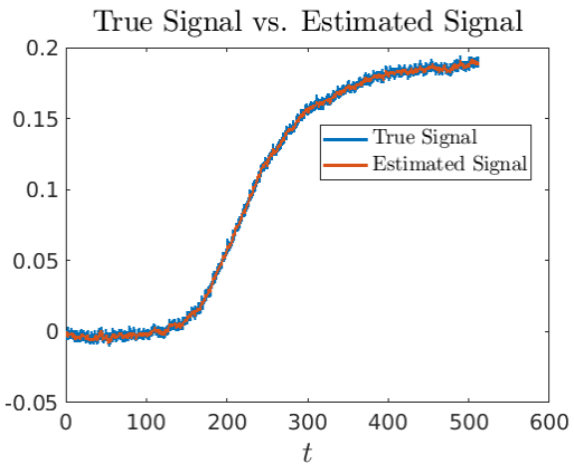

Figure 36. *An overlay of the true and estimated signals.*

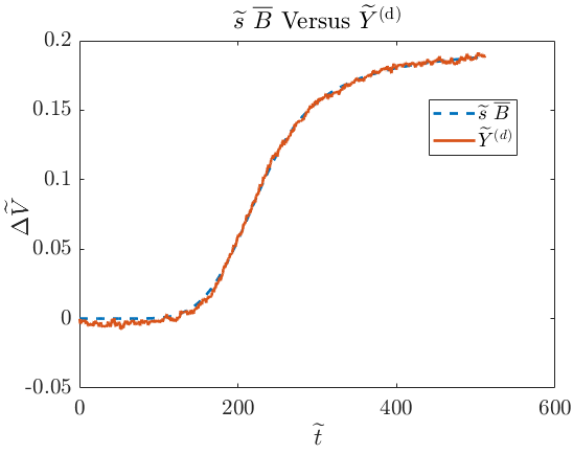

Figure 37. *An overlay of the spatially-averaged solution to our IDE model* $\tilde{\boldsymbol{s}}\overline{\boldsymbol{B}}$ *and the estimated deterministic component of the signal* $\widetilde{\boldsymbol{Y}}^{(\boldsymbol{d})}$. *Here,* $\tilde{\boldsymbol{s}}$ *is a proportionality constant.*

The coefficients $a_0(t), a_1(t)$,and $b_0(t)$were determined using a local weighted regression and maximum likelihood estimation as described in [5]. Figure 36 shows an overlay of the measured signal and the estimated signal $X_t = (a_0(t) + a_1(t)X_t)dt$. Parameters were estimated using a rust region method implemented in lsqnonlin() in MATLAB. Figure 37 shows excellent agreement with experimental data. Future work will explore the estimation of kinetic coefficients associated with more complex physiologically relevant reactions.

[1] K. Fosgerau and T. Hoffmann. Peptide Therapeutics: Current Status and Future Directions. *Drug Discovery Today* **20** (2015), 122-128.

[2] B. K. Binukumar, Y.-L. Zheng, V. Shukla, N. D. Amin, P. Grant, and H. C. Pant. TFP5, a Peptide Derived from P35, a CDK5 Neuronal Activator, Rescues Cortical Neurons from Glucose Toxicity. *Journal of Alzheimer's Disease* **39**:4 (2014), 899909.

[3] P. K. Drain, L. Gounder, F. Sahid, and M.-Y. Moosa. Rapid Urine LAM Testing Improves Diagnosis of Expectorated Smear-Negative Pulmonary Tuberculosis in an HIV-Endemic Region. *Scientific Reports* **6** (2016), 19992.

[4] A. J. Kearsley, Y. Gadhyan, and W. E. Wallace. Stochastic Regression Modeling of Chemical Spectra. *Chemometrics and Intelligent Laboratory Systems* **139** (2014), 26-32.

[5] W. Knoll. Interfaces and Thin Films as Seen by Bound Electromagnetic Waves. *Annual Review of Physical Chemistry* **49**:1 (1998), 569-638.

[6] D. K. Armani, T. J. Kippenberg, S. M. Spillane, and K. J. Vahala. Ultra-high-Q Toroid Microcavity on a Chip. *Nature* **421** (2003), 925-928.

[7] Y. Cui, Q. Wei, H. Park, and C. M. Lieber. Nanowire Nanosensors for Highly Sensitive and Selective Detection of Biological and Chemical Species. *Science* **293** (2001), 1289-1292.

[8] P. Mohanty, Y. Chen, X. Wang, M. K. Hong, C. L. Rosenberg, D. T. Weaver, and S. Erramilli. Field Effect Transistor Nanosensors for Breast Cancer Diagnostics. arXiv:1401.1168 [q-bio.QM], 2014.

[9] F. Pouthas, C. Gentil, D. Cote and U. Bockelmann. DNA Detection on Transistor Arrays Following Mutation-specific Enzymatic Amplification. *Applied Physics Letters* **84**:9 (2004), 1594-1596.

[10] A. Cardone, H. Pant, and S. A. Hassan. Specific and Non-Specific Protein Association in Solution: Computation of Solvent Effects and Prediction of First-Encounter Modes for Efficient Configurational Bias Monte Carlo Simulations. *The Journal of Physical Chemistry B* **117**:41 (2013), 12360-12374.

[11] S. Baumgartner, M. Vasicek, A. Bulyha, N. Tassotti, and C. Heitzinger. Analysis of Field-Effect Biosensors Using Self-Consistent 3D Drift-Diffusion and Monte-Carlo Simulations. *Procedia Engineering* **25** (2011), 40700410.

[12] C. Heitzinger, N. J. Mauser, and C. Ringhofer. Multiscale Modeling of Planar and Nanowire Field-effect Biosensors. *SIAM Journal on Applied Mathematics* **70**:4 (2010), 1635–1654

[13] D. A. Edwards. Estimating Rate Constants in a Convection-Diffusion System with a Boundary Reaction. *SIAM Journal on Applied Mathematics* **8** (1999), 10–14.

[14] R. M. Evans, A. Balijepalli, and A. J. Kearsley. Diffusion-Limited Reaction in Nanoscale Electronics. In review.

Mathematical Modeling of Cryopreservation

Daniel Anderson
James Benson (University of Saskatchewan, Canada)
Anthony J. Kearsley

Cryobiology broadly impacts medicine, agriculture and forensics and is important in the fight to maintain earth's biodiversity. Not surprisingly, there have been a growing interest in the development of mathematical models to explain phenomena, explore potential theories of damage or success, aid in the development of equipment, and refinement of optimal cryopreservation or cryoablation strategies.

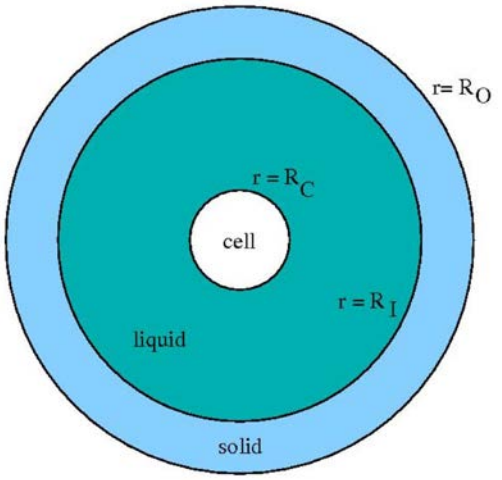

Figure 38. *Spherical cell inside a liquid-solid structure.*

Cryopreservation involves the freezing of cells, tissues, organs and other, typically biological, compounds that are feared to be susceptible to damage caused by chemical kinetics. If correctly performed, cooling to very low temperatures (typically -80 °C using solid carbon dioxide or -196 °C using liquid nitrogen) can prevent damage. Cryoprotocols, strategies used to direct laboratory procedures that cool and warm biospecimens, have a variety of objectives ranging from preserving the viability of a cell as in assisted reproduction, to locally destroying cells or tissue in cryosurgery, to optimally preserving chemical, genetic or proteomic information for archival and/or forensics applications.

Cryopreservation procedures permit cells to be stored indefinitely using extremely cold temperatures to suspend all metabolic activities and therefore preserve the cell and cell function. Loosely speaking, there are two main types of cryopreservation procedures: equilibrium (conventional slow freezing) and non-equilibrium or ultra-rapid freezing (vitrification). Both procedures employ the use of cryoprotectants, chemicals behaving like antifreeze to prevent cellular damage during the freezing process. After proper freezing, cells should be able to be stored for an indefinite amount of time. This can be done, for example, by immersing them in liquid nitrogen, an extremely cold fluid with an approximate temperature of -196 C. Cryoprotectants must be removed later during thawing, when the water balance in the cell can be slowly restored, and normal activity in the cell should return. Procedures exist for the freezing of single cells, tissue comprised of many cells, and even entire organs. Size, amount of cytoplasm (or biofluid),

and structural complexity change the freezing procedures employed. For example, cells with less cytoplasm, like sperm cells, are generally considered to be less difficult to freeze than those cells with more cytoplasm, like eggs. Slow freezing or equilibration has been successfully employed to freeze and store a wide range cells, but research is ongoing to optimize the cryobiology of cells.

Mathematical and computational sciences play a critical role as a means of effectively and efficiently exploring these complex bio-chemical and/or bio-physical systems and their overcrowded parameter spaces [1-3]. Recently we studied the use of optimization techniques [4] to determine or improve the equilibration of cryoprotectant when applied to a spherical cell (Figure 38). We considered the case of cells and tissues with high concentrations of permeating chemicals known as cryoprotective agents, or CPAs. Despite their protective properties, CPAs can cause damage because of osmotically-driven cell volume changes, as well as chemical toxicity. In this study, data was used to determine a toxicity cost function, a quantity that represents the cumulative damage caused by toxicity. We then used this cost function to define and numerically solve the optimal control problem for CPA equilibration, using human oocytes as representative cell type with high clinical relevance. The resulting toxicity-optimal procedures are predicted to yield significantly less toxicity than conventional procedures. Results showed that toxicity is minimized during CPA addition by inducing the cell to swell to its maximum tolerable volume and then loading it with CPA while in the swollen state. This counterintuitive result is considerably different from the conventional stepwise strategy, which involves exposure to successively higher CPA concentrations to avoid excessive shrinkage. The procedures identified are a first step in deriving protocols that significantly reduce toxicity damage [5].

[1] D. M. Anderson, J. D. Benson, and A. J. Kearsley. Foundations of Modeling in Cryobiology—I: Concentration, Gibbs Energy, And Chemical Potential Relationships. *Cryobiology* **69**:3 (2014), 349-60.

[2] D. M. Anderson, J. D. Benson, and A. J. Kearsley. Foundations of Modeling in Cryobiology—II: Heat and Mass Transport in Bulk and at Cell Membrane and Ice-liquid Interfaces. In review.

[3] D. M. Anderson, J. D. Benson, and A. J. Kearsley. Foundations of Modeling in Cryobiology—III: Inward Solidification of a Ternary Solution Towards a Permeable Spherical Cell in the Dilute Limit. In review.

[4] D. M. Anderson, J. D. Benson, and A. J. Kearsley. Numerical Solution of Inward Solidification of a Dilute Ternary Solution Towards a Semi-permeable Spherical Cell. In review.

[5] J. D. Benson, A. J. Kearsley, and A. Z. Higgins. Mathematical Optimization Procedures for Cryoprotectant Equilibration Using A Toxicity Cost Function. *Cryobiology* **64**:3 (2012),144-151.

Quantitative MRI

Andrew Dienstfrey
Zydrunas Gimbutas
Michael Boss (NIST PML)
Kathryn Keenan (NIST PML)
Karl Stupic (NIST PML)
Stephen Russek (NIST PML)

Magnetic resonance imaging (MRI) is maturing as a quantitative biomedical imaging technology. For example, imaging facilities routinely report tumor volumes in units of mm^3, blood perfusion in units of ml g^{-1} min^{-1}, apparent diffusion coefficient in mm^2 s^{-1}, and temperature in K. In addition to these biophysical quantities, new parameters specific to MRI physics such as as longitudinal and transverse proton relaxation times (T_1 and T_2, respectively), reported in s, are being considered as biomarkers for a wide range of pathologies including: traumatic brain injury, multiple sclerosis, and liver disease. Despite such use, as of a few years ago the attachment of SI units to MRI-based measurements of these quantities was potentially unwarranted as SI traceability chains for these MRI measurement modalities were unclear if not non-existent. In FY 2018 we continued our collaboration with researchers from NIST's Applied Physics Division (686) to extend SI traceability for this important medical imaging technology.

In May we completed the launch of a new NIST measurement service reporting proton relaxation times. Under this service, customers provide NIST with sample solutions exhibiting mono-exponential spin relaxation behavior. Using the NIST-built nuclear magnetic resonance measurement system, NIST returns SI-traceable measurements of T_1 and T_2 over the range of 4 ms to 3000 ms. This range is significantly larger than current assessments of medically relevant values for these biomarkers, assumed to be approximately 100 ms to 1500 ms. More than 20 sources of uncertainty are accounted for in the calibration analysis. Total uncertainties (bias and variance) for both relaxation times are less than 0.300 ms. Thus, for the first time, measurements of these MRI parameters can be obtained from a national metrology institute with traceability to the SI system. The measurement service website was made public in Feb 2018 [1] and the service was formally documented in the NIST Special Publication 250 series published in May 2018 [2]. In addition, this new service was highlighted by Dr. James Olthoff, Associate Director of NIST Labs, in his invited plenary talk delivered at the XXII IMEKO World Congress in Belfast, Ireland [3].

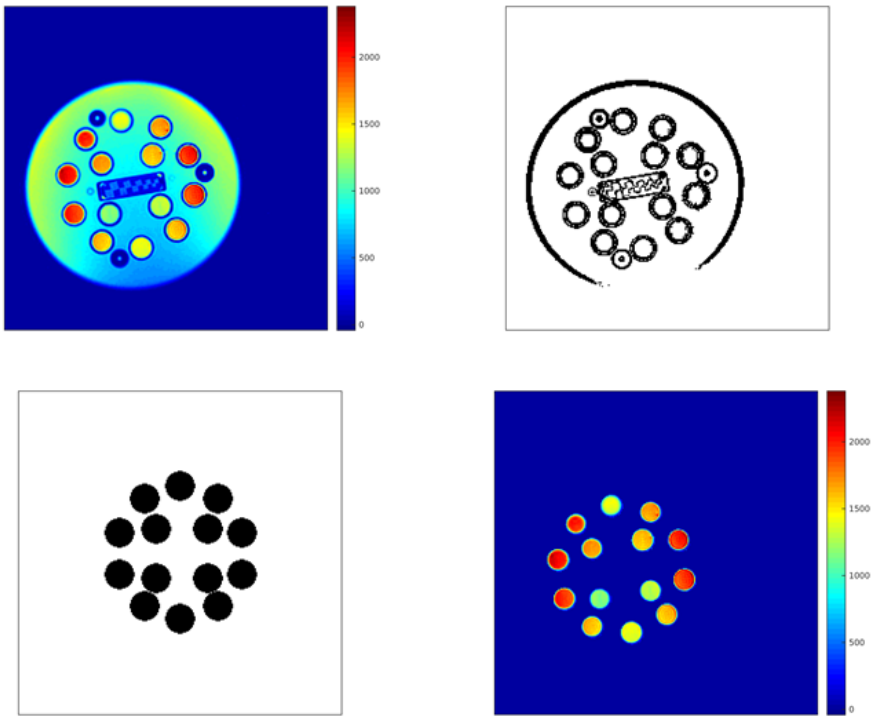

Figure 39. *ROI determination*. Upper left: *MRI measurement image. Note: translation and rotation have been introduced to illustrate the performance of ROI determination algorithm. Phantom placement is visibly more consistent in practice. Nevertheless, quantitative analysis reveals significant variability even to these small shifts.* Upper right: *A thresholded gradient algorithm reveals edge features.* Lower left: *Phantom specifications define an ROI mask which is used to compute initial estimates of ROI centers.* Lower right: *Refinement results in the fourteen regions containing measurement data.*

In a different but related vein, in 2018 we began analysis of cross-sectional measurements of the ISMRM/NIST system phantom. In this study, external collaborators including academic and clinical researchers made measurements of this phantom using distinct MRI scanners with fixed magnetic fields of both 1.5 T and 3 T. The goal of this study is to determine repeatability and reproducibility of measurements of T_1 and T_2 in more clinical-like settings.

The large volume of data in this study required development of new image segmentation algorithms customized for automatic determination of regions of interest (ROI) within the scanned image of the system phantom. As the geometry of this phantom is both known and fixed, we implemented a two-stage algorithm. In the first stage, 2D cross-correlation is used to estimate the Euclidean transformation (rotation and translation) that registers the known phantom mask with a binarized image of measurement edges (thresholded gradient). This step results in initial estimates of ROI centers. These estimates are subsequently refined by an iterative process which alternately: (i) uses existing edge pixels to estimate a disk center and radius, (ii) captures edge pixels in a slightly expanded disk at this center, (iii) if the list of edge pixels is changed, return to (i). This refinement step proceeds independently for each ROI. Once converged, the data within ROI is averaged for signal analysis. Furthermore, the displacements of ROI centers from nominal points determined by the Euclidean transformation of the first step can be analyzed for geometric distortion of the MRI scanner. Figure 39 depicts the steps of this procedure.

Through extensive experiments on the clinical data, we determined that this algorithm is sufficiently robust to analyze the clinical data in a consistent and stable manner. Previously, this registration was performed manually for each ROI. As there are 14 ROI's within each image and nearly 100 images in this preliminary study alone, the newly developed algorithm is essential for consistency and scalability in the future.

With the images properly segmented, data within each ROI were analyzed to return estimates of T_1 and T_2. These clinical MRI-based measurements were compared against known values of these quantities as determined by the NIST NMR calibration service for proton relaxation times. Statistical analyses of these variations have been completed. A paper discussing this work is in preparation.

FY 2019 will continue to be a busy year for NIST's quantitative MRI program. In early 2018 we were contacted by representatives of the National Health Service of the United Kingdom (NHS). Multiple medical MRI facilities in Northern Ireland have acquired scans of the ISMRM/NIST phantom as a component of a quality assurance and control protocol implemented three years ago. At the request of NHS, NIST obtained this longitudinal dataset in November 2018. We intend to begin its analysis in the coming year.

Finally, our proposal "Deep Learning for MRI Reconstruction and Analysis" received seed-funding under NIST's Fundamental and Applied Research and Standards for AI Program. Here we proposed to develop a suite of novel, AI-based MRI inversion programs and to compare these results to physics-based models of MRI measurement process. All computational models will be assessed by comparison against true MRI measurements

made at NIST. We look forward to reporting on these developments in the future.

[1] K. E. Keenan and S. Russek, Magnetic Resonance Measurements for MRI Biomarkers. https://www.nist.gov/calibrations/magnetic-resonance-measurements-mri-biomarkers, accessed Jan 29, 2019.

[2] M. Boss, A. Dienstfrey, Z. Gimbutas, K. E. Keenan, J. D. Splett, K. F. Stupic, and S. E. Russek. Magnetic Resonance Imaging Biomarker Calibration Service: Proton Spin Relaxation Times. NIST Special Publication 250-97, 2018.

[3] J. Oltoff. "Ultra-precision Metrology—Unexpected Applications," XXII IMEKO World Congress, Belfast, Ireland, October 2018.

The Constrained Orthogonal Procrustes Problem

Javier Bernal
James F. Lawrence
Christoph Witzgall

In the *orthogonal Procrustes problem*, matrices P and Q of size $d \times n$ are given, and the problem is that of finding a $d \times d$ orthogonal matrix U that minimizes $\|UQ - P\|_F$, where $\|\cdot\|_F$ denotes the Frobenius norm of a matrix. On the other hand, in the *constrained orthogonal Procrustes problem*, the same function is minimized but U is constrained to be a rotation matrix, i.e., an orthogonal matrix of determinant 1. Applications for the constrained orthogonal Procrustes problem can be found, for example, in the field of functional and shape data analysis [1, 2].

In the past three or four decades the algorithm of choice for solving the constrained orthogonal Procrustes problem has been the algorithm by Kabsch and Umeyama [3-5] which is based on the concept of the singular value decomposition of a matrix. The justification of this algorithm as presented separately by Kabsch and Umeyama is not totally algebraic as it is based on exploiting the optimization technique of Lagrange multipliers. In [6], we have presented a purely algebraic justification of the algorithm through the exclusive use of simple concepts from linear algebra.

Currently we are developing and implementing other methods for solving the constrained orthogonal Procrustes problem in 2, 3, and higher dimensions without the use of singular value decompositions. The new methods promise to be more efficient than the methods using singular value decompositions.

[1] G. Doğan, J. Bernal, and C. R. Hagwood. FFT-based Alignment of 2D Closed Curves with Application to Elastic Shape Analysis. In *Proceedings of the 1st DIFF-CV Workshop*, British Machine Vision Conference, 2015.

[2] A. Srivastava and E. P. Klassen. *Functional and Shape Data Analysis.* Springer, New York, 2016.

[3] W. Kabsch. A Solution for The Best Rotation to Relate Two Sets of Vectors. *Acta Crystallographica Section A: Crystal Physics* **32**:5 (1976), 922-923.

[4] W. Kabsch. A Discussion of the Solution for the Best Rotation to Relate Two Sets of Vectors. *Acta Crystallographica Section A: Crystal Physics* **34**:5 (1978), 827-828.

[5] S. Umeyama. Least-Squares Estimation of Transformation Parameters Between Two Point Patterns. *IEEE Transactions on Pattern Analysis and Machine Intelligence* **13**:4 (1991), 376-380.

[6] J. Lawrence, J. Bernal, and C. Witzgall. A Purely Algebraic Justification of the Solution by Singular Value Decomposition to the Constrained Orthogonal Procrustes Problem. In review.

High-energy Heavy Ion Projectiles in Diatomic Molecular Mediums

Heman Gharibnejad
David R. Schultz (University of Northern Arizona)
Thomas E. Cravens (University of Kansas)
Stephen J. Houston (University of Kansas)

The main objective of this research is to obtain comprehensive cross sections and energy losses of high energy heavy ionic plasma colliding with diatomic molecules, with application to planetary astrophysics.

During the flybys of Jupiter in 1979, NASA's Voyager spacecraft detected a significant ion population within the Jovian system. These observations are consistent with physical chemistry models for the region between six and nine Jovian radii inferring the presence of O^+, S^{2+}, O^{2+}, S^{3+}, and S^+ [1]. These abundances are supported by data from the subsequent observations made when the Ulysses probe passed by Jupiter in 1992 to gain an orbital assist, by the Galileo mission to Jupiter (1995-2003), by the Cassini spacecraft on its way to Saturn (2000), and by the Juno spacecraft that has recently arrived at Jupiter (2016-2021). They originate from Jupiter's Galilean satellites, principally volcanic Io, with a population also possible from the entertainment of the solar wind by Jupiter's magnetic field.

The heavy ions, present in the magnetosphere, also precipitate into the Jovian atmosphere as evidenced by the existence of both north and south polar x-ray auroras identified [1] as originating from de-excitation emission following charge transfer between the precipitating ions and molecules of the upper atmosphere, principally molecular hydrogen. In this process low-charge-state, heavy ions are accelerated by Jupiter's prodigious magnetic field to energies just below 1 MeV/u (depending on their species), strip to high-charge states in collisions with H_2, slow down in their passage through the

atmosphere, and produce secondary electrons, dissociation of H_2, and photon emission from H_2 and from the precipitating ions. These atomic processes heat the atmospheric molecules and contribute to the atmospheric ion and electron currents. In particular, this physical chain of events links the sources of these ions, the Jovian moons and possibly the solar wind, with the magnetosphere, ionosphere, and atmosphere.

Unique observations are being made by the Juno mission of the polar regions in which these ions precipitate along magnetic field lines, made possible by its unique highly elliptical polar orbit with perigee very near the planet. This has motivated the production of data required to simulate the physics of the ion and secondary electron currents, photon emission, and molecular dissociation associated with oxygen ion precipitation [2, 3]. In the most recent work [3] we investigated the viability of having mixtures of reaction channels happening simultaneously as opposed to separately. As an example of simultaneous processes, the probability of single ionization verses single ionization combined with excitation or stripping was explored.

As noted from in situ observations, data for hydrogen and oxygen was important owing to its high abundance, but next in importance is data for sulfur. For example, as evidenced by analysis of x-ray observations from Earth's orbit, sulfur is required in addition to oxygen to model the precipitation-emission process.

Calculation of projectile charge states, and impact energies is presently only achievable using the classical trajectory Monte Carlo (CTMC) method, as described in the previous work for oxygen. The sulfur data was produced over the past year, making extensive use of the ACMD's KNL nodes, and is in the process of verification and completion. The scarcity or the non-existence of measurements to test the very wide range of data for inelastic processes required for ion-electron-transport simulations precludes a direct test of the present comprehensive set of inelastic cross sections and energy losses. However, as part of verification, use of an ion-transport simulation with the present integral cross sections and average energy losses allows the calculation of the stopping power [4] representing the energy loss and charge evolution as sulfur ions pass through molecular hydrogen gas. The stopping-power is a measure that can be compared with the available measurements and accepted values as a function of impact energy.

The validity of our proposed simultaneous interaction model for oxygen [3] still needs to be verified for sulfur. We plan to accomplish this task through our Monte-Carlo electron transport simulations for hydrogen on hydrogen and sulfur on hydrogen interactions.

[1] L. P. Dougherty, K. M. Bodisch, and F. Bagenal. Survey of Voyager Plasma Science Ions at Jupiter: Heavy Ions. *Journal of Geophysical Research: Space Physics* **122**:8 (2017), 8257–8276.

[2] D. R. Schultz, N. Ozak, T. E. Cravens, and H. Gharibnejad. Ionization of Molecular Hydrogen and Stripping of Oxygen Atoms and Ions in Collisions of $O^{q+}+H_2$ (q=0-8): Data for Secondary Electron Production from Ion Precipitation at Jupiter. *Atomic Data and Nuclear Data Tables* **113**:1 (2017), 116.

[3] D. R. Schultz, H. Gharibnejad, T.E. Cravens, and S.J. Houston. Data for Secondary-Electron Production from Ion Precipitation at Jupiter II: Simultaneous and Non-Simultaneous Target and Projectile Processes in Collisions of $O^{q+}+H_2$ (q=0-8). *Atomic Data and Nuclear Data Tables*, 2018, in press.

[4] J. F. Ziegler, M.D. Ziegler, and J.P. Biersack. SRIM: The Stopping and Range of Ions in Matter. *Nuclear Instruments and Methods in Physics Research Section B: Beam Interactions with Materials and Atoms* **268**:11 (2010), 1818–1823.

Modeling Magnetic Fusion

Geoffrey McFadden
Eugenia Kim (New York University)
Harold Weitzner (New York University)

A future source of commercial energy may be based on the controlled fusion of a hot plasma of hydrogen isotopes that is confined by a strong magnetic field. Quite often a toroidal geometry is envisioned in which the ions fuse to form helium and release energetic neutrons. A number of computational methods to model such magnetic fusion devices have been developed by researchers at New York University (NYU) and elsewhere to allow effective numerical simulations of the most essential features of modern tokomak and stellarator experiments. We are currently participating in the continuing development of a code, NSTAB, that computes three dimensional equilibria of toroidal plasmas, and determines their nonlinear stability [1, 2].

In NSTAB the solenoidal magnetic field is represented as a cross product of two potential functions, and the magnetic energy is minimized subject to a given pressure profile and "rotational transform," which represents a winding number of magnetic field lines on a given flux surface [1]. Another assumption is that of "nested" flux surfaces, which preclude the possibility of magnetic "islands" that would result in undesirably rapid particle transport across magnetic surfaces. It turns out, however, that the assumption of nested flux surfaces can lead to the formation of singular current sheets at magnetic surfaces where the rotational transform is a rational number, particularly for low values of the corresponding numerator and denominator. So-called "quasi-symmetric" configurations [2] are designed to avoid these undesirable singularities at rational surfaces by carefully choosing the shape of the plasma boundary in such a way as to avoid resonances at these surfaces.

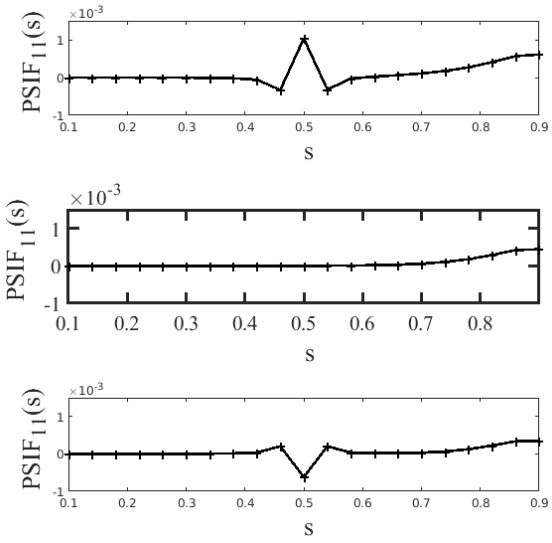

Figure 40. *The (1,1) Fourier component $PSI_{11}(s)$ of a potential function of the magnetic field as a function of the toroidal flux, s, that labels a family of nested flux surfaces. For the surface with s = ½ the rotational transform is unity, which can cause a singular current there which appears as a localized "blip" in the potential at this surface. By systematically varying the amplitude $\boldsymbol{\Delta_{01}}$ of a perturbation to the plasma boundary, this singularity is successfully suppressed. Top: $\boldsymbol{\Delta_{01} = 0.017}$. Middle: $\boldsymbol{\Delta_{01} = 0.01783}$ (singularity is suppressed). Bottom: $\boldsymbol{\Delta_{01} = 0.018}$*

To better study this procedure, we have developed a simplified version of NSTAB that applies in a rectangular geometry and avoids the complication of the magnetic axis that occurs in toroidal geometries. The same variation principle is used to derive governing equations, which are nonlinear partial differential equations of a non-standard type. In Figure 40 we show a sample calculation in which a singularity at a rational surface with a winding number of unity is generated by a wall perturbation with wavenumber $(k_x, k_y) = (1,1)$. By generating a nonlinear resonance with neighboring non-resonant wavenumbers of (1,0) and (0,1) of the proper amplitude, this singularity is suppressed [3]. These studies could provide design principles that can be used to generate quasi-symmetric stellarators with improved performance in future fusion power plants.

[1] M. Taylor. A High Performance Spectral Code for Nonlinear MHD Stability. *Journal of Computational Physics* **110** (1994), 407-418.

[2] P. R. Garabedian and G. B. McFadden. Design of the DEMO Fusion Reactor Following ITER. *Journal of Research of the National Institute of Standards and Technology* **114** (2009), 229-236.

[3] E. Kim, G. McFadden, and H. Weitzner. "Computational Study of Magnetohydrodynamic Equilibria with Emphasis on Fragility of Flux Surfaces." 60th Annual Meeting of the APS Division of Plasma Physics, Portland, OR, November 7, 2018.

Large Scale Dynamic Building System Simulation

Anthony Kearsley
Aaron Chen (Drexel University)
Amanda Pertzborn (NIST MML)
Jin Wen (Drexel University)

The building sector represents the largest primary energy-consuming sector in the United States, responsible for 41 % of the country's primary energy, in comparison to 28 % for the transportation sector and 32 % for industry. Moreover, buildings consume 74 % of the electricity in the United States, which makes the building sector significant to the overall smart grid infrastructure. Given the rapid development of the smart grid and the potential of buildings to store and generate electricity through demand shifting and transactive control, there is an urgent need to improve the dynamic interactions between buildings and the smart grid, which further calls for robust and accurate dynamic building energy system modeling and simulation.

Unlike traditional dynamic building simulations, which typically focus on a single building, dynamic building simulations used for smart grid applications simulate large and complex building energy systems and their interactions within building clusters that are composed of multiple buildings. These simulations result in large systems of coupled, potentially ill-conditioned nonlinear equations (easily including thousands of equations), will need to be solved rapidly and robustly.

Efficiently, robustly and accurately solving large and sparse nonlinear algebraic and differential equation system for dynamic building simulation is becoming more and more essential to meet the increasing demands to simulate large scale multiple-building heating ventilation and air conditioning (HVAC) scenarios that are coupled to various complicated energy sources either through the smart-grid or other means, such as district heating/cooling.

In practice, these large simulations are decomposed through geometric zones (see Figure 41) where one expects air flow and thermal conductivity to be similar. Typically, these zones are comprised of rooms or collections of closely connected rooms. The HVAC systems then control temperature and air flow in these zones through coupled boundary conditions that are matched in what is called a "super-block." It is interesting that something as simple as a fan/coil unit (see Figure 42) can result in an approximation whose discretized system that is quite hard to solve (see Figure 43). More detailed mathematical models which would more accurately predict the physics of a simple fan coil unit would result in simulations that would be prohibitively expensive. Less

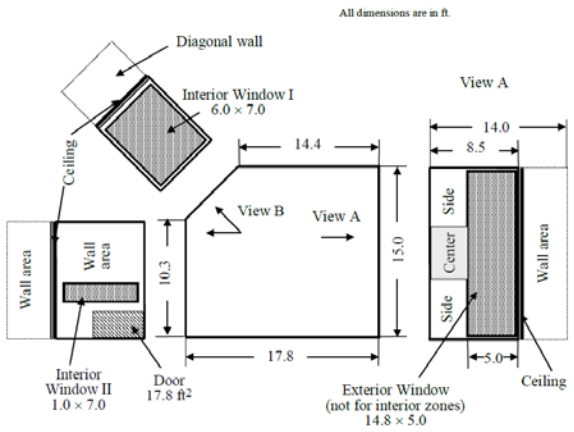

Figure 41. *A floor and window view of a typical zone.*

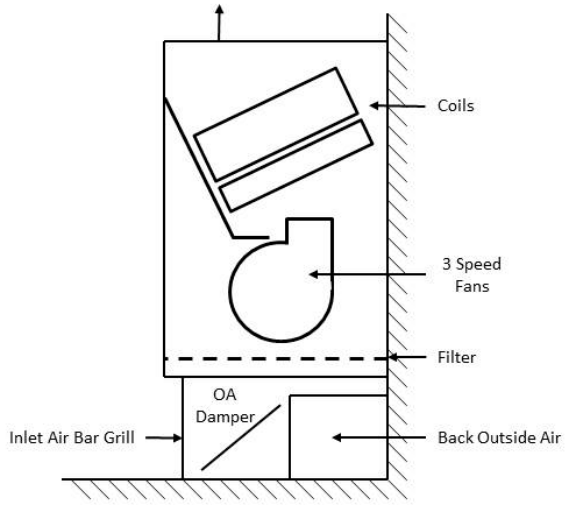

Figure 42. *A simple fan/coil unit schematic.*

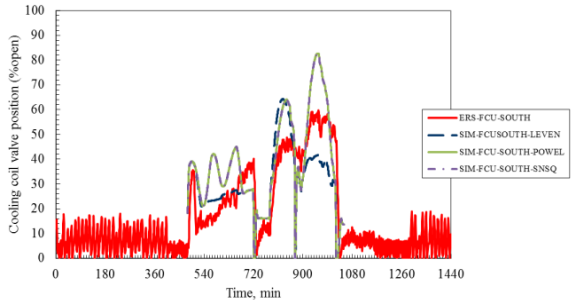

Figure 43. *A collection of nonlinear-solvers behaving very differently on a very simple HVAC simulation.*

detailed mathematical models yield more well-conditioned systems that can be solved quickly but do not provide the flexibility of, for example, more complicated scenarios through various degrees of occupancy, seasons or other factors that must be considered.

In [1], Z. Chen seeks to develop a class of large-scale Krylov methods for solving these nonlinear systems that automatically build pre-conditioners based on building geometries. Comprised of smaller models, like the one used to predict fan/coil dynamics, the resulting large-scale systems will be assembled at the same time as a preconditioner, both of which would be made available to a building engineer seeking to simulate and evaluate a building HVAC system.

[1] Z. Chen. Large-Scale Dynamic Building System Simulation. PhD Thesis in preparation, Drexel University, Philadelphia PA.

Numerical Solutions of the Time Dependent Schrödinger Equation

Barry I. Schneider
Heman Gharibnejad
Luca Argenti (University of Central Florida)
Nico Douguet (University of Central Florida)
Jeppe Olsen (Aarhus University)

We have been collaborating with scientists developing numerically robust methods for solving the time dependent Schrödinger equation (TDSE). L. Argenti, a new Assistant Professor from the University of Central Florida and his postdoc, N. Douguet, joined the effort in 2016. H. Gharibnejad, a NIST/NRC postdoctoral associate, joined the group in January of 2017 to collaborate on our ongoing efforts.

There are two related research threads underway. The primary effort has been to develop a hybrid finite element discrete variable (FEDVR)-Gaussian approach to treat the interaction of attosecond (10^{-18} sec) radiation with molecular targets. In addition, we are examining the performance of various numerical time propagation techniques for the TDSE. This past summer, a SURF student, H. Schmale, continued the work started the previous summer with another SURF student, Mark Leadingham, to develop a simple one spatial dimension, time propagation code to test some of the numerical methods. While the model is simple, it serves well to illustrate the problems that would be faced in higher spatial dimensions while being simple enough for a talented undergraduate to tackle in a summer research program. A paper on this research has been submitted to *Computer Physics Communications* [1].

The hybrid finite element approach that has been developed is quite general, but the applications to date have concentrated on describing the single and double ionization of electrons exposed to intense, ultrafast, laser radiation in many-body atomic and molecular systems. These attosecond (10^{-18} sec) pulses provide a new window to study electronic motion in atoms and molecules

on their natural timescale. To put this in context, the motion of electrons responsible for chemical binding and electron transfer processes in nature, have a characteristic timescale of about 100 attoseconds (It takes an electron 152 attoseconds to go around the hydrogen atom.) These processes can only be described using time dependent quantum mechanics and, where appropriate, need to be coupled to Maxwell's equations to describe macroscopic phenomena. At the end of the day, we wish to image quantum phenomena with sub-femtosecond temporal and sub-Angstrom spatial resolution. Eventually, one can contemplate producing "molecular movies" of this motion in much the same way as it is done in molecular dynamics simulations of heavy particle processes.

The basic methodology as applied to atoms and simple diatomic molecules, has been described in [2-11] and [12] provides a detailed review of the work. The essential aspects have been

- development of the finite element discrete variable method (FEDVR) spatially discretize the coordinates of the electrons, and
- use of the short iterative Lanczos method to propagate the wavefunction in time.

The method has been efficiently parallelized using MPI and scales linearly with the size of the FEDVR basis. Large scale calculations have been performed on a number of atoms and molecules using resources provided by the NSF Extreme Science and Engineering Discovery Environment (XSEDE). The group has received a competitively awarded allocation of more than 3.0 million service units for the current fiscal year.

We have begun a study to employ a mixed basis of Gaussian functions at short range and FEDVR functions at long range to extend our methods to complex polyatomic molecules. This approach has several important advantages over using a single basis over all of space. First, the use of nuclear centered Gaussians preserves the local atomic symmetry around each nucleus and avoids the poor convergence of using a single-center FEDVR basis at all distances. Second, once the electron is far enough away from the nuclear cusps, a single center expansion converges quickly and importantly, can represent the electrons out to very large distances using an approach that is very amenable to domain decomposition. The major issue is to compute the one and two electron integrals between the two types of basis functions. In 2016-2017, a new and efficient formalism, using transition density matrices, was developed so that an optimal use can be made of existing quantum chemistry codes to extract the information required to compute the additional integrals. We have been lucky enough to interest J. Olsen from Aarhus University, an extremely talented quantum chemist, to collaborate with us on the project. The NIST-UCF-Aarhus group has already met three times and substantial progress has been made. It should be noted, that this is a very complex many-body problem and even with the most talented of researchers, it is a long-term effort. We are in the process of implementing our approach and interfacing with the quantum chemistry code of Olsen. Computing the required hybrid one and two electron integrals is the major responsibility of Gharibnejad.

For the time propagation problem, Schneider, Gharibnejad, Leadingham, and Schmale have taken a simple one-dimensional model of the hydrogen atom in an intense electric field and examined the propagation of wavepackets as the system evolved in time. The model uses a soft-core to treat the interactions of the electron with the nucleus and a three-point finite difference approach to the second derivative operator. While this problem has been studied before, and the model is a reasonable representation of the three-dimensional hydrogen atom, our objective was to determine how various time propagation schemes performed as well as to suggest a new approach that might be more robust than those currently being used. The two senior researchers felt that this was an excellent problem for summer SURF students to tackle and indeed that turned out to be the case. Leadingham and Schmale made excellent progress over their summer stays at NIST and Gharibnejad has worked to refine the initial research to the point where a publication has been submitted to *Computer Physics Communications*.

The study found that for very simple propagation schemes such as the Crank-Nicholson (CN), variants of the split-operator (SO) method and real-space propagation (RSP) methods are very efficient per time step, the size of the time steps must be quite small to obtain accurate results. In contrast, more elaborate schemes, such as the short-iterative-Lanczos (SIL) method, are more expensive per time step but allow time steps two orders of magnitude larger than CN, SO or RSP for the same accuracy. While we suspected that might be the case, a careful study confirmed the results. The conclusion was that the SIL performed much more efficiently in practice than the other methods. The basic reason is that the SIL only depends on the natural time scale of the laser field and not on issues of the spectrum of the operator being discretized. The SIL does not rely on a second order expansion to be accurate. We have also examined higher order spatial discretization schemes and also have found them to be even more efficient and accurate than the three-point approach. We are now looking into an integral equation technique that would combine the best of the SIL with perhaps even larger time steps for high accuracy.

[1] H. Gharibnejad, B. I. Schneider, M. Leadingham, and H. J. Schmale. A Comparison of Numerical Approaches to the Solution of the Time-Dependent Schrödinger Equation in One Dimension, arXiv:1809.09164, Sept. 24, 2018. Under review for special 50thYear Anniversary issue of *Computer Physics Communications.*

[2] J. Feist, S. Nagele, R. Pazourek, E. Persson, B. I. Schneider, L. A. Collins, and J. Burgdörfer. Nonsequential Two-Photon Double Ionization of Helium. *Physical Review A* **77** (2008), 043420.

[3] X. Guan, K. Bartschat, and B. I. Schneider. Dynamics of Two-photon Ionization of Helium in Short Intense XUV Laser Pulses. *Physical Review A* **77** (2008), 043421.

[4] X. Guan, K. Bartschat, and B. I. Schneider. Two-photon Double Ionization of H_2 in Intense Femtosecond Laser Pulses. *Physical Review A* **82** (2010), 041407.

[5] X. Guan, E. Secor, K. Bartschat, and B. I. Schneider, Double-slit Interference Effect in electron Emission from H_2^+ Exposed to X-Ray Radiation. *Physical Review A* **85** (2012), 043419.

[6] X. Guan, K. Bartschat, B. I. Schneider, and L. Koesterke. Resonance Effects in Two-Photon Double Ionization of H_2 by Femtosecond XUV Laser Pulses. *Physical Review A* **88** (2013), 043402.

[7] J. Feist, O. Zatsarinny, S. Nagele, R. Pazourek, J. Burgdörfer, X. Guan, K. Bartschat and B. I. Schneider. Time Delays for Attosecond Streaking in Photoionization of Neon. *Physical Review A* **89** (2014), 033417.

[8] X. Guan, K. Bartschat, B. I. Schneider, and L. Koesterke. Alignment and Pulse-duration Effects in Two-Photon Double Ionization of H_2 by Femtosecond XUV Laser Pulses. *Physical Review A* **90** (2014), 043416.

[9] B. I. Schneider, L. A. Collins, X. Guan, K. Bartschat, and D. Feder. Time-Dependent Computational Methods for Matter Under Extreme Conditions, In *Advances in Chemical Physics 157, Proceedings of the 240 Conference: Science's Great Challenges*, (A. Dinner, Ed.), John Wiley and Sons, 2015.

[10] B. I. Schneider, X. Guan, and K. Bartschat. Time Propagation of Partial Differential Equations Using the Short Iterative Lanczos Method and Finite-Element Discrete Variable Representation, In *Advances in Quantum Chemistry 72* (2016), A Tribute to Frank E. Harris.

[11] B.I. Schneider. How Novel Algorithms and Access to High Performance Computing Platforms are Enabling Scientific Progress in Atomic and Molecular Physics. *IOP Journal of Physics Conference Series* **759** (2016).

[12] B. I. Schneider, J. Feist, S. Nagele, R. Pazourek, S. Hu, L. Collins, and J. Burgdörfer. Recent Advances in Computational Methods for the Solution of the Time-Dependent Schrödinger Equation for the Interaction of Short, Intense Radiation with One and Two Electron Systems. In *Dynamic Imaging, Theoretical and Numerical Methods: CRM Series in Mathematical Physics* **XV** (A. Bandrauk and M. Ivanov, Eds.), 2011.

A Science Gateway for Atomic and Molecular Physics

Barry I. Schneider
Naduvalath Balakrishhan (UNLV)
Klaus Bartschat (Drake University)
Igor Bray (Curtin University, Australia)
Robert Foray (Penn State)
Armin Scrinzi (Ludwig-Maximilians U., Germany)
Fernando Martín (U. Autónoma de Madrid, Spain)
Jonathan Tennyson (University College London)
Sudhakar Pamidighantam (Indiana University)

B. Schneider (chair), R. Foray and N. Balakrishhan organized an NSF supported workshop entitled, "Developing Flexible and Robust Software in Computational Atomic and Molecular (A&M) Physics," which was held at the Harvard-Smithsonian Institute for Theoretical Atomic and Molecular Physics (ITAMP) on May 14-16, 2018. The workshop brought together a group of internationally known researchers in computational atomic and molecular physics to

- identify and prioritize the outstanding problems in A&M science which would benefit from a concerted community effort in developing new software tools and algorithms which would lead to more rapid and productive scientific progress for the entire community,
- determine what would be the best approaches to achieving that goal, and
- produce and disseminate a report of the workshop to the entire community.

A concerted community effort is now required to develop and maintain these tools to ensure continued scientific progress. The group acknowledged that, in contrast to some other communities, the A&M physics has lagged behind in developing community software packages that are robust and used by others. The software packages are typically poorly documented, poorly written and only usable by a set of local "experts." The tools themselves are capable of treating scientific and technologically interesting problems but are only accessible to a small group of people. The codes are not always maintained and the lack of coordination among the developers has led to a lot of "reinventing the wheel." The group felt strongly that the efforts being expended in developing these computational tools be available and easily used by future generations of A&M scientists.

The workshop was a great success. A very tangible outcome was that six of the groups decided to work together to develop a proposal to the NSF XSEDE facility to build and maintain a Science Gateway devoted to the codes developed in these groups. That proposal was

funded, and since May there has been some initial progress. A number of the codes are already ported and running on various XSEDE platforms. Progress has already been achieved in making them usable by others within the group but not yet the outside world. We are now in an excellent position to take another step forward.

A proposal has been written to the Molecular Sciences Software Institute to

(i) Promote our ideas to a larger more diverse group of scientists than the ITAMP workshop participants both in A&M physics as well as other related fields to help us solidify our ideas.

(ii) Conduct a three-day workshop, most likely held before or after one of the major A&M international conferences such as the International Conference on Photonic, Electronic, and Atomic Collisions (ICPEAC) in late July of 2019. ICPEAC is in Deauville, France, and has about 800 attendees. The exact location of the workshop needs more discussion but holding it close to the conference site has many advantages. Doing this would clearly reduce the cost of the workshop and be more convenient for the Europeans. We envision inviting about 30 participants consisting of both A&M scientists and quantum chemists. The workshop will consist of a number of general sessions discussing the codes and what they can and cannot do. In addition, there will be hands on sessions on how to use the codes on the Science Gateway.

(iii) Develop a roadmap for other workshops focusing more on a specific code or codes for specialists.

Advanced Materials

Delivering technical support to the nation's manufacturing industries as they strive to out-innovate and out-perform the international competition has always been a top priority at NIST. Mathematical modeling, computational simulation, and data analytics are key enablers of emerging manufacturing technologies. The Materials Genome Initiative (MGI), an interagency program with the goal of significantly reducing the time from discovery to commercial deployment of new materials using modeling, simulation, and informatics, is a case in point. To support the NIST role in the MGI, ACMD develops and assesses modeling and simulation techniques and tools, with emphasis on uncertainty quantification, and collaborates with other NIST Laboratories in their efforts to develop the measurement science infrastructure needed by the materials science and engineering community.

Micromagnetic Modeling

Michael Donahue
Donald Porter
Robert McMichael (NIST CNST)
June Lau (NIST MML)
Justin Shaw (NIST PML)
Hans Nembach (NIST PML)

http://math.nist.gov/oommf/

Advances in magnetic devices such as recording heads, field sensors, spin torque oscillators, and magnetic nonvolatile memory (MRAM) are dependent on an understanding of magnetization processes in magnetic materials at the nanometer level. Micromagnetics, a mathematical model used to simulate magnetic behavior, is needed to interpret measurements at this scale. ACMD is working with industrial and academic partners, as well as with colleagues in the NIST CNST, MML, and PML, to improve the state-of-the-art in micromagnetic modeling.

The research of the Micromagnetic Modeling project was honored twice in 2018. At the 46th Annual NIST Awards Ceremony on December 12, M. Donahue and D. Porter received the Jacob Rabinow Applied Research Award, an annual NIST award for outstanding achievements in the practical application of the results of scientific engineering research.[8] On August 30, the same work was honored with the ITL Outstanding Technology Transfer award.[9]

We have developed a public domain computer code for performing computational micromagnetics, the Object-Oriented Micromagnetic Modeling Framework (OOMMF). OOMMF serves as an open, well-documented environment in which algorithms can be evaluated on benchmark problems. OOMMF has a modular structure that allows independent developers to contribute extensions that add to its basic functionality. OOMMF also provides a fully functional micromagnetic modeling system, handling three dimensional problems, with extensible input and output mechanisms.

In FY 2018 alone, the software was downloaded by more than 3700 users and employed by over 200 additional users through the nanohub[10] and JOOMMF[11] services. During the same period, use of OOMMF was acknowledged in more than 200 peer-reviewed journal articles. OOMMF has become an invaluable tool in the magnetics research community.

Key developments over the last year include the following:

- Continued development of extended precision numerics and an alternative approach to the demagnetization energy calculation based on hybrid fine/coarse grid computations.
- Fixed inefficient thread allocation on two-dimensional problems.
- Completed a book chapter on standard problems in micromagnetics.
- Released OOMMF versions 1.2b2[12] and 2.0a1 in Sept. 2018[13].

OOMMF is a part of a larger activity, the Micromagnetic Modeling Activity Group (μMAG), formed to address fundamental issues in micromagnetic modeling through two activities: the development of public domain reference software, and the definition and dissemination of standard problems for testing modeling software. ACMD staff members are involved in development of the standard problem suite as well. A contributed solution to Standard Problem 5[14] was received and published.[15] The history of μMAG standard

[8] https://www.nist.gov/nist-awards/2018-jacob-rabinow-applied-research-award-donahue-porter
[9] https://content.govdelivery.com/accounts/USNIST/bulletins/1fb7feb#link_1521651422112
[10] https://nanohub.org/
[11] https://nanohub.org/resources/oommfnotebooks/
[12] https://math.nist.gov/oommf/software-12.html
[13] https://math.nist.gov/oommf/software-20.html
[14] https://www.ctcms.nist.gov/~rdm/std5/spec5.xhtml
[15] https://www.ctcms.nist.gov/~rdm/std5/Finnochio.html

problems is the subject of a book chapter soon to be published [1]. Donahue serves as editor of the volume containing that chapter [2].

In addition to the continuing development of OOMMF, the project also does collaborative research using OOMMF. Donahue provides technical guidance on micromagnetic modeling for the DARPA M3IC (Magnetic, Miniaturized, and Monolithically Integrated Components) project[16], which aims to integrate magnetic components into the semiconductor materials fabrication process. The goal is to improve electromagnetic systems for communications, radar, and related applications. Donahue is also a team member on the new NIST Innovations in Measurement Science (IMS) nanothermometry project Thermal MagIC.

In total, the ACMD micromagnetic project produced a book chapter [1], a journal article [3], and two conference presentations [4, 5] during this past year.

[1] D. G. Porter and M. J. Donahue. Standard Problems in Micromagnetics. In *Electrostatic and Magnetic Phenomena: Particles, Macromolecules, Nanomagnetics*, (M. J. Donahue, ed.). World Scientific Publishing, to appear.

[2] Electrostatic and Magnetic Phenomena: Particles, Macromolecules, Nanomagnetics, (M. J. Donahue, ed.). World Scientific Publishing, to appear.

[3] M. J. Donahue. Novel Low Loss and Lightweight Magnetic Material for Electrical Machinery. *IEEE Transactions on Magnetics*, to appear.

[4] M. J. Donahue. "Hybrid Fine/Coarse Stray Field Computation for Micromagnetics." 62nd Annual Conference on Magnetism and Magnetic Materials (MMM 2017), Pittsburgh, PA, November 10, 2017.

[5] M. J. Donahue and D. G. Porter. "Quantitative Evaluation of Errors in Calculation of the Demagnetization Tensor." Joint MMM-Intermag Conference, Washington, DC, January 2019.

OOF: Finite Element Analysis of Material Microstructures

Stephen A. Langer
Andrew C.E. Reid (NIST MML)
Günay Doğan (Theiss Research)
Shahriyar Keshavarz (Theiss Research)

http://www.ctcms.nist.gov/oof/

The OOF Project, a collaboration between ACMD and MML, is developing software tools for analyzing real material microstructure. The microstructure of a material is the (usually) complex ensemble of polycrystalline grains, second phases, cracks, pores, and other features occurring on length scales large compared to atomic sizes. The goal of OOF is to use data from a micrograph of a real or simulated material to compute its macroscopic behavior via finite element analysis.

The OOF user loads images into the program, assigns material properties to the features of the image, generates a finite element mesh that matches the geometry of the features, chooses which physical properties to solve for, and performs virtual experiments to determine the effect of the microstructural geometry on the material. OOF is intended to be a general tool, applicable to a wide variety of microstructures in a wide variety of physical situations. It is currently used by academic, industrial, and government researchers worldwide.

There are two versions of OOF, OOF2 and OOF3D, each freely available on the OOF website. OOF2 starts with two-dimensional images of microstructures and solves associated two-dimensional differential equations, assuming that the material being simulated is either a thin freely suspended film or a slice from a larger volume that is unvarying in the third dimension (generalizations of plane stress and plane strain, respectively). OOF3D starts with three-dimensional images and solves equations in three dimensions.

As large software projects, OOF2 and OOF3D rely on many external libraries, including VTK (3D graphics), GTK (user interface components), and Python (scripting). These libraries are always evolving, and their old versions eventually become obsolete. The OOF philosophy has been to use old versions as long as possible so as to minimize the number of disruptive and time-consuming upgrades. A major project in the past year was to bring OOF3D up-to-date with VTK. VTK 5 was many years old and no longer supported. Major changes were required to make OOF3D compatible with VTK 8, including switching from X11 graphics to native macOS graphics on Macintoshes. Upgrades from GTK2 to GTK3 and from Python 2 to 3 are anticipated soon.

Because building OOF3D and VTK 8 and all of their dependencies on macOS is now significantly more difficult than with earlier versions of VTK, a binary installer is now available for OOF3D. OOF3D users no longer have to compile OOF3D from source on Macintosh computers. A side-benefit of the binary installer for macOS is that OOF3D development is now free to use uncommon libraries and tools, since users won't need to build and install anything. This will enable OOF to use the same compilers on both Linux and macOS. Re-implementing many parts of OOF in parallel had been postponed because the Apple compilers stopped supporting OpenMP, but that effort will now proceed using the GNU compilers on both Linux and macOS.

An OOF3D development reported in FY 2017 was the implementation of a new, robust method for computing the intersection of a tetrahedral finite element with

[16] https://www.darpa.mil/program/magnetic-miniaturized-and-monolithically-integrated-components/

a set of voxels, which is at the heart of many OOF3D operations. During FY 2018 it was discovered that the analogous intersection routine in OOF2 suffers (extremely rarely) from the same pathologies that necessitated the modifications to OOF3D. A 2D analog of the new OOF3D method was devised and implemented in OOF2. These new methods ensure that small numerical errors in the positions of finite element nodes with respect to voxel corners (or vice versa) cannot lead to large errors in the computed volume of the intersection. A manuscript about these methods is being prepared.

During this year, A. Reid and S. Keshavarz continued to make progress in incorporating crystal plasticity into the main OOF code. A small number of architectural issues were identified with the prototype code, and work began on modifications to the OOF code base itself. Several additional minor "impedance mismatches" between the prototype code and the main OOF code arose during this effort and were largely worked through. The OOF Crystal Plasticity base class, which does the heavy lifting in this implementation, is now substantially complete. It remains to modify the Equation infrastructure to take the correct divergence for the large-strain formulation implicit in crystal plasticity, and then identify suitable validation problems to exercise the resulting capability.

[1] A. Reid. "OOF3D: New Developments in a Materials-Focused Finite Element System." 4th International Congress on 3D Materials Science, Elsinore, Denmark, June 10-13, 2018.

[2] A. Reid. "Exploring Crystal-Plastic Constitutive Rules with the OOF Tool." 9th International Conference on Multiscale Materials Modeling, Osaka, Japan, October 28 – November 2, 2018.

[3] S. Langer. "Meshing Images with OOF3D." 13th World Congress on Computational Mechanics, New York, July 22-27, 2018.

[4] A. Reid, S. Langer, and S. Keshavarz. "A Materials Scientists View of Crystal Plasticity -- The OOF Project." 13th World Congress on Computational Mechanics, New York, July 22-27, 2018.

[5] M. Tzimas, S. Papanikolaou, S. Langer, A. Reid, and H. Song. "A Machine Learning Approach for Plastic Deformation History Using Spatial Strain Correlations." 13th World Congress on Computational Mechanics, New York, July 22-27, 2018.

Numerical Methods for Reliable Computing with Equations of State

Bradley Alpert
Ian Bell (NIST MML)

Equations of state (EOS) provide quantitative relationships between thermodynamic variables of fluid mixtures, such as temperature, pressure, volume, and internal energy, that enable determination of key fluid properties by exploiting statistical physics to interpolate or extrapolate beyond where laboratory measurements are economical or feasible. The NIST data facilities REFPROP (Reference Fluid Thermodynamic and Transport Properties Database) and TDE (ThermoData Engine), which are widely accessed by the chemical engineering community, are developed from critically evaluated laboratory data in combination with EOS.

Increasing reliance on, and automation of, retrieval of such thermodynamic property data imposes heightened demands on the reliability and generality of algorithms both for deriving and for exploiting the EOS. Calculation of the density of a mixture for a given temperature, pressure, and mixture composition from multiparameter mixture models sometimes fails, due to insufficiently accurate root finding, but also insufficiently robust algorithms that may miss certain roots entirely. The initial result of this collaboration has been to represent transcendental equations in one dimension with orthogonal polynomial (Chebyshev) expansions that enable reliable root finding. A concomitant requirement for very fast evaluations, achieved here, arises since typical applications may involve an extremely large number of root-finding steps.

This year B. Alpert introduced efficiencies available for computing derivatives of analytic function representations, both that recalled in recent articles by N. Higham of the University of Manchester for truncation-free computation of the first derivative, and that due to improved discretization of the Cauchy integral representation of higher derivatives. These have led to order of convergence $2n$ versus n for n quadrature points. I. Bell has determined that these capabilities will significantly improve performance, and flexibility through greater simplicity, of software manipulating EOS.

Extension of the EOS root-finding software to two independent variables, with increased geometric structure and its attendant complications, is planned.

[1] I. H. Bell and B. K. Alpert. Exceptionally Reliable Density-solving Algorithms for Multiparameter Mixture Models from Chebyshev Expansion Rootfinding. *Fluid Phase Equilibria* **476** Part B (2018) 89-102. DOI: 10.1016/j.fluid.2018.04.026

[2] I. H. Bell, B. Alpert, and L. Bouck, ChebTools: C++11 (and Python) Tools for Working with Chebyshev Expansions. *The Journal of Open Source Software* 12 February 2018. DOI: 0.21105/joss.00569

Data Analysis and Uncertainty Quantification for Molecular Modeling of Advanced Materials

Paul Patrone
Andrew Dienstfrey

Advances in computer simulations have led to a dramatic paradigm shift in the way that new materials are created and tested. For example, molecular dynamics (MD) simulations are now routinely used to aid in the development of next generation composites for passenger airplanes [1-4]. Similarly, chemical companies are exploiting MD to speed up discovery of lubricants with desirable properties, such as extended service-life in automobile engines. From an economic perspective, the motivations behind this trend are clear: traditional "make-it-and-break it" testing approaches can consume entire R&D budgets, so that there are significant incentives to develop cheaper alternatives [5]. Given that MD can often replicate experimental procedures in an inexpensive, virtual environment, this tool has become a mainstay in materials modeling.

Despite their growing usefulness, however, simulations are often accompanied by distinct sources of uncertainty that can sometimes render predictions questionable. This issue largely arises from the fact that computers, while more powerful than ever, are still limited in their ability to model sufficiently many degrees of freedom. Practically speaking, this limitation means that simulations cannot resolve bulk structures (e.g., airplane wings) with atomistic detail, so modelers are forced to simulate microscopic systems that may not be fully representative of the desired material. As a result, finite size effects, thermal noise, and related issues manifest as noise in data, confounding attempts to accurately predict a materials' properties [3]. Scientists therefore need robust uncertainty-quantification tools if the full benefits, economic and otherwise, of simulations are to be realized.

Building on work from FY 2016 and FY 2017, ACMD staff have collaborated with scientists from Boeing, Solvay, Exxon Mobil, and Schrodinger to develop UQ methods relevant to their associated simulation protocols. While the details cover a broad range of topics [4, 6], our key objectives this year have been to address: (i) the issue of model validation for MD; and (ii) ensuring successful technology transfer to stakeholders. Despite being seeming unrelated, model validation, i.e. the assessment that a model is an accurate representation of experimental data, is generally necessary before industry is willing to support widespread adoption of a simulation technique. Thus, our collaborative efforts on industry-specific validation problems provided a key route by which we could show the usefulness of our UQ methods and thereby ensure they are adopted in commercial settings.

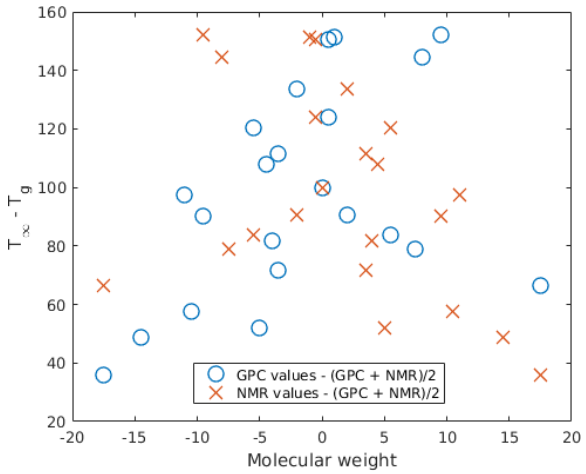

Figure 44. *Example of $\boldsymbol{T_g}$ data versus variation in molecular weight data. Gel-phase chromatography (GPC) and nuclear magnetic resonance (NMR) are two separate techniques for determining molecular weight $\boldsymbol{M_n}$. These correspond to $\boldsymbol{g_i}$ and $\boldsymbol{h_i}$ in the equations above. Blue circles show $\boldsymbol{g_i - m_i}$, whereas orange × show $\boldsymbol{h_i - m_i}$. The quantity $\boldsymbol{\sigma}$ discussed in the main text characterizes the horizontal variation in this data and thereby provides an estimate of our uncertainty in any given molecular weight $\boldsymbol{m_i}$.*

A typical problem that illustrates these points is the task using MD to estimate the glass-transition temperature T_g of a polymer. Roughly speaking, T_g corresponds to the temperature at which the material becomes soft. In FY 2016 and FY 2017, we developed modeling and UQ protocols to estimate this quantity from high-throughput MD simulations. In FY 2018, we began the task of comparing these estimates with experimental counterparts. Ironically, this validation exercise also requires that we develop UQ methods for experimental data, since disagreement with simulated predictions may be due to inaccuracy in the former. This is particularly important when experimental results are provided without uncertainty estimates, as may happen with archival data generated for other purposes.

In the context of T_g predictions, we addressed the task of validating simulated results against experimental counterparts as a function of molecular weight M_n, i.e., the polymer length. This quantity is exactly controlled in simulations but unknown in experiments, so additional measurements are required to characterize it. For the case under consideration, two independent techniques were used to determine M_n, but we were only provided one measurement per sample-technique combination, for a total of two measurements per sample. Importantly, a single measurement is insufficient to determine uncertainty in a technique, as are two per sample if the corresponding uncertainties are both different and unknown. Thus, our main task, which amounted to estimating uncertainties in all experimental M_n values, seemed intractable.

The main idea that led to a breakthrough in this case was the assumption that the uncertainty in M_n is fixed (albeit unknown) for each measurement protocol, so that an uncertainty in the mean value per sample is also fixed. Stated mathematically, we take h_i and g_i to be the estimates of M_n values associated with the two measurements of the *i*th sample and postulate models of the form

$$h_i = M_n(i) + \mathcal{N}_i(0, {\sigma_h}^2)$$
$$g_i = M_n(i) + \mathcal{N}_i(0, {\sigma_g}^2)$$

where $\mathcal{N}(0,*)$ is a normal random variable with mean zero and variance $*$, and $M_n(i)$ is the true molecular weight. Note that σ_h and σ_g are unknown, although they only depend on the experimental protocol. In this case, it is possible to show that

$$m_i = (h_i + g_i)/2$$
$$\sigma^2 = \frac{1}{N}\sum_{i=1}^{N}(h_i - m_i)^2 + (g_i - m_i)^2$$

are unbiased and consistent estimates of the true mean $M_n(i)$ and uncertainty $({\sigma_h}^2 + {\sigma_g}^2)/4$ as the number of samples $N \to \infty$. Note that σ^2 is the uncertainty in the experimentally determined estimate m_i, which is what we seek. Estimating this quantity is equivalent to characterizing the spread in molecular weights shown Figure 44.

Having determined these molecular weights (and corresponding experimental T_g values), we were able to demonstrate that the simulated and experimental predictions were consistent to within the uncertainties computed for each. Ultimately, we used these results to test the validity of the well-established Fox-Flory model for polypropylene, a commercially important plastic. These results are discussed in more detail in a manuscript under review [6].

In addition to these more basic research tasks, we have also been engaging the MD community in an effort to better communicate best-practices for MD and UQ thereof. To this end, P. Patrone and A. Dienstfrey have published an invited book chapter on UQ of MD for the series *Reviews in Computational Chemistry* [7]. The chapter provides a tutorial on basic UQ tools to graduate-level modelers learning MD. Moreover, Patrone was involved in a collaborative effort to write a best-practices document for uncertainty quantification of molecular dynamics, which has been published in the new journal *LiveCoMS* [8]. Future work aims to extend these methods to other material properties and continue technology transfer activities.

[1] S. Christensen and J. Senger. Distortional Matrix of Epoxy Resin and Diamine. U.S. Patent 7,745,549 B2, filed December 20, 2006, issued June 29, 2010.

[2] S. Christensen and J. Senger. Distortional Matrix of Epoxy Resin and Diamine. U.S. Patent 7,985,808 B2, filed April 23, 2010, issued July 26, 2011.

[3] V. Sundararaghavan and A. Kumar. Molecular Dynamics Simulations of Compressive Yielding in Cross-Linked Epoxies in the Context of Argon Theory. *International Journal of Plasticity* **47** (2013), 111-125.

[4] P. N. Patrone, A. J. Kearsley, and A. Dienstfrey. The Role of Data Analysis in Uncertainty Quantification: Case Studies for Materials Modeling. In *Proceedings of the 2018 American Institute of Aeronautics and Astronautics SciTech Forum* (AIAA SciTech 2018), Kissimmee, Florida, January 8-12, 2018. DOI: 10.2514/6.2018-0927

[5] Gerhard Goldbeck, *The Economic Impact of Molecular Modelling: Impact of The Field on Research, Industry, And Economic Development.* Goldbeck Consulting Ltd., St. John's Innovation Centre, Cambridge, UK, 2012.

[6] P. N. Patrone, P. Brant, J. Younker, D. J. Crowther, C. J. Ruff, M. K. Ng, M. Vadlamudi, and J. E. Lee. Revisiting Fox-Flory: Detailed Study of the Glass-transition Temperature for Polypropylene Systems, in review.

[7] P. Patrone and A. Dienstfrey. Uncertainty Quantification for Molecular Dynamics. *Reviews in Computational Chemistry* **31** (2018). DOI: 10.1002/9781119518068.ch3

[8] A. Grossfield, P. N. Patrone, D. R. Roe, A. J. Schultz, D. Siderius, and D. M. Zuckerman. Best Practices for Quantification of Uncertainty and Sampling Quality in Molecular Simulations. *LiveCoMS* **1** (2018), 1-24. DOI: 10.33011/livecoms.1.1.5067

Modeling of Emulsion Stability using a Diffuse Interface Model

Sean Colbert-Kelly
Geoffrey McFadden
Trevor Keller (NIST/MML)
Frederick Phelan, Jr. (NIST/MML)

An outstanding problem in computational physics that arises in emulsion science is the modeling of binary emulsions stabilized by a surfactant. The amphiphilic structure of surfactants results in their migration to the fluid interface in a binary mixture [1]. In general, this alters the interfacial tension, interfacial viscosity and diffusion between the two phases, leading to greater emulsion stability. The lowering of the interfacial tension between the two fluids generates gradients in the surfactant concentration on the drop surface under flow, which, in turn, introduces Marangoni forces that alter drop shape, breakup, and coalescence dynamics [2]. The altering of the stability, equilibrium properties, and droplet dynamics of the mixture due to surfactants govern the long-time stability of emulsions. Although surfactants are very low in overall concentration, they have a dominant effect at the interface, which makes the modeling problem challenging.

The goal of this project is to develop an emulsion model that simulates the long-term stability of a predominantly binary fluid system stabilized by a

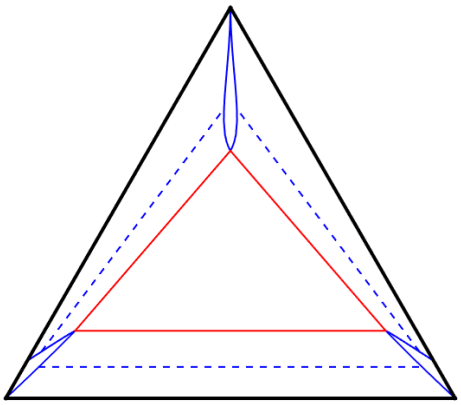

Figure 45. *A Gibbs triangle (solid black lines) depicting the concentrations of equilibrium phases of the ternary system for the free energy **G** with W = 1.75. Mole fractions are represented along the sides of the Gibbs triangle. The blue solid curves in each corner of the Gibbs triangle delimit the extent of single phases, with a surfactant phase near the top corner and the two fluid phases at the bottom two corners. Tie lines (dashed blue lines) that connect edges of the blue regions represent two-phase equilibria. A region of three-phase equilibria (red triangle) is delimited by the three vertices of the blue single-phase regions.*

surfactant. We take into consideration the effect that the composition of each component in the emulsion has on viscosity, as well as the relationship between the viscosity and the diffusion coefficients in the surfactant phase in the mathematical description of the system.

In this study, a diffuse interface model is formulated to investigate binary emulsions with a ternary surfactant component. This formulation extends previous models [3] for the free energy of two-phase systems to include a third stabilizing surfactant phase, resulting, for example, in a modified three-phase Ginzburg-Landau formulation. Many of these models represent the two-phase fluid in terms of a conserved order parameter φ, with $\varphi \in [-1,1]$, where $\varphi = -1$ represents one phase and $\varphi = 1$ represents the second. In this work the surfactant phase is added by introducing a second conserved order parameter ψ, with $\psi \in [0,1]$, where $\psi = 0$ represents the surfactant-free system. The isothermal free energy density is then a double well function of both φ and ψ, $G = G(\varphi, \psi)$. The Ginzburg-Landau free energy functional is written as an integral of $G(\varphi, \psi)$ plus a gradient energy term in φ, where the gradient energy coefficient, $(\kappa - \varepsilon\psi)$, is taken to depend on ψ in order to introduce a surface energy that depends on the level of surfactant.

To aid in the physical interpretation of the model, the order parameters can be re-expressed in terms of an equivalent ternary alloy system, letting X_1 and X_2 represent mole fractions of the majority species composing the two fluid phases and X_3 representing the mole fraction of the surfactant, with $X_1 + X_2 + X_3 = 1$ at each point in the system. The relation between the order parameters and the mole fractions are given by [1]

$$X_1 = \frac{(1-\varphi)(1-\psi)}{2}, \quad X_2 = \frac{(1+\varphi)(1-\psi)}{2}.$$

The properties of such models can be analyzed by means of ternary phase diagrams that represent the equilibrium phases supported by each model. An example of a phase diagram that includes regions of single-phase equilibria, two-phase equilibria, and three phase equilibria for the free energy $G(\phi, \psi)$ is given in Figure 45.

Governing Equations. The hydrodynamic equations that govern this system represent a fundamental diffuse interface model for the flow of two macroscopically immiscible viscous, incompressible Newtonian fluids with the same densities [4], with the addition of a surfactant component. This system consists of equations that govern the flow dynamics, which are the conservation of momentum and conservation of mass. The system also includes equations that govern the concentration dynamics, which are species balance equations for the two-phase fluid and surfactant components, respectively. The density and viscosity distributions both depend on the densities and viscosities of the bulk components. By re-expressing the governing equations in terms of the ternary system X_1, X_2 and X_3, the interfacial viscosity in this system can incorporate the effects from surfactant concentration explicitly.

To complete the model, dependence of the diffusion coefficients on composition and viscosity are introduced. Since surfactants migrate to the interface and stabilize emulsions, an increase in surfactant concentration at the interface should decrease the diffusion of the two-phase fluid across the interface. Using the Stokes-Einstein relation, it can be argued that the diffusion coefficients, D_ϕ and D_ψ, are inversely proportional to the viscosity.

Results. In studying the effects of the model on emulsion stability, the average domain size is defined as

$$L(t) = 2\pi \sqrt{\frac{1}{< k_x{}^2 >} + \frac{1}{< k_y{}^2 >}}$$

where $< k_i^2 >$ is the second-moment of the structure factor in the i-th direction. Plotting the quantity $L(t)$ allows us to determine if the emulsion is stabilized, i.e., if no growth of domain size is observed after a particular time.

The left-hand plot in Figure 46 depicts the average domain size as a function of time, where the viscosity has no dependence on the interfacial viscosity. The ratio ε/κ is increased from 0.1 to 0.7. This graph shows that the growth of the domain slows down with the introduction of surfactant in the system but does not stabilize. This observation suggests that introducing a surfactant component alone does not lead to emulsion stability via surface tension. The right-hand plot in Figure 46 shows

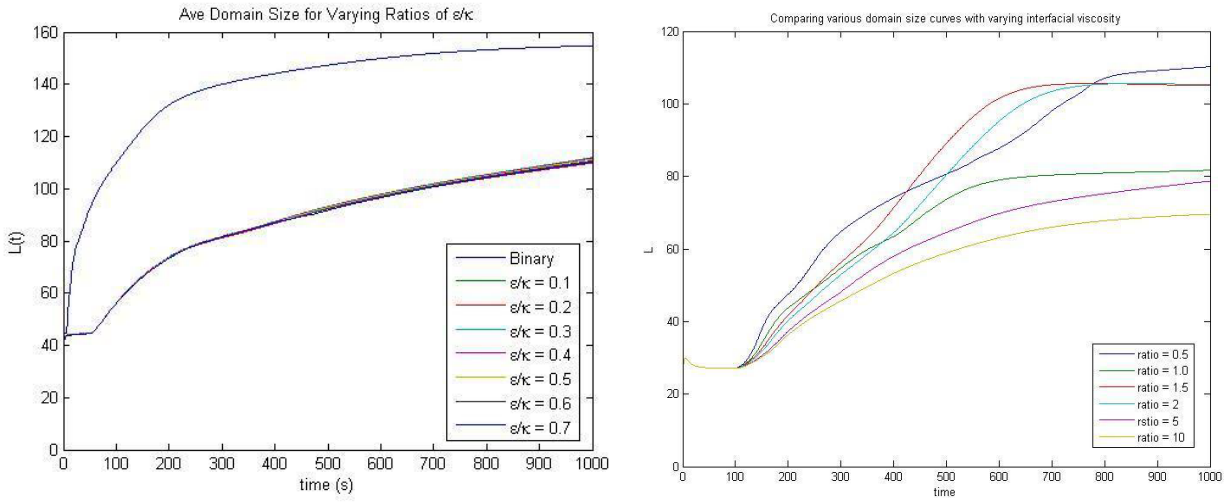

Figure 46. *Left: The average domain size L(t) as a function of time while increasing the ratio between* $\boldsymbol{\varepsilon}$ *and* $\boldsymbol{\kappa}$ *with the viscosity varying by mole fraction values only. Right: The average domain size L as a function of time for increasing values of the ratio* η_1/η_2 *of the viscosities in the bulk phases.*

the average domain size as a function of time, with the ratio η_1/η_2 of bulk viscosities increasing from 0.5 to 10.

Expressing the phase field equations as a ternary system allows explicit representation of the effects of surfactant concentration on the viscosity and diffusion coefficients. This formulation is expected to enable modeling of stable emulsions and the examination of droplet dynamics. Furthermore, the inclusion of simple velocity fields that influence droplet dynamics is planned, focusing on the effect of the flows on drop size distributions.

[1] S. Engblom, M. Do-Quang, G. Amberg, and A.-K. Tornberg. On Diffuse Interface Modeling and Simulation of Surfactants in Two-Phase Fluid Flow. *Communications in Computational Physics* **14**:4 (2013), 879-915.

[2] J. T. Schwalbe, F. R. Phelan, Jr., P. M. Vlahovska, and S. D. Hudson. Interfacial Effects on Droplet Dynamics in Poiseuille Flow. *Soft Matter* **7** (2011), 7797–7804.

[3] C.-H. Teng, I.-L. Chern, and M.-C. Lai. Simulating Binary Fluid-surfactant Dynamics by a Phase Field Model. *Discrete and Continuous Dynamical Systems Series B* **17**:4 (2011), 1289–1307.

[4] P.C. Hohenberg and B.I. Halperin. Theory of Dynamic Critical Phenomena. *Reviews of Modern Physics* **49**:3 (1977), 435—479.

The Effect of Vacancy Creation and Annihilation on Grain Boundary Motion

Geoffrey McFadden
Yuri Mishin (George Mason University)
William Boettinger (NIST MML)

Many important applications in materials science involve the interaction of stress and grain boundary behavior in crystalline solids. A crystalline solid typically consists of grains with given crystal orientations that are separated by grain boundaries where the orientation changes. Typical grain sizes can range from hundreds of micrometers to large single crystals that can be on the order of centimeters.

A common technological problem in the electronics industry is that when metallic or semiconductor grains are subject to lateral mechanical stresses, diffusion along the grain boundary can lead to “whiskers’’ that can extend normally to a substrate and provide unwanted electrical connections between neighboring components (see Figure 47). Often whiskers can be prevented by the addition of various components to the substrate, such as lead, but these additives can be undesirable for environmental reasons. In particular, lead-free solder commonly has a high composition of tin, which is prone to the whisker development in high-stress conditions.

Modeling whisker growth involves the derivation of governing equations that couple the effects of mechanical stress and compositional diffusion in a multi-grain geometry. Of particular interest is the development of appropriate boundary conditions that apply at moving grain boundaries. In previous research such derivations

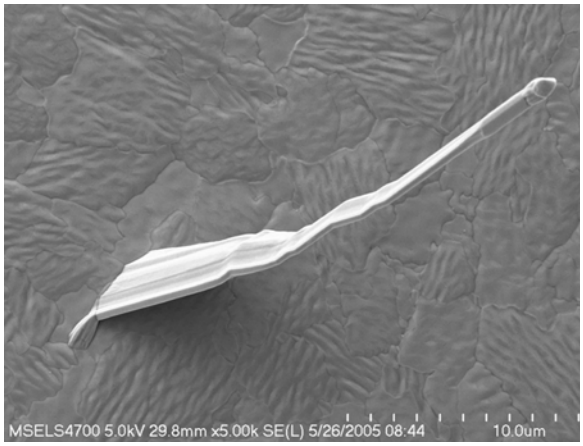

Figure 47. *Tin whisker growing on a stressed substrate.*

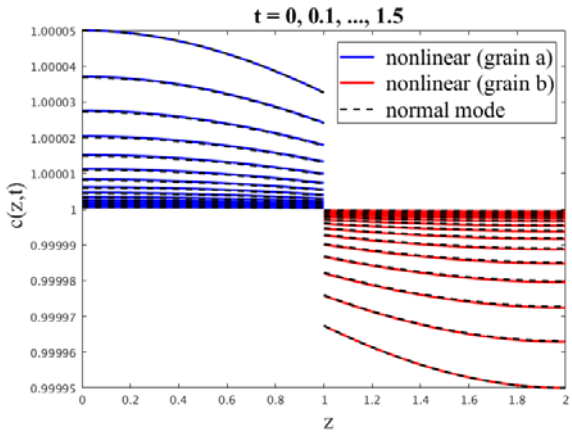

Figure 48. *Comparison of vacancy concentration profiles at various times [4]. The diffusion takes place in a bi-crystal, with nonlinear simulation results shown as the solid blue and red curves, and corresponding normal mode solutions shown as dashed curves. The concentration is discontinuous at the grain boundary (which is fixed in these computational coordinates).*

were carried out by using positive entropy production arguments that are based upon the second law of thermodynamics [1]. The resulting boundary conditions contain kinetic coefficients that relate vacancy diffusion across grain boundaries to thermodynamic driving forces such as jumps in chemical potential, and also include the effects of sources or sinks of vacancy concentrations at the grain boundary and their effect on conditions of thermodynamic equilibrium at the interface.

Recent research in this area has consisted of numerical simulations and theoretical stability studies for one-dimensional bi-crystals that illustrate the effects of the grain-boundary boundary conditions [2]. The motion of grain boundaries is simulated using a mapping to a fixed computational domain which is computed along with the evolution of the diffusion fields from various initial conditions (see Figure 48). The dynamics can also be studied analytically by considering small-amplitude perturbations to equilibrium states which can described by a normal mode analysis of the linearized governing equations, illustrating the roles played by the various terms in the boundary conditions.

Future work is anticipated to include the effects of surface energy and surface stress in curved geometries during grain growth, as well as the implementation of related phase-field models [3] that could aid in the description of whisker growth.

[1] Y. Mishin, G. B. McFadden, R. F. Sekerka, and W. J. Boettinger. Sharp Interface Model of Creep Deformation in Crystalline Solids. *Physical Review B* **92** (2015) 064113. DOI: 10.1103/PhysRevB.92.064113

[2] G. B. McFadden, Y. Mishin, and W. J. Boettinger, The Effect of Vacancy Creation and Annihilation on Grain Boundary Motion. In preparation.

[3] Y. Mishin, J. A. Warren, R. F. Sekerka, and W. J. Boettinger. Irreversible Thermodynamics of Creep in Crystalline Solids. *Physical Review B* **88** (2013) 184303. DOI: 10.1103/PhysRevB.88.184303

Shear Localization in Bulk Metallic Glasses

Timothy Burns

Metallic glasses (MGs) are produced by cooling alloy melts under conditions that prevent crystallization. Also known as amorphous alloys and liquid metals, these materials have excellent physical and chemical properties, such as high toughness and corrosion resistance, but the original specimen sizes that have been achievable (typically on the order of microns) have severely restricted their study and application.

These limitations were overcome by the development of bulk metallic glasses (BMGs), which were produced under lower critical cooling rates (<100 K/s). BMGs have received considerable attention during the last two decades, due to their high strength and very large resilience, which is the capacity of a material to absorb energy when it is deformed elastically; this energy can be recovered upon unloading [1-3]. Microscopically, BMGs are different from common polycrystalline metallic alloys, because their atoms do not assemble on a crystalline lattice. Instead, they have an amorphous microstructure, which lacks the dislocations and associated slip planes that are found in polycrystalline metallic alloys. This glassy structure makes these materials candidates for important applications, including medical devices such as prosthetics [2, 3].

A major problem with BMGs is the tendency of these materials to deform with a localized shear-banded

$$\rho\,\partial v/\partial t = \partial \tau/\partial y \qquad \text{(Momentum)}$$

$$\partial \gamma/\partial t = \partial v/\partial y \qquad \text{(Compatibility)}$$

$$\rho\, C_p\, \partial \theta/\partial t = k\,\partial^2\theta/\partial y^2 + A\tau\, f(\xi,\theta,\tau) \qquad \text{(Energy)}$$

$$\partial \xi/\partial t = D\,\partial^2\xi/\partial y^2 + g(\xi,\theta,\tau) \qquad \text{(Free Volume)}$$

$$\partial \gamma^p/\partial t = f(\xi,\theta,\tau) \qquad \text{(Plastic Flow)}$$

$$\partial \tau/\partial t = \mu\,(\partial\gamma/\partial t - \partial\gamma^p/\partial t) \qquad \text{(Force Balance)}$$

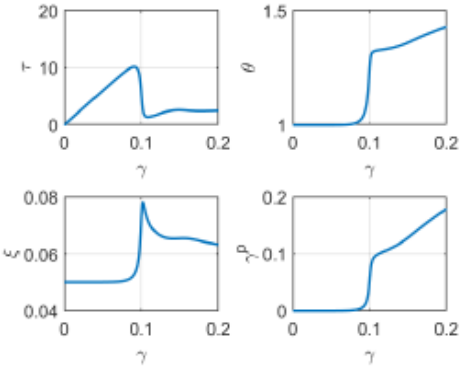

Figure 49. *(left) Continuum model of shear flow in a BMG. (right) Time–dependent homogeneous simple shear solution at a constant strain rate of* $\mathbf{2 \times 10^{-4}}$*/s.*

structure under high stress [1-5]. Several research groups have been investigating this problem, because this shear localization can render BMGs mechanically unstable [3-11]. Some theoretical studies have argued that this strain localization is controlled not by rapid heating, as is the case with adiabatic shear band formation in polycrystalline metals [12, 13], but rather by a change in the concentration of free volume in the material [8, 9]. Others argue that it is controlled by a combination of heating and free volume effects [7]. Whatever controls the localization, there is some interesting experimental work which has shown that these localized regions can still be hot [10].

A number of studies of shear band formation in BMGs mimic the analysis that has been done to study the formation of adiabatic shear bands in polycrystalline metallic alloys. This is done by analyzing the linear stability of a geometrically simple homogeneous shear flow of a BMG [4, 6-9]. Just as in the polycrystalline case, there are two main difficulties with this approach. First, a physics-based model of the response of the material to shear loading is required. In the BMG case, there is a generally accepted material response model which has been proposed by Spaepen [10]. This includes a function $f(\xi,\theta,\tau)$ describing the irreversible part of the strain rate, and a function $g(\xi,\theta,\tau)$ that governs the creation or annihilation of free volume; see Figure 49(left). Here, ξ is the scaled free volume, θ is the scaled temperature, and τ is the scaled shear stress, which is homogeneous. Second, because the shear stress depends upon the shear strain, the reference shear flow solution is time-dependent; see Figure 49(right), in which the abscissa γ is scaled time t times the constant strain rate. As a result, the matrix of the linearization of the model equations about the reference solution is also time-dependent.

An approach that has frequently been used in this field is to "freeze'' the coefficients in the time-dependent matrix at a fixed reference time, and to study the characteristic equation associated with the eigenvalues of the matrix [6]. Another approach is to make physical arguments about the behavior of the coefficients in the perturbed equations [4]. A better method is to study the problem computationally. By computing the perturbed equations together with the homogeneous shear solution, the conclusions of several authors about the behavior of the perturbed equations are shown to be incorrect. In particular, numerical simulations show that there is not a critical frequency for which the perturbed equations are unstable; see Figure 49 and Figure 50. Furthermore, they show that the controlling term is $\partial f/\partial \xi$, the rate of change of plastic strain with respect to free volume. In this sense, the instability is driven by the free volume, not the temperature. However, as depicted on the right in Figure 50, there is a large increase in the perturbed temperature associated with the growth in the free volume, so that the associated shear bands are hot [10]. A paper on this work is in preparation.

[1] M. F. Ashby and A. L. Greer. Metallic Glasses as Structural Materials. *Scripta Materialia* **54** (2006), 321–326.

[2] E. Axinte. Metallic Glasses from "Alchemy" to Pure Science: Present and Future of Design, Processing and Applications of Glassy Metals. *Materials and Design* **35** (2012), 518–556.

[3] M. M. Trexler and N. N. Thadhani. Mechanical Properties of Bulk Metallic Glasses. *Progress in Materials Science* **55** (2010), 759–839.

[4] Y. F. Gao, B. Yang and T. G. Nieh. Thermomechanical Instability Analysis of Inhomogeneous Deformation in Amorphous Alloys. *Acta Materialia* **55** (2007), 2319–2327.

[5] E. S. Park. Understanding of the Shear Bands in Amorphous Metals. *Applied Microscopy* **45**:2 (2015), 63–73.

[6] L. H. Dai, M. Yan, Y. F. Liu, and Y. L. Bai. Adiabatic Shear Banding Instability in Bulk Metallic Glasses. *Applied Physics Letters* **87** (2005), 14196-1–3.

[7] L. H. Dai and Y. L. Bai. Basic Mechanical Behaviors and Mechanics of Shear Banding in BMGs. *International Journal of Impact Engineering* **35** (2008), 704–716.

[8] R. Huang, Z. Suo, J. H. Prevost, and W. D. Nix, Inhomogeneous Deformation in Metallic Glasses. *Journal of the Mechanics and Physics of Solids* **50** (2002), 1011–1027.

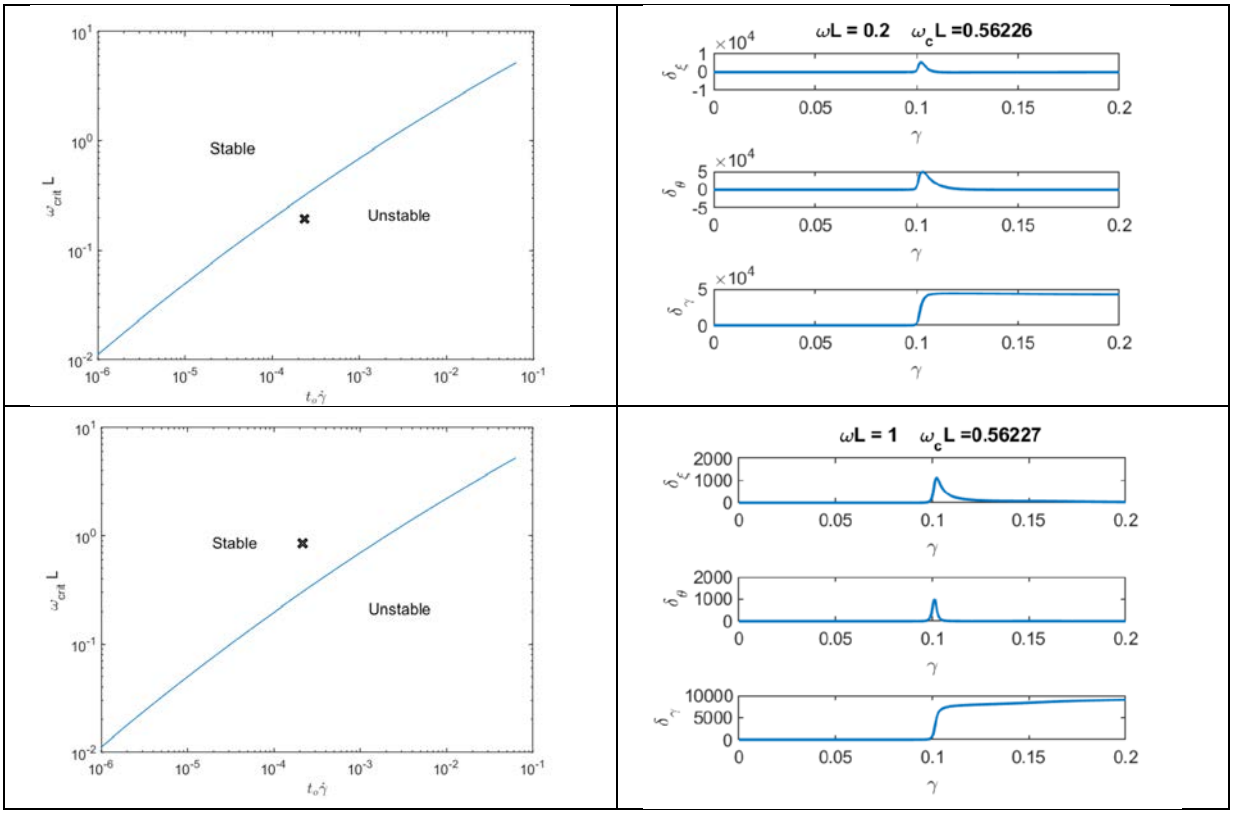

Figure 50. *(left) Stability curve of Gao, Jiang and Ni [7]; x denotes scaled wavelength. (right) Numerical analysis of perturbed homogeneous solution indicates that the homogeneous solution is unstable in both cases.*

[9] M. Q. Jiang and L. H. Dai, On the Origin of Shear Banding Instability in Bulk Metallic Glasses. *Journal of the Mechanics and Physics of Solids* **57** (2009), 1267–1292.

[10] F. Spaepen. Must Shear Bands Be Hot? *Nature Materials* **5** (2006), 7–8.

[11] F. Spaepen. A Microscopic Mechanism for Steady State Inhomogeneous Flow in Metallic Glasses. *Acta Metallurgica* **25** (1977), 407–415.

[12] T. J. Burns. Approximate Linear Stability Analysis of a Model of Adiabatic Shear Band Formation. *Quarterly of Applied Mathematics* **43** (1985), 65–84.

[13] M. A. Davies and T. J. Burns. Thermomechanical Oscillations in Material Flow During High–speed Machining. *Philosophical Transactions of the Royal Society of London, A* **359** (2001), 821–846.

Approximate Solution of the Abel Equation

Timothy Burns
Bert Rust

We are revising our method [1] for obtaining an approximate solution of an ill-posed inverse problem, which is part of a long-term research program in the modeling and simulation of high-speed machining operations [2, 3]. The problem can be described as follows: Given a discrete set of temperature measurements on the face of a cutting tool, which are contaminated by random experimental noise, with estimated 2σ error bars at each data point, determine the flow stress in the material near the tool face. The mathematical problem is to determine the *source* function $f(x)$ given a smooth *data* function $g(x)$, that is defined only by a finite set of data measurements, which have been contaminated by noise, with known statistical properties, in Abel's integral equation

$$g(x) = I_a^{\mu} f(x) := \frac{1}{\Gamma(\mu)} \int_a^x (x-y)^{\mu-1} f(y)\, dy$$

Here, $a \le x \le b, 0 < \mu < 1$, and Γ is Euler's Gamma function. We have developed a finite-dimensional spectral projection method for separating signal from noise

in $g(x)$. The method determines a smooth, closed-form regularization of the data function $g(x)$. Key assumptions are that the residual corresponding to the noise is a realization of a white noise time series, and the measurements are from a process which preferentially damps high-frequency content in the data. Our method also provides closed-form estimates of the derivative, $f(x) = D_a g := dg/dx$, and fractional derivative of $g(x)$,

$$f(x) = D_a^{\mu} g(x) := \frac{1}{\Gamma(1-\mu)} \frac{d}{dx} \int_a^x (x-y)^{-\mu} g(y)\, dy$$

which are based on known singular value decompositions of the associated compact Volterra integral operators on and into weighted L_2 spaces. In our revision of the method, we take advantage of a technique for solving the Volterra integral equation of the first kind

$$g(x) = \int_a^x f(y)\, dy, \quad -\infty < a \le x \le b < \infty$$

which is based on a novel singular value decomposition of the associated Volterra integral operator [4].

[1] T. J. Burns and B. W. Rust. Closed-Form Projection Method for Regularizing a Function Defined by a Discrete Set of Noisy Data and for Estimating its Derivative and Fractional Derivative. arXiv:1805.09849v1 [math.NA], 24 May 2018.

[2] S. P. Mates, R. L. Rhorer, E. P. Whitenton, T. J. Burns, and D. Basak. A Pulse-Heated Kolsky Bar Technique for Measuring Flow Stress of Metals Subjected to High Loading and Heating Rates. *Experimental Mechanics* **48** (2008), 799–807.

[3] T. J. Burns, S. P. Mates, R. L. Rhorer, E. P. Whitenton, and D. Basak. Inverse Method for Estimating Shear Stress in Machining. *Journal of the Mechanics and Physics of Solids* **86** (2016), 220–236.

[4] Z. Zhao, Z. Meng, and G. He. A New Approach to Numerical Differentiation. *Journal of Computational and Applied Mathematics* **232** (2009), 227-239.

Mathematics of Uncertainty in Engineering Reliability

Jeffrey T. Fong
James J. Filliben (NIST ITL)
N. Alan Heckert (NIST ITL)
D. D. Leber (NIST ITL)
Stephen Freiman (NIST MML)
Li Ma (NIST MML)
Pedro V. Marcal (MPACT Corp.)
Robert Rainsberge (XYZ Scientific)
Stephen R. Doctor (PNNL)
Ned Finney (Duke Energy)
Marvin Cohn (Intertek)

To ensure the safe operation of an engineering structure or system, be it a chemical processing plant, a nuclear power plant, a jet airliner, or a steel bridge, engineers need to design, manufacture, assemble and install, test in laboratories and in the field, and then operate with continuous monitoring and scheduled maintenance for all necessary components and connections that are required to make a system work as a whole without failure. This requires that one estimate the reliability of all components and connections and construct a fault tree to evaluate the system reliability of the whole structure or system.

In such work, two categories of problems of uncertainty come up that require independent study, namely, (i) Uncertainty in Loads, and (ii) Uncertainty in Resistance. In this project, we restrict ourselves to the study of category (ii), Uncertainty in Resistance. More specifically, we address three types of uncertainty that are essential for predicting the reliability of an ageing component as it operates with a known defect. The three types of uncertainty are: (1) Material Property Sampling Uncertainty (Global), (2) Laboratory-to-Full-Size Scaling Uncertainty (Global), and (3) Life Prediction Uncertainty (Local) based on Continuous Monitoring and Damage-Physics Assessment of a Detected Small Defect. To enable continuous, and autonomous monitoring, we have written a code in Python to address type (3) uncertainty and linked it to a crack monitoring code to yield an early warning signal for an aging component in service with a known small defect

The accurate prediction of the ultimate fracture of a pipe with the detection of a small crack of irregular shape is accomplished using a sophisticated analysis code [1-3] that is attached to a structural health monitoring (SHM) program [4-8] capable of detecting and monitoring the growth of a small crack in a pipe either continuously or periodically with short intervals [9-12]. We use the concept of a topological crack that mimics a real crack of irregular shape [13-14] and a powerful meshing software named TrueGrid [15-16] that can remesh efficiently the region around a growing crack of

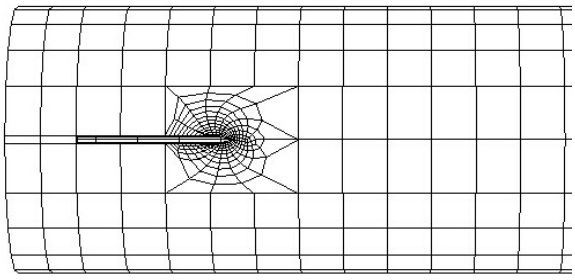

Figure 51. *Finite element mesh in the neighborhood of a small crack with (a) an all-hexagonal-element-and-optimally-dense-at-crack-tip design, and (b) an automatic re-meshing capability such that when the initial crack length, a_i , is increased to, say, $a_i + d_1$, with d_1 not necessarily collinear with the initial crack, the crack-tip mesh design follows the new crack with the increment, d_1 , as shown in Figure 52.*

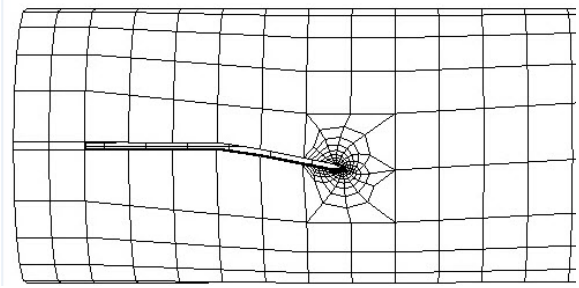

Figure 52. *Finite element mesh in the neighborhood of a small crack of initial length, a_i , and a first increment of d_1 not collinear with the initial crack but with the cracl-tip mesh design same as the initial crack length. Such re-meshing capability is automatic and independent of the angle of orientiation of the increment.*

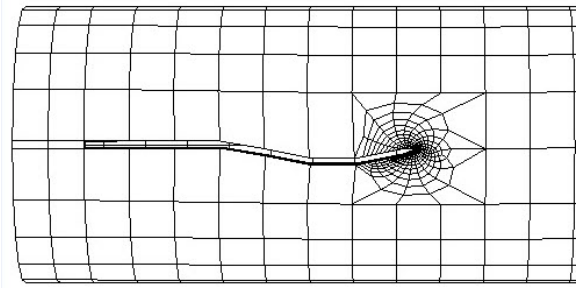

Figure 53. *Finite element mesh in the neighborhood of a small crack of initial length, a_i , and two increments of d_1 and d_2 not collinear with any of its preceding increment but with the crack-tip mesh design same as the initial crack. Such re-meshing capability is automatic and independent of the angle of orientiation of any new increment. Such crack of an irregular shpae is called a topological crack, and the algorithm that generates the optimally-dense-crack-tip mesh is furnished by a finite-element-pre-processor named TrueGrid and its commands based on geometric and topological concepts.*

irregular shape. See Figure 51, Figure 52, and Figure 53. Based on this, we have developed a code that embeds two finite element analysis platforms to compute and predict the stress and crack geometry of a growing crack such that the crack growth exponent of an initial crude model is refined as more information on the crack advancement becomes available from the SHM code. Since the initial model is based information in a crack growth exponent database that is global in nature and contains large uncertainty, this approach allows us to learn from local crack growth information to obtain a field-based estimate of the appropriate crack growth exponent for a specific cracked pipe under monitoring. Such a code serves, therefore, as an early warning assistant to the SHM code with the ability to predict accurately the onset of the ultimate fracture of the pipe with uncertainty quantification. Such an approach is essential to the implementation of a new ASME Boiler and Pressure Vessel Section XI Division 2 Code named the "Reliability and Integrity Management (RIM) Code" [17-20].

[1] R. E. Neapolitan and X. Jiang. *Artificial Intelligence: with an Introduction to Machine Learning*, 2nd ed. Chapman and Hall/CRC, 2018.

[2] T. Boobier. *Advanced Analytics and AI: Impact, Implementation, and the Future of Work*. Wiley, 2018.

[3] F. Chollet. *Deep Learning with Python*. Manning Publications, 2017.

[4] N. E. Dowling. *Mechanical Behavior of Materials*, 2nd ed. Prentice Hall, 1999.

[5] H. Tada, P.C. Paris, and G. R. Irwin. *The Stress Analysis of Cracks Handbook,* 3d ed. Wiley, 2000.

[6] J. T. Fong, O. F. Hedden, J. J. Filliben, and N. A. Heckert. A Web-based Data Analysis Methodology for Estimating Reliability of Weld Flaw Detection, Location, and Sizing. In *Proceedings of the 2008 ASME Pressure Vessels & Piping Division Conference*, July 27-31, 2008, Chicago, IL, PVP2008-61612.

[7] J. T. Fong, J. J. Filliben, and N. A. Heckert. Robust Engineering Design for Failure Prevention. In *Proceedings of the 2008 ASME Pressure Vessels & Piping Division Conference*, July 27-31, 2008, Chicago, IL, PVP2008-61602.

[8] D. Frolov. How Machine Learning Empowers Models for Digital Twins. *BENCHMARK, the International Magazine for Engineering Designers and Analysts from NAFEMS*, July 2018, 48-53.

[9] J. T. Fong, W. F. Ranson III, E. I. Vachon, and P. V. Marcal. Structural Aging Monitoring via Web-based Nondestructive Evaluation (NDE) Technology. In *Proceedings of the 2008 ASME Pressure Vessels & Piping Division Conference*, July 27-31, 2008, Chicago, IL, PVP2008-61607.

[10] J. T. Fong, P. V. Marcal, O. F. Hedden, Y. J. Chao, and P. S. Lam. A Web-based Uncertainty Plug-in (WUPI) for Fatigue Life Prediction Based on NDE Data and Fracture Mechanics Analysis. In *Proceedings of the ASME 2009 Pressure Vessels & Piping Division Conference*, July 26-30, 2009, Prague, Czech Republic, PVP2009-77827.

[11] J. T. Fong and P. V. Marcal. A Dataplot-Python-Anlap (DPA) Plug-in for High Temperature Mechanical Property Databases to Facilitate Stochastic Modeling of Fire-Structural Interactions. In *Proceedings of the ASME 2009 Pressure Vessels & Piping Division Conference*, July 26-30, 2009, Prague, Czech Republic, PVP2009-77867.

[12] P. V. Marcal, J. T. Fong, and N. Yamagata. Artificial Intelligence (AI) Tools for Data Acquisition and Probability Risk Analysis of Nuclear Piping Failure Databases. In *Proceedings of the ASME 2009 Pressure Vessels & Piping Division Conference,* July 26-30, 2009, Prague, Czech Republic, PVP2009-77871.

[13] S. Osovski, A. Srivastava, L. Ponson, E. Bouchaud, V. Tvergaard, K. Ravi-Chandar, and A. Needleman. The Effect of Loading Rate on Ductile Fracture Toughness and Fracture Surface Roughness. *Journal of the Mechanics and Physics of Solids* **76** (2015), 20-46.

[14] J. T. Fong, N. A. Heckert, J. J. Filliben, and S. R. Doctor. Three Approaches to Quantification of NDE Uncertainty and a Detailed Exposition of the Expert Panel Approach Using the Sheffield Elicitation Framework. In *Proceedings of the 2018 ASME PVP Division Conference*, Prague, Czech Republic, July 15-20, 2018, PVP2018-84771.

[15] R. Rainsberger, J. T. Fong, and P. V. Marcal. A Super-Parametric Approach to Estimating Accuracy and Uncertainty of the Finite Element Method. In *Proceedings of the ASME 2016 Pressure Vessels & Piping Division Conference,* July 17-21, 2016, Vancouver, British Columbia, Canada, PVP2016-63890.

[16] R. Rainsberger, J. T. Fong, and P. V. Marcal. Application of an *a priori* Jacobian-based Error Estimation Metric to the Accuracy Assessment of 3D Finite Element Simulations. In *Proceedings of the 2018 ASME PVP Division Conference*, Prague, Czech Republic, July 15-20, 2018, PVP2018-84784.

[17] *ASME Boiler and Pressure Vessel Code, Section XI, Division 2 - Requirements for Reliability and Integrity Management (RIM) Program for Nuclear Power Plants.* November 11, 2018 Draft for Public Comment. American Society of Mechanical Engineers, New York, 2018.

[18] J. T. Fong, J. J. Filliben, N. A. Heckert, D. D. Leber, P. A. Berkman, and R. E. Chapman. Uncertainty Quantification of Failure Probability and a Dynamic Risk Analysis of Decision Making for Maintenance of Aging Infrastructure. In *Risk Based Approaches to Complex Systems* (P. V. Varde, R. V. Prakash, and N. S. Joshi, Eds.), Springer, 2018.

[19] J. T. Fong, N. A. Heckert, J. J. Filliben, and S. W. Freiman. A Multi-Scale Failure-Probability-based Fatigue or Creep Rupture Life Model for Metal Alloys *International Journal of Pressure Vessel Technology,* to appear.

[20] J. T. Fong, P. V. Marcal, R. Rainsberger, N. A. Heckert, and J. J. Filliben. Design of an Intelligent Python Code for Validating Crack Growth Exponent by Monitoring a Crack of Zig-Zag Shape in a Cracked Pipe. In *Proceedings of the 2019 ASME Pressure Vessels & Piping Division Conference,* July 27-31, 2019, San Antonio, TX, USA, PVP2019-93502, to appear.

High Performance Computing and Visualization

Computational capability continues to advance rapidly, enabling modeling and simulation to be done with greatly increased fidelity (e.g., higher resolution and more complex physics). However, doing so often requires computing resources well beyond what is available on the desktop. Developing software that make effective use of such high-performance computing platforms remains very challenging, requiring expertise that application scientists rarely have. And, as the hardware landscape continues to evolve, new algorithmic techniques must constantly be developed. We maintain such expertise for application to NIST problems. Such computations, as well as modern laboratory experiments, typically produce large volumes of data, which cannot be readily comprehended without some form of analysis. We are developing the infrastructure necessary for advanced interactive, quantitative visualization and analysis of scientific data, including the use of 3D immersive environments, and applying the resulting tools to NIST problems. One of our goals is to develop the 3D immersive environment into an interactive measurement laboratory.

Simulation of Dense Suspensions: Cementitious Materials

William George
Nicos Martys (NIST EL)
Clarissa Ferraris (NIST EL)
Steven Satterfield
Judith Terrill

A suspension is a collection of solid inclusions embedded in a fluid matrix. Suspensions play an important role in a wide variety of applications including paints, cement-based materials, slurries, and drilling fluids. Understanding the flow properties of a suspension is necessary in many such applications. However, measuring and predicting flow properties of suspensions remains a great scientific challenge. Suspensions can be quite complex, as the inclusions may have a wide range of shapes and a broad size distribution. Further complicating matters is that different matrix fluids may have quite disparate flow behavior. While the simplest type of matrix fluid is Newtonian, where the local stress is proportional to the shear rate, the matrix fluid can also be non-Newtonian, exhibiting quite complex behavior including shear thinning (viscosity decreases with shear rate), shear thickening (viscosity increases with shear rate), viscoelasticity (exhibiting both viscous and elastic properties), or even have a time dependent viscosity (thixotropic).

We have two on-going studies on the rheology of cementitious materials, which are dense suspensions in non-Newtonian matrix fluids.

SRMs for Mortar and Concrete. Rotational rheometers, devices that measure fluid properties such as viscosity, are routinely used for homogeneous materials such as oils, but their use on dense suspensions, such as concrete, is a relatively new phenomenon. Since measurements with rheometers involve flow in a complex geometry, it is important that they are calibrated with a well characterized standard reference material (SRM). We are developing such SRMs in collaboration with the NIST Engineering Laboratory.

NIST produced an SRM for cement paste (SRM 2492) as the first step in the development of a reference material for concrete rheometers. The second step, the development of an SRM for mortar (SRM 2493) was completed in the past year and is now available. The material properties of the mortar SRM, such as viscosity, could not be measured in fundamental units with certainty. Thus, simulation was used to determine the viscosity of the mortar. To obtain the necessary fidelity in the simulations, a high-performance computing facility was used. Results of these simulations were compared with physical experiments as validation.

We are currently developing the final SRM, for concrete, which we expect to be released in calendar year 2019. The concrete SRM will be comprised of the mortar SRM with the addition of suspended 10 mm diameter hard glass spheres. In support of this development, we are running a suite of simulations to determine the rheological properties of this SRM. As with the mortar SRM, the simulation will be used to certify the values of the concrete SRM material properties.

Flow of Dense Suspensions in Pipes. Understanding the flow of suspensions in pipes is important for a wide variety of applications. For example, in the construction industry, concrete is often placed by pumping it through extensive pipe systems. However, research on predicting the pumpability of concrete has been limited due to the heavy equipment and large amounts of material needed. Suspension flow is also important in the developing field of 3D additive manufacturing.

Predicting the flow of this complex fluid, which is composed of a non-Newtonian matrix fluid with suspended solid inclusions flowing under pressure, is challenging. Flow in these systems is also complicated by variety of phenomena such as slip at the wall and shear induced migration, which has only been studied for the simpler case of a suspensions with a Newtonian

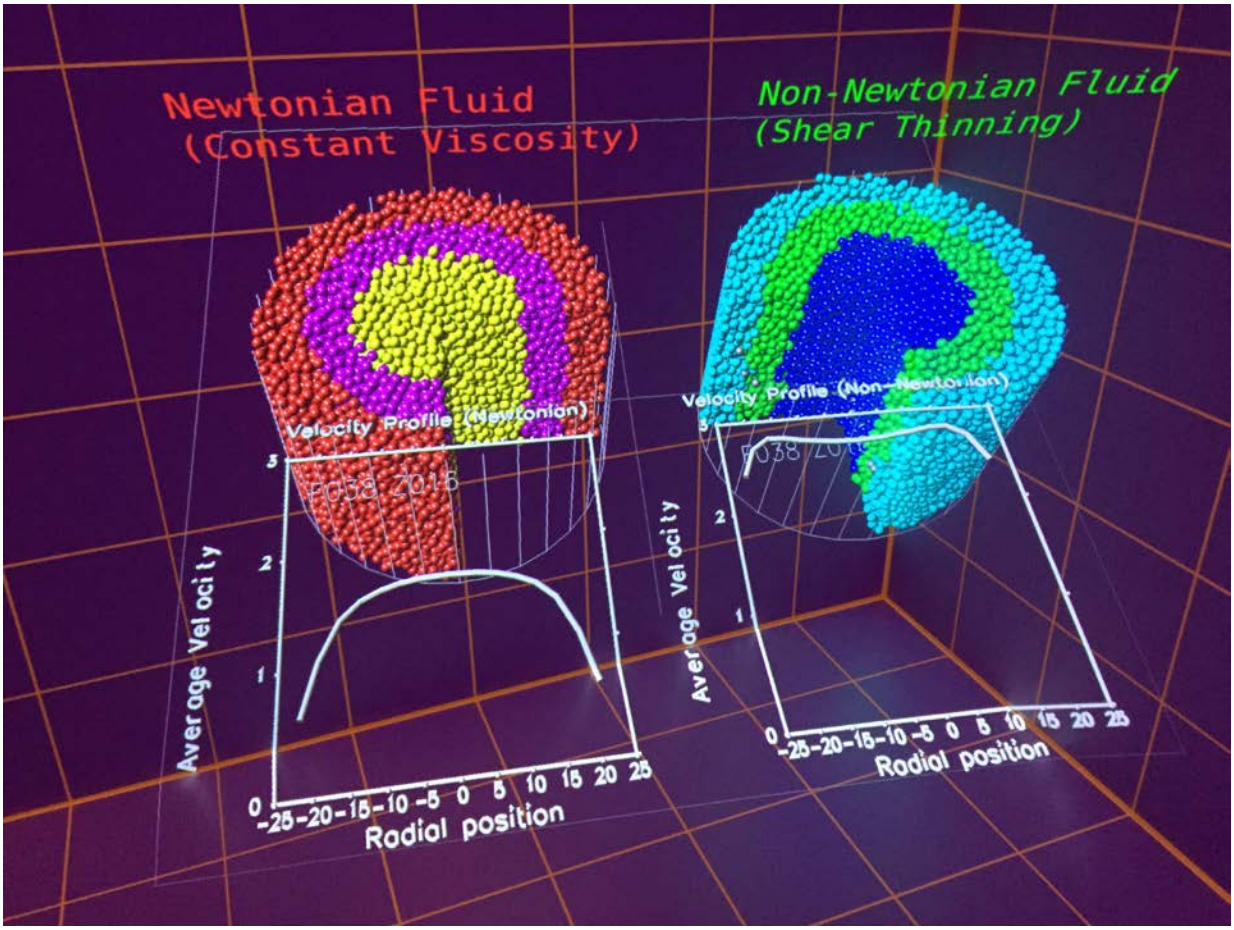

Figure 54. *A snapshot of two similar simulations showing the difference in the system velocity due primarily to slip at the wall.*

matrix fluid. A detailed discussion of this topic is available in a NIST Technical Note [1]. It is also the case, especially in the 3D additive manufacturing, that the placement of these materials is time sensitive, from the time the material is initially mixed to the time it is pumped and placed [2].

We have been conducting detailed simulations of the flow of suspensions through pipes to enable the development of predictive flow models and to advance measurement science in this field. Through quantitative analysis and visualization of results, we have gained insight into shear-induced migration and slip behavior in these systems. For example, Figure 54 shows a side-by-side comparison of identical systems with only the property of the matrix fluid changed, one Newtonian and the other non-Newtonian (shear thinning). Over the last year we have been conducting a suite of simulations of shear thinning and shear thickening suspensions, varying the properties of the matrix fluid and the driving force.

Studying the flow velocity fields as a function of driving force we have discovered a useful scaling relationship. Given that the matrix fluids have a viscosity, μ, that relates to the strain rate $\dot{\gamma}$ such that

$$\mu \propto \dot{\gamma}^n,$$

we have determined that the system velocity in the pipe, v, is related to the driving force, g, as

$$v \propto g^{1/(1+n)}.$$

So, for example, with a shear thinning matrix fluid with $n = -0.5$, we have

$$v \propto g^{1/(1-0.5)} = g^2$$

and with a matrix fluid which is shear thickening, with $n = 0.5$, we have

$$v \propto g^{1/(1+0.5)} = g^{2/3}$$

Notice that this scaling relation depends on the power-law behavior of the non-Newtonian matrix fluid. As a consequence, given a few measurements of the flow velocity versus the driving force of the suspension, one can determine the power law behavior of the suspension, and indeed we can then also determine the power law behavior of the matrix fluid.

Although our simulations have not yet completed, they appear at this time to confirm this model to within about 15 % accuracy. We will continue to examine this model in the coming year. We have presented preliminary results [3] and expect to complete this study this year and produce a final paper detailing our findings.

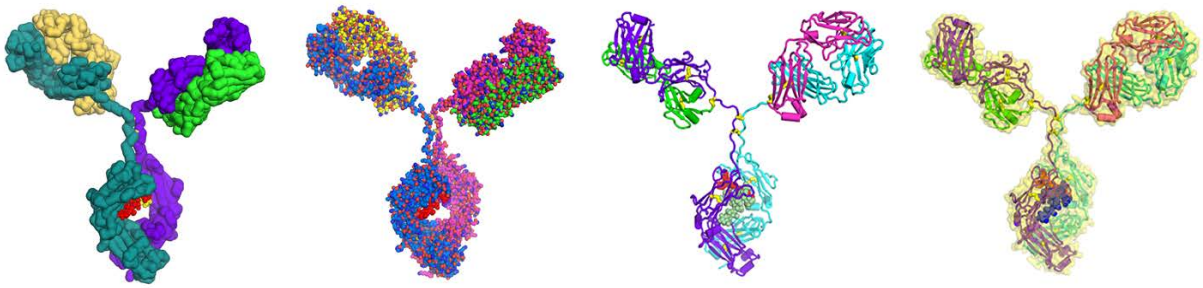

Figure 55. *Structure of the NIST Monoclonal Antibody Reference Material 8671.*

[1] M. Choi, C. F. Ferraris, N. S. Martys, V. K. Bui, H. R. Trey Hamilton, and D. Lootens. Research Needs to Advance Concrete Pumping Technology. NIST Technical Note 1866, 2015.

[2] S. Z. Jones, D. P. Bentz, N. S. Martys, W. L. George, and A. Thomas. "Rheological Control of 3D Printed Cement Paste." Digital Concrete 2018: First International Conference on Concrete and Digital Fabrication, Zurich Switzerland, September 9-12, 2018.

[3] N. S. Martys, W. L. George, S. G. Satterfield, and S. Z. Jones. "Computational Modelling of Suspension Flow in Pipes: Application to Cement Based Materials." 90th Annual Meeting of The Society of Rheology, Houston, TX October 14-18, 2018.

Monoclonal Antibodies Under High Shear

William George
Nicos Martys (NIST EL)
Steven Satterfield
Judith Terrill

Recent advances at the NIST Center for Neutron Research (NCNR) have enabled neutron scattering experiments for the study of the development of long-range structure and phase transitions under pressure driven flow conditions in a tube geometry. This capability was developed, in part, to study therapeutic proteins, such as monoclonal antibodies, as they flow under high shear rate, such as would be encountered during direct injection via a hypodermic needle.

Such direct injection is desired because it would simplify the delivery of these therapeutic proteins, which are currently only administered intravenously. However, since such injections can lead to shear rates on the order of 10^6/s there is concern that this could lead to structural degradation of the molecules. Even small distortions of the molecular structure could cause aggregation of the protein. The most dangerous potential consequence of such distortion and agglomeration is that the patient may develop an allergic reaction to the medication. Recorded fatalities have occurred where immunogenic response to such aggregates is suspected. For these reasons it is necessary for the pharmaceutical companies to demonstrate that the structure of protein therapeutics is not degrading before high shear rate delivery methods can be utilized.

In support of this research, we have begun extending the capabilities of our dense-suspension simulator, QDPD, to match the physical experiments being performed at the NCNR. Recent experiments are in good agreement with preliminary QDPD simulations of similar systems, that is, the flow of suspensions in a tube.

The extensions to QDPD will enable the simulation of suspensions of the NIST monoclonal antibody (NIST mAb) Reference Material (SRM 8671) shown in Figure 55. In collaboration with NCNR, the NIST Engineering Lab, and the NIST Material Measurement Lab, we will carry out a suite of simulations designed to determine the effect of the flexibility within monoclonal antibodies on the suspension's viscosity for a set of volume fractions and shear rates like that studied at NCNR.

In addition to the rheological studies, we will also modify QDPD to generate pertinent data from our NIST mAb simulations that will assist in the analysis of neutron scattering data from NCNR experiments on such systems. This is needed since experimental neutron scattering results so far have been shown to be difficult to interpret, primarily due to their complexity.

HydratiCA: A Parallelized Numeric Model of Cement Hydration

Judith Terrill
Wesley Griffin
Steve Satterfield
Jeffrey Bullard (NIST EL)

HydratiCA is a stochastic reaction-diffusion model of cement hydration. Hydration occurs when cement powder is mixed with water that subsequently transforms the paste from a fluid suspension into a hardened solid. This process involves complex chemical and microstructural changes. Developing a deep understanding of this process which would allow accurate prediction of the rates of these changes is a longstanding goal.

Computational modeling of cement hydration is challenging because it involves many coupled nonlinear rate equations that must be solved in a highly irregular three-dimensional spatial domain. HydratiCA addresses these challenges with a computational model that has several advantages over others. Parallelization of the model and visualization of the output are important components of this project. With parallelization we can simulate systems that are large enough to be realistic, avoid finite size effects, and complete the simulations in a reasonable amount of time. Visualization of the data produced by HydratiCA is important both for validation and for understanding of the results.

Several of the solid products of cement hydration, especially portlandite and ettringite, are crystals that have markedly anisotropic growth properties. Portlandite often grows in the shape of large but thin plates while ettringite and secondary gypsum grow as long needles. These anisometric shapes have a significant influence on the setting time and mechanical properties of concrete at early times because they change the rigidity percolation threshold that marks the transition of the material from a fluid suspension to a solid. With most of the important chemical kinetic mechanisms having been simulated and validated with HydratiCA, this year we focused on incorporating this crystal growth anisotropy into the model.

As a first approximation to modeling the most important growth shapes, we defined a *growth aspect ratio* that the user inputs for each solid material. This aspect ratio can be any positive real value; a value of unity produces an equiaxed, isotropic shape, while values close to zero produce thin plates, and values much greater than unity produce long needles. The algorithms in HydratiCA were modified to encode the appropriate aspect ratio within newly nucleated solid material at any lattice site, along with a randomly chosen orientation for the growth axis using Euler angles. We demonstrated that the simulations can reproduce randomly oriented plates and needles, as well as intermediate shapes between these extremes. We are still working to relate these shapes to changes in the rigidity percolation thresholds for simple microstructures.

Although the current state of development is already sufficient to simulate reasonably realistic microstructures in cement paste and gypsum wallboard, several challenges remain to be resolved. For one, the growth shapes are still influenced noticeably by the geometry of the underlying computational lattice. The lattice imparts artifacts to the overall shape, especially when the growth directions are not aligned with the lattice basis vectors. For example, isotropic, equiaxed shapes should be approximately spherical, but in the simulations, they are more octahedral. A second challenge is the need to simulate growth shapes that are not defined solely by a single aspect ratio, such as cubes. This latter challenge can, in principle, be addressed by adding more realistic crystal growth physics in the form of so-called “M-plots” which contain the growth rate constant in every direction rather than just along a single growth axis. However, this is quite challenging to implement within the existing framework of HydratiCA and we are still thinking through possible approaches. Nevertheless, the current state of the model is a major step forward in producing realistic microstructures.

Besides this change to the basic simulation algorithms, we redesigned the input file formats from XML to JSON. This significantly reduced the size and complexity of the input files and also removed the model’s dependence on XML libraries for schema validation and file parsing.

[1] J. Bullard, E. Garboczi, P. Stutzman, P. Feng, A. Brand, L. Perry, J. Hagedorn, W. Griffin, and J. Terrill. Measurement and Modeling Needs for Microstructure and Reactivity of Next-generation Concrete Binders. Cement and Concrete Composites (2017), in press. DOI: 10.1016/j.cemconcomp.2017.06.012

[2] J. Bullard, J. Hagedorn, T. Ley, Q. Hu, W. Griffin, and J. Terrill. A Critical Comparison of 3D Experiments and Simulations of Tricalcium Silicate Hydration. *Journal of the American Ceramic Society* **101** (2017), 1453-1470. DOI: 10.1111/jace.15323

In Situ Analysis, Machine Learning, and Visualization

Judith Terrill
Wesley Griffin
Steve Satterfield
Jeffrey Bullard (NIST EL)

The simulations that we now work on are large, complex, and run for long periods of time. To make the best use of limited high-performance computing resources, we need to monitor and analyze simulation results while the simulation is in process. Ideally, the results of such analysis can allow intervention to improve outcomes. Unfortunately, for simulations at this scale, it is not feasible to write out detailed data to analyze during the runs. The only way to do needed analysis is to do it as part of the runs. We are using machine learning to help with this analysis.

We used a large-scale simulation code, HydratiCA, to develop and test our techniques. HydratiCA integrates a partial differential equation forward in time using small time steps on a 3D lattice of sites. Data analysis is challenging because a single timestep generates a large, many-dimensional data set. Furthermore, at any one point in time there are large parts of that data that are either empty or not interesting to the scientists.

The most important factor that influences the effectiveness of machine learning is the representation space in which the problem is solved. The representation space is spanned by a set of descriptors which, in general terms, are useful ways to group or characterize the data. We analyzed a great deal of data to look for suitable descriptors to describe the representation space on a local (per-lattice-site) basis. We found that reaction saturation index—a quantitative measure of how far a reaction is from equilibrium— as well as its time derivative provided valuable information on the state of the simulation at each site. It also warned of approaching nucleation. This is very important since nucleation causes steep drops in the simulation time step which we would like to model better for faster code.

Nucleation will be sparse in typical applications of HydratiCA, even in a 1000×1000×1000 site simulation, so we need only take notice when nucleation is approaching and then take steps to reduce its impact on computational efficiency. It is not feasible to save the saturation indices and their derivatives at each site and each time iteration for external analysis. To reduce the amount of saved information, we modeled the saturation index over time with Chebyshev polynomials. This successfully reduced a data set spanning one million time iterations to just 22 parameters: the start time, end time, and 20 Chebyshev coefficients; see Figure 56.

We have developed code that outputs these 22 parameters and from them recreates the entire saturation index time history. The Chebyshev polynomial representation also enables us to compute time derivatives of the saturation indices analytically, an advantage which we expect to be useful for detecting the onset of nucleation events. With this method, we can do local analysis that greatly reduces the amount of data that needs to be analyzed. Finally, this same representation of the saturation index history for each reaction serves as input to our immersive visualization monitoring procedure that displays the data.

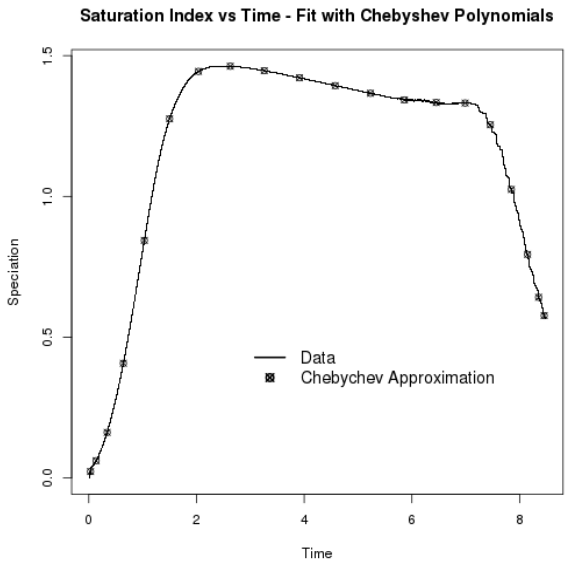

Figure 56. *Chebyshev fit of saturation index vs time for one million iterations.*

We have embedded a Python interpreter in the hydration code to gain access to the math and machine learning algorithms already written. We are working with the University of Maryland to develop a method to obtain a data-driven compact representation using a deep convolutional autoencoder network from an existing cement hydration simulation that produces large, multivariate volumetric data. This has been used to facilitate volume visualization. But adding in the new descriptor may lead to insight into the hierarchical structures learned by the deep convolutional autoencoder.

In the coming year, we will greatly expand our study of saturation indices, modeling them as Chebyshev polynomials and examining their derivatives with respect to time, searching for features in the derivatives that signal the onset of phase transformations and other chemical events. We will also seek and test a state-based model of entire simulation runs using the saturation indices, their derivatives, and other information.

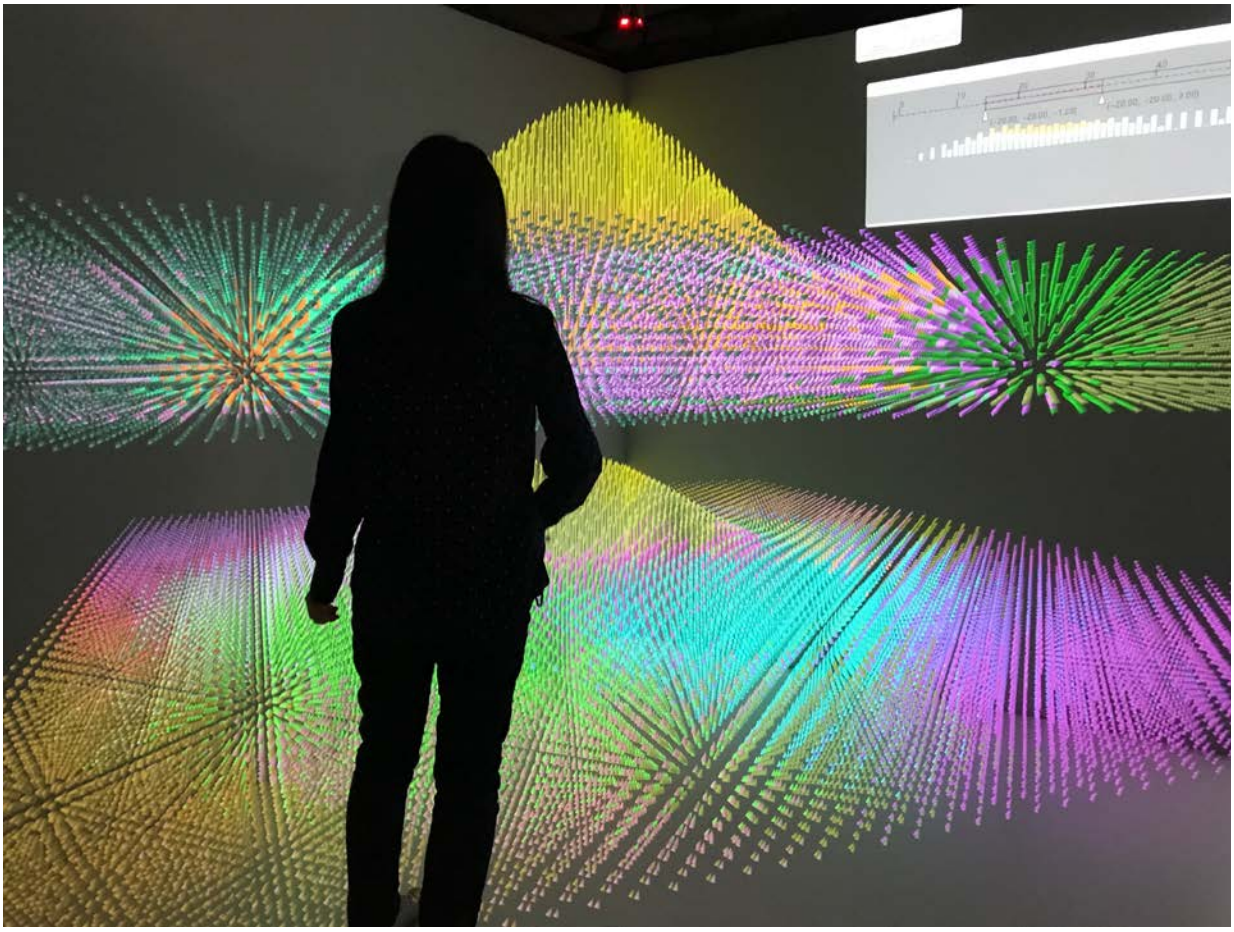

Figure 57. *Analysis of a nanostructure in the NIST CAVE.*

Nano-structures and Nano-optics

James S. Sims
Steve Satterfield
Wesley Griffin
Judith Terrill
Garnett W. Bryant (NIST PML)
Jian Chen (Ohio State University)
Henan Zhao (UMBC)

Research and development of nanotechnology, with applications ranging from smart materials to quantum computing to biolabs on a chip, remains a national priority. Semiconductor nanoparticles, also known as nanocrystals and quantum dots (QDs), are one of the most intensely studied nanotechnology paradigms. Nanoparticles are typically 1 nm to 10 nm in size, with a thousand to a million atoms. Precise control of particle size, shape and composition allows one to tailor charge distributions and control quantum effects to tailor properties completely different from the bulk and from small clusters. Due to enhanced quantum confinement effects, nanoparticles act as artificial atoms with discrete electronic spectra that can be exploited as light sources for novel enhanced lasers, discrete components in nanoelectronics, qubits for quantum information processing, and enhanced ultrastable fluorescent labels for biosensors to detect, for example, cancers, malaria or other pathogens, and to do cell biology.

We are working with the NIST Physical Measurement Lab to develop computationally efficient large-scale simulations of such nanostructures, and to develop immersive visualization techniques and tools to enable analysis of highly complex computational results of this type. The electrical, mechanical, and optical properties of semiconductor nanocrystals and quantum dots are studied. In the most complex structures this entails modeling structures with on the order of a million atoms. Highly parallel computational and visualization platforms are critical for obtaining the computational speeds necessary for systematic, comprehensive study.

Our current code considers wave functions with maximum spin up, with maximum spin down, and two intermediate states. The addition of a magnetic field provides a probe to split excitonic states, providing a more complete spectroscopy of quantum dot optics. This allows us to isolate contributions from spin-orbit

coupling, Zeeman and spatial motion. Magnetic field response depends sensitively on quantum dot (QD) size and shape. The addition of a magnetic field also allows for the intrinsic spins of the electrons to lead to different effects depending on QD size, shape, and arrangements. Without visualization, it becomes very difficult to understand what this distribution is and how it changes for different magnetic fields, electric fields or strain. This distribution is critical for understanding exchange interactions or electron/nucleus interactions in quantum devices, properties that are intimately connected with the performance of these structures for quantum information processing.

As the device size in Si electronics continues to decrease, the devices are rapidly approaching the atomic scale where a change in only a few atoms can make a significant change in device performance. At the same, the ability to make Si nanodevices with only a few, deterministically placed dopant atoms opens up the possibility of creating quantum information processing devices with these structures. We currently are participating in a program to make, characterize and model both traditional and quantum Si devices at this few-dopant atom limit.

During the past year, the computational nanodevices project has focused on using the atomistic tight-binding simulation tool and the visualization tools to analyze the electronic and spin properties of quantum dot systems where alloy effects are critical. This includes studies of InGaAs quantum dots where the alloy character of the quantum dot plays an essential role in determining hole states in this structure. This modeling work supports experimental work in a collaboration with the Naval Research Labs. In addition, simulations of quantum dot molecules, i.e., stacked pairs of quantum dots, have been done to understand how an alloy barrier with bismuth inserted into the GaAs barrier between the dots can be used to tailor the mixing of spins in the quantum dot molecule. This could lead to novel ways to use these hole spins as qubits with ultrafast, optical control. This work was done in collaboration with students from the Joint Quantum Institute and with researchers at the University of Delaware who are trying to make these structures.

The current serial codes used to simulate dopant-based devices in silicon will be extended this year to be a parallel code to exploit the computing power of NIST's Linux cluster. The current parallel simulation tool is being used as a template for implementing the parallel version of this new code.

Ongoing analysis of results from the simulations of various nanodevices are supported by enhanced visualization tools developed in ITL. The significant speedup of these visualization tools makes them practical to use on data from million-atom device simulations both for visualization at the desktop and for immersive 3D visualization. This has greatly facilitated analysis of these systems with large amounts of data. This is especially important for systems for random alloys. These tools allow one to determine which results are configuration-specific and which apply to all random configurations of the same structure; see Figure 57. These simulation tools are also now being applied to atomic-scale dopant-based Si electronic, quantum and photonic devices.

[1] H. Zhao and J. Chen. Bivariate Separable-Dimension Glyphs Can Improve Visual Comparison of Holistic Features for Large-Range Magnitude Vector Data Visualization. In Review.

High Precision Calculations of Fundamental Properties of Few-Electron Atomic Systems

James Sims
Stanley Hagstrom (Indiana University)
Maria Ruiz (University of Erlangen, Germany)
Bholanath Padhy (Khallikote College, India)

NIST has long been involved in supplying critically evaluated data on atomic and molecular properties such as the atomic properties of the elements contained in the Periodic Table and the vibrational and electronic energy level data for neutral and ionic molecules contained in the NIST Chemistry WebBook. Fundamental to this endeavor is the ability to predict, theoretically, a property more accurately than even the most accurate experiments. It is our goal to be able to accomplish this for few-electron atomic systems.

While impressive advances have been made over the years in the study of atomic structure, in both experiment and theory, the scarcity of information on atomic energy levels is overwhelming, especially for highly ionized atoms. The availability of high precision results tails off as the state of ionization increases, not to mention higher angular momentum states. In addition, atomic anions have more diffuse electronic distributions, thus representing more challenging computational targets than the corresponding ground states.

In the past two decades, there have been breathtaking improvements in computer hardware and innovations in mathematical formulations and algorithms, leading to "virtual experiments" becoming a more and more cost-effective and reliable way to investigate chemical and physical phenomena. Our contribution in this arena has been undertaking the theoretical development of our hybrid Hylleraas-CI (Hy-CI) wave function method to bring sub-chemical accuracy to atomic systems with more than two electrons.

Hy-CI has from its inception been an attempt to extend the success of the Hylleraas (Hy) method to systems with more than three electrons, and hence is an

attempt to solve not just the three-body problem but the more general N-body problem [1]. Fundamental to the method is the restriction of one r_{ij} per configuration state function (CSF).[17] In the case of three electron lithium systems, we have computed four excited states of the lithium atom to two orders of magnitude greater than has ever been done before [2]. At the four-electron level, to get truly accurate chemical properties like familiar chemical electron affinities and ionization energies, it is important to get close to the nanohartree level we achieved for the three-election atom, a significantly more difficult problem for four electrons than for three. By investigating more flexible atomic orbital basis sets and better configuration state function filtering techniques to control expansion lengths, we have been able to successfully tackle the four-electron case.

Progress to date has included computing the nonrelativistic ground state energy of not only beryllium, but also many members of its isoelectronic sequence to eight significant digit accuracy. With the results from our calculations and a least-squares fit of the calculated energies, we have been able to compute the entire beryllium ground state isoelectronic sequence for Z = 4 through Z = 113 [3]. Li^- (with Z=3), nominally the first member of this series, has a decidedly different electronic structure and was not included in those calculations. Work this past year has included correcting this "omission" and carrying out a large, comparable calculation for the Li^- ground state. A paper reporting the results of this study has been published [4].

The first member of the Be isoelectronic ground state sequence, the negative Li^- ion, is also a four- electron system in which correlation plays a very important part in the binding. However due to the reduced nuclear charge, it is a more diffuse system in which one of its outer two L shell electrons moves at a greater distance from the nucleus than the other, and hence its nodal structure is different from that of a coupled L shell with an identical pair of electrons. The ground state of the singlet S state of Li^- is the same type of problem as the first excited state of Be; it is like Be(2s3s), not Be(2s2s). Completing this calculation has provided the necessary insight to enable the calculation of the Be first excited state of singlet S symmetry, Be(2s3s) to an order of magnitude better than previous calculations.

Our goal now is to investigate how far we can continue with this level of accuracy as we continue to calculate the higher excited singlet S states of Beryllium. Current plans for this year are to investigate the Be(2s3s) through Be(2s7s) states of singlet S symmetry. As we continue to go to higher and higher excited states with the more complicated nodal structures of the diffuse Rydberg states, we will be determining how well Hy-CI can represent four electron atomic states other than the ground state.

[1] J. S. Sims and S. A. Hagstrom. Combined Configuration Interaction – Hylleraas Type Wave Function Study of the Ground State of the Beryllium Atom. *Physical Review A* **4**:3 (1971), 908. DOI: 10.1103/PhysRevA.4.908

[2] J. S. Sims and S. A. Hagstrom. Hy-CI Study of the 2 Doublet S Ground State of Neutral Lithium and the First Five Excited Doublet S States. *Physical Review A* **80** (2009), 052507. DOI: 10.1103/PhysRevA.80.052507

[3] J. S. Sims and S. A. Hagstrom. Hylleraas-Configuration Interaction Nonrelativistic Energies for the Singlet S Ground States of the Beryllium Isoelectronic Series Up Through Z = 113. *Journal of Chemical Physics* **140** (2014), 224312. DOI: 10.1063/1.4881639

[4] J. S. Sims. Hylleraas-Configuration Interaction Study of the Singlet S Ground State of the Negative Li Ion. *Journal of Physics B: Atomic, Molecular and Optical Physics* **50** (2017), 245003. DOI: 10.1088/1361-6455/aa961e

[17] For atomic systems with greater than four electrons, all relatively precise calculations nowadays adopt the Hy-CI methodology of one r_{ij} per CSF.

Parallelization of an Overset Mesh Framework

Justin A. Kauffman
William George
Jonathan S. Pitt (Virginia Tech)

Simulating full scale fluid-structure interaction (FSI) is important in a variety of applications. For example, in the space industry, FSI simulations are used to assist in the design of parachutes that are used during spacecraft landings. Additionally, FSI is important in many biomechanical applications, such as blood flow through arteries or artificial heart valves. To get accurate results from FSI simulations modelers need to represent the true geometry, regardless of its complexity, while also adequately solving the systems of partial differential equations (PDEs) describing the physics of the problem.

Each of these requirements can be difficult to achieve independently, so developing a technology that can do both is a challenge. We want the capability to allow complex geometrical features to be able to move throughout the computational domain. Overset meshes are used to fully describe the geometrical features in addition to maintaining initial mesh quality, even when bodies or features in the domain have relative motion. Overset mesh methods enhance the flexibility in how the physical domain is discretized by allowing different meshes to overlap in the computational domain.

Once the physical domain is discretized, we use the hybridizable discontinuous Galerkin (HDG) finite element method to solve the system of partial differential equations on each mesh of the computational domain. There are two motivating factors for use of the HDG method in conjunction with an overset mesh method. First, the amount of overlap between meshes is completely arbitrary, as long as there are no gaps (or holes) in the computational domain, and second, the coupling necessary to stitch the meshes together is inherently constructed in the HDG method.

This particular hybridization of a discontinuous Galerkin (DG) method reduces the size of the global linear system by reformulating the governing equations through the elimination of volumetric degrees of freedom (DoFs) for a smaller set of surface/face DoFs [1]. Historically, overset mesh methods have been used with finite volume and finite difference methods, but within the last decade overset mesh methods have been extended to DG methods. The drawback for the traditional overset mesh methods is that approximation order and amount of overlap are coupled. To obtain a higher-order approximation more cells must be used in the communication of data between meshes for finite volume and finite difference methods; therefore, these overset mesh methods are mainly used for second-order approximations. DG overset schemes enable researchers to obtain high order accurate solutions with no additional cost for the data communication between meshes. The drawback for DG overset schemes is that the resulting linear system becomes large compared to traditional linear systems in the computational fluid dynamics (CFD) community. It will then take more computational resources and computational time to solve that resulting linear system.

To date a serial algorithm has been developed to identify acceptor-donor cell pairs, which are necessary for overset communication. An acceptor cell is a cell that exists on the overset boundary of a mesh that will receive numerical contributions from a cell on a different mesh, or a donor cell. Acceptor cells are known only at run-time because they exist on a mesh boundary, but the donor cells are not known *a priori*. The serial version of the overset-HDG method has been implemented to solve PDEs of linear convection-diffusion, linear static elasticity, and Navier-Stokes in both Eulerian and arbitrary Langrangian-Eulerian (ALE) reference frames, but this method uses an inefficient linear solver, a brute force approach to obtain the acceptor-donor pairs and does not properly utilize the embarrassingly parallel structure to obtain the local solution of the HDG method.

To start solving full scale FSI problems, each building block is first tested via verification and validation. Verification results are obtained through the method of manufactured solutions and validation is performed by comparing our results to benchmark problems and experimental data. The main effort of this work is to create efficient parallel algorithms that identify the acceptor-donor cell pairs. The parallel algorithms being developed first identify potential donor cells and then determine which of those potential donors is the true donor cell. Care is then taken to communicate with only one mesh in the event of more than two meshes overlap at the same physical location. Finally, a robust and efficient linear solver must be designed. We hope to demonstrate in this work that the increased cost associated with the HDG method, compared to finite volume (or finite difference) [2], is an acceptable trade-off for the increased accuracy, while minimizing the data communication between the overset meshes. These advantages make the overset-HDG method a viable candidate to compete with the traditional finite volume/difference overset mesh methods currently used in the CFD community.

[1] B. Cockburn and J. Gopalakrishnan. New Hybridization Techniques. *GAMM-Mitteilungen* **2** (2005), 154-183.

[2] T. Ahnert and G. Bärwolf., Numerical Comparison of Hybridizable Discontinuous Galerkin and Finite Volume Methods for Incompressible Flow. *International Journal for Numerical Methods in Fluids* **76** (2014), 267-281.

Immersive Visualization Systems

Wesley Griffin
Steve Satterfield
Terence Griffin
William George
Judith Terrill

https://www.nist.gov/programs-projects/visualization

ACMD's High Performance Computing and Visualization Group develops tools and maintains facilities to enable high-performance 3D immersive visualization and analysis to be applied to NIST measurement science problems. This past year we worked on three things

HEVx: High End Visualization. The High-End Visualization (HEV) Software that drives the NIST CAVE [1] currently uses an OpenGL-based rendering engine which has been sufficient for the CAVE up until now. This year, however, NVIDIA announced new graphics processing units (GPUs) that have several new features including real time hardware-accelerated ray-tracing [2] and global illumination. These new features, combined with the evolving application programming interfaces (APIs) for programming GPUs, required a reevaluation of the rendering engine in HEV. There is a new cross-platform standard API for programming GPUs, called Vulkan [3], that brings GPU programming more in-line with how GPU hardware is organized. The OpenGL API, while still being an actively supported cross-platform standard, no longer maps well to the hardware and

thus there is now significant overhead in using OpenGL in the traditional way.

This summer we launched new project HEVx [4], that will replace the OpenGL-based rendering engine with a Vulkan-based rendering engine. This will ensure that the CAVE can continue to take advantage of the latest GPU hardware while also re-writing the rendering engine to improve performance of large dataset visualizations. This work will directly benefit CAVE users in that rendering performance of large datasets will improve. Also, head mounted displays (HMDs), such as the Oculus Rift or HTC Vive, will be directly supported by HEVx thus extending the types of immersive visualization environments that can be used for visualizations.

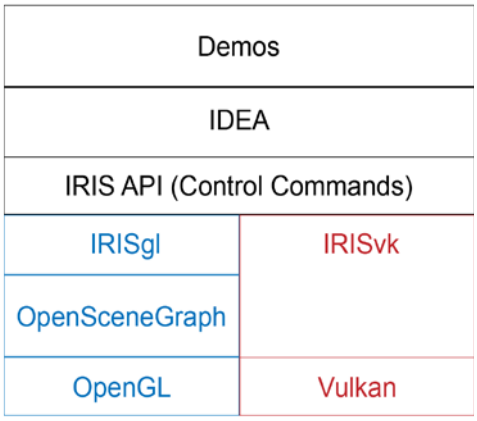

Figure 58. *HEV system architecture.*

Thus far we performed a design phase and review and have begun implementing the Vulkan-based rendering engine. Figure 58 shows the system architecture of HEV and HEVx. The OpenGL-based rendering engine is referred to as IRISgl and the Vulkan-based rendering engine is referred to as IRISvk. Thanks to the use of an IRIS API, which is implemented as a set of text-based control commands issued via a UNIX named pipe, the majority of the existing HEV tools will continue to work regardless of the rendering engine.

Render Testing. Our immersive visualization environment (IVE) consists of a three-wall cave as well as Linux desktops and laptops that all run the Linux operating system. This environment is heterogenous and changing. The hardware is not the same everywhere, which includes different NVIDIA graphics cards This is likewise true for our operating system, which may be at different versions on different machines.

Our IVE software consists of a combination of vendor supplied, open source, and locally written software. In order to have confidence that our environment is functioning correctly, we have implemented three types of tests: hardware tests, software functional tests, and render tests. The render tests are necessary because the hardware does not guarantee that the pixels displayed will be the same when displayed with different GPUs and different drivers. So, the images generated with identical inputs at two different times may both be correct, but not identical.

We have developed a software utility that enables us to run an application from a text file called a timeline file. Using this we can start and stop navigation, snap images, and issue commands to the application. The commands enable us to modify the visualization in various ways, such as adding or deleting objects or modifying object properties such as color.

For each test, we develop a timeline file to run the application and capture rendered images at specific times during the execution. To initialize the test, we run the timeline file and save the captured images as baseline images. We run the test on multiple machines.

We have designed a three-tiered success evaluation. First, the generated and baseline images are checked to see if they are identical. If they are not, they are evaluated for perceptual sameness. Finally, the evaluation uses a variety of image processing techniques to give us some information on the differences. After all the tests are run, they are published to a web page where they can be examined.

This year, we expanded our render tests. We also incorporated two types of perceptual sameness tests: The International Commission on Illumination (CIE) ΔE [5] and the structural similarity metric [6]. We are collecting information on these metrics on our images. In the coming year, we will continue to add tests and study the values returned by these metrics.

MERSIV - Monitor, Explore, Review Simulations with Immersive Visualization. The goal of this project is to develop an application that gives the user access to the status of a computation, such as a long-running simulation, without necessarily having access to the compute host where the computation is running. Collaboration between research project members can be improved if all can see the progress and status of the supporting computations at any time convenient to them. This application is not tied to any particular computation, but instead relies on a set of conventions (file naming and placement), which, if followed by the computation owner, allows the computation to be easily monitored by MERSIV users. The extent of this monitoring, which relies on scripts and other programs, can range from simply showing the MERSIV user whether the computation is currently running or not, to showing the user a 3D immersive animation of the simulation, up to its latest state. Thus, the power of MERSIV rests in the scripts and programs, along with the computation output, provided to MERSIV by the computation owner.

A proto-type of this application, shown in Figure 59, was developed in the summer of 2018 in collaboration with an intern in the NIST SURF program. An initial stable version of this application was completed in September 2018. We will be testing its functions this year, using both local users, i.e., within ACMD, and remote users, i.e., collaborators in other NIST Labs.

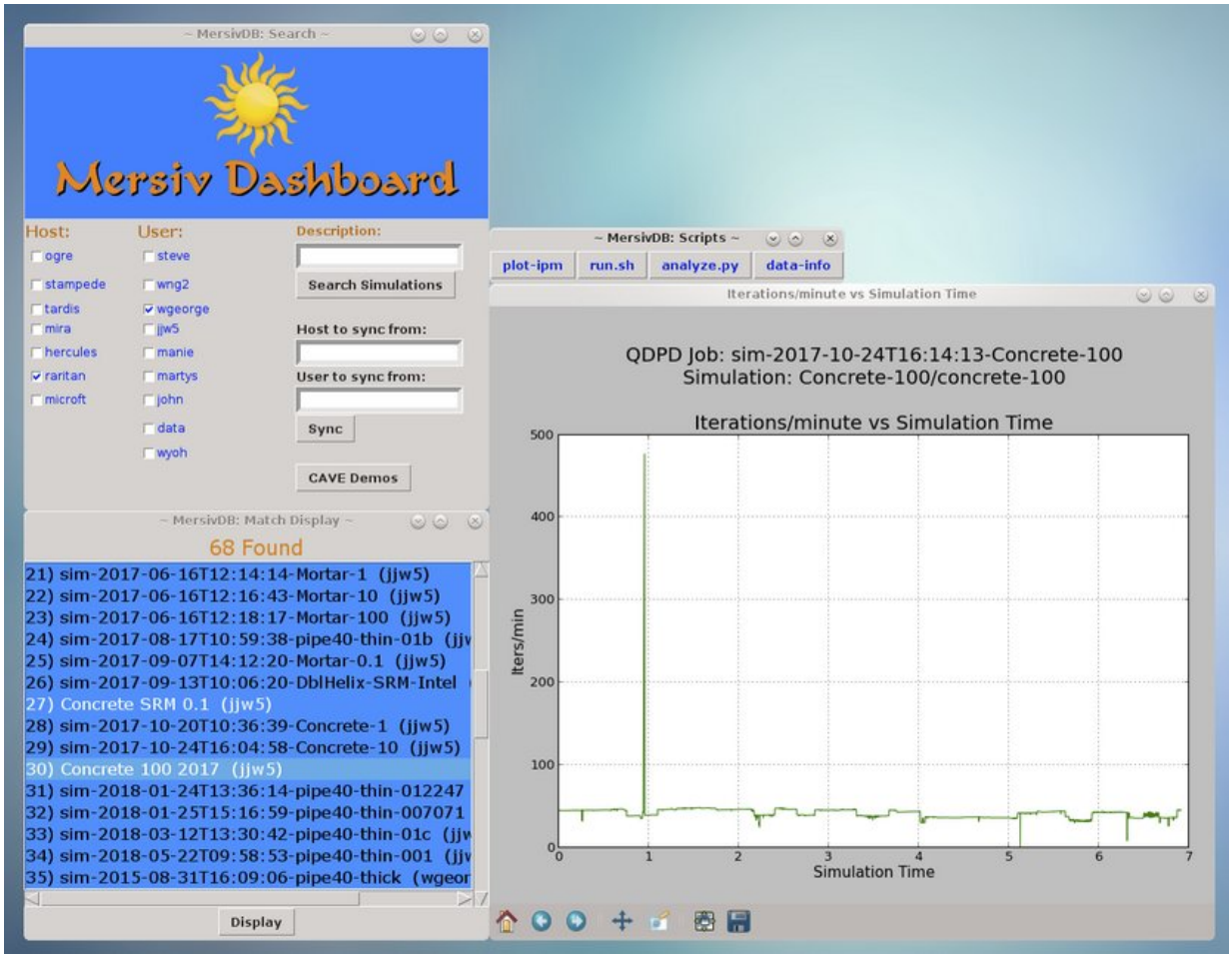

Figure 59. *The MERSIV application displaying plotted information from a selected computation.*

[1] https://www.nist.gov/programs-projects/visualization
[2] https://www.nvidia.com/en-us/geforce/turing/
[3] https://www.khronos.org/vulkan/
[4] https://github.com/usnistgov/hevx
[5] https://en.wikipedia.org/wiki/Color_difference#CIE94
[6] https://en.wikipedia.org/wiki/Structural_similarity

Figure 60. *Left: STM with menu on the VR controller. Right: Exploded parts view of the STM.*

WebVR Graphics

Sandy Ressler
Kevin Chen (Poolesville High School)
James Biggins (University of Maryland)
Paul Armstrong (University of Maryland)

WebVR is a technology that enables some types of virtual reality (VR) content to be displayed in a Web page. 2017 was a breakthrough year for WebVR, when Firefox's Mozilla browser out of the box understood VR devices (Oculus Rift and HTC Vive). 2018 continues the trend as Google Chrome's production version also includes native Oculus and Vive support with the setting of a Chrome browser flag. WebVR content remains the simplest most ubiquitous method to distribute VR content. After development, one simply transmits a URL to the user and no additional software is required, reducing a major point of friction.

We continue work on two exemplar applications. The first is a navigable scanning tunneling microscope (STM) head, and the second are walkthroughs of several

NIST locations using 360-degree images. This year we also began a significant third new application of VR with the Digital Library of Mathematical Functions. As a multi-disciplinary agency, NIST performs research across a wide variety of domains. The techniques we are developing and exploring serve to expose NIST research in a simple yet powerful way.

STM head. An entirely new user interface has been developed for the scanning tunneling microscope (STM) head which functions more robustly and vastly improves the navigation. Improvements this year include being able to use the STM head environment with both an Oculus Rift and HTC Vive. The Rift hand controllers have small joysticks and using those to navigate is particularly effective. Figure 60 shows the STM with menu and the STM with several parts moved aside to allow viewing of the interior, as well as an exploded view of the STM, one of several new visualization features accessible via the new menu system that has been developed. This demo has been made publicly available [1].

Virtual Walkthroughs. Last year we had a walkthrough of the NIST library. This year the software was completely reworked to use the widely supported Unity software platform. We have completed walkthroughs of the NIST Library, the NIST Shops (Building 304) and the NIST Net Zero House; see Figure 61 and Figure 62. Each location was filmed by placing a tripod in a number of locations and then capturing 360-degree images. The images were then made navigable by placing them into a Unity structure which allowed us the freedom to define the interaction we desired. In our case we defined "gaze" type navigation which allows interaction by simply looking at a "hot button" area. The areas are linked to other virtual spheres which are locations (those tripod locations) in other areas of the Library, Shops or NetZero House (whichever demo is being used). Unity offered us the ability to define a template into which we can quickly implement new locations. This demo has been made publicly available [2].

DLMF and Virtual Reality. The NIST Digital Library of Mathematical Functions (DLMF) is a long-standing project at NIST [3]. Interactive web-based computer graphic representations of the surfaces of many of the functions has been a key feature of the online version of the DLMF website for many years. As a point of curiosity and as an experiment (created initially by a high school summer student) in using virtual reality for a novel application, we started with the question: "What would happen if we placed all of the DLMF surfaces in a VR environment simultaneously?" There was, of course, an educated preconceived notion that this would be useful. The question of whether there would be any advantages to such an environment has not been scientifically answered yet. However, the reaction of virtually all users is "yes."

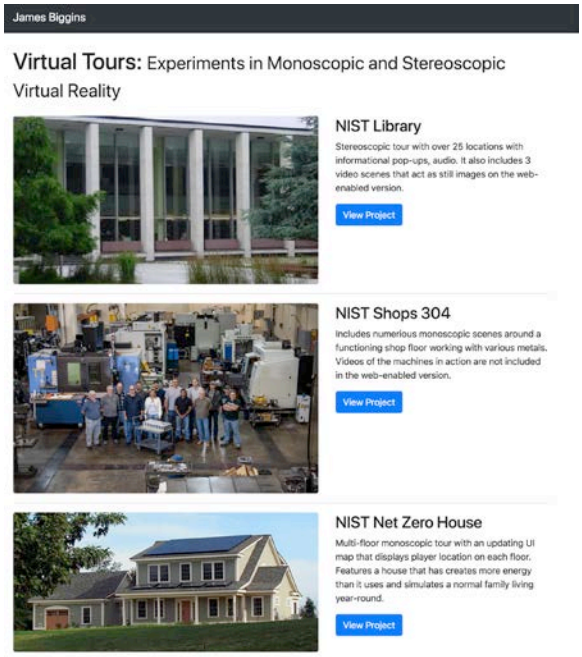

Figure 61. *Virtual tour home page.*

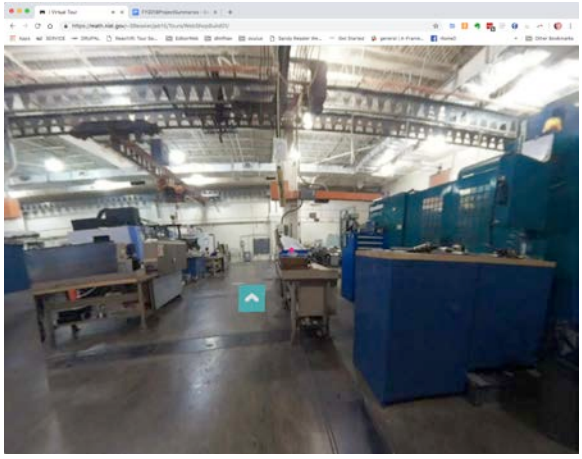

Figure 62. *View of Shops (Bldg. 301) virtual tour.*

Users have the ability to virtually grab the surfaces, using an Oculus Rift Controller which is very close to the sensation of physically grabbing an object. The surface responds in real time as if the user is actually holding it just like a real physically object. You can bring the surface close to your eyes, move it around in front of your face, inspect all sides of it and get a genuine physical sense as to its often-complex shape. This is the first time that shapes from the DLMF have been able to be inspected so "naturally." Users can grab the shapes and scale them up or down just like images on phones with a pinch-type move using both hands, that many find quite intuitive. See Figure 63 and Figure 64. When finished with a particular surface you can toss the surface and it spins and flies away in an appropriate way.

This is a very early implementation of this experiment. We next need to make the surfaces available in the environment with much more information. We need to add information about the types of surfaces, the values used for the ranges, provide filtering mechanisms to select some of the surfaces according to those filters and perhaps start filtering according to shapes. We also intend on experimenting with other coloring methods to exploit more fully the possibilities of using shaders for real-time displays that are mathematically meaningful. This is an exploratory project with an unknown set of applications, however one clearly useful application is simply getting people interesting in the concepts of special functions and interactive mathematical surfaces. This demo has been made publicly available [4].

[1] S. Ressler and P. Armstrong. NIST VR Scanning Tunneling Microscope Head. December 10, 2018. URL: https://math.nist.gov/~SRessler/stm_scene/

[2] J. Biggins and S. Ressler. Virtual Tours: Experiments in Monoscopic and Stereoscopic Virtual Reality. December 10, 2018. URL: https://math.nist.gov/~SRessler/jab15/HomePage/

[3] F. Olver, et al. NIST Digital Library of Mathematical Functions. URL: https://dlmf.nist.gov

[4] S. Ressler and K. Chen. Digital Library of Mathematical Functions in VR. December 10, 2018. URL: https://math.nist.gov/~SRessler/dlmfvr.html

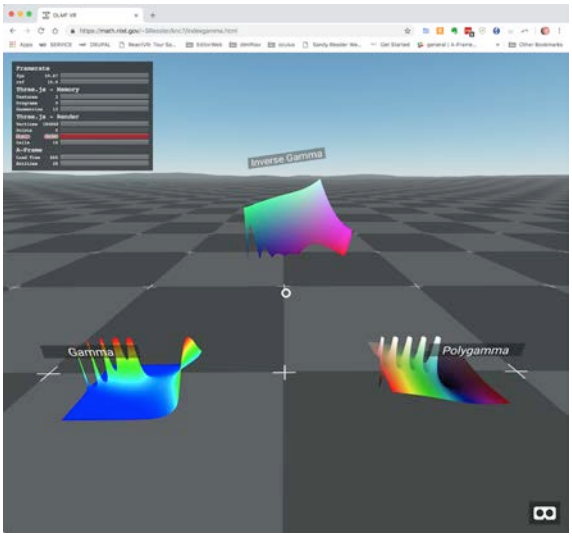

Figure 63. *Gamma function with labels.*

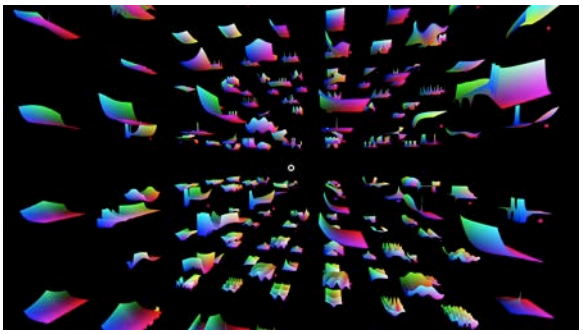

Figure 64. *All DLMF surfaces in a grid layout.*

Quantum Information

An emerging discipline at the intersection of physics and computer science, quantum information science is likely to revolutionize 21st century science and technology in the same way that lasers, electronics, and computers did in the 20th century. By encoding information into quantum states of matter, one can, in theory, enable phenomenal increases in information storage and processing capability. At the same time, such computers would threaten the public-key infrastructure that secures all of electronic commerce. Although many of the necessary physical manipulations of quantum states have been demonstrated experimentally, scaling these up to enable fully capable quantum computers remains a grand challenge. We engage in (a) theoretical studies to understand the power of quantum computing, (b) collaborative efforts with the multi-laboratory experimental quantum science program at NIST to characterize and benchmark specific physical realizations of quantum information processing, and (c) demonstration and assessment of technologies for quantum communication.

Quantum Information Science

Scott Glancy
Emanuel Knill
Peter Bierhorst (University of Colorado)
Karl Mayer (University of Colorado)
James R. van Meter (University of Colorado)
Lynden K. Shalm (University of Colorado)
Sae Woo Nam (NIST PML)
Yanbao Zhang (NTT Corporation, Japan)
Gerardo Ortiz (Indiana University)

Quantum information technology is experiencing rapid expansion with growing commercial interest, availability of devices for quantum randomness and quantum key distribution, and publicly accessible small quantum computers. Characterizing and utilizing the increasingly complex quantum devices being developed requires highly efficient analytical tools, algorithms and protocols. ACMD researchers are helping develop these essentials. Recent contributions include highly efficient randomness generation protocols and their demonstration with loophole-free Bell tests, process fidelity bounds with fewer experimental resources, benchmarks for verifying Majorana modes and simpler realizations of entangling gates for decoherence-free subsystems carried by spins.

Randomness Generation. Uniformly random bits are a valuable resource. Public random bits are required for fair sampling in statistics, Monte-Carlo simulations and auditing. Private random bits are essential for generating keys when initiating secure internet connections, which is one of the most common applications of randomness. Quantum correlations, such as those exhibited in Bell tests, imply the presence of fundamental randomness and can be exploited for certified public or private randomness without requiring trust in the underlying quantum devices or their manufacturer [1]. However, the protocols for extracting randomness from Bell tests required extraordinary experimental resources before any randomness could be obtained. Our work reduced the resources required by orders of magnitude, reducing the experimental effort for producing 512 very high-quality random bits to less than 5 minutes [2,3]. This was enabled by our development of a general framework for randomness generation based on quantum randomness estimation [4], which simplifies the analysis of randomness generation of all kinds and ensures that the random bits are uniform with respect to the most general, quantum-capable agents. We expect to improve the experiments to generate 512 random bits in less than 1 minute, which would enable the use of our quantum randomness source in the NIST randomness beacon [5].

Quantum Gate Fidelity Estimation. When building and commissioning quantum devices for quantum computing, a common task is to verify that the fundamental quantum gates have sufficiently high fidelity after calibration. This can be done by applying the gates to sufficiently many input states and comparing the output to the desired one. This process can be speeded up by reducing the number of input states. In many cases, it is not necessary to determine the fidelity exactly and it suffices to obtain a lower bound that approaches 1 for nearly ideal gates. We found that the minimum number of states required is less than previously thought. For two-qubit gates, four states suffice, where previously it was thought that five were necessary. More generally, we determined a semidefinite program for lower bounds on gate fidelities given fidelities at any given number of states and investigated classes of states yielding better fidelity bounds [6]. Future work will integrate the methods found into benchmarks used in our quantum laboratories.

Topological Quantum Computing. Among the many proposals for building quantum computers, topological quantum computers stand out as one of the most theoretically attractive ones. Such quantum computers exploit an esoteric class of emergent quantum phenomena to achieve an intrinsic robustness that otherwise requires the use of sophisticated fault-tolerance strategies. One approach to topological quantum computers is

based on what are known as Majorana modes in topological superconductors. Although this approach lacks universal robustness, there are now significant experimental resources dedicated to realizing it. The first step is to verify the presence and measurability of the Majorana modes. Only indirect signatures of such modes have been found so far. We are investigating the use of quantum self-testing procedures to verify that an experimental system has the state space and behavior required of Majorana modes. For this purpose, we draw on our experience with verification of quantum correlations in Bell tests and related self-testing experiments.

A unique feature of Majorana modes experiments is the lack of a single, natural partition into local subsystems. This requires a generalization of the self-testing scenarios. We determined such a generalization and have established that Majorana modes can be self-tested accordingly, meaning that with minimal assumptions on the physical system being measured and with only the statistics from randomized measurements, we can determine how close the system is to behaving like ideal Majorana modes and measurements. Future work includes completion of a framework for our more general self-testing scenarios and the development of Majorana benchmarks for sequential measurements as may be performed for realizing a quantum computation.

Computing with Quantum Dots. A very promising proposal for building quantum computers is based on electrically defined quantum dots in a semiconductor. Progress on such quantum dot computers has been rapid in the last few years, with good fidelity two-qubit gates demonstrated. One of the best methods for encoding a qubit in quantum dots is based on the decoherence-free subsystem defined by three two-level systems with respect to collective noise. It has the advantage that universal gates can be implemented with exchange interactions naturally associated with the dot's electrons, which can be electrically controlled. The known methods for implementing universal gates, such as the controlled NOT (CNOT) gate, are involved, requiring many distinct steps with exchange interactions. The methods have been obtained by numerical optimization and difficult analytical analyses.

We have determined that for high-fidelity gates, a conceptually and operationally simpler approach is obtained by decoupling unwanted interactions associated with the native exchange processes [7]. CNOT fidelities sufficient for near-term quantum devices can thereby be implemented with less effort than previous, exact CNOT realizations. Our method has the flexibility to directly implement entangling evolutions under some circumstances. Next steps include generalizing the theory to all decoherence-free subsystems contained in d-level systems with respect to collective noise.

[1] R. Colbeck. Quantum and Relativistic Protocols for Secure Multi-Party Computation. arXiv:0911.3814, 2006.

[2] Y. Zhang, E. Knill, and P. Bierhorst. Certifying Quantum Randomness by Probability Estimation. *Physical Review A* **98** (2018), 040304(R). DOI: 10.1103/PhysRevA.98.040304

[3] Y. Zhang et al. Experimental Low-Latency Device-Independent Quantum Randomness. arXiv:1812.07786, 2018.

[4] E. Knill, Y. Zhang, H. Fu. Quantum Randomness Generation by Quantum Probability Estimation with Quantum Side Information. arXiv:1806.04553, 2018.

[5] NIST Randomness Beacon. https://beacon.nist.gov/home.

[6] K. Mayer and E. Knill. Quantum Process Fidelity Bounds from Sets of Input States. *Physical Review A* **98** (2018), 052326. DOI: 10.1103/PhysRevA.98.052326

[7] James R. van Meter and E. Knill. Approximate Exchange-only Entangling Gates for the Three-Spin-1/2 Decoherence-Free Subsystem. arXiv:1812.08853, 2018.

Quantum Estimation Theory and Applications

Arik Avagyan (University of Colorado)
Charles Baldwin
Scott Glancy
Emanuel Knill
Karl Mayer (University of Colorado)
Hilma Vasconcelos (University of Colorado)
Stephen Erickson (NIST PML)
Alexey Gorshkov (NIST PML)
Daniel Kienzler (NIST PML)
Dietrich Leibfried (NIST PML)
Alan Migdall (NIST PML)
Trey Porto (NIST PML)
Kartik Srinivisan (NIST PML)
Ting Rei Tan (NIST PML)
Yong Wan (NIST PML)
David Wineland (NIST PML)
Andrew Wilson (NIST PML)
Jenny Wu (NIST PML)
Leonardo Silva (Federal University of Ceará, Brazil)

Many emerging technologies will exploit quantum mechanical effects to enhance metrology, computation, and communication. Developing these technologies requires improved methods to measure the states of quantum systems. Quantum estimation is a statistical problem of estimating an underlying quantum state, measurement, or process by using a collection of measurements made on independently prepared copies of the state or applications of the measurement or process. Accurate quantum estimation allows experimentalists to answer the question "What is happening in my quantum experiment?" and to characterize uncertainty in that answer.

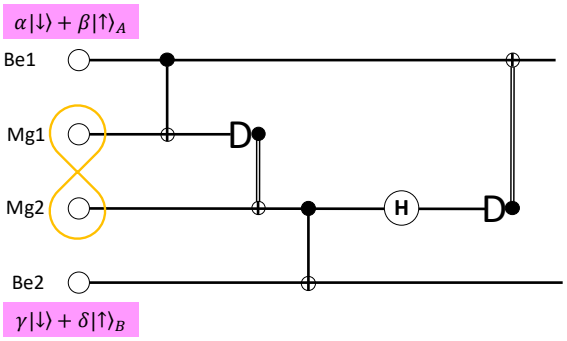

Figure 65. *Simplified diagram of CNOT teleportation. The Magnesium qubits Mg1 and Mg2 are prepared in an entangled state, and the two Berillium qubits Be1 and Be2 are prepared in arbitrary logical states. Each Be ion interacts with its partner Mg ion through conventional quantum CNOT operations. Then the Mg ions are measured, and depending on the measurement results, single qubit operations are applied to the Be ions. After these corrections, the action of the circuit is equivalent to application of CNOT between the Be ions.*

NIST's Ion Storage Group has pioneered one of the world's most successful quantum computer development projects. To keep pace with their recent advances in qubit preparation, logical operation, and measurement fidelities, ACMD researchers have developed more advanced statistical techniques to characterize the trapped ion quantum computers [1]. In collaboration with NIST's Ion Storage Group, ACMD researchers applied these techniques to an experiment demonstrating a controlled-NOT (CNOT) quantum logic operation that is transferred from two magnesium ion qubits to two beryllium ion qubits through quantum teleportation. As shown in Figure 65, the entangled magnesium ions are used to teleport the beryllium ions. After teleportation, the beryllium ions have received the CNOT operation, even though they do not directly interact with one another. According to the ACMD analysis, the fidelity of the teleportation is in the interval [0.85, 0.87] with 95 % confidence [2]. By applying a likelihood-ratio consistency check to the experimental data, ACMD researchers discovered significant drift in the laser power controlling some logic operations. The Ion Storage Group is now building better laser controls to increase the fidelities and consistency of logic operations. Analysis software used in this experiment has been published on Github [3].

ACMD researchers are contributing to the Metrology with Interacting Photons project, which is funded by the NIST Innovations in Measurement Science (IMS) program. This project's goals are to demonstrate photon-photon interactions that are mediated by Rydberg atoms and to exploit those for metrology and quantum information processing. ACMD researchers have theoretically explored adaptation of traditional homodyne detection so that they can verify that the photons have interacted with one another despite noise, loss, and a strict limit on the power of the homodyne reference field (or "local oscillator"). They have characterized what properties of optical quantum states can be inferred from the measured data even when the signal is contaminated by noise photons in nearby modes, when the reference field is very weak, and when the reference phase and power can be varied [4].

When measuring the state of a quantum harmonic oscillator (such as a nano-mechanical resonator or a quantum optical field), the natural measurements are continuous variables that are phase variants of position and momentum. The fact that every measurement outcome may be unique can cause estimation of the quantum state to be computationally expensive. ACMD researchers have designed a scheme for discretizing the measurement outcomes based on an estimate of the number of photons in the state. They have conducted extensive numerical tests to compare this and other discretization strategies. These tests show that discretization allows much faster estimation while keeping high fidelity of the state estimate [5]. ACMD researchers are preparing their continuous variable quantum state tomography for public release.

Characterizing uncertainty in the estimates provided by quantum state tomography remains challenging. Without computationally tractable and statistically rigorous methods to produce confidence intervals for parameters characterizing quantum states, interpreting experimental results can be problematic. To address this problem most researchers use bootstrap-based methods to characterize uncertainty. However, bootstrap estimates are biased, so bootstrap confidence intervals may not achieve the desired coverage probabilities. ACMD researchers have begun a numerical study of several bootstrap-based methods for constructing confidence intervals. The studies show that these methods are useful for relatively low confidence levels (≈68 %), but they are not reliable for high confidence levels (≈95 %).

[1] A. C. Keith, C. H. Baldwin, S. Glancy, and E. Knill, Partial Quantum Tomography Using Maximum Likelihood Estimation. *Physical Review A* **98** (2018), 042318.

[2] Y. Wan, D. Kienzler, S. Erickson, K. H. Mayer, T. Rei Tan, J. Wu, H. H. Macedo De Vasconcelos, C. H. Baldwin, S. Glancy, E. H. Knill, D. J. Wineland, A. Wilson, and D. Leibfried. Deterministic Teleportation of a Controlled-NOT Gate in a Trapped Ion System. In preparation.

[3] A. C. Keith, C. H. Baldwin, S. Glancy, and E. Knill. State-meas-tomo: Joint Quantum State and Measurement Tomography. URL: https://github.com/usnist-gov/state_meas_tomo

[4] Arik Avagyan, Emanuel Knill, Scott Glancy, and Hilma Vasconcelos. State Tomography with Photon Counting after a Beam Splitter. In preparation.

[5] J. L. E. Silva, H. M. Vasconcelos, and S. Glancy. Quadrature Histograms in Maximum Likelihood Quantum State Tomography. *Physical Review A* **98** (2018), 022325.

Robust Quantum Process Tomography via Phase Retrieval

Yi-Kai Liu
Ingo Roth (Free University of Berlin)
Richard Kueng (Caltech)
Shelby Kimmel (Middlebury College)
David Gross (University of Cologne)
Jens Eisert (Free University of Berlin)
Martin Kliesch (Heinrich Heine University Dusseldorf)
Felix Krahmer (Technical University of Munich)

Quantum process tomography is the task of characterizing an unknown quantum operation, such as a gate operation performed by a quantum computer. This is done for calibration purposes, and to diagnose possible sources of error. Ultimately, this is a crucial step towards implementing quantum error correction and fault-tolerant quantum computation.

In practice, the accuracy of quantum process tomography is limited by state preparation and measurement (SPAM) errors. To obtain accurate estimates, one must resort to alternative characterization procedures, such as randomized benchmarking (RB) and gate set tomography (GST). These methods are robust to SPAM errors, but they have significant drawbacks: RB is much less informative than conventional process tomography, while GST is much more resource intensive.

In our recent work [1], we developed a new method for quantum process tomography that is robust to SPAM errors and avoids the main drawbacks of RB and GST. The key idea is to focus on processes that are close to unitary operations, which can be written in the form

$$E(\rho) = U\rho U^{+}.$$

Many processes that arise in practice, such as quantum gates and coherent errors, belong to this class.

For these processes, we show that tomography can be performed more efficiently by combining algorithms from compressed sensing and phase retrieval with robust measurements based on interleaved RB. In particular, we use random Clifford measurements, and a variant of PhaseLift semidefinite programming (SDP) relaxation.

To justify our method for robust tomography of unitary processes, we provide a rigorous theoretical analysis, which upper-bounds the required number of random Clifford measurements, as well as the error in the reconstruction of the unknown process. This analysis required several technical innovations, including an adaptation of Mendelson's small-ball method for proving recovery guarantees in compressed sensing and phase retrieval, and a new characterization of the low-order moments of certain representations of the Clifford group. This builds on a line of work by several researchers at NIST and elsewhere.

Finally, we are continuing to investigate methods for phase retrieval using different kinds of measurements, such as random Bernoulli measurements [2]. This has applications in optical imaging, in situations where one can only measure the intensity of the light field, and not its phase.

[1] I. Roth, R. Kueng, S. Kimmel, Y.-K. Liu, D. Gross, J. Eisert, and M. Kliesch. Recovering Quantum Gates from Few Average Gate Fidelities. *Physical Review Letters* **121** (Oct. 2018), 170502.

[2] F. Krahmer and Y.-K. Liu. Phase Retrieval Without Small-Ball Probability Assumptions. *IEEE Transactions on Information Theory* **64**:1 (January 2018), 485-500.

Pseudorandom Quantum States and Quantum One-Time Programs

Yi-Kai Liu
Zhengfeng Ji (University of Technology - Sydney)
Fang Song (Portland State University)

In our recent work [1], we gave the first construction for *pseudorandom quantum states* – quantum states that look "random" to an observer that is computationally bounded. These states have several important applications in quantum cryptography and quantum information science.

First, pseudorandom states can be used to implement private-key quantum money, a natural cryptographic functionality which cannot be achieved using classical resources alone. In quantum statistical mechanics, pseudorandom states provide a simple example of how probabilistic ensembles on subsystems can emerge from a highly-entangled pure state of the universe.

Finally, pseudorandom states provide a pathological example that demonstrates the worst-case hardness of quantum state estimation: despite the fact that these states have compact (polynomial-size) classical descriptions and can be prepared efficiently (using polynomial-size quantum circuits), they cannot be characterized by *any* efficient method (using a sub-exponential number of measurements and a sub-exponential amount of computation).

Pseudorandom quantum states are related to quantum t-designs, which have been studied previously. Pseudorandom states differ from quantum t-designs in two ways: they are only computationally secure (not information-theoretically secure), and they can be constructed more efficiently, using logarithmic-depth (rather than polynomial-depth) quantum circuits.

In ongoing work, we are developing more sophisticated techniques for constructing pseudorandom unitary

operations. We expect that these will be useful for encryption of quantum states, and potentially for quantum algorithms.

In addition, we are continuing to develop theoretical proposals for quantum implementations of *one-time programs.* These are trusted computing devices that perform a pre-programmed computation exactly once, and then self-destruct. One-time programs can be used to perform actions that should not be repeated, such as spending a set amount of money, or casting a vote in an election. They can also be used to protect mobile devices, such as smartphones or autonomous drones, from being stolen and reverse-engineered by an adversary.

In previous work, we developed techniques for constructing one-time programs based on *isolated qubits*, such as nuclear spins in solid-state quantum systems. To improve the efficiency of these constructions, we are now investigating new techniques that use *program obfuscation*, in concert with isolated qubits. These techniques use fewer qubits and are more robust to noise.

[1] Z. Ji, Y.-K. Liu, and F. Song. Pseudorandom Quantum States. In *Proceedings of CRYPTO 2018*. Lecture Notes in Computer Science **10993**, 126-152.

Correlated Noise in Quantum Devices

Yi-Kai Liu
Alireza Seif (University of Maryland)
Mohammad Hafezi (University of Maryland)

Noise and decoherence are an important concern in the development of quantum devices for metrology and computation. In order to realize quantum advantages at these tasks, one must mitigate the effects of noise, using a combination of better experimental hardware, more sophisticated quantum control techniques, and active quantum error correction. These problems are becoming increasingly challenging, as experimentalists start to build so-called NISQ (noisy intermediate-scale quantum) devices. These devices can have tens to hundreds of qubits, with noise levels that are low but still non-negligible.

To this end, it is important to have mathematical models that can accurately describe noise processes on many qubits over fairly long time scales. In particular, it is important to understand temporal correlations in noise (e.g., non-Markovian memory effects), and spatial correlations (e.g., cross-talk between qubits). While there is a large literature on this subject, we believe that new approaches may be needed to address NISQ devices. In this project, we are taking a first step in this direction, by developing methods for characterizing sparse cross-talk among many qubits using compressed sensing.

In addition, we are investigating an approach called *quantum system tomography*, where one tries to discover the sources of noise in a quantum device by looking at the classical "side information" that leaks out of the device into its environment.

Post-Quantum Cryptography

Yi-Kai Liu
Gorjan Alagic (NIST/ITL Computer Security Division)
Jacob Alperin-Sheriff (NIST/ITL Comp. Security Div.)
Daniel Apon (NIST/ITL Computer Security Division)
Lily Chen (NIST/ITL Computer Security Division)
David Cooper (NIST/ITL Computer Security Division)
Quynh Dang (NIST/ITL Computer Security Division)
John Kelsey (NIST/ITL Computer Security Division)
Carl Miller (NIST/ITL Computer Security Division)
Dustin Moody (NIST/ITL Computer Security Division)
Rene Peralta (NIST/ITL Computer Security Division)
Ray Perlner (NIST/ITL Computer Security Division)
Angela Robinson (NIST/ITL Computer Security Div.)
Daniel Smith-Tone (NIST/ITL Computer Security Div.)

NIST is currently engaged in a formal process to develop standards for post-quantum cryptosystems [1]. The goal of this process is to standardize one or more cryptosystems that could replace those currently-used schemes that are vulnerable to attack by quantum computers, including RSA, Diffie-Hellman and elliptic curve cryptosystems. These play a crucial role in Internet commerce and cybersecurity. While large quantum computers have not yet been built, NIST believes it is prudent to begin preparing for that possibility.

NIST is focusing on three main functionalities: public-key encryption, key exchange, and digital signatures. These are fundamental cryptographic primitives that enable a variety of applications, including secure web browsing, digital certificates, and secure software updates.

There are a number of candidate cryptosystems that are believed to be quantum-secure. These are based on a variety of mathematical techniques, including high-dimensional lattices, coding theory, systems of multivariate polynomial equations, elliptic curve isogenies, hash-based signatures, and many others. However, further research is needed in order to increase confidence in the security of these schemes, and to improve their practical performance.

NIST has solicited proposals for post-quantum cryptosystems, which were due in November 2017. NIST received a total of 82 proposals. Since then, NIST has been carrying out a first round of review, including both internal reviews by NIST staff, and public discussions with experts and stakeholders in academia, government and industry. In these reviews, NIST is

evaluating the key properties of these cryptosystems for security, performance, and ease of deployment in the real world.

As part of this review process, NIST organized the First PQC Standardization Conference, on April 11-13, 2018, co-located with the PQCrypto conference in Fort Lauderdale, Florida. In addition, NIST hosts the "PQC forum" mailing list, which has served to communicate a large amount of feedback and technical analysis on the proposed post-quantum cryptosystems. NIST is also carrying out independent research on post-quantum cryptography and quantum cryptanalysis [2-4].

In January 2019, NIST announced that 26 of the proposed cryptosystems that will move onto the second round of the standards development process. In the second round, these candidates will be subjected to further analysis, to prepare them for possible standardization.

[1] Announcing Request for Nominations for Public-Key Post-Quantum Cryptographic Algorithms. *Federal Register*, 81 FR 92787, December 20, 2016.

[2] J. Ding, R. A. Perlner, A. Petzoldt, and D. Smith-Tone. Improved Cryptanalysis of HFEv- via Projection. In *Proceedings of PQCrypto 2018*, Lecture Notes in Computer Science **10786**, 375-395.

[3] Y. Ikematsu, R. A. Perlner, D. Smith-Tone, T. Takagi, and J. Vates. HFERP - A New Multivariate Encryption Scheme. In *Proceedings of PQCrypto 2018*, Lecture Notes in Computer Science **10786**, 396-416.

[4] S. Jordan and Y.-K. Liu. Quantum Cryptanalysis: Shor, Grover, and Beyond. *IEEE Security & Privacy* **16**:5 (September/October 2018), 14-21.

Analog Quantum Algorithms

Lucas Brady
Chris Baldwin (NIST PML)
Alexey Gorshkov (NIST PML)
Aniruddha Bapat (University of Maryland)
Jake Bringewatt (University of Maryland)
Brad Lackey (Microsoft Research)

As quantum computers and quantum technologies begin to be realized and become more powerful, it is important to develop algorithms that can exploit these small devices to best utilize any quantum advantage. Such devices are usually noisy and prone to errors, making it difficult to implement many circuit-based quantum algorithms that require a specific sequence of quantum operations. Another class of quantum algorithms that is thought to be more suitable to these small noisy devices is analog quantum algorithms. Rather than being described in terms of discrete quantum operations or gates, these algorithms are described in terms of how the system or Hamiltonian evolve with time.

One of the most promising algorithmic approaches to utilizing small quantum devices involves applying a variational approach. In this approach, we use classical computation to pick some set of parameters for a quantum calculation or state preparation, using the small quantum computer to sample from the distribution of outputs that results from those parameters. This output is then used to update the classical algorithm, leading to a loop until a desired problem is solved or the state is prepared.

For instance, one of the most prominent quantum variational algorithms is the Quantum Approximate Optimization Algorithm (QAOA) [1]. In this algorithm, a system of quantum bits, or qubits, are exposed to two alternating Hamiltonians. These Hamiltonians are applied for p alternations, with the times for each pulse being fed to the classical computer as its variational parameters. The goal is to approximately prepare the ground state of one of the Hamiltonians (or any other desired state), and the output of sampling the quantum computer for a given parameter set is used in a classical loop to optimize the energy of the produced state (or another desired quantity).

The outer loop can require significant computational resources, and one of the big open questions is how best to choose initial parameters as the size of the problem or the number of allowed parameters is increased. In collaboration with experimentalists at the University of Maryland, we are exploring these questions numerically, experimentally, and analytically. Notably, we see that an optimized set of QAOA parameters for p steps can be used to make good initial guesses at the optimal parameters for a larger number of steps. We are currently working on an analytic proof of this fact, and we are also looking at how the structure of these optimal parameters relates to the complexity of the problem being solved.

Another important class of analog quantum algorithms is Quantum Adiabatic Optimization (QAO) [2] or its slightly more generalized form, Quantum Annealing (QA). In this algorithm, the system is initialized in the ground state of some initial Hamiltonian. If the Hamiltonian changes slowly enough, the quantum adiabatic theorem says that the system will stay in the ground state, allowing us to find the ground state of desired Hamiltonians that might encode some classical problem.

One of the key challenges from these QA algorithms is how slowly they must be run and when during the process it is okay to go faster or slower. Toward that end, we are looking at the problem of doing unstructured search via an annealing algorithm. This problem, which is the analog equivalent of the digital quantum Grover's algorithm, exhibits a speed-up over the best possible classical algorithm, but only if a very careful annealing schedule is followed.

We are looking at this unstructured search problem as a testbed, trying to find new ways to dynamically update an annealing schedule using preliminary preparations of the desired state. We are also looking at the structure of the naive quantum adiabatic search algorithm, looking for ways that it could be improved. Toward this goal, we are also looking into classical search algorithms and Monte Carlo methods to see if any heuristics from classical algorithms can find new meaning in a quantum context.

[1] Edward Farhi, Jeffrey Goldstone, and Sam Gutmann. A Quantum Approximate Optimization Algorithm. arXiv:1411.4028, 2014.

[2] Edward Farhi, Jeffrey Goldstone, Sam Gutmann, and Michael Sipser. Quantum Computation by Adiabatic Evolution. arXiv:quant-ph/0001106, 2000.

Quantum Repeater R&D

Oliver Slattery
Lijun Ma
Xiao Tang

Current quantum repeater research is focused on the applications of long-distance point-to-point quantum communication and distributed quantum computational networks; see Figure 66. Quantum repeaters are essential in overcoming the distance limits of single photon transmission in optical fibers. At the same time, quantum repeaters may be used as nodes to connect separate and/or dissimilar quantum computing technologies to combine their computational capabilities or form multipoint quantum networks. Proposals for quantum repeaters have been based on the principles of entanglement swapping (teleportation). The key components of a quantum repeater include entangled photon sources, quantum memories, quantum interfaces, and Bell state measurements (BSM).

To date, several prototypes of quantum repeaters have been proposed, (partially) implemented and demonstrated in laboratory experiments. However, their performance has been poor and thus there remain huge technical challenges in the implementation of quantum repeaters. Repeater performance is limited mainly by inefficiencies of its key components as well as the challenge of integrating these components into complex quantum systems.

Quantum Memories. Quantum memory is an essential requirement for quantum computing and quantum communication. Fidelity is one of its most important performance parameters and noise greatly reduces fidelity. In an optically controlled quantum memory, the quantum signal carried by single photons needs to be controlled by a strong laser beam for storage and retrieval. Unfortunately, residual light from the control beam is a serious source of noise, especially since it may be spectrally and spatially close to the single photon signal carrying the quantum information. Many research groups, including ours, have developed noise reduction techniques which we detailed in an invited review article published in *Modern Physics Letters B.* [1].

Ensuring single photon sources are compatible in wavelength and bandwidth with quantum is a significant measurement and control challenge for quantum systems integration. Therefore, it is necessary to have a dedicated ultra-high resolution, accuracy and sensitivity spectral characterization method for single photon sources. During this period, we developed and demonstrated such a spectrometer that exploits the inherent characteristics of the same atoms that are used for quantum memories. These results were published in *Optics Express* [2] and we have applied for a patent based on this principle.

We have continued to further improve the performance of our electromagnetically-induced-transparency (EIT) quantum memory systems based on a warm atomic vapor cell and on laser trapped atoms, respectively. These improvements include a new coating on the atomic cell inner-wall that will ultimately enhance storage times and the design and implementation of a two-dimensional magneto-optical trap (MOT) for quantum memory based on cold atoms.

Quantum Interfaces. Any fully capable quantum communications system, especially a quantum network, will use a mixture of technologies and frequencies for its key components and will connect quantum systems that are based on different technologies. In this case, the interface between these various components becomes an essential consideration. A set of interfaces can, for example, convert the frequency of a signal from a shared single photon source to be compatible with different quantum memory frequencies or different quantum computing technologies. An interface can convert a telecommunications frequency that is suitable for long-distance transmission to a more optimal detection frequency while preserving the quantum characteristics of the signal. Quantum interfaces will also enable hybrid quantum networks that operate at different frequencies for different target applications.

During this period, we have continued to work with industry to develop a quantum interface to convert single photon signals from the telecommunications wavelength at 1550 nm to the atomic system wavelength of 895 nm, and vice versa. The novel design of this quantum interface will allow the pump laser to double pass through the conversion crystal to increase system efficiency and allow for lower pump power. This, combined with a pump wavelength which is longer than the input signal and converted output signal, will help reduce noise, in particular the dominant Raman noise typically associated with the pump laser.

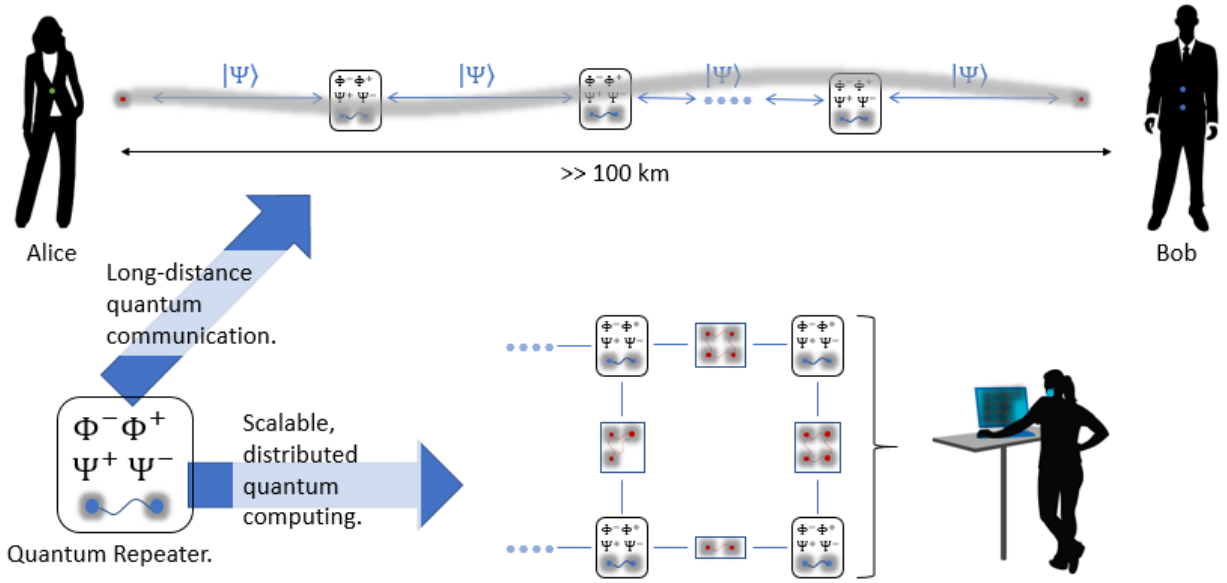

Figure 66. *A Quantum Repeater can enable long-distance ground-based quantum communications and distributed quantum computing.*

Single photon sources. We previously implemented a narrow linewidth (28 MHz) single photon source based on cavity enhanced spontaneous parametric down-conversion (SPDC) that generates photons at both the telecommunications (1310 nm) and cesium atomic (895 nm) wavelengths. Integration of this source with our cesium quantum memory is ongoing. We are also continuing our development of single photon sources based on four-wave-mixing (FWM) in a micro-resonator. These high-Q micro-resonators have the potential of generating very narrow linewidth sources that can be tailored to connect to atomic systems.

More recently, we have been working with industry to develop a novel type of single photon source based on an on-chip non-linear waveguide formed into a tunable cavity. This source uses a waveguide cavity whose index can be varied by a voltage to allow us to change the effective optical length of the waveguide at a high enough rate to potentially lock the emission (using our previously developed technique) to a desired frequency. This is a new concept based on integrated waveguide optical gyroscope (iWOG) technology. If successful, it will have high impact as a compact integrated source.

Future research. As the development of quantum system components in laboratories continues, more attention is being paid to integrating these components into complete interconnected systems such as quantum networks. However, implementing a quantum communication system in the "real world" is very different from and much more challenging than the controlled environment of the laboratory. For example, the transmission of single photons that carry quantum states is influenced by environmental fluctuations such as temperature, humidity and vibration as well as the presence of strong classical optical signals in the same infrastructure. During the next several years, we plan to work with colleagues in other ITL and NIST divisions to implement a field testbed for quantum communication and quantum networks on the NIST campus. The system will be developed for field testing of components, devices and systems related to quantum communications, and for studying the feasibility and compatibility of multiplexing quantum communication with conventional optical communication. This is an important priority because integrating into existing fiber-optic infrastructure is an economic and practical choice for deployment of quantum communication systems in the future.

[1] L. Ma, O. Slattery, and X. Tang. Noise Reduction in Optically Controlled Quantum Memory. *Modern Physics Letters B* **32**:14 (2018), 1830001.

[2] L. Ma, O. Slattery, and X. Tang. Spectral Characterization of ingle Photon Sources with Ultra-high Resolution, Accuracy and Sensitivity. *Optics Express* **25**:23, 2017, 28898-28907.

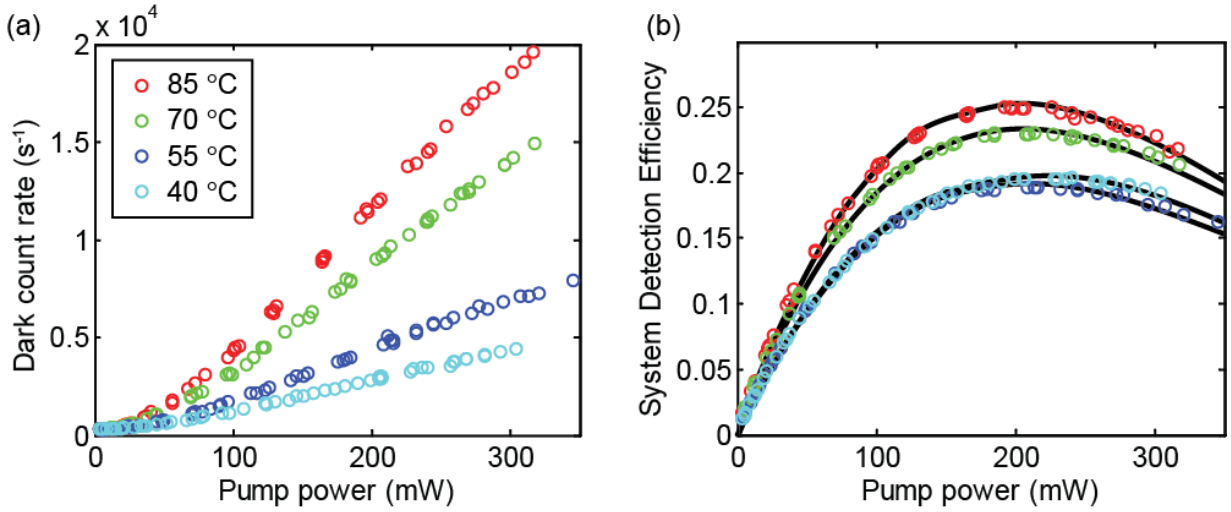

Figure 67. *(a) Dark (or noise photon) count rates as a function of device temperature. (b) System detection efficiency (SDE) at different device temperatures, which includes wavelength-dependent filter loss. After accounting for variations in SDE, the noise photon generation rate decreases with decreasing temperature.*

Technologies for Hybrid Quantum Networks

Paulina Kuo
Brian Alberding (NIST PML)
Jason Pelc (Stanford University)
Carsten Langrock (Stanford University)
Martin Fejer (Stanford University)

Future quantum information networks are envisioned to consist of a heterogenous mixture of nodes that offer different functions including quantum computation and quantum memory. These nodes operate at different wavelengths, which will require interconnects that convert between the wavelengths while preserving quantum information. ACMD researchers have contributed to improvements in technologies that support hybrid quantum networks.

One problem that has plagued the wavelength-converting interconnects is the addition of noise due to the wavelength-conversion process. ACMD researchers have studied this noise and have recently demonstrated a new strategy to reduce it [1]. By decreasing the operating temperature of the wavelength-conversion device, the number of noise photons can be lowered (see Figure 67). Experimental observations presented in this work show very good agreement with theoretical predictions based on temperature-dependent Raman scattering.

Another challenge for interconnects is the preservation of quantum information. For photonic qubits, the quantum information is often encoded in the polarizations of the photons. Unfortunately, wavelength-conversion devices are typically made of lithium niobate, which only works for one polarization. ACMD researchers are investigating wavelength-conversion devices made of other materials that are capable of dual-polarization wavelength conversion. The polarization-diverse response of this class of materials was explored theoretically in recent work [2]. There, a framework for describing the coupled-wave equations is presented and implications for wavelength-conversion devices are described.

Another key enabling technology for quantum information networks are single-photon detectors. Superconducting nanowire single photon detectors (SNSPDs) are increasingly being incorporated into quantum networks. SNSPDs offer high detection efficiency and low noise but are inconvenient to use due to their cryogenic operating-temperatures. The long-wavelength performance of commercial SNSPD systems is currently limited by the optical-fiber interconnect that delivers photons to the cryogenic detectors. ACMD researchers noted that the published data for the long-wavelength cutoff of optical fibers was highly scattered and inconsistent. They performed measurements of fiber transmission of standard optical fibers (see Figure 68) and determined that standard silica fibers offer excellent transmission up to 2.2 μm wavelength [3]. These measurements provide a path towards extending operation of SNSPDs into the infrared wavelength range.

[1] P. S. Kuo, J. S. Pelc, C. Langrock, and M. M. Fejer. Using Temperature to Reduce Noise in Quantum Frequency Conversion. *Optics Letters* **43**:9 (2018), 2034. DOI: 10.1364/OL.43.002034

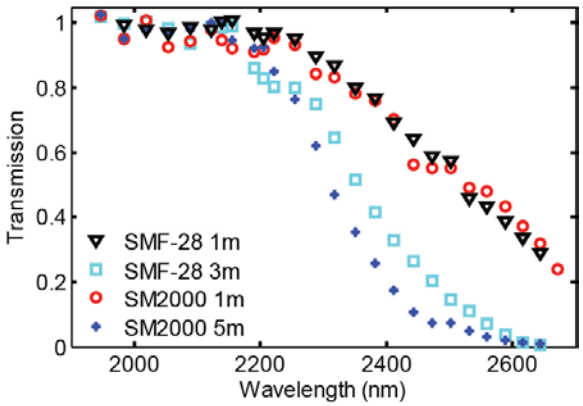

Figure 68. *Measured transmission of several different lengths of two types of silica optical fibers. The data show excellent transmission at wavelengths below 2200 nm and decreased transmission above this wavelength with 3 dB/m loss at 2500 nm.*

[2] P. S. Kuo and M. M. Fejer. Mixing of Polarization States in Zincblende Nonlinear Optical Crystals. *Optics Express* **26**:21 (2018), 26971. DOI: 10.1364/OE.26.026971

[3] P. S. Kuo. Using Silica Fiber Coupling to Extend Superconducting Nanowire Single-Photon Detectors into the Infrared. *OSA Continuum* **1**:4 (2018), 1260. DOI: 10.1364/OSAC.1.001260

Joint Center for Quantum Information and Computer Science

Stephen Jordan
Yi-Kai Liu
Carl Miller (NIST ITL)
Jacob Taylor (NIST PML)
Carl Williams (NIST PML)
Andrew Childs (University of Maryland)

http://quics.umd.edu/

Established in October 2014, the Joint Center for Quantum Information and Computer Science (QuICS) is a cooperative venture of NIST and the University of Maryland (UMD) to promote basic research in understanding how quantum systems can be effectively used to store, transport and process information. QuICS brings together researchers from the University of Maryland Institute for Advanced Computer Studies (UMIACS) and the UMD Departments of Physics and Computer Science with NIST's Information Technology and Physical Measurement Laboratories, together with postdocs, students and a host of visiting scientists.

QuICS has quickly established itself as a premier center for research in quantum information science. Twelve Fellows, 2 Adjunct Fellows, 11 postdocs, and 31 graduate and undergraduate students are currently associated with the center. In CY 2018 a total of 75 research papers were produced by those associated with the center. Some 55 seminars were held through the year, many by visiting researchers. Stephen Jordan and Yi-Kai Liu of ACMD serve as QuICS Fellows, holding research appointments at the University.

In September 2018 QuICS hosted a Workshop on Quantum Machine Learning, which attracted 60 participants. In June 2019, QuICS will host the Theoretical Quantum Computing (TQC) conference, a major annual event in the field. It will be followed by a workshop on Noisy Intermediate Scale Quantum (NISQ) Computing. During 2019 QuICS will also double its footprint in the Atlantic Building on the College Park campus, obtaining 5400 square feet of additional space, which will include 15 new offices and an expanded seminar room.

Figure 69. *Co-Director Andrew Childs in a technical discussion with QuICS fellows, postdocs and students in the QuICS offices at the University of Maryland.*

Foundations of Measurement Science for Information Systems

ITL assumes primary responsibility within NIST for the development of measurement science infrastructure and related standards for IT and its applications. ACMD develops the mathematical foundations for such work. This can be very challenging. For example, many large-scale information-centric systems can be characterized as an interconnection of many independently operating components (e.g., software systems, communication networks, the power grid, transportation systems, financial systems). A looming new example of importance to NIST is the Internet of Things. Exactly how the structure of such large-scale interconnected systems and the local dynamics of its components leads to system-level behavior is only weakly understood. This inability to predict the systemic risk inherent in system design leaves us open to unrealized potential to improve systems or to avoid potentially devastating failures. Characterizing complex systems and their security and reliability properties remains a challenging measurement science problem for ITL.

Neuromorphic Computing

Andrew Dienstfrey
Yi-Kai Liu
Alan Mink
Sonia Buckley (NIST PML)
Adam McCaughan (NIST PML)
Jeff Shainline (NIST PML)

The era of Moore's law, characterized by the exponential growth of computing performance per dollar, is now ending [1]. As this growth enabled the spectacular expansion of industries relying on the internet, cell phones, and big data, its sunset presents challenges for the next generation of products relying on technologies such as the Internet of Things (IoT) and artificial intelligence (AI). In response, companies including Intel, IBM, and Google are in a multi-billion-dollar race to develop new computational paradigms [2]. Spiking neural networks (SNNs) are one such paradigm motivated by their potential high performance for AI and IoT applications, fault tolerance, and resolution of the fundamental barriers to the future of Moore's law.

SNNs are motivated by observations of biological nervous systems, hence the term neuromorphic computation. Here intercellular communication takes the form of electrical spike-trains propagating along pathways connecting neuron cells. Information is encoded in the combination of: spike-rates, time between successive spikes, and partitioning of the neuron population into synchronized groups. From this description one recognizes that SNNs resemble artificial neural networks in that both rely on parallel information processing in layered networks. However, the time dynamics inherent in SNNs introduce a new dimension of complexity into algorithmic design and computational possibilities. A representation of their interrelationship is shown in Figure 70.

This past year we initiated a project with a long-term goal to research and develop an implementation of a spike-based computer using super-conducting optoelectronics. Such devices leverage NIST's world class expertise in few-photon generation and detection to create optical spike trains organized for neuromorphic computation. These novel devices are prime SNN candidates due to their high speed, scalability, and incredibly low power consumption [3].

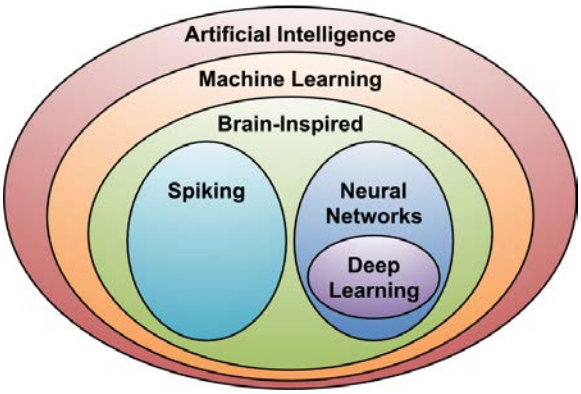

Figure 70. *Schematic representation of AI problem space and the relationship between spiking and deep neural networks. (Reproduced from [5]).*

ACMD contributions to this project include analysis of algorithms which admit novel solutions in a spike-based model of computation. In FY 2018 we focused attention on recent results indicating that the problem of finding a sparse-representation of a signal from a given dictionary can be implemented in a spiking format [4]. We have developed a simulation of this algorithm and will research hardware implementations in the future.

[1] T. N. Theis and H.-S. P. Wong. The End of Moore's Law: A New Beginning for Information Technology. *Computing in Science and Engineering* **19**:2 (2017), 41-50.

[2] J. Pavlus. The Billion-dollar Race to Reinvent the Computer Chip. *Scientific American* (May 2015).

[3] J. M. Shainline, S. M. Buckley, R. P. Mirin, and S. W. Nam. Superconducting Optoelectronic Circuits for Neuromorphic Computing. *Physical Review Applied* **7** (2017), 034013.

[4] P. T. P. Tang. Convergence of LCA Flows to (C)LASSO Solutions. arXiv:1603.01644 (2016).

A New Metric for Robustness of Complex Systems – Identifying Nodes Vulnerable to Cascading Failures

Richard J. La

Many critical systems (e.g., smart grids, manufacturing systems, transportation systems) are comprised of multiple heterogeneous component systems (CSs) which depend on and support each other. For instance, a modern power system not only includes an electrical grid/network that consists of many elements, but also utilizes an information and communication network (ICN) to monitor the state of (the elements in) the electrical network and to take appropriate control actions based on the observed state. Intricate dependence among CSs makes the analysis of such complex systems challenging. Moreover, in many cases, a local failure of even a small number of CSs can cause widespread failures in the system, affecting many CSs. For instance, an outage in a part of an electrical network can trigger cascading failures and lead to a large-scale blackout, affecting millions of people (e.g., Northeast blackout of 2003 and India blackouts of 2012).

With the increasing reliance of modern societies on such complex yet fragile systems for important services, there is a growing interest in modeling and understanding the interaction between CSs and the robustness of the overall systems. The goals of this project are:

(i) develop a new sound model for capturing the interdependence among CSs;
(ii) investigate the likelihood of suffering widespread failures in large complex systems; and
(iii) identify more vulnerable CSs that will serve as the "weak" links in critical systems.

The expected outcomes will help researchers and engineers to better understand the fragility/robustness of critical systems and develop new guidelines for improving their resilience against attacks and failures.

In order to achieve these goals, borrowing advanced tools from random graphs, branching processes, and optimization theory, we first developed a novel model that allows us to estimate the likelihood that a large system will experience widespread failures, beginning with a local failure. We call this the Probability of Cascading Failures (PoCF). Because the PoCF depends on the CS that suffers the initial failure, it helps us identify "vulnerable" CSs that are more likely to cause widespread failures. Using the new model, we investigated how the underlying structure of dependence among the CSs affects their PoCFs. Second, we proposed two computationally efficient methods for identifying vulnerable nodes with limited historical data and/or detailed simulation.

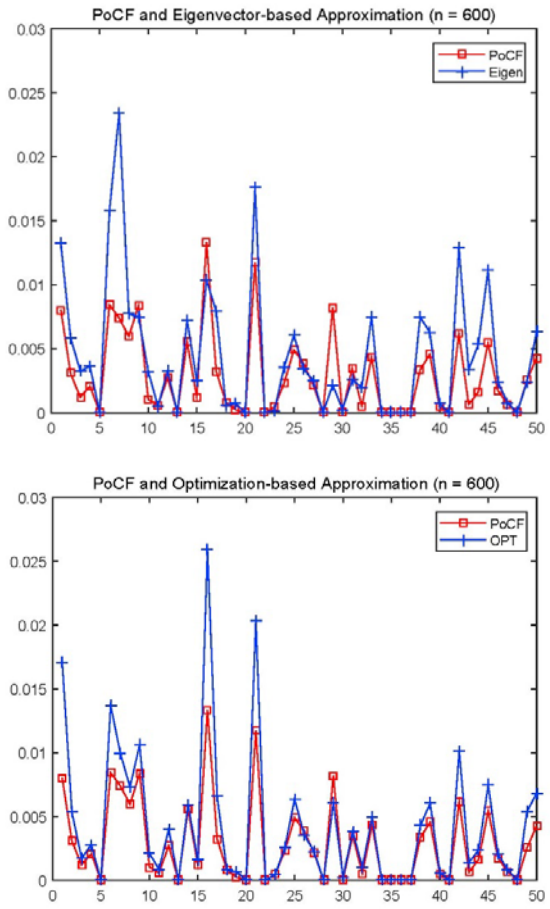

Figure 71. *Plots of normalized PoCFs and their approximations using eigenvector-based and optimization-based approaches for a network of 600 CSs. (All vectors are normalized so the sum of the elements is equal to one.)*

Some of our key results are:

a) there is an intriguing relationship between the clustering (also known as transitivity) exhibited by real networks and the average PoCF. But, in the critical regime where a large system can suffer widespread failures, clustering tends to help keep failures localized in a small neighborhood, thus diminishing the PoCF in large systems; and
b) under some assumptions, there is a close relation between the PoCFs of CSs and their non-backtracking centralities, which serve as a measure of their importance in a network.

Furthermore, our proposed methods for identifying vulnerable nodes (eigenvector-based approach and optimization-based approach) suggest that, even in the

absence of sufficient historical data or detailed simulation, we may be able to identify many, if not most, of vulnerable nodes that are far more likely to trigger cascading failures in the system in a computationally efficient manner.

Figure 71 shows the PoCFs and their approximations for CSs 1 through 50 in a system with 600 CSs. They are normalized so that their ℓ_1 norm is equal to one. It is clear from the plots that, although the proposed methods do not give the exact values, the trend and variations in PoCFs are correctly captured to a large extent, helping us find most of vulnerable nodes.

[1] R. J. La. Influence of Clustering on Cascading Failures in Interdependent Systems. *IEEE Transactions on Network Science and Engineering*, in press. DOI: 10.1109/TNSE.2018.2805720

[2] R. J. La. Identifying Vulnerable Nodes to Cascading Failures: Centrality to the Rescue. In *Complex Networks and Their Applications VII. COMPLEX NETWORKS 2018* (L. Aiello, C. Cherifi, H. Cherifi, R. Lambiotte, P. Lió, and L. Rocha, eds.), 866-878. *Studies in Computational Intelligence* **812** (2019). Springer. DOI: 10.1007/978-3-030-05411-3_69

Towards Balancing Cyber Resiliency with Economic Efficiency

Vladimir Marbukh

Numerous recent systemic failures in various performance oriented networked infrastructures demonstrated systemic risks associated with economic benefits of interconnectivity. We have argued in [1, 2] that while interconnectivity allows a system to accommodate "small" demand/capacity imbalances, sufficiently large imbalances may result in abrupt/discontinuous instabilities, which is a form of *robust yet fragile* phenomenon. Fragility risks are aggravated by economic pressures driving networked system design/operation towards the boundary of the system capacity/operational region, where all system resources are fully utilized Interconnectivity results in a hard/discontinuous stability loss as the system breaches this boundary due to unavoidable exogenous uncertainties.

Our current work emphasizes cyber resilience implications of this robust yet fragile phenomenon, which can be exploited by an adversary capable of triggering a super-critical adversarial event which causes a system transition to a persistent undesirable regime. For example, a distributed denial of service (DDoS) attacker may cause a super-critical demand/capacity imbalance. The National Academies define resilience as "the ability to prepare and plan for, absorb, recover from, and more successfully adapt to adverse events." Managing system resilience involves balancing numerous tradeoffs, e.g.,

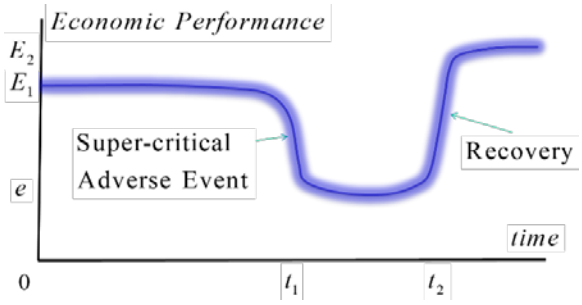

Figure 72. *System performance through failure/recovery cycle.*

the tradeoff between robustness and recoverability as well as the tradeoff between performance in normal and failed regimes. IEEE Standard 610.12.1990 defines robustness as "the degree to which a system operates correctly in the presence of exceptional inputs or stressful environmental conditions."

Figure 72 depicts the evolution of the economic performance of a robust yet fragile system operating under variable exogenous conditions. During period of "normal" operation $t \in [0, t_1)$, when exogenous variability does not exceed certain threshold, networked infrastructure performance fluctuates at acceptable level E_1. The length of the time interval $t \in [0, t_1)$ represents system robustness. Once the exogenous variability/adversity exceeds a certain critical level at some moment $t = t_1$, the system fragility manifests itself as unacceptable performance deterioration to level e. This transition typically has a form of cascading failure. The system recovery during time interval $t \in [t_1, t_2)$, raises system performance to level E_2, which may be different from the previous "normal" performance level E_1. The situation $E_2 > E_1$ $(E_2 < E_1)$ corresponds to successful (unsuccessful) adaptation to supercritical exogenous uncertainty/adversity.

Our efforts [1-7] are directed towards exposing, quantifying, and ultimately managing, the various tradeoffs required for balancing resiliency with economic efficiency. Our results indicate that, given system resources, increase in the economic efficiency by increasing resource utilization, reduces the stability margin of the operational regime, which reduces system robustness to exogenous shocks and thus negatively affects system resilience. Currently we are investigating the robustness vs. recoverability tradeoff which is due to competition between investment in adding capacity to enable the system to better withstand exogenous shocks vs. investment in the recovery capability to reduce recovery time $\tau = t_2 - t_1$.

[1] V. Marbukh. "Towards Resilient Yet Economically Viable Networked Infrastructures: Quantitative Metrics and Systemic Risk-Aware Design." International Conference on Infrastructure Resilience, ETH Zurich, February 2018.

[2] V. Marbukh. "Dynamic Job Replication for Balancing Fault Tolerance, Latency, and Economic Efficiency:

Work in Progress." IEEE World Congress on Services 2018 (IEEE Services 2018), San Francisco, CA, July 2-7, 2018.

[3] V. Marbukh. "Economics of Networked Infrastructures at the Edge of Undesirable Contagion: A Case of SIS Infection." Poster, IEEE Infocom 2018, Honolulu, HI, April 15-19, 2018.

[4] V. Marbukh. "Network Formation by Contagion Averse Agents: Modeling Bounded Rationality with Logit Learning." Workshop on Dynamics on and Of Networks (DYNO 2018) co-located with the 2018 IEEE/ACM International Conference on Advances in Social Networks Analysis and Mining (ASONAM 2018).

[5] V. Marbukh. "Towards Efficient Offloading in Fog/Edge Computing by Approximating Effect of Externalities." Workshop on Integrating Edge Computing, Caching, and Offloading in Next Generation Network co-located with IEEE Infocom 2018, Honolulu, HI, April 15-19, 2018.

[6] V. Marbukh. "On Mitigation Inefficiency of Selfish Investment in Network Recovery from High Loss SIS Infection." Workshop on Cyber-Physical Systems and Applications (IWCPSA 2018), co-located with the 17th IEEE International Conference on Trust, Security and Privacy in Computing and Communications 2018 (IEEE TrustCom-18).

[7] V. Marbukh. Towards Managing Age of Network State Information in Challenged Networks. In *Proceedings of IEEE Infocom 2018*, Honolulu, HI, April 15-19, 2018.

Algorithms for Identifying Important Network Nodes for Communication and Spread

Fern Y. Hunt
Roldan Pozo

The identification of nodes in a network that enable the fastest spread of information is an important if not fundamental problem in network control and design. It is applicable to the optimal placement of sensors, the design of secure networks, and the problem of control when network resources are limited. Our approach to this problem has its origins in models of opinion dynamics and the spread of innovation in social networks. The mode of communication between nodes is described by simple models of random or deterministic propagation of information from a node to its neighbors. During the past few years, we have made progress in understanding the structural requirements for sets of nodes for effective spread in networks and have developed scalable algorithms for constructing these sets in real world networks.

We consider a discrete time model of information spread (represented by a variable assigned to each node) in a network with a set of nodes V and a subset $A \subseteq V$ of k nodes representing leaders or stubborn agents that are initially assigned a single value. Propagation occurs by iterated averaging or diffusion defined by a stochastic matrix P. All node values will eventually converge to the single value at a speed determined by the sub-stochastic matrix $P_{\sim A}$, the matrix P restricted to the complement of A. An effective spreader in this situation is then a set of nodes for which convergence to this single value is fastest, i.e., the set A for which the Perron-Frobenius eigenvalue of $P_{\sim A}$ is largest. Using a classical result of Markov chain theory, the problem can be recast in terms of finding the set A of cardinality k that minimizes the mean first hitting time, i.e., the average or expected time a random walker reaches the target set A for the first time.

We have developed a polynomial time algorithm for finding an approximation to the optimal set. It is an extension of the classic greedy algorithm and it begins with a class of optimal and near optimal starter sets of cardinality $m < k$, rather than the best singleton set. For a graph with N nodes, the complexity of the method is $O(N^m E)$ where E is the complexity of calculating $F(A)$ for a single set A. $F(A)$ is the sum of all arrival times to the vertex set A from nodes outside of A, where the arrival time for any vertex is the average random-walk path length to A. If one calculates F by solving an appropriate sparse eigenproblem, then $E = O(N^2)$, but if fast Laplacian methods are used then $E = O(N(\log N)^2)$; see [2]. In actual computations $m = 1$ or 2 is used.

Direct comparison of the algorithm results with the actual optimal solution and lower bounds on the performance ratio can be obtained because F is a supermodular set function [2]. However, for large complex networks commonly encountered in applications, another approach is needed.

Recently, we developed a set of fast heuristics that work well on graphs with large hubs, a common feature of complex networks. When the desired set cardinality is k, subsets of hub vertices are rapidly screened to produce candidate sets. Each set consists of k nodes whose first (or higher order) neighborhoods have minimal overlap. After further screening, the offered approximation is selected by ranking the results of a Monte Carlo calculation of F for each candidate. This process allows us to find near optimal and optimal spreaders in networks with millions of nodes and dozens of millions of edges in less than a few seconds on a typical laptop.

This past year, we investigated the validity of this procedure. After realizing that the resulting offered set was an approximate solution of a discrete stochastic optimization problem, we established sufficient conditions that imply that it is also an approximate solution of the original problem, the degree of approximation being the same in both cases. The fact that the first hitting time to a set A has a distribution with exponential tails means that a sample average of simulated hitting times produces a consistent estimate of F in the limit of large sample size. Establishing the degree of optimality of any

offered solution is very difficult since supermodularity cannot be used and the size of the graphs are so large. However, the methods we use make it possible to rapidly sample the distribution of possible *F* values. We are leveraging this capability to produce estimates and confidence intervals for the optimal value by using bootstrapping and other resampling techniques. Thus, the validity of this approach can be justified in a statistical sense. The results of our work on this phase of the project are reported in paper in preparation [3].

[1] F. Hunt. Using First Hitting Times to Maximize the Rate of Convergence to Consensus. arXiv:1812.08881.

[2] F. Hunt. An Algorithm for Identifying Optimal Spreaders in a Random Walk Model of Network Communication. *Journal of Research of the National Institute of Standards and Technology* **121** (2016), 180-195.

[3] F. Hunt and R. Pozo. Algorithms for Effective Spread and Communication in Real Complex Networks. In preparation.

Algorithmic Tools for Network Modeling and Analysis

Brian Cloteaux

Studying interactions within systems, such as biological, social or communications, is an active area of pursuit in the research community. Commonly, such interactions are modeled as networks or graphs. As these areas of investigation mature, researchers increasingly need to be domain specialists, not experts in programming and graph algorithms. Providing such researchers with a tool set of fast and efficient algorithms for network modeling and analysis is the central idea behind this project. As a byproduct of this research, there have been a number of theoretical discoveries.

Recent results coming from this project have given extremely efficient algorithms for testing if a sequence is graphic [1], and for generating random instances of a network with a given degree sequence [2]. In addition to these new algorithms, we have been looking at approaches to improving existing algorithms. We found several new bounds that have direct algorithmic application [3, 4], leading to faster modeling algorithms, and interesting applications in graph theory.

As an example of the results from this project, we recently worked on the problem of random graph generation. The most common approach used for this problem is to create a non-random instance and then to modify it using a Monte Carlo Markov chain approach. A serious problem with this approach is that it requires holding an entire graph in memory. For random graph generation, sequential importance sampling methods have also been developed, but suffer from slow run times. We introduced a new algorithm for creating random instances

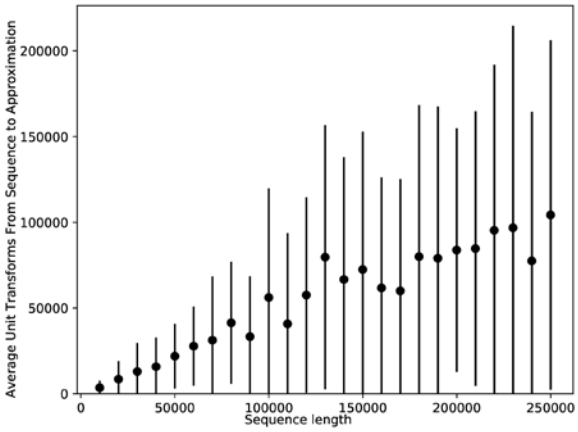

Figure 73. *The average number of unit transformations between a non-graphic sequence selected from a power-law distribution with exponent of 2 and its approximation created from the algorithm in [6]. Each point represents the average number of unit transformations for 30 sequences created at a given length. The error bars represent one standard deviation.*

[2], which overcomes the space and time limitations of earlier methods. At the same time, we also published results that can be used to speed-up some instances of the traditional Monte Carlo Markov chain approach [4].

Recently we have given attention to the problem of generating random graphs created using a graphic degree sequence selected from some given probability distribution. More specifically, how do we deal with a randomly drawn integer sequence that is not graphic (i.e., a degree distribution that is not realized in any graph)? There have been two approaches to this problem. The first is to simply discard the sequence and repeatedly select a new sequence until a graphic sequence is found. This approach is used by the NetworkX graph library. A disadvantage to this approach is that for some probability distributions, such as a power-law distribution, the probability of selecting a graphic sequence can be very small. For these distributions, we have a very small chance of finding a graphic sequence in reasonable time.

Last year, we contributed a new and extremely fast algorithm for this problem [5]. One disadvantage of our approach was that it can greatly affect the size of the hub nodes in a distribution. This year we produced a new algorithm that is both fast and protects the hub nodes [6]. Figure 73 shows the average number of sequence modifications needed for this algorithm. This figure shows the linear run-time expected for this new algorithm. We are currently publishing this new algorithm and enhancements for the benefit of the public. We are further looking to see if we can parallelize these algorithms for even greater speed up. In addition, we are continuing to examine other fundamental algorithms needed by the network research community.

[1] B. Cloteaux. Is This for Real? Fast Graphicality Testing. *Computing in Science & Engineering* **17**:6 (2015), 91-95.

[2] B. Cloteaux. Fast Sequential Creation of Random Realizations of Degree Sequences. *Internet Mathematics* **12**:3 (2016), 205-219.

[3] B. Cloteaux. A Sufficient Condition for Graphic Lists with Given Largest and Smallest Entries, Length and Sum. *Discrete Mathematics and Theoretical Computer Science* **20**:1 (2018), Number 25.

[4] B. Cloteaux. Forced Edges and Graph Structure. In review.

[5] B. Cloteaux. One-Pass Graphic Approximation of Integer Sequences. In review.

[6] B. Cloteaux. Fast Graphic Approximation of Very Large Integer Sequences. In review.

Counting the Number of Linear Extension of a Directed Acyclic Graph

Isabel Beichl
Alathea Jensen (George Mason University)
Francis Sullivan (IDA Center for Computing Sciences)

We have developed a new algorithm for approximating the number of linear extensions of a directed acyclic graph (DAG). A DAG is a set of nodes and directed edges and can be used to model many data that arise in information technology. A linear extension is a topological sort of this data that preserves the DAG ordering. For example, if the data is a list of tasks to be done with some tasks needing to be completed before others are started, then a linear extension is a legal schedule of the tasks. Ideally one would like to optimize something among the schedules. Fast counting of the number of such legal schedules, without actually optimizing, would give an estimate of how hard one might need to work to optimize. It gives information on modeling the computation.

There are algorithms for counting the number of linear extensions based on the Markov Chain Monte Carlo method (MCMC), but they are impractical for large data sets. We have developed several methods based on sequential importance sampling. In particular, we have developed a new importance function related to the Moebius function that works extremely well on large data.

[1] I. Beichl, A. Jensen, and F. Sullivan. A Sequential Importance Sampling Algorithm for Estimating Linear Extensions. arXiv:1902.01704 [cs.DS].

Using Sequential Importance Sampling to Speed Up the Monte Carlo Markov Chain Method

Isabel Beichl
Francis Sullivan (IDA Center for Computing Sciences)

Monte Carlo methods have become central to scientific computing and their importance is growing because of applications in machine learning and stochastic optimization. An important issue in the use of the Markov Chain version of Monte Carlo (MCMC) is the rate of convergence and determining optimal fugacity. In earlier research joint with D. P. O'Leary we proposed some methods for addressing these issues. We have now discovered and developed some improved methods based on sequential importance sampling (SIS) to determining optimal fugacity and to give estimates for the rate of convergence. By using SIS, we can learn much about aggregation of states and how the MCMC would have to behave. We are now engaged in writing up our results.

A New Metric for Resilient Intelligent Transportation Systems

Richard J. La
Mohammad Hassan Lotfi (University of Maryland)
Nuno C. Martins (University of Maryland)

Over the past decades, many metropolitan areas have experienced a significant increase in traffic congestion. As a result, existing transportation infrastructure is strained, and drivers suffer many lost hours every year, resulting in significant economic losses to society. Unfortunately, increasing the capacity of the transportation system is expensive and is not always economically feasible. Moreover, in many cases, traffic congestion is caused not only by high traffic volume, but also by unpredictable exogenous factors, such as accidents, construction activities, or new traffic patterns. When this happens, without access to current traffic information, drivers who often plan their routes based on the past experience cannot avoid congestion.

On the other hand, there are already existing infrastructure and information technologies (e.g., smart navigation tools) that can be utilized to provide more up-to-date information to drivers. Somewhat surprisingly, recent studies showed that providing more information to drivers is not always beneficial; the overall network congestion increases as a result of offering information to (more) drivers. For this reason, it is important to understand the coupling between the transportation system and the information technologies used to provide (real-

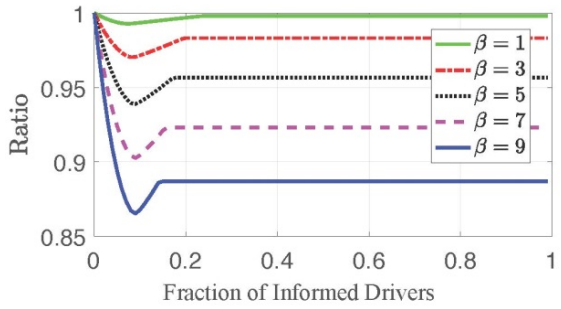

Figure 74. *The ratio of the network cost at a new equilibrium with traffic information to informed drivers to that with no traffic information to drivers.*

time) traffic information to drivers, to avoid preventable congestion or exacerbating severe network congestion.

Any study of such coupling and its effects requires examining how drivers' behavior change in response to information. Moreover, their response to the information will depend on (i) how other drivers respond as well, creating further coupling in the behavior among the drivers, and (ii) how sensitive congestion delays are to traffic volume. The main goals of this project are:

a) to understand the change in drivers' behavior in response to different forms of traffic information, and
b) to design effective means of communicating traffic information to drivers via information technologies in intelligent transportation systems with the objective of minimizing network congestion.

As a starting point, we investigated a simple scenario where a set of drivers choose one of two available routes (routes 1 and 2) from a source to a destination. However, one of the routes (route 1) suffers from more unpredictable traffic conditions due to, for example, frequent accidents or long-term construction projects, the distribution of which is known to all drivers (who can learn it from experience). In the first scenario, the drivers select one of two routes based on their beliefs regarding the traffic conditions on both routes with the goal of minimizing the expected delay. This leads to a Bayesian Wardrop equilibrium at which the expected delay is the same for both routes.

In the second scenario, a subset of drivers is informed by a traffic manager of the traffic condition on route 1 through a binary signal ("High" vs. "Normal"). The uninformed drivers, in the absence of additional information, act on the prior beliefs and pick a route in accordance with the Bayesian Wardrop equilibrium strategies. The "informed" drivers, on the other hand, update their beliefs about the traffic condition on route 1 and choose one of the routes that will minimize the expected delay. Note that the posterior beliefs of the informed drivers depend on how the traffic manager selects the signal to send ("High" or "Normal"). The goal of the traffic manager is to select a binary signal in such a way to minimize the average congestion delay in the network.

Our main findings include the following:

(i) even with a simple binary signal, a judicially selected signal can reduce the overall network congestion;
(ii) as the congestion delay becomes more sensitive to traffic volume, the traffic manager should send the "High" signal only if the traffic congestion is more severe; and
(iii) there is an optimal fraction of drivers the traffic manager should inform of the traffic condition, which is less than one (even when all drivers are capable of receiving the signal), which minimizes the overall network congestion. The last observation suggests that, in some cases, the traffic manager may wish to restrict the information regarding traffic condition to some drivers to minimize the congestion delay in a network.

Figure 74 plots the ratio of the minimum network cost (measured by overall average delay) the traffic manager can achieve by informing varying fraction of drivers of the traffic condition on route 1 to that of the first scenario (in which no driver receives any signal). The parameter β determines how sensitive the congestion delay is to traffic volume; the larger it is, the more sensitive are congestion delays. The plot indicates that, indeed, only a small fraction of drivers (about 10 percent) should be informed of the traffic condition on route 1 to minimize the network congestion. Furthermore, the more sensitive congestion delays are to traffic volume, the greater the benefits are, i.e., a larger reduction in congestion delays can be achieved by signaling drivers.

[1] M. H. Lotfi, R. J. La, and N. C. Martins. Bayesian Congestion Game with Traffic Manager: Binary Signal Case. In *Proceedings of the 57th IEEE Conference on Decision and Control (CDC)*, Miami (FL), December 17-19, 2018.

Estimating the Orientation of a Wireless Capsule Endoscopy

Katjana Krhac (University of Zagreb, Croatia)
Kamran Sayrafian
Mehdi Alasti (Adgen Telecom Group)
Kamya Yazdandoost (Aalto University, Finland)
Dina Simunic (University of Zagreb, Croatia)

Endoscopy procedures play a significant part in nearly all gastro-intestinal (GI) related diseases, as well as a crucial role in clinical research. It is estimated that more than 20 million GI endoscopies are performed each year in the United States [1]. A wireless capsule endoscopy is an ingestible capsule equipped with a miniaturized

camera. It provides a minimally invasive alternative imaging technology for the entire GI tract of the human body. Wireless capsule endoscopy (WCE) is the only painless and effective diagnostic technology for various diseases such as obscure gastrointestinal bleeding, tumors, cancer, Crohn's disease, and celiac disease. The breakthrough impact of WCE in medicine is that it allows observation of abnormalities in the entire 5 m to 7 m length of the small intestine from locations that are not accessible by today's conventional endoscopy or colonoscopy technology.

Eighteen years after the invention of this technology, positioning and mapping metrology in this area is still in its infancy. As a result, doctors receive clear pictures of abnormalities such as bleeding and tumors inside the GI tract, but they have no way to determine their precise locations within the body or the relative distance of the abnormality from an anatomic landmark, such as the pylorus or the ileocecal valve. This is due to lack of knowledge about location and orientation of a capsule at the time when the image is taken. Lack of such critical information necessitates follow-on use of expensive and invasive testing such as deep endoscopy, CT enterography, or even surgery to determine the site of the tumor, lesion, or bleeding. The elasticity of the GI tract, and the looped and folded nature of some its components (e.g., small intestine), along with variable speed and irregular motion pattern of a WCE, pose several unique metrology challenges for this problem.

Since the next generation of endoscopy capsules are expected to deliver higher quality images, or even videos as well as more diagnosis and therapeutic functionality, in this study, ultra-wideband (UWB) technology has been considered for the wireless communication links between the transmitter antenna inside the capsule and the receiver's nodes located on the body. Despite the high attenuation, higher bandwidth (i.e., data rate) and lower complexity of the transceiver makes UWB an attractive candidate for future WCE.

Research activities on WCE have been mostly focused on developing accurate position estimation methodologies [2-4]; however, as the miniaturized camera in these capsules do not have a wide view angle, knowledge of the capsule orientation inside the GI tract could also be valuable information for the physicians who review the transmitted images. This adds another layer of complexity to the already challenging localization problem for such capsules.

Another challenge in studying localization or orientation estimation of a WCE is the platform that should be used to evaluate potential methodologies. Clearly, physical experimentation on patients is nearly impossible. Therefore, computational models or liquid phantoms are often used to carry out such studies. Liquid phantoms are aqueous solutions that mimic the electromagnetic properties of human tissues (e.g., muscle). Although they enable simple physical

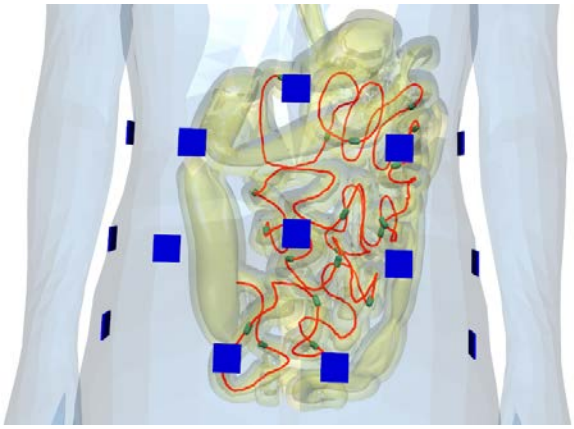

Figure 75. *Computational human body model with enhanced GI tract.*

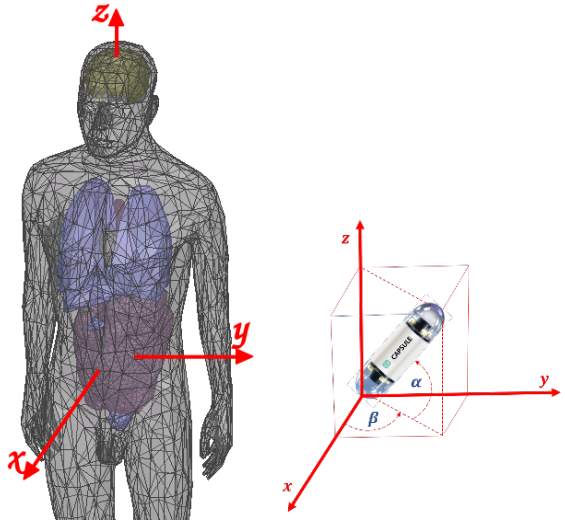

Figure 76. *Specification of the capsule orientation (α and β).*

experimentation, the results might not be so accurate as they fail to capture the inhomogeneous nature of the human body. On the other hand, computational human body models can capture details of the inhomogeneous environment between the capsule and the on-body receivers. However, extensive computational time and high memory requirements often create an obstacle in performing sophisticated simulation involving a WCE.

In this study, a novel 3D computation and immersive platform visualization that emulates the communication links between a WCE and several on-body sensors has been developed [5]. A high-resolution 3D GI tract model without self-intersections or other "non-manifold" features has also been developed and integrated with a 3D computational human body model of an adult male (Figure 75). The 3D body model has a resolution of 2 mm and includes frequency-dependent dielectric properties of 300+ parts of a male human body. These dielectric properties are user-definable in case custom modifications or changes are desired. Validated models of practical antennas have also been

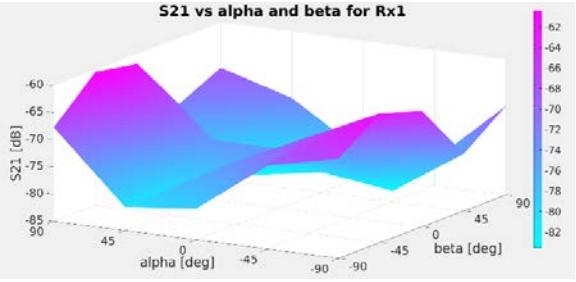

Figure 77. *Magnitude of S_{21} at receiver 1 versus orientation angles α and β.*

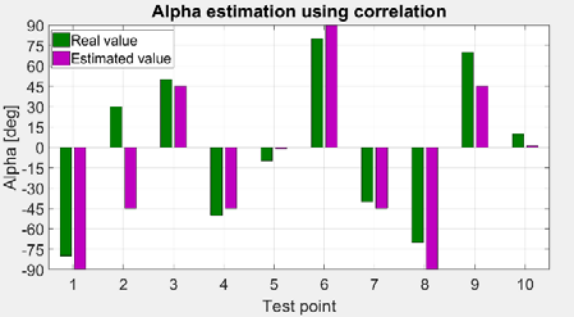

Figure 78. *α versus $\hat{\alpha}$ using correlation coefficient.*

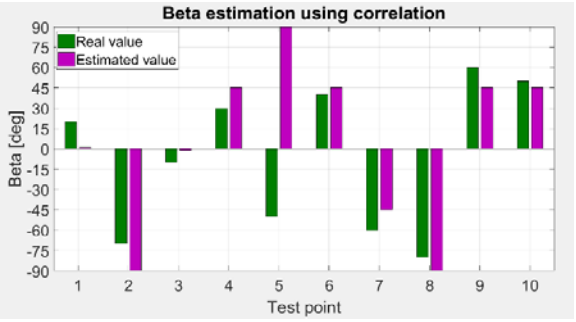

Figure 79. *β versus $\hat{\beta}$ using correlation coefficient.*

incorporated in the computational system to accurately characterize the wireless link between the capsule and the on-body receivers' antennas.

The center-line that passes through the GI tract (e.g., small intestine) in 3D space has been calculated and used as the reference line for the capsule placement within the GI tract (shown as a red line in Figure 75). Multiple on-body receivers (indicated with blue squares in Figure 75) have been considered around the abdomen area. The collection of the signal strength at these receivers are typically used to estimate the location of the capsule within the GI tract. This data can also be processed to infer further information about the orientation of the transmit antenna (or equivalently the orientation of the capsule) at a given location. To see this possibility, consider the coordinate system illustrated in Figure 76. The angles α and β specify the orientation of the capsule located at the origin of a coordinate system that is completely parallel to the global body coordinate.

Figure 77 demonstrates the magnitude of the forward transmission coefficient (i.e., S_{21}) between the transmit antenna (inside the capsule located at a sample position inside the small intestine) and one of the receivers on the body surface (e.g., Rx1). As observed, variations in α and β directly impact the magnitude of S_{21} and therefore the received signal strength at Rx1. In this project, we study this impact by using the complex correlation coefficient defined as the cross correlation between the S_{21} vector at position $\overline{P}_k$ with orientation α and β and the S_{21} vector at position $\overline{P}_{k+j}$ with orientation $\alpha+m\Delta$ and $\beta+n\Delta$. High values of this coefficient could be translated to similarities between two capsule positions or orientations. Therefore, if prior knowledge of the S_{21} vector at a reference location is available, then some information regarding orientation α, β and $\overline{P}_k$ can be obtained by looking at the values of this coefficient.

The correlation coefficient is sensitive to rotations in α and β. Changes in the values of α or β will effectively change the direction where the null of the antenna is pointing. For the specific WCE antenna [6], the orientation of the null in its pattern is indeed equivalent to the orientation of the camera which is typically mounted in one end of the capsule. Estimation of α and β can effectively identify the direction of this null, and in turn the capsule. Following this methodology, and using 10 different sample points, Figure 78 and Figure 79 show the real and estimated values of α and β.

Although for data communication purposes, it is clearly preferred to have a completely omni-directional antenna for the capsule, the initial results obtained so far indicate that any directionality (or equivalently any nulls) in the capsule antenna pattern could be exploited to estimate its orientation through observation of the signal strength by a set of on-body receivers [7]. It is conjectured that a larger number of sensors on the abdomen area could lead to higher accuracy in the estimated orientation. Further studies are needed to determine the optimal locations for these sensors around the abdomen.

[1] J. E. Everhart. Burden of Digestive Diseases in the United States Report, National Institutes of Health. NIH Publication 09-6443. URL: http://www.niddk.nih.gov/about-niddk/strategic-plans-reports/Pages/burden-digestive-diseases-in-united-states-report.aspx

[2] H. Mateen, M. D. Basar, A. U. Ahmed, and M. Y. Ahmad, Localization of Wireless Capsule Endoscope: A Systematic Review. *IEEE Sensors Journal* **17**:5 (March 2017), 1197-1206.

[3] Y. Geng and K. Pahlavan. On the Accuracy of RF and Image Processing Based Hybrid Localization for Wireless Capsule Endoscopy. In *Proceedings of the IEEE Wireless Communications and Networking Conference* (WCNC), New Orleans, LA, March 9-12, 2015. DOI: 10.1109/WCNC.2015.7127512

[4] N. Dey, A. S. Ashour, F. Shi, and R. S. Sherratt. Wireless Capsule Gastrointestinal Endoscopy: Direction-of-Arrival Estimation Based Localization Survey. *IEEE Reviews in Biomedical Engineering* **10** (2017), 2-11. DOI: 10.1109/RBME.2017.2697950

[5] K. Sayrafian, J. Hagedorn, W. B. Yang, and J. Terrill. A Virtual Reality Platform to Study RF Propagation in Body Area Networks. In *Proceedings of the 3rd IEEE International Conference on Cognitive Infocommunications (CogInfoCom)*, Kosice, Slovakia, December 2-5, 2012.

[6] K. Y. Yazdandoost. Antenna for Wireless Capsule Endoscopy at Ultra-Wide Band Frequency. In *Proceedings of the IEEE Symposium on Personal Mobile Radio Communications (PIMRC)*, Valencia, Spain, September 4-7, 2016. DOI: 10.1109/PIMRC.2016.7794781

[7] K. Krhac, K. Sayarafian, M. Alasti, K. Y. Yazdandoost, and D. Simunic. A Study of Capsule Endoscopy Orientation Estimation at UWB Frequencies. In *Proceedings of the IEEE International Symposium on Personal, Indoor and Mobile Radio Communications (PIMRC'18)*, Bologna, Italy, September 9-11, 2018.

Combinatorial Testing for Software Based Systems

Raghu N. Kacker
D. Richard Kuhn (NIST ITL)
Yu Lei (University of Texas at Arlington)
Dimitris E. Simos (SBA-Research, Austria)
Mohammad S. Raunak (Loyola University, Maryland)
Nicky Mouha (NIST ITL)
Eric Wong (University of Texas at Dallas)
James F. Lawrence
Itzel Dominguez-Mendoza (CENAM, Mexico)

https://csrc.nist.gov/projects/automated-combinatorial-testing-for-software

In 1997 the Mars Pathfinder began experiencing system resets at seemingly unpredictable times soon after it landed and began collecting data. Fortunately, engineers were able to deduce and correct the problem, which occurred only when (1) a particular type of data was being collected, and (2) intermediate priority tasks exceeded a certain load, resulting in a blocking condition that eventually triggered a reset. Situations of this type are known as *interaction faults*. Many real-time failures of software-based systems have been traced to interaction faults. These are often insidious in that they may remain hidden until the unfortunate combination is encountered during system operation.

Combinatorial testing (CT) is a versatile methodology for detecting interaction faults. CT is based on an empirical observation, referred to as the *interaction rule*, that while the behavior of a software system may be affected by a large number of factors, only a few are involved in any given failure. NIST investigations of failures in actual systems have shown that while most faults involved single factors or interactions between two factors, some faults involved three or more factors [1]. (A fault involving more than six factors has not yet been reported.). Thus, while pairwise (2-way) testing is useful, i.e., testing all cases in which two particular factor values are present, it may not be sufficient.

About a decade ago, NIST took the initiative to extend 2-way CT to higher strength t-way CT for $t > 2$. NIST has helped make CT practical by developing research tools and techniques for generating combinatorial test suites. CT has now gained significant interest from the international software testing community. Many successful results from the use of CT in aerospace, automotive, and financial service industries, as well as defense, security, and electronic medical systems have since been reported.

A suite of test cases for combinatorial t-way testing covers (includes) all t-way combinations of factor values among the complete set of k-factors that are tested ($k > t$). Selecting test cases using mathematical objects called *covering arrays* make it possible to test all t-way combinations with a small number of test cases. Table 2 shows a covering array of only 13 rows which covers all 960 3-way combinations of ten 2-valued factors.[18] One wants a minimal covering array, that is, one containing all t-way combinations in the smallest number of rows possible, since this leads to the least number of tests. In practice, many factors have dependencies and constraints, with the consequence that not all t-way combinations may be logically or physically valid. A

Table 2. *A covering array of 13 rows includes all eight triplets (000, 001, 010, 011, 100, 101, 110, and 111) between two possible values (0 and 1) for every three of the 10 parameters represented by columns (for example, see colored entries).*

	Parameters									
Rows	**1**	**2**	**3**	**4**	**5**	**6**	**7**	**8**	**9**	**10**
1	0	0	0	0	0	0	0	0	0	0
2	1	1	1	1	1	1	1	1	1	1
3	1	1	1	0	1	0	0	0	0	1
4	1	0	1	1	0	1	0	1	0	0
5	1	0	0	0	1	1	1	0	0	0
6	0	1	1	0	0	1	0	0	1	0
7	0	0	1	0	1	0	1	1	1	0
8	1	1	0	1	0	0	1	0	1	0
9	0	0	0	1	1	1	0	0	1	1
10	0	0	1	1	0	0	1	0	0	1
11	0	1	0	1	1	0	0	1	0	0
12	1	0	0	0	0	0	0	1	1	1
13	0	1	0	0	0	1	1	1	0	1

[18] $\binom{10}{3} \times 2^3 = 960$

combinatorial test suite must avoid such forbidden combinations. Generating minimal covering arrays that avoid forbidden combinations is a difficult mathematical and computational problem. A great deal of research has been done to develop mathematical and computational methods to generate minimal covering arrays of this type. NIST has developed several such algorithms.

NIST-Developed Tools. NIST has developed several research tools to make CT practical. ACTS (for Automated Combinatorial Testing for Software), which was developed in cooperation with the University of Texas at Arlington, includes several algorithms to generate high strength test suites for CT. The ACTS algorithms are optimized to efficiently avoid forbidden combinations of test settings. More than 3 100 users have downloaded executable versions of the ACTS algorithms from NIST.[19]

A second research tool, CCM (for Combinatorial Coverage Measurement), developed jointly by NIST and a guest researcher from CENAM, the National Metrology Institute of Mexico, determines the combinatorial coverage of a test suite that may not have been developed from a CT viewpoint. This can be considered as one measure of the effectiveness of a test suite. The extent of combinatorial coverage of a test suite may be illustrated by graphing the percentage (ordinate) of the fraction (abscissa) of all *t*-way combinations that are covered. Figure 80 shows combinatorial *t*-way coverage of a test suite of 7 489 tests of 82 factors for $t = 2, 3, 4,$ and 5. The area under a curve represents the proportion of combinations that are covered by the test suite. Conversely, the area above the curve represents input parameter combinations that are not covered. The combinatorial deficiency of a test suite can be remedied by additional tests. Thus, CCM can help guide the expansion of a test suite to satisfy stated combinatorial requirements [2]. The latest version of CCM supports constraints. A parallel processing version is also available.

Impact of NIST Research. NIST efforts have sparked a surge of research and application of combinatorial testing technology. A NIST Special Publication on CT has been downloaded more than 30 000 times [3]. In 2013, we published a book on this topic [4].

One of the first large-scale users that we worked with is a group at the U.S. Air Force Base in Eglin, Florida. The behavior of one of their systems depended on the sequential order of certain events. This led to the problem of testing sequences of events, which required development of new mathematical objects called *sequence covering arrays* [5-7].

Lockheed-Martin, a large U.S. defense contractor, reported (based on eight projects) that use of CT reduced cost of testing by about 20 %, with 20 % to 50 % improvement in test coverage [8]. CT methods are now being used in diverse areas such as financial services, automotive, automation, avionics, video coding standards, and for security testing.

CT is now included in software engineering courses taught in more than 18 U.S. universities. NIST efforts on technology transfer of CT tools and techniques received the 2009 Excellence in Technology Transfer Award from the Federal Laboratory Consortium-Mid Atlantic Region.

CT has also gained significant interest from the software testing research community. In 2012, NIST took lead in organizing an International Workshop on CT (IWCT) in conjunction with the IEEE International Conference on Software Testing, Verification, and Validation (ICST), a premier conference in this field.[20] Since then, IWCT has become an annual event for sharing advancements in CT tools and techniques, as well as results from practical industrial use of CT.[21] The seventh such IWCT was held in Vasteras, Sweden during April 9 to 13, 2018. Four of us (Kacker, Kuhn, Lei, and Simos) were among co-organizers. The IWCT 2018 received 15 high quality submissions, out of which 11 papers were accepted for publication (six full papers, four short ones, and one extended abstract). The program contained research papers as well as papers on applications and use cases of CT.

Recent Research Efforts. We are jointly investigating the use of CT methods for cyber-security applications with a consortium of universities and industry led by SBA-Research, a leading Austrian research center for information security. A tutorial on combinatorial testing for cyber-security was presented at the Symposium on Hot Topics in the Science of Security (HoTSoS 2018) in Raleigh, North Carolina on April 10-11, 2018.[22]

We investigated the cybersecurity vulnerabilities reported in the National Vulnerabilities Database (NVD),[23] where we found that almost two thirds of the vulnerabilities resulted from implementation errors [9]. A poster on this topic received the Best Poster Award from the 2018 Symposium on Hot Topics in the Science of Security.[24] We investigated use of combinatorial testing ideas for detecting bugs in implementations of cryptographic hash functions. The results were presented at a conference held at NIST [10].

Fault localization is a generic problem in software and system testing; it refers to detecting from pass/fail results of testing a fault that triggers a failure. Our research paper on tools and techniques for fault

[19] The actual number of users is difficult to ascertain, since some users have redistributed to others.

[20] http://www.es.mdh.se/icst2018/

[21] https://iwct2018.sba-research.org/

[22] https://cps-vo.org/node/47533

[23] https://nvd.nist.gov/

[24] https://cps-vo.org/node/48134

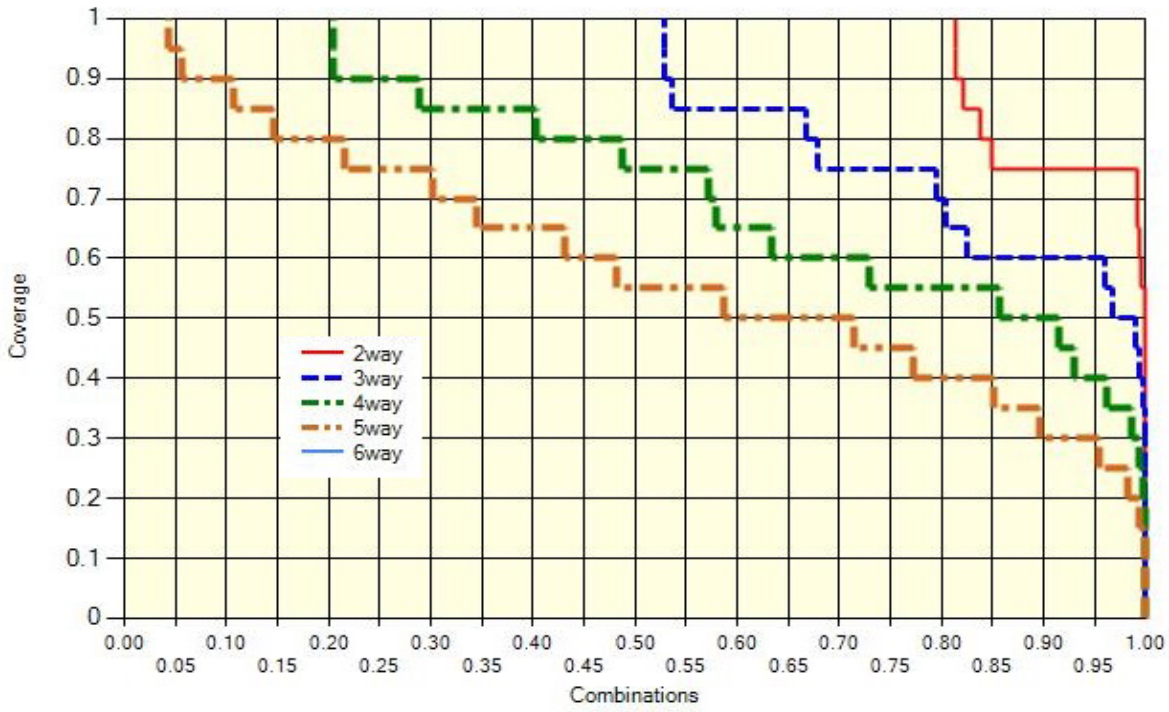

Figure 80. *Combinatorial t-way coverage of a test suite of 7489 tests of 82 variables for t=2, 3, 4, and 5. The graph show the percentage (ordinate) of the fraction (abscissa) of all t-way combinations that are covered by a given test suite.*

localization using combinatorial testing has been accepted for publication in the IEEE Transactions on Software Engineering [11].

CT has been found to be effective in testing and verifying rule-based security systems. A paper was presented at the Thirtieth International Conference on Software Engineering and Knowledge Engineering (SEKE 2018) held in San Francisco July 1-3, 2018 [12].

[1] D. R. Kuhn, D. R. Wallace, and A. M. Gallo, Jr. Software Fault Interactions and Implications for Software Testing. *IEEE Transactions on Software Engineering* **30** (June 2004), 418-421. DOI: 10.1109/TSE.2004.24

[2] D. R. Kuhn, R. N. Kacker, and Y. Lei. Combinatorial Coverage as an Aspect of Test Quality. *CrossTalk: The Journal of Defense Software Engineering*, (March/April 2015), Hill AFB, 19-21.

[3] D. R. Kuhn, R.N. Kacker, and Y. Lei. Practical Combinatorial Testing. Special Publication 800-142, National Institute of Standards and Technology, Gaithersburg, MD. URL: http://nvlpubs.nist.gov/nistpubs/Legacy/SP/nistspecialpublication800-142.pdf

[4] D. R. Kuhn, R.N. Kacker, and Y. Lei. *Introduction to Combinatorial Testing*. CRC Press, 2013.

[5] D. R. Kuhn, J. M. Higdon, J. F. Lawrence, R. N. Kacker, and Y. Lei. Combinatorial Methods for Event Sequence Testing. In *Proceedings of the 5th IEEE International Conference on Software Testing, Verification and Validation Workshops (ICSTW)*, Montreal, Canada, April 17-21, 2012, 601-609. DOI: 10.1109/ICST.2012.147

[6] D. R. Kuhn, J. M. Higdon, J. F. Lawrence, R. N. Kacker, and Y. Lei. Efficient Methods for Interoperability Testing using Event Sequences. *CrossTalk: The Journal of Defense Software Engineering* (July/August 2012), Hill AFB, 15-18.

[7] Y. M. Chee, C. J. Colbourn, D. Horsley, and J. Zhou. Sequence Covering Arrays. *SIAM Journal of Discrete Mathematics* **27** (2013), 1844-1861.

[8] J. Hagar, D. R. Kuhn, R. N. Kacker, and T. Wissink. Introducing Combinatorial Testing in a Large Organization. *IEEE Computer* **48** (April 2015), 64-72.

[9] D. R. Kuhn, M. S. Raunak, and R. N. Kacker. It Doesn't Have to Be Like This: Cybersecurity Vulnerability Trends. *IT Professional* **19**:6 (November/December 2017), 66-70. URL: https://ieeexplore.ieee.org/document/8123486

[10] N. Mouha, M. S. Raunak, D. R. Kuhn, and R. N. Kacker. "Finding Bugs in Cryptographic Hash Function Implementations." 28th IEEE Software Technology Conference (STC 2017), Gaithersburg, MD, USA, September 25-28, 2017.

[11] L. Sh. Ghandehari, Y. Lei, R. Kacker, D. R. Kuhn, T. Xie, and D. Kung. A Combinatorial Testing-Based Approach to Fault Localization. *IEEE Transactions on Software Engineering*, in press.

[12] D. R. Kuhn, D. Yaga, R. N. Kacker, Y. Lei, and V. Hu. Pseudo-exhaustive Verification of Rule Based Systems. In *Proceeding of the International Conference on Software Engineering and Knowledge Engineering (SEKE 2018)*, July 1-3, 2018, Redwood City, CA, 586-591. URL: http://ksiresearchorg.ipage.com/seke/seke18.html

Mathematical Knowledge Management

We work with researchers in academia and industry to develop technologies, tools, and standards for representation, exchange, and use of mathematical data. Of particular concern are semantic-based representations which can provide the basis for interoperability of mathematical information processing systems. We apply these representations to the development and dissemination of reference data for applied mathematics. The centerpiece of this effort is the Digital Library of Mathematical Functions, a freely available interactive and richly linked online resource, providing essential information on the properties of the special functions of applied mathematics, the foundation of mathematical modeling in all of science and engineering.

Digital Library of Mathematical Functions

Barry I. Schneider
Daniel W. Lozier
Bruce R. Miller
Bonita V. Saunders
Howard S. Cohl
Marjorie A. McClain
Ronald F. Boisvert
Adri B. Olde Daalhuis (University of Edinburgh)
Charles W. Clark (NIST PML)
Brian Antonishek (NIST EL)
Nina Tang (Poolesville High School)
Amanda Hu (Poolesville High School)
Ananya Krishnan (Richard Montgomery High School)
Jeff Tran (Richard Montgomery High School)
Jonathan Lin (Richard Montgomery High School)
Derek Yao (Richard Montgomery High School)

http://dlmf.nist.gov/

Progress in science has often been catalyzed by advances in mathematics. More recently, developments in the physical sciences, such as investigations into string theory, have influenced pure mathematics. This symbiotic relationship has been extremely beneficial to both fields. Mathematical developments have found numerous applications in practical problem-solving in all fields of science and engineering, while cutting-edge science has been a major driver of mathematical research**.** Often the mathematical objects at the intersection of mathematics and physical science are mathematical functions. Effective use of these tools requires ready access to their many properties, a need that was capably satisfied for more than 50 years by the *Handbook of Mathematical Functions with Formulas, Graphs, and Mathematical Tables*, which was published by the National Bureau of Standards (NBS) in 1964 [1].

The 21st century successor to the NBS Handbook, freely accessible online Digital Library of Mathematical Functions (DLMF) together with the accompanying book, the *NIST Handbook of Mathematical Functions* [2], published by Cambridge University Press in 2010,

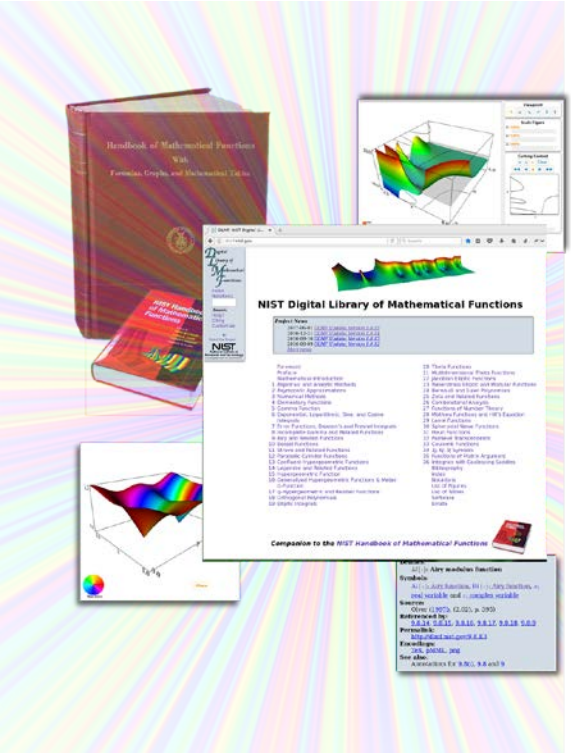

Figure 81. *A visual history of the DLMF from its roots in the 1964 NBS Handbook to the eye catching and informative graphical contents of the present DLMF.*

are collectively referred to as the DLMF. The DLMF continues to serve as the gold standard reference for the properties of what are termed the special functions of applied mathematics.

The DLMF has considerably extended the scope of the original handbook, as well as improving accessibility to the worldwide community of scientists and mathematicians. To cite a few examples, the new handbook contains more than twice as many formulas as the old one, coverage of more functions, in more detail, and an up-to-date list of references. The website covers everything in the handbook and much more: additional formulas and graphics, interactive search, live zooming

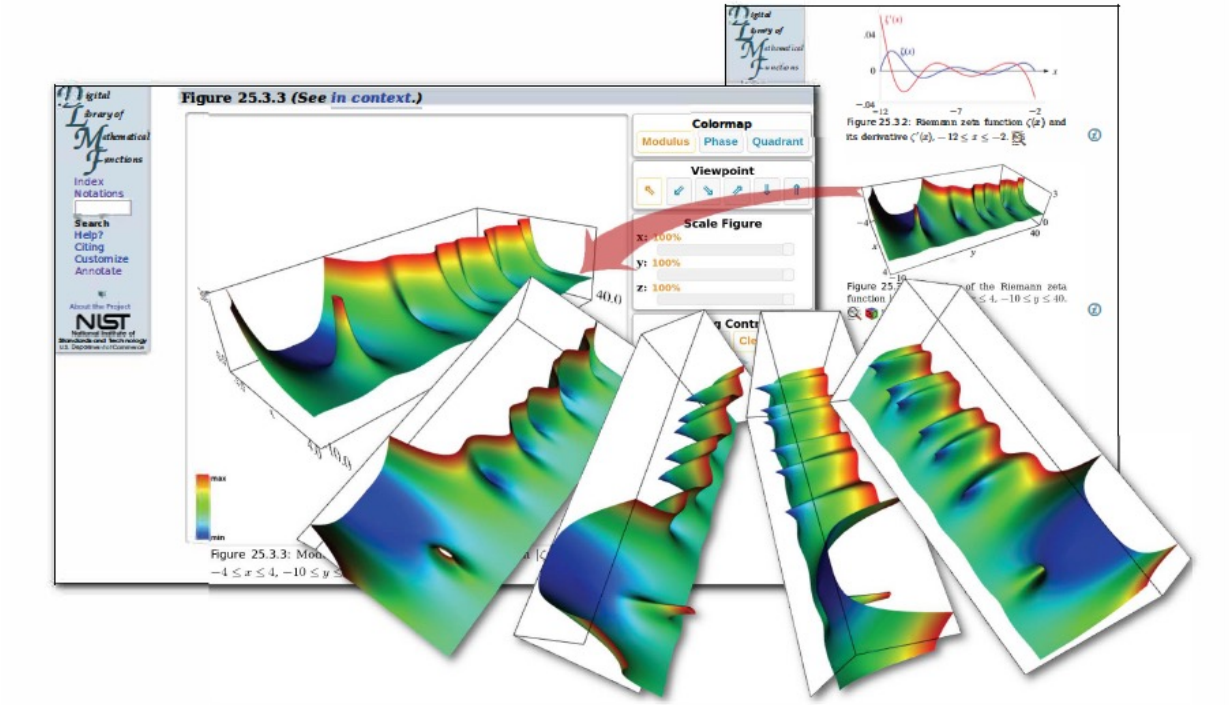

Figure 82. *DLMF graphics can be used to manipulate the 3D images to show the mathematical features of the functions.*

and rotation of 3D graphs, internal links to symbol definitions and cross-references, and external links to online references and sources of software.

While the original Handbook still receives an enormous number of citations, citations to the DLMF are steadily growing. Google Scholar reports more than 4600 citations of the DLMF in the technical literature. In CY 2018 DLMF web server delivered 4.46M pages in 415 286 sessions by 263 047 unique users.

Today's DLMF is the product of many years of effort by more than 50 expert contributors. Its appearance in 2010, however, was not the end of the project. Corrections to errors, clarifications, bibliographic updates, and addition of important new material are all continually being made. New chapters covering emerging subject areas are both planned and under active development. Such active curation is necessary to assure the continued vitality of the DLMF deep into the 21st century.

In the past year, there were four releases of the DLMF containing additions and corrections to various DLMF chapters: 1.0.18 (2018-03-27), 1.0.19 (2018-06-22), 1.0.20 (2018-09-15) and 1.0.21(2018-12-15). This achieved our goal of quarterly releases.

New chapters, and substantial revisions to others, are also under development. These include a new chapter on Orthogonal Polynomials of Several Variables and a major update of the chapters on Orthogonal Polynomials, Algebraic Methods and Painlevé Transcendents. Four external authors were identified to carry out the work. Early drafts of the full chapters are now available and are being internally reviewed. External validation of the chapters will follow in much the same manner as the original DLMF.

An article on the DLMF authored by Schneider, Miller, and Saunders appeared in the February 2018 issue of *Physics Today* magazine [6]. In Figure 81, we show a montage designed to provide a visual history of the DLMF from its roots in the 1964 NBS Handbook to the eye catching and informative graphical contents of the present DLMF. In Figure 82, we illustrate how the DLMF graphics engine can be used to manipulate the 3D images in various ways to show the mathematical features of the functions.

One of the design goals for the DLMF was that each formula would be connected to a proof in the literature. This data, visible as annotations on the website, provides either a proof for the formula, a reference to the proof for the formula or for definitions, a reference which gives that definition. Unfortunately, this information has not been provided in all cases. In FY 2015 we began an effort to systematically verify the completeness and traceability of DLMF formulae to published proofs. This audit is first being undertaken for Chapter 25 (Zeta and

Related Functions) and is actively continuing for Chapters 1-5, 22-30. In addition, work has progressed to make proof-related information visible in metadata at the equation level. Improvements in markup to more accurately identify the nature of the added material have been developed and deployed (see Chapter 9, Airy and Related Functions).

During the past year, the DLMF project has seen continued progress on several related fronts. DLMF Tables [3], an on-demand table generation web service for special functions, and the Digital Repository of Mathematical Formulae (DRMF) [4,5], a community-based context-free compendium of mathematical formulas and associated mathematical data continue to evolve and remain important parts of the overall NIST goal to present important and useful mathematical information to the community in a trustworthy manner. These are described in more detail elsewhere in this report.

[1] M. Abramowitz and I. Stegun, eds. *Handbook of Mathematical Functions with Formulas, Graphs and Mathematical Tables*. Applied Mathematics Series 55, National Bureau of Standards, Washington, DC 1964.

[2] F. Olver, D. Lozier, R. Boisvert and C. Clark, eds. *NIST Handbook of Mathematical Functions*. Cambridge University Press, 2010.

[3] D. Lozier. "Outgrowths of the Digital Library of Mathematical Functions Project, Part I: DLMF Standard Reference Tables," Challenges in 21st Century Experimental Mathematical Computation, Institute for Computational and Experimental Research in Mathematics (ICERM), Providence, RI, July 2014. URL: http://icerm.brown.edu/video_archive/?play=661

[4] H. S. Cohl, M. A. McClain, B. V. Saunders, and M. Schubotz, "Outgrowths of the Digital Library of Mathematical Functions Project, Part II: NIST Digital Repository of Mathematical Formulae," Challenges in 21st Century Experimental Mathematical Computation, Institute for Computational and Experimental Research in Mathematics, Providence, RI, July 2014. URL: https://icerm.brown.edu/materials/Slides/tw-14-5/Outgrowths_of_the_Digital_Library_of_Mathematical_Functions_Project_]_Howard_Cohl_and_Daniel_Lozier,_National_Institute_of_Standards_and_Technology.pdf

[5] H. S. Cohl, M. A. McClain, B. V. Saunders, M. Schubotz, and J. C. Williams. Digital Repository of Mathematical Formulae, *Lecture Notes in Artificial Intelligence* **8543** (2014), Proceedings of the Conferences on Intelligent Computer Mathematics, Coimbra, Portugal, July 7-11, 2014, (S. M. Watt, J. H. Davenport, A. P. Sexton, P. Sojka, and J. Urban, eds.), Springer, 419-422.

[6] B. Schneider, B. Miller, and B. Saunders. NIST's Digital Library of Mathematical Functions. *Physics Today*, **71:2** (2018), 48-53. DOI: https://doi.org/10.1063/PT.3.3846

Visualization of Complex Functions Data

Bonita Saunders
Bruce Miller
Brian Antonishek (NIST EL)
Sandy Ressler
Qiming Wang (NIST retired)

Our work on visualizing complex functions encompasses research areas crossing several mathematical and technical disciplines. It includes the study and design of grid generation techniques to create meshes that capture key function features, the utilization and enhancement of 3D web graphics technology to develop interactive surface visualizations that spur user exploration, and the investigation of function definitions, properties and numerical software to validate data accuracy.

Since the NIST Digital Library of Mathematical Functions (DLMF) provides much of the motivation for this work, priorities change throughout the fiscal year based on feedback from users or DLMF team members. The recent move of DLMF files to a Github repository led to a concerted effort to reorganize and purge unnecessary graphics files. In place of large executable files, the repository will store script files that can quickly regenerate visualization executables when necessary.

Adaptive mesh development to improve our underlying computational grids continues, with results presented at recent conferences [1, 2]. Also, we are making progress in increasing the visibility of our function visualizations. Our work was prominently featured in an invited article on DLMF technologies published in *Physics Today* [3]. In fact, during the past three years our visualizations have been publicized in numerous technical articles, conference presentations, career articles, a blog, and an art exhibition [1-9].

Although increased exposure can be accomplished through additional publications in prominent journals and presentations at appropriate venues, we also need to increase visibility inside the DLMF site. Discussions with visiting DLMF authors showed they had little familiarity with the capabilities available in the visualizations. A short impromptu briefing and follow-on discussions led to several suggestions. For example, a small animation on the opening DLMF page might attract attention, and an interesting visual or animation near the static 3D figures could link to a brief tutorial of some of the interesting visualization options.

Related work may also help. Currently, some DLMF chapters show a small gallery of images related to the chapter on the title page. DLMF Physical Sciences Editor Charles Clark suggested that creating galleries for all chapters will add visual interest to the DLMF. Each

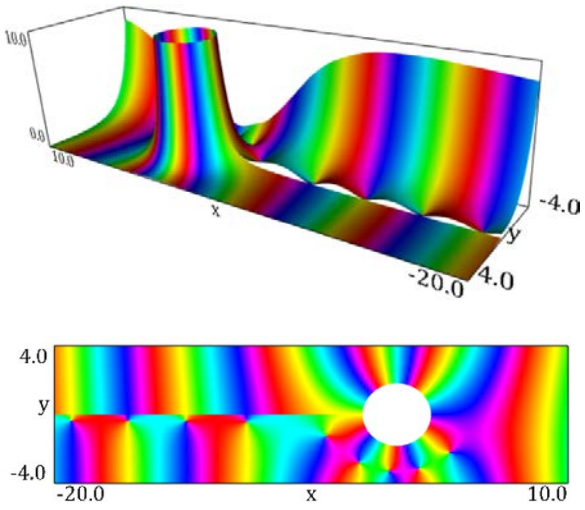

Figure 83. *Hankel function $|H_5^{(1)}(x+iy)|$ is shown with a phase colormap. The surface height was collapsed to 0 to obtain the phase density plot below it.*

image would be linked to an information page explaining its significance. The page would also link to the chapter's application section or related visualizations.

To maintain the quality of our visualizations it is important that we continue to incorporate new ideas. We continue to monitor developments in mesh generation, 3D Web graphics, and graphics in computer algebra packages to see how our work measures up and to find inspiration for future enhancements.

[1] B. Saunders. "An Adaptive Curvature and Gradient Based Grid Generation Method." MASCOT 2018, Rome, Italy, October 5, 2018.

[2] B. Saunders. "Adaptive Curvature-Based Grid Generation for 3D Web Graphics." Curves and Surfaces 2018, Arcachon, France, July 3, 2018.

[3] B. Schneider, B. Miller, and B. Saunders. NIST's Digital Library of Mathematical Functions. *Physics Today*, **71:2** (2018), 48-53. DOI: https://doi.org/10.1063/PT.3.3846

[4] B. Saunders. "NIST's Digital Library of Mathematical Functions and the Digital Age." MD-DC-VA Spring Section Meeting, Mathematical Association of America, Virginia Military Institute/Washington & Lee University, Lexington, VA, April 14, 2018.

[5] B. Saunders. Somebody Else's Dream. *SIAM News* **51:2** (2018), 5-6. URL: https://sinews.siam.org/Details-Page/somebody-elses-dream.

[6] B. Saunders. "Adaptive Grids for Accurate Visualizations of Complex Function Data," SIAM Conference on Industrial and Applied Geometry (GD17), Pittsburgh, Pennsylvania, July 12, 2017.

[7] B. Saunders. "Plotting a Path from NASA Grids to NIST Graphics." NIST Taking Measure Blog, NIST Public Affairs Office, April 27, 2017.

[8] C. Clark and B. Saunders. DLMF gamma, digamma phase plot display, MICRO/MACRO: Big Images of Small Things from NIST Labs. Johns Hopkins University Montgomery County Campus, Rockville, MD, September 6 – November 11, 2016.

[9] B. Saunders, B. Antonishek, B. Miller, and Q. Wang. "Adaptive Curvature-Based Composite Grid Generation Techniques Applied to 3D Visualizations." 9th International Conference on Mathematical Methods for Curves and Surfaces, Tonsberg, Norway, June 23, 2016.

DLMF Standard Reference Tables on Demand

Bonita Saunders
Bruce Miller
Marjorie McClain
Daniel Lozier
Andrew Dienstfrey
Annie Cuyt (University of Antwerp)
Stefan Becuwe (University of Antwerp)
Franky Backeljauw (University of Antwerp)
Chris Schanzle

http://dlmftables.uantwerpen.be/

DLMF Standard Reference Tables on Demand (DLMF Tables) is an online service under development for the generation of tables of special function values with an error certification for comparison with various software implementations for computing special functions. The system might be used by a software developer or researcher to test his own code or to confirm the accuracy of results obtained from a commercial or publicly available package. The project is a collaboration between ACMD and the University of Antwerp Computational Mathematics Research Group (CMA) [1-5].

A challenging, but critical part of developing such a system is determining the likely users and assessing their needs. To address this problem, we have released a beta version that includes design features we feel are crucial. By publicizing this fully operational site, we hope to obtain feedback that can be considered as we expand and enhance the service.

Preliminary feedback indicates the name of our site may mask its intended use for software testing. Some users associate the term 'reference table' with the historical use of published tables for computing function values by interpolation. One possibility is to keep the current name to suggest a connection to the 1964 NBS *Handbook of Mathematical Functions* [6] but add a subtitle such as "A Software Testing System" to make the focus of our service clear.

Other feedback dramatically demonstrates the importance of communicating with potential users throughout the development process. For example, although the strength of our system is the certifiably

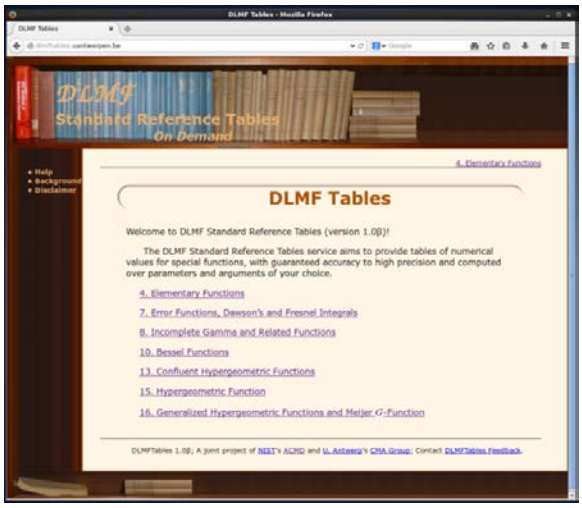

Figure 84. *Table of contents for DLMF Tables website.*

correct high precision function values it provides, interactions with NIST physicists have shown us there are applications where the ability to input extremely large parameter values may be more important [9]. We are currently studying this work to help us implement options that strike a balance between the size of the input parameters and the precision needed in the result. Undoubtedly it will be necessary to define a threshold that sparks a user alert when real time computation is unreasonable because of time or resource considerations. Depending on the situation, various choices might be presented, such as *continue*, *submit a batch job* for later results, or *suspend the computation* to change the input choices.

Of course, an important problem is helping potential users understand why such a system is needed. Many feel that reference values for testing their software can be computed using several well-known computer algebra packages. However, most of these packages produce a string of digits with no claims about correctness. Admittedly, the user's application and the quality of the package may be such that finding agreement between "*n*" consecutive digits is enough to foster confidence. Our system is for those cases where this is not enough. Perhaps the scientific application requires very accurate high precision results, or large input parameters make it hard to ensure the correctness of even a small number of digits, or results are needed near the edge of a regime where a particular numerical method is stable, or the user simply wants to test his "agreement equals correct" theory. Our system provides the added confidence of a certified result with error bound information.

To encourage more feedback, we are publicizing the site through talks and publications [10-14]. A brief overview of the project appears in a *Physics Today* article on the DLMF [11]. A fortuitous meeting between team leaders B. Saunders (ACMD) and A. Cuyt (CMA) at two summer conferences in France and Italy led to an infusion of constructive ideas for keeping the project on track and included an invitation to work with CMA at U. Antwerp for a month. A renewed commitment to project status meetings by Skype every 1-2 months has already led to better communication between the teams. However, key to the expansion and improvement of DLMF Tables is the development and integration of more functions. We are starting a search for personnel who can assist our ongoing work in these areas. We are also exploring other research on high precision codes that might be relevant to our project [15, 16].

[1] F. Backeljauw, S. Becuwe, A. Cuyt, J. Van Deun, and D. Lozier. Validated Evaluation of Special Mathematical Functions. *Science of Computer Programming* **10** (2013), 1016.

[2] M. Colman, A. Cuyt and J. Van Deun. Validated Computation of Certain Hypergeometric Functions. *ACM Transactions on Mathematical Soft*ware **38**:2 (January 2012), Article 11.

[3] F. Backeljauw. A Library for Radix-independent Multiprecision IEEE-compliant Floating-point Arithmetic. Technical Report 2009-01, Department of Mathematics and Computer Science, Universiteit Antwerpen, 2009.

[4] A. Cuyt, V. B. Petersen, B. Verdonk, H. Waadeland and W. B. Jones. *Handbook of Continued Fractions for Special Functions*. Springer, New York, 2008.

[5] A. Cuyt, B. Verdonk, and H. Waadeland. Efficient and Reliable Multiprecision Implementation of Elementary and Special Functions. *SIAM Journal of Scientific Computing* **28** (2006), 1437-1462.

[6] M. Abramowitz and I. Stegun, eds. *Handbook of Mathematical Functions*. Applied Mathematics Series **55**, National Bureau of Standards, Washington, DC, 1964.

[7] NIST Digital Library of Mathematical Functions. http://dlmf.nist.gov/, Release 1.0.17 of 2017-12-22. Online companion to [8].

[8] F. W. J. Olver, D. W. Lozier, R. F. Boisvert, and C. W. Clark, eds. *NIST Handbook of Mathematical Functions*. Cambridge University Press, New York, NY, 2010. Print companion to [7].

[9] E. L. Shirley, M. Furst, and U. Arp. Refined Analysis of Synchrotron Radiation for NIST's SURF III facility. *Review of Scientific Instruments* **89** (2018), 041301.

[10] B. Saunders, B. Miller, F. Backeljauw, S. Becuwe, M. McClain, D. Lozier, A. Cuyt, and A. Dienstfrey. DLMF Tables: A Computational Resource Inspired by the NIST Digital Library of Mathematical Functions. In review.

[11] B. Schneider, B. Miller, and B. Saunders. NIST's Digital Library of Mathematical Functions. *Physics Today*, **71:2** (2018), 48-53. DOI: https://doi.org/10.1063/PT.3.3846

[12] B. Saunders, "Who Needs Standard Reference Tables on Demand?" Mathematical Association of America MD-DC-VA Section Meeting, Frostburg State University, Frostburg, MD, April 29, 2017.

[13] B. Saunders, B. Miller, M. McClain, D. Lozier, A. Dienstfrey, A. Cuyt, S. Becuwe, and F. Backeljau. "DLMF Standard Reference Tables on Demand (DLMF Tables)." Minisymposium on Orthogonal Polynomials

and Special Functions: Computational Aspects, 2015 International Conference on Orthogonal Polynomials, Special Functions and Applications, Gaithersburg, MD, June 1, 2015.

[14] B. Saunders. "NIST Projects: Graphics in the Digital Library of Mathematical Functions (DLMF) and DLMF Standard Reference Tables on Demand (DLMF Tables)." Careers in Mathematical Sciences Workshop for Underrepresented Groups, Institute for Mathematics and Its Applications, University of Minnesota, Minneapolis, MN, March 29, 2015.

[15] J. Le Maire, N. Brunie, F. de Dinechin, and J. Muller. Computing Floating-point Logarithms with Fixed-point Operations. In Proceedings of the *IEEE 23nd Symposium on Computer Arithmetic (ARITH)*, 2016, 156-163.

[16] N. Brunie, F. de Dinechin, O. Kupriianova, and C. Lauter. Code Generators for Mathematical Functions. In Proceedings of the *IEEE 22nd Symposium on Computer Arithmetic (ARITH)*, 2015, 66-7.

NIST Digital Repository of Mathematical Formulae

Howard S. Cohl
Marjorie A. McClain
Bonita V. Saunders
Abdou Youssef
Moritz Schubotz (University of Konstanz)
André Greiner-Petter (Technische Universität Berlin)
Alan Sexton (University of Birmingham)

The NIST Digital Repository of Mathematical Formulae (DRMF) is an online compendium of formulae for orthogonal polynomials and special functions (OPSF) designed to

a) facilitate interaction among a community of mathematicians and scientists interested in OPSF;
b) be expandable, allowing the input of new formulae from the literature;
c) provide information for related linked open data projects;
d) represent the context-free full semantic information concerning individual formulas;
e) have a user friendly, consistent, and hyperlinkable viewpoint and authoring perspective;
f) contain easily searchable mathematics; and
g) take advantage of modern MathML tools for easy-to-read, scalably rendered content-driven mathematics.

Our DRMF implementation, previously built using MediaWiki (the wiki software used by Wikipedia), is now in migration to a different software platform, namely the platform used by the NIST Digital Library of Mathematical Functions (DLMF). See Figure 85 for the current draft of the DRMF home page, and Figure 86 for a sample DRMF formula page. The DRMF has been described in a series of papers and talks [1-9].

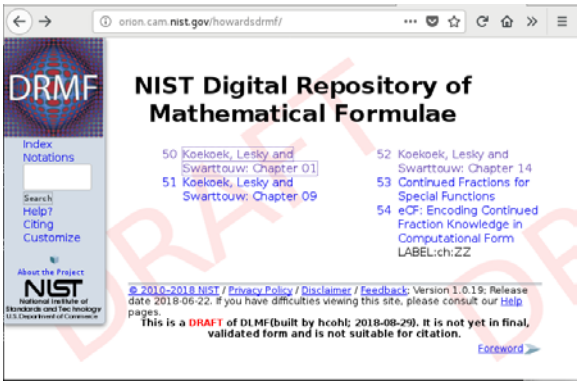

Figure 85. *Current Draft of the DRMF home page displaying the current table of contents.*

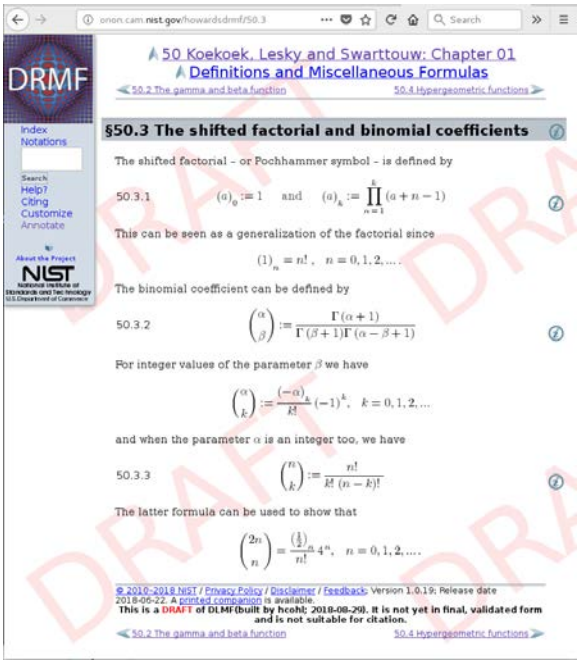

Figure 86. *Sample DRMF formula page, taken from the KLS Chapter 1 dataset.*

A key asset in the development of DRMF context free semantic content is the utilization of a set of LaTeX macros originally created by Bruce Miller (ACMD) to achieve the encapsulation of semantic information within the NIST Digital Library of Mathematical Functions (DLMF) [10]. These macros give us the capability to tie LaTeX commands in a mostly unambiguous way to mathematical functions defined in an OPSF context. There are currently 540 DLMF LaTeX macros, as well as an additional 156 which have been created specifically for the DRMF. All DLMF macros have at least one DLMF web page associated with them, and the goal is to have definition pages for all additional DRMF macros. The use of DLMF and DRMF macros guarantees

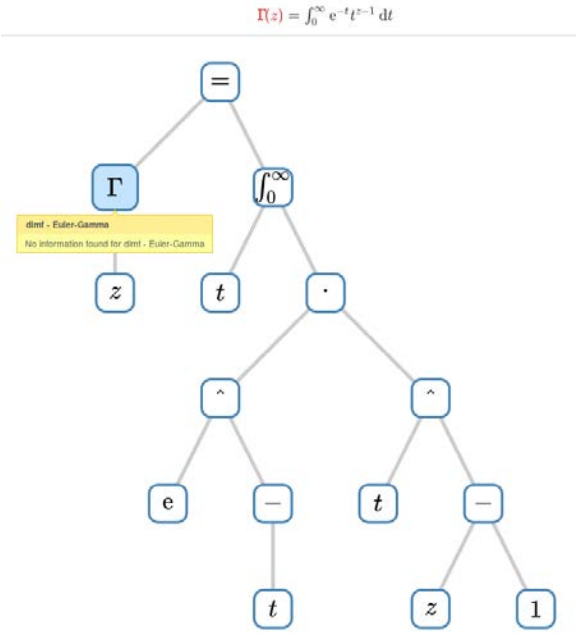

Figure 87. *VMEXT visualization of (5.2.1) in the DLMF. The corresponding MathML XML file is 89 lines and 6293 characters long.*

mathematical and structural consistency throughout the DRMF. We refer to LaTeX source with incorporated DLMF and DRMF macros as semantic LaTeX.

DRMF formula seeding is currently focused on

1) Koekoek, Lesky, and Swarttouw (KLS) chapters 1 (Definitions and Miscellaneous Formulas), 9 (Hypergeometric Orthogonal Polynomials), and 14 (Basic Hypergeometric Orthogonal Polynomials [11];
2) Koornwinder KLS addendum LaTeX data [12];
3) Wolfram Computational Knowledge of Continued Fractions Project (eCF) [3];
4) Continued Fractions for Special Function (CFSF) Maple dataset hosted by the University of Antwerp [3,14];
5) Bateman Manuscript Project (BMP) books [13]; and
6) Magnus, Oberhettinger, and Soni (MOS) books [13].

For these seed projects, we are developing Python and Java software to incorporate DLMF and DRMF macros into the corresponding LaTeX source. Our coding efforts have also focused on extracting formula data from LaTeX source as well as generating DRMF semantic LaTeX. We have developed Java software for the seeding of the eCF and CFSF projects which involve conversion from Mathematica and Maple format to DLMF and DRMF macro incorporated semantic LaTeX [3]. Moreover, in [4] we developed the VMEXT visualization that helps us to investigate the content structure of MathML expressions without reading the verbose parallel MathML markup; see Figure 87.

In August 2014, the DRMF Project obtained permission and license to use BMP material as seed content for the DRMF from Adam Cochran, Associate General Counsel of Caltech. Caltech has loaned us copies of the BMP. In February 2018, we received permission and license to use the KLS and MOS material as seed content for the DRMF from Springer Nature. We have forwarded the copies of BMP and MOS to A. Sexton, Scientific Document Analysis Group, School of Computer Science, University of Birmingham, UK. Sexton has scanned the BMP and MOS and is developing software to perform mathematical optical character recognition to obtain LaTeX source. To enhance the development process of the OCR software, we have developed an automated testing framework that uses visual diffs of the original scanned source and the rendering of the generated LaTeX source.

Current and future DRMF MediaWiki development projects include the production of formula output representations (such as semantic LaTeX, MathML, Mathematica, Maple, and Sage); incorporation of sophisticated DLMF and DRMF macro related formula search; and the development of capabilities for user community formula input. In this vein, A. Youssef has written a grammar-based mathematical language processor (MLP) that uses JavaCC to parse mathematical LaTeX expressions [15]. Based on the MLP, A. Greiner-Petter has developed a Java tool to convert mathematical LaTeX expressions, which contain DLMF and DRMF macros, to a given computer algebra system source format. This Java tool provides further information of the conversion about possible ambiguities and differences in definitions, domains and branch cuts between the semantic LaTeX source and the CAS source. Furthermore, it is designed to be easily extendable to other computer algebra systems and currently supports Maple and Mathematica input sources.

The KLS datasets have been uploaded to our DLMF platform as well as the CFSF and eCF datasets. By working with Andrea Fisher-Scherer, Rights Administrator, Artists Rights Society, New York, NY, we have received permission from Foundation Vasarely, to use an image of one of Victor Vasarely's paintings as the DRMF logo; see Figure 88.

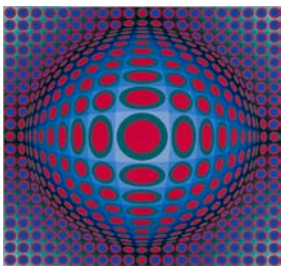

Figure 88. *DRMF Logo.*

[1] H. S. Cohl, M. A. McClain, B. V. Saunders, M. Schubotz and J. C. Williams. Digital Repository of Mathematical Formulae. *Lecture Notes in Artificial Intelligence* **8543** (2014), Proceedings of the Conferences on Intelligent Computer Mathematics 2014, Coimbra, Portugal, July 7-

11, 2014, (S. M. Watt, J. H. Davenport, A. P. Sexton, P. Sojka, and J. Urban, eds.), Springer, 419-422.

[2] H. S. Cohl, M. Schubotz, M. A. McClain, B. V. Saunders, Cherry Y. Zou, Azeem S. Mohammed, and Alex A. Danoff. Growing the Digital Repository of Mathematical Formulae with Generic LaTeX Sources. *Lecture Notes in Artificial Intelligence* **9150** (2015), Proceedings of the Conference on Intelligent Computer Mathematics 2015, Washington DC, USA, July 13-17, 2015, (M. Kerber, J. Carette, C. Kaliszyk, F. Rabe, and V. Sorge, eds.), Springer, 280-287.

[3] H. S. Cohl, M. Schubotz, A. Youssef, A. Greiner-Petter, J. Gerhard, B. V. Saunders, M. A. McClain, J. Bang, and K. Chen. Semantic Preserving Bijective Mappings of Mathematical Formulae between Word Processors and Computer Algebra Systems. *Lecture Notes in Computer Science* **10383** (2017), Proceedings of the Conference on Intelligent Computer Mathematics 2017, Edinburgh, Scotland, U.K., July 17-21, 2017, (H. Geuvers, M. England, O. Hasan, F. Rabe, O. Teschke, eds.), Springer, 115-131.

[4] M. Schubotz, N. Meuschke, T. Hepp, H.S. Cohl, and B. Gipp. VMEXT: A Visualization Tool for Mathematical Expression Trees. *Lecture Notes in Computer Science* **10383** (2017), Proceedings of the Conference on Intelligent Computer Mathematics 2017, Edinburgh, Scotland, U.K., July 17-21, 2017, (H. Geuvers, M. England, O. Hasan, F. Rabe, O. Teschke, eds.), Springer, 340-345.

[5] M. Schubotz and H.S. Cohl. "Content Dictionary Description: Select Symbols from Chapter 9 of the KLS Dataset in the DRMF." OpenMath Workshop, Conference on Intelligent Computer Mathematics 2017, Edinburgh, Scotland, U.K., July 17-21, 2017.

[6] M. Schubotz, A. Greiner-Petter, P. Scharpf, N. Meuschke, H. S. Cohl, and B. Gipp. Improving the Representation and Conversion of Mathematical Formulae by Considering their Textual Context. In *Proceedings of the Joint Conference on Digital Libraries* (JCDL'18), Fort Worth, Texas, USA, June 3-6, 2018, 233-242.

[7] H. S. Cohl, A. Greiner-Petter, and M. Schubotz. Automated Symbolic and Numerical Testing of DLMF Formulae using Computer Algebra Systems. *Lecture Notes in Computer Science* **11006** (2018), Proceedings of the Conference on Intelligent Computer Mathematics 2018, Hagenberg, Austria, August 13-17, 2018, (F. Rabe, W. Farmer, G.O. Passmore, A. Youssef, eds.), Springer, 39-52.

[8] A. Greiner-Petter, M. Schubotz, H. S. Cohl, and B. Gipp. MathTools: An Open API for Convenient MathML Handling. *Lecture Notes in Computer Science* **11006** (2018), Proceedings of the Conference on Intelligent Computer Mathematics 2018, Hagenberg, Austria, August 13-17, 2018, (F. Rabe, W. Farmer, G.O. Passmore, A. Youssef, eds.), Springer, 104-110.

[9] A. Greiner-Petter, M. Schubotz, H. S. Cohl, and Bela Gipp. Semantic Preserving Bijective Mappings for Expressions Involving Special Functions in Computer Algebra Systems and Document Preparation Systems. *ASLIB Journal of Information Management*, to appear.

[10] B. Miller. "Drafting DLMF Content Dictionaries." OpenMath Workshop, 9th Conference on Intelligent Computer Mathematics, CICM 2016, Bialystok, Poland.

[11] R. Koekoek, P. A. Lesky, and R. F. Swarttouw. *Hypergeometric Orthogonal Polynomials and their q-Analogues*. Springer Monographs in Mathematics, Springer-Verlag, Berlin, 2010.

[12] T. H. Koornwinder. Additions to the Formula Lists in Hypergeometric Orthogonal Polynomials and their q-analogues by Koekoek, Lesky and Swarttouw. arXiv:1401.0815, June 2015.

[13] A. Erdelyi, W. Magnus, F. Oberhettinger, and F. G. Tricomi. *Higher Transcendental Functions*. Vols. I, II, III, Robert E. Krieger Publishing Co., Melbourne, FL, 1981.

[14] A. Cuyt, V. Petersen, H. Waadeland, W. B. Jones, F. Backeljauw, C. Bonan-Hamada, and S. Becuwe. *Handbook of Continued Fractions for Special Functions*. Springer, New York, 2008.

[15] A. Youssef. Part-of-Math Taggin and Applications. *Lecture Notes in Computer Science* **10383** (2017), Proceedings of the Conference on Intelligent Computer Mathematics 2017, Edinburgh, Scotland, U.K., July 17-21, 2017, (H. Geuvers, M. England, O. Hasan, F. Rabe, O. Teschke, eds.), Springer, 356-374.

Mathematical Knowledge Management

Bruce Miller
Tom Wiesing (University of Erlangen, Germany)
Deyan Ginev (Jacobs University, Germany)

Providing a collection of useful information about the special functions of applied is, of course, the purpose of the Digital Library of Mathematical Functions (DLMF) project. We might call it tactical that our initial focus was to put these definitions, relationships, properties and other data into a form readable by the scientists and engineers who make up our readership. But the longer-term strategy calls for the data to be machine-readable. When appropriately indexed by either major search engines, or special purpose ones, this will support richer search and discoverability. Most important is the goal that DLMF's formula can be imported directly into other software systems and used within the computations of those systems.

The first, most fundamental question immediately reveals itself: Are the functions treated in DLMF actually the same as those in Mathematica, or Maple or the NAG libraries? As it turns out, usually they are, but sometimes they are not, and the differences can be subtle. Establishing these correspondences is exactly the purpose of the Special Function Concordance activity of the International Mathematical Knowledge Trust (IMKT) established by the Global Digital Mathematical Library (GDML) working group of the International

Mathematical Union. We are participating in this effort to establish this concordance between the various special functions, in all their flavors, as used within various handbooks, such as the DLMF, and software systems, such as Mathematica, Maple and NAG, to assure interoperability.

For our part, we are developing a catalog of the special functions as defined in DLMF. Obviously, we start by listing those formulas which we consider to be the defining ones for each function. However, the key is to focus on those aspects, those choices, that potentially distinguish our version of a particular function from those of other systems. Choices of argument conventions (e.g., elliptic functions sn(u,k) versus sn(u,m)) are significant. Patterns of singularities and type signatures help distinguish different extensions and generalizations of functions. A trickier class of difference are the choices made for the location of branch-cuts or which value is taken on the cuts, or indeed the choice made to avoid them entirely as multi-valued functions.

Given this set of distinguishing features, we are now proceeding to collect and encode that information for each of the functions treated in DLMF and present the result in the form of OpenMath Content Dictionaries.

Part-of-Math Tagging

Abdou Youssef

A part-of-math (POM) tagger is a system that determines the mathematical categories or role(s), called tags, of every mathematical symbol in a given math expression or equation. Also, the POM tagger should often be able to determine the mathematical meaning of a symbol by using the symbol's expression-level context and manuscript-level context, as well as broad domain-level and sub-domain-level knowledge.

This project, which started in 2016, developed a first phase of a POM tagger that computes, for each math symbol, a list of tags, where some of the tags are certain and some are tentative. This tagger is being utilized in the above described project on deep-leaning-based extraction of semantics by providing the latter with basic tag information. In turn, the latter project will feed back to the POM tagger by providing semantic tags to add to the list of tags of math symbols. In this past year, the POM tagger was refined and enhanced extensively to better serve the needs of the deep-leaning-based semantics-extraction project.

Deep Learning for Math and Science Knowledge Processing

Abdou Youssef
Bruce Miller

The amount of literature in STEM fields is growing so rapidly that it is impossible to keep current. Therefore, automated semantic-processing of math and science documents is essential for future progress in knowledge discovery and use, and for the synthesis of large and exponentially growing volumes of technical text. Many researchers are now using automated techniques to mine the scientific literature. Success in doing this relies on being able to determine the meaning, i.e., semantics, of the literature in an automated way [1].

In this multi-year project, started in 2017, we are using the fast-evolving deep learning paradigm to develop techniques for extracting and disambiguating semantics from text in math and science documents. We are also creating "labeled" (i.e., annotated) datasets, which are essential for training deep learning models.

In the first phase, funded internally by ITL's Building the Future program in 2018 [2], we developed considerable infrastructure (software and datasets). Specifically, we collected and annotated datasets from the arXiv and from the NIST's Digital Library of Mathematical Functions (DLMF). These datasets are needed for training deep neural networks (DNNs). We also designed and have already started the training, testing and comparative evaluation of deep learning models.

In the second phase and beyond, we will complete the dataset collection and annotation, and will train and test the deep learning models that we designed in the first phase [3]. Additionally, we will exploit recent advances in deep learning, such as the incorporation of attention mechanisms and the use of more advanced numerical encoding (aka embedding) of textual terms. We will also start to explore new applications of our work, such as in math document classification and the enhancement of math search.

[1] A. Youssef and B. Miller. Deep Learning Neural Networks for Math & Science Knowledge Processing – Phase I. Grant, ITL Building the Future Program, NIST, $100,000, 2017-2018.

[2] A. Youssef and B. Miller. Deep Learning Neural Networks for Math & Science Knowledge Processing – Phase II. Grant, ITL Building the Future Program, NIST, $100,000, 2018-2019.

[3] A. Youssef and B. Miller. Deep Learning for Math Knowledge Processing. *11th Conference on Intelligent Computer Mathematics* (CICM), Hagenberg, Austria, August 2018.

Fundamental Solutions and Expansions for Special Functions and Orthogonal Polynomials

Howard S. Cohl
Roberto S. Costas-Santos (University of Alcala)
Hans Volkmer (University of Wisconsin-Milwaukee)
Gestur Olafsson (Louisiana State University)
T. Mark Dunster (San Diego State University)
Mourad E. H. Ismail (University of Central Florida)
Michael A. Baeder (Citigroup Inc.)
Jessica E. Hirtenstein (University of California Davis)
Philbert R. Hwang (University of Maryland)
Wenqing Xu (Caltech)
Thinh H. Dang (George Washington University)
Tanay Wakhare (University of Maryland)
Justin Park (Poolesville High School)
Jason Zhao (University of California Los Angeles)

The concept of a function expresses the idea that one quantity (the input) completely determines another quantity (the output). Our research concerns special functions and orthogonal polynomials. A special function is a function that has appeared in the mathematical sciences so often that it has been given a name. Green's functions (named after the British mathematician George Green, who first developed the concept in the 1830s) describe the influence of linear natural phenomena such as electromagnetism, gravity, heat and waves. For example, in electrostatics, a Green's function describes the influence of a point charge, called the source, over all of space. The inputs for fundamental solutions (Green's functions) are all of space (with the exception of a singular region), and the output is the "force" exerted from the point throughout space. Green's functions are fundamental to the study of inhomogeneous partial differential equations and are powerful in that they provide a mechanism for obtaining their solutions.

We investigate fundamental solutions of linear partial differential equations on highly symmetric Riemannian manifolds (harmonic, rank-one symmetric spaces) such as real, complex, quarternionic, and octonionic Euclidean, hyperbolic, and projective spaces. Our recent focus has been on applications of fundamental solutions for linear elliptic partial differential operators on spaces of constant curvature. We have constructed closed-form expressions of a fundamental solution for the Helmholtz equation in d-dimensional, R-radius spaces of constant positive and negative curvature. These were in the hyperboloid model of hyperbolic geometry, in terms of associated Legendre functions, and on the d-dimensional hypersphere, in terms of Ferrers functions [1]. With G. Olafsson, we are also preparing work on fundamental solutions for the Laplace-Beltrami operator on rank one symmetric spaces of compact and noncompact type [2]. H. Cohl is working with J. E. Hirtenstein on deriving Gegenbauer expansions and addition theorems for binomial and logarithmic fundamental solutions of the polyharmonic equation in even-dimensional space with powers of the Laplacian greater than or equal to the dimension divided by two [3]. In conjunction with J. Park and H. Volkmer, Cohl is computing all Gauss hypergeometric representations of Ferrers functions of the second kind by starting with the full list of 18 Gauss hypergeometric representations for the associated Legendre function of the second kind [4].

In the following works, we derive and use properties of hypergeometric orthogonal polynomials. In particular, we compute specializations and generalizations of generalized and basic hypergeometric orthogonal polynomial generating functions as well as corresponding definite integrals using orthogonality. We present the power collection method for hypergeometric orthogonal polynomials and summarize for which orthogonal polynomials in the Askey and q-Askey schemes it can be applied [5]. Here, we apply the power collection method to Meixner polynomials and compute a series of connection and connection-type relations for these orthogonal polynomials. We also apply these connection and connection-type relations to generating functions for Meixner and Krawtchouk polynomials. Our series-rearrangement technique is extended to generalizations of generating functions for basic hypergeometric orthogonal polynomials in [6]. Here, we derive generalizations of generating functions for Askey-Wilson, q-ultraspherical/Rogers, q-Laguerre, and little q-Laguerre/Wall polynomials, and also derive a new quadratic transformation for basic hypergeometric series, and a Wilson polynomial expansion which corresponds to the generalized Rogers generating function given by M. E. H. Ismail and P. Simeonov. We give contour integral orthogonality relations for the Al-Salam-Carlitz polynomials which is valid for arguments in the complex plane and complex-valued parameters in [7]. Here, we compute generalized generating functions for the Al-Salam-Carlitz polynomials using connection relation for these polynomials. We obtain q-analogues of the Sylvester, Cesaro, Pasternack, and Bateman polynomials and generating functions for these polynomials in [8]. We derive generalized linearization formulas for generalized and basic hypergeometric orthogonal polynomials by applying connection relations to them in [9]. Here, we generalize linearization formulae for Laguerre, Gegenbauer, continuous q-ultraspherical/Rogers, Jacobi, and continuous q-Jacobi polynomials. We derive 5-term contiguous relations for linearization coefficients of generalized and basic hypergeometric orthogonal polynomials such as Laguerre, Gegenbauer, Hermite, Jacobi, continuous q-ultraspherical/Rogers, and continuous q-Jacobi polynomials [10].

Cohl served on the Scientific and Local Organizing committees for the Orthogonal Polynomials and Special Functions Summer School 6 (OPSF-S6) workshop

which was held on June 17-23, 2016 at the Norbert Wiener Center for Harmonic Analysis and Applications at the University of Maryland. The OPSF-S6 lecture notes will be published by Cambridge University Press, edited by Cohl and Ismail, including lecture notes by A. Duran, M. E. H. Ismail, E. Koelink, H. Rosengren, and J. Zeng [11].

[1] H. S. Cohl, T. H. Dang, and T.M. Dunster. Fourier and Gegenbauer Expansions for a Fundamental Solution of the Helmholtz Operator in Riemannian Spaces of Constant Curvature. *Symmetry, Integrability and Geometry: Methods and Applications (SIGMA)* **14**:136 (2018), Special Issue on Orthogonal Polynomials, Special Functions and Applications (OPSFA14), 45 pages. DOI: 10.3842/SIGMA.2018.136

[2] G. Olafsson and H. S. Cohl. Fundamental Solutions for the Laplace-Beltrami Operator on the Rank One Symmetric Spaces. In preparation.

[3] H. S. Cohl and J. E. Hirtenstein. Binomial and Logarithmic Gegenbauer Expansions for the Even-dimensional Polyharmonic Equation. In preparation.

[4] H. S. Cohl, J. Park, and H. Volkmer. Gauss Hypergeometric Representations of Ferrers Functions of the Second Kind. In preparation.

[5] M. A. Baeder, R. S. Costas-Santos, and W. Xu. The Power Collection Method for Connection Relations: Meixner Polynomials, *Journal of Classical Analysis* **11**:2 (2017), 107-128.

[6] H. S. Cohl, R. S. Costas-Santos, P. R. Hwang, and T. V. Wakhare. Generalizations of Generating Functions for Basic Hypergeometric Orthogonal Polynomials. In review.

[7] H. S. Cohl, R. S. Costas-Santos, and W. Xu, The Orthogonality of Al-Salam-Carlitz Polynomials for Complex Parameters. In *Frontiers in Orthogonal Polynomials and q-Series*, (Z. Nashed and X. Li, eds.), World Scientific Publishing (2017), 155-167.

[8] H. S. Cohl, R. S. Costas-Santos, and T. V. Wakhare. Some Generating Functions for *q*-polynomials. *Symmetry* **10**:12 (2018), 758. DOI: 10.3390/sym10120758

[9] H. S. Cohl, R. S. Costas-Santos, and J. Zhao. Generalizations of Linearization Formulae for Continuous Hypergeometric Orthogonal Polynomials. In preparation.

[10] H. S. Cohl, M. E. H. Ismail. Two-dimensional Contiguous Relations for Linearization Formulae. In preparation.

[11] *Lecture Notes from the Sixth Orthogonal Polynomials and Special Functions Summer School 2016* (M. E. H. Ismail and H. S. Cohl, eds.), Cambrige University Press, in preparation.

Part IV

Activity Data

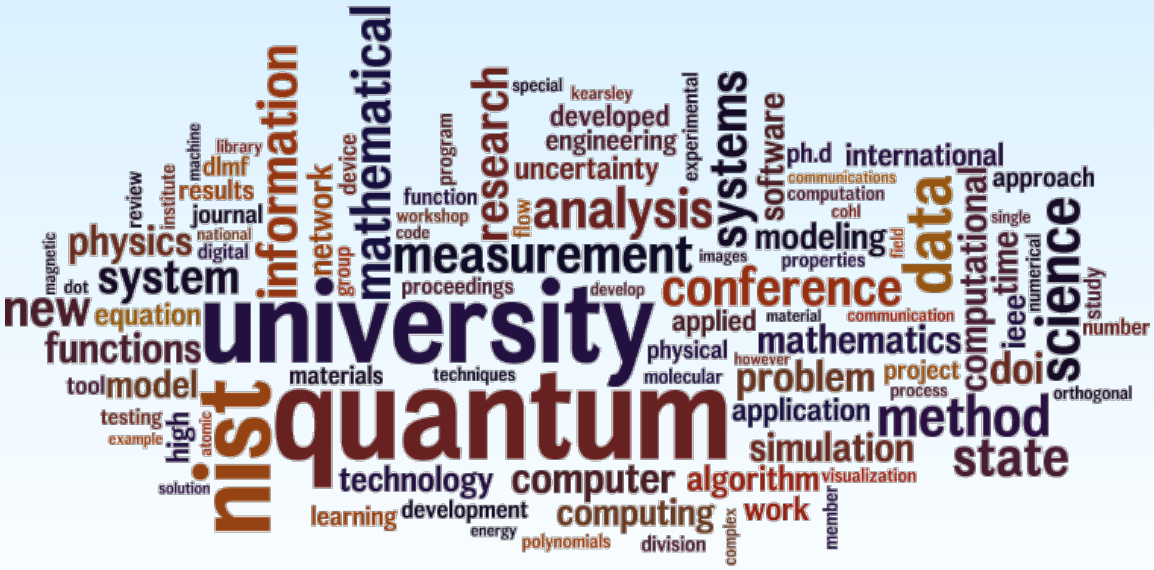

Publications

Note: Names of (co-)authors with a Division affiliation during this reporting period are underlined.

Appeared

Refereed Journals

1. C. Abellán, A. Acín, A. Alarcón, O. Alibart, C. K. Andersen, F. Andreoli, A. Beckert, F. A. Beduini, A. Bendersky, M. Bentivegna, P. Bierhorst, D. Burchardt, A. Cabello, J. Cariñe, S. Carrasco, G. Carvacho, D. Cavalcanti, R. Chaves, J. Cortés-Vega, A. Cuevas, A. Delgado, H. de Riedmatten, C. Eichler, P. Farrera, J. Fuenzalida, M. García-Matos, R. Garthoff, S. Gasparinetti, T. Gerrits, F. Ghafari Jouneghani, S. Glancy, E. S. Gómez, P. González, J.-Y. Guan, J. Handsteiner, J. Heinsoo, G. Heinze, A. Hirschmann, O. Jiménez, F. Kaiser, E. Knill, L. T. Knoll, S. Krinner, P. Kurpiers, M. A. Larotonda, J.-Å. Larsson, A. Lenhard, H. Li, M.-H. Li, G. Lima, B. Liu, Y. Liu, I. H. López Grande, T. Lunghi, X. Ma, O. S. Magaña-Loaiza, P. Magnard, A. Magnoni, M. Martí-Prieto, D. Martínez, P. Mataloni, A. Mattar, M. Mazzera, R. P. Mirin, M. W. Mitchell, S. Nam, M. Oppliger, J.-W. Pan, R. B. Patel, G. J. Pryde, D. Rauch, K. Redeker, D. Rieländer, M. Ringbauer, T. Roberson, W. Rosenfeld, Y. Salathé, L. Santodonato, G. Sauder, T. Scheidl, C. T. Schmiegelow, F. Sciarrino, A. Seri, L. K. Shalm, S.-C. Shi, S. Slussaren-ko, M. J. Stevens, S. Tanzilli, F. Toledo, J. Tura, R. Ur-sin, P. Vergyris, V. B. Verma, T. Walter, A. Wallraff, Z. Wang, H. Weinfurter, M. M. Weston, A. G. White, C. Wu, G. B. Xavier, L. You, X. Yuan, A. Zeilinger, Q. Zhang, W. Zhang, and J. Zhong. Challenging Local Realism with Human Choices. *Nature* **557** (2018) 212. DOI: 10.1038/s41586-018-0085-3

2. M. A. Baeder, H. S. Cohl, R. S. Costas-Santos, and W. Xu. The Power Collection Method for Connection Relations: Meixner Polynomials. *Journal of Classical Analysis* **11**:2 (2017), 107-128. DOI: 10.7153/jca-2017-11-02

3. I. H. Bell and B. K. Alpert. Exceptionally Reliable Density-Solving Algorithms for Multiparameter Mixture Models from Chebyshev Expansion Root-finding. *Fluid Phase Equilibria* **476** Part B, 89-102 (2018). DOI: 10.1016/j.fluid.2018.04.026

4. I. H. Bell, B. K. Alpert, and L. Bouch. ChebTools: C++11 (and Python) Tools for Working with Chebyshev Expansions. *The Journal of Open Source Software* (2018). DOI: 10.21105/joss.00569

5. P. Bierhorst, E. Knill, S. Glancy, Y. Zhang, A. Mink, S. Jordan, A. Rommal, Y. K. Liu, B. Christensen, S. W. Nam, M. J. Stevens, and L. K. Shalm. Experimentally Generated Randomness Certified by the Impossibility of Superluminal Signals. *Nature* **556** (2018), 223. DOI: 10.1038/s41586-018-0019-0

6. W. J. Boettinger, M. E. Williams, K. W. Moon, G. B. McFadden, P. N. Patrone, and J. H. Perepezko. Interdiffusion in the Ni-Re System: Evaluation of Uncertainties. *Journal of Phase Equilibria and Diffusion* **38** (2017), 750-763. DOI: 10.1007/s11669-017-0562-7

7. J. W. Bullard, E. J. Garboczi, P. Feng, A. S. Brand, L. Perry, J. G. Hagedorn, W. Griffin, and J. E. Terrill. Measurement and Modeling Needs for Next-Generation Concrete Binders. *Cement and Concrete Composites* (2017). DOI: 10.1016/j.cemconcomp.2017.06.012

8. J. W. Bullard, J. G. Hagedorn, M. T. Ley, Q. Hu, W. Griffin, and J. E. Terrill. A Critical Comparison of 3D Experiments and Simulations of Tricalcuim Silicate Hydration. *Journal of the American Ceramic Society* **101**:4 (2017) 1453-1470. DOI: 10.1111/jace.15323

9. A. S. Carasso. Stabilized Backward in Time Explicit Marching Schemes in the Numerical Computation of Ill-Posed Time-Reversed Hyperbolic/Parabolic Systems. *Inverse Problems in Science and Engineering* **27**:2 (2018). DOI: 10.1080/17415977.2018.1446952

10. A. S. Carasso. Stable Explicit Stepwise Marching Scheme in Ill-Posed Time-Reversed 2D Burgers' Equation. *Inverse Problems in Science and Engineering* (September 21, 2018). DOI: 10.1080/17415977.2018.1523905

11. B. Cloteaux. A Sufficient Condition for Graphic Sequences with Given Largest and Smallest Entries, Length, and Sum. *Discrete Mathematics and Theoretical Computer Science* **20**:1 (2018), 5. DOI: 10.23638/DMTCS-20-1-25

12. H. S. Cohl, R. S. Costas-Santos, and T. V. Wakhare. Some Generating Functions for *q*-Polynomials. *Symmetry* **10:**12 (2018), 758. DOI: 10.3390/sym10120758

13. H. S. Cohl, T. H. Dang, and T. M. Dunster. Fundamental Solutions and Gegenbauer Expansions of Helmholtz Operators in Riemannian Spaces of Constant Curvature. *Symmetry, Integrability, and Geometry: Methods and Applications (SIGMA)* **14**:136 (2018), Special Issue on Orthogonal Polynomials, Special Functions and Applications (OPSFA14), 45 pages. DOI:10.3842/SIGMA.2018.136

14. R. Dou, E. Brewe, G. Potvin, J. P. Zwolak, and Z Hazari. Understanding the Development of Interest

and Self-Efficacy in Active-Learning Undergraduate Physics Courses. *International Journal of Science Education* **40**:13, 1587-1605 (2018). DOI: 10.1080/09500693.2018.1488088

15. N. Douguet, B. I. Schneider, and L. Argenti. Application of the Complex Kohn Variational Method to Attosecond Spectroscopy. *Physical Review A* **98** (2018), 023403. DOI: 10.1103/PHYSREVA.98.023403
16. T. G. Downes, J. R. Van Meter, E. Knill, G. J. Milburn, and C. M. Caves. Quantum Estimation of Parameters of Classical Spacetimes. *Physical Review D* **96** (2017) 105004. DOI: 10.1103/PhysRevD.96.105004
17. R. M. Evans and D. A. Edwards. Receptor Heterogeneity in Optical Biosensors. *Journal of Mathematical Biology* **76** (2018), 795-816. DOI: 10.1007/s00285-017-1158-x
18. J. T. Fong, N. A. Heckert, J. J. Filliben, and S. W. Freiman. Uncertainty in Multi-Scale Fatigue Life Modeling and a New Approach to Estimating Frequency of Inservice Inspection of Aging Components. *Strength, Fracture and Complexity* **11** (2018), 195-217. DOI: 10.3233/SFC-180223
19. J. W. Fowler, C. G. Pappas, B. K. Alpert, W. B. Doriese, G. C. O'Neil, J. N. Ullom, and D. S. Swetz. Approaches to the Optimal Nonlinear Analysis of Microcalorimeter Pulses. *Journal of Low Temperature Physics* **193** (3-4), 539-546, (2018). DOI: 10.1007/s10909-018-1892-5
20. A. Grossfield, P. N. Patrone, D. R. Roe, A. J. Schultz, D. Siderius, D. M. Zuckerman. Best Practices for Quantification of Uncertainty and Sampling Quality in Molecular Simulations. *LiveCoMS* **1** (2018), 1-24. DOI: 10.33011/livecoms.1.1.5067
21. P. D. Hale, D. F. Williams, and A. Dienstfrey. Waveform Metrology: Signal Measurements in a Modulated World. *Metrologia* **55**:5 (2018). DOI: 10.1088/1681-7575/aa1cd
22. A. C. Keith, C. H. Baldwin, S. Glancy, and E. Knill. Joint Quantum State and Measurement Tomography with Incomplete Measurements. *Physical Review A* **98** (2018), 042318. DOI: 10.1103/PhysRevA.98.042318
23. S. Keshavarz, Z. Molaeinia, A. C. E. Reid, and S. A. Langer. Morphology Dependent Flow Stress in Nickel-Based Superalloys in the Multi-Scale Crystal Plasticity Framework. *Crystals* **7** (2017), 334. DOI: 10.3390/cryst7110334
24. L. Kocia and P. Love. Measurement Contextuality and Planck's Constant. *New Journal of Physics* **20**:7 (2018), 073020. DOI: 10.1088/1367-2630/aacef2
25. F. Krahmer and Y.-K. Liu. Phase Retrieval Without Small-Ball Probability Assumptions. *IEEE Transactions on Information Theory* **64** (2018), 485-500. DOI: 10.1109/TIT.2017.2757520
26. P. S. Kuo, J. S. Pelc, C. Langrock, and M. M. Fejer. Using Temperature to Reduce Noise in Quantum Frequency Conversion. *Optics Letters* **43**:9 (2018) 2034. DOI: 10.1364/OL.43.002034
27. P. S. Kuo and M. M. Fejer. Mixing of Polarization States in Zincblende Nonlinear Optical Crystals. *Optics Express* **26**:21 (2018) 26971. DOI: 10.1364/OE.26.026971
28. P. S. Kuo. Using Silica Fiber Coupling to Extend Superconducting Nanowire Single-Photon Detectors into the Infrared. *OSA Continuum* **1**:4 (2018) 1260. DOI: 10.1364/OSAC.1.00126
29. R. J. La. Cascading Failures in Interdependent Systems: Impact of Degree Variability and Dependence. *IEEE Transactions on Network Science and Engineering* **5**:2 (2018). DOI: 10.1109/TNSE.2017.2738843
30. B. Lester, Y. Lin, M. Brown, A. Kauffman, R. Ball, E. Knill, A. M. Rey, and C. Regal. Measurement-Based Entanglement of Non-Interacting Bosonic Atoms. *Physical Review Lett.* **120** (2018) 193602. DOI: 10.1103/PhysRevLett.120.193602
31. D. Li, B. K. Alpert, D. T. Becker, D. A. Bennett, G. A. Carini, H. M. Cho, W. B. Doriese, J. E. Dusatko, J. W. Fowler, J. C. Frisch, J. D. Gard, S. Guillet, G. C. Hilton, M. R. Holmes, K. D. Irwin, V. Kotsubo, S. J. Lee, J. A. B. Mates, K. M. Morgan, K. Nakahara, C. G. Pappas, C. D. Reintsema, D. R. Schmidt, S. R. Smith, D. S. Swetz, J. B. Thayer, C. J. Titus, J. N. Ullom, L. R. Vale, D. D. Van Winkle, A. Wessels, and L. Zhang. TES X-ray Spectrometer at SLAC LCLS-II. *Journal of Low Temperature Physics* **193** (5-6), 1287-1297, (2018). DOI: 10.1007/s10909-018-2053-6
32. L. Ma, O. Slattery, and X. Tang. Noise Reduction in Optically Controlled Quantum Memory. *Modern Physics Letters B* **32** (2018), 1830001. DOI: 10.1142/S0217984918300016
33. L. Ma, O. Slattery, and X. Tang. Spectral Characterization of Single Photon Sources with Ultra-High Resolution, Accuracy and Sensitivity. *Optics Express* **25**:23 (2017), 28898. DOI: 10.1364/OE.25.028898
34. H. Mahboubi, K. Moezzi, A. Aghdam, and K. Sayrafian. Distributed Sensor Coordination Algorithms for Efficient Coverage in a Network of Heterogeneous Mobile Sensors. *IEEE Transactions on Automatic Control* **62**:11 (2017).DOI: 10.1109/TAC.2017.2714102

35. A. Nucciotti, B. K. Alpert, M. Balata, D. Becker, D. Bennett, A. Bevilacqua, M. Biasotti, V. Ceriale, G. Ceruti, D. Corsini, M. De Gerone, R. Dressler, M. Faverzani, E. Ferri, J. Fowler, G. Gallucci, J. Gard, F. Gatti, A. Giachero, J. Hays-Wehle, S. Heinitz, G. Hilton, U. Köster, M. Lusignoli, J. Mates, S. Nisi, A. Orlando, L. Parodi, G. Pessina, A. Puiu, S. Ragazzi, C. Reintsema, M. Ribeiro-Gomez, D. Schmidt, D. Schuman, F. Siccardi, D. Swetz, J. Ullom, and L. Vale. Status of the HOLMES Experiment to Directly Measure the Neutrino Mass. *Journal of Low Temperature Physics* **193**:5-6 (2018), 1137-1145. DOI: 10.1007/s10909-018-2025-x

36. C. G. Petra and F. A. Potra. A Homogeneous Model for Monotone Mixed Horizontal Linear Complementarity Problems. *Computational Optimization and Applications* **72** (2019), 241-267. DOI: 10.1007/s10589-018-0035-x.

37. A. L. Plant, C. A. Becker, R. J. Hanisch, R. F. Boisvert, A. M. Possolo, and J. T. Elliot. How Measurement Science Can Improve Reliability of Research Results. *PLOS Biology* **16**:4 (2018), e2004299. DOI: 10.1371/journal.pdio.2004299.

38. A. P. Reed, K. H. Mayer, J. D. Teufel, L. D. Burkhart, W. Pfaff, M. Reagor, L. Sletten, X. Ma, R. J. Schoelkopf, E. Knill, and K. W. Lehnert. Faithful Conversion of Propagating Quantum Information to Mechanical Motion. *Nature Physics* **13** (2017), 1163-1167. DOI: 10.1038/nphys4251

39. I. Roth, R. Kueng, S. Kimmel, Y.-K. Liu, D. Gross, J. Eisert, and M. Kliesch. Recovering Quantum Gates from Few Average Gate Fidelities. *Physical Review Letters* **121** (2018), 170502. DOI: 10.1103/PhysRevLett.121.170502

40. B. I. Schneider, B. R. Miller, and B. V. Saunders. NIST's Digital Library of Mathematical Functions. *Physics Today* **71**:2 (2018), 48. DOI: 10.1063/PT.3.3846

41. J. P. Schneider, P. N. Patrone, and D. Margetis. Steric Hindrance of Crystal Growth: Nonlinear Step Flow in 1 + 1 Dimensions. *Multiscale Modeling and Simulation* **16** (2018), 266-299. DOI: 10.1137/16M1110017

42. J. L. E. Silva, S. Glancy, and H. M. Vasconcelos. Quadrature Histograms in Maximum Likelihood Quantum State Tomography. *Physical Review A* **98** (2018), 022325. DOI: 10.1103/PhysRevA98.022325

43. E. Simiu, F. A. Potra, and T. N. Nandi. Determining Longitudinal Integral Turbulence Scales in the Near-Neutral Atmospheric Surface Layer. *Boundary-Layer Meteorology* (2018). DOI: 10.1007/s10546-018-0400-4

44. J. S. Sims. Hylleraas-Configuration-Interaction Study of the Singlet S Ground State of the Negative Li Ion. *Journal of Physics B: Atomic, Molecular, and Optical Physics* **50** (2017), 245003. DOI: 10.1088/1361-6455/aa961e

45. J. P. Zwolak, S. S. Kalantre, X. Wu, S. Ragole, and J. M. Taylor. QFlow Lite Dataset: A Machine-Learning Approach to the Charge States in Quantum Dot Experiments. *PLoS ONE* **13**:10 (2018), e0205844. DOI: 10.1371/journal.pone.0205844

46. J. P. Zwolak, M. Zwolak, and E. Brewe. Educational Commitment and Social Networking: The Power of Informal Networks. *Physical Review: Physics Education Research* **14**:1 (2018), 010131. DOI: 10.1103/PhysRevPhysEducRes.14.010131

Book Chapters

1. H. S. Cohl, R. S. Costas-Santos, and W. Xu. The Orthogonality of Al-Salam-Carlitz Polynomials for Complex Parameters. In *Orthogonal Polynomials and q-Series* (Z. Nashed and X. Li, eds.), World Scientific Publishing, 2017, 155-167. DOI: 10.1142/9789813228887_0008

2. P. N. Patrone and A. Dienstfrey. Uncertainty Quantification for Molecular Dynamics. *Reviews in Computational Chemistry* **31**, Wiley, 2018, 115-162. DOI: 10.1002/9781119518068.ch3

In Conference Proceedings

1. M. Barbi, K. Sayarafian, and M. Alasti. Application of Link Adaptation in Body Area Networks. In *IEEE 28th International Symposium on Personal, Indoor and Mobile Radio Communications (PIMRC'17)*, Montreal, Canada, October 8-13, 2017. DOI: 10.1109/PIMRC.2017.8292629

2. M. Barbi, K. Sayarafian, and M. Alasti. A Study of Capsule Endoscopy Orientation Estimation at UWB Frequencies. *IEEE 29th International Symposium on Personal, Indoor and Mobile Radio Communications (PIMRC'18)*, Bologna, Italy, September 9-11, 2018. DOI: 10.1109/PIMRC.2018.8580786

3. H. S. Cohl, A. Greiner-Petter, and M. Schubotz. Automated Symbolic and Numerical Testing of DLMF Formulae Using Computer Algebra Systems. In *Intelligent Computer Mathematics (CICM 2018)*, Lecture Notes in Computer Science **11006** (2018), 39-52. DOI: 10.1007/978-3-319-96812-4_4

4. J. T. Fong, N. A. Heckert, J. J. Filliben, P. V. Marcal, R. Rainsberger, K. F. Stupic, and S. E. Russek. MRI Birdcage RF Coil Resonance with Uncertainty and Relative Error Convergence Rates. In *Proceedings of the 2017 International COMSOL Users' Conference*, Boston, MA, October 4-6, 2017. URL: https://www.comsol.com/paper/mri-birdcage-rf-coil-resonance-with-uncertainty-and-relative-error-convergence-r-52751

5. J. T. Fong, N. A. Heckert, J. J. Filliben, and M. J. Cohn. Uncertainty in Multi-Scale Creep Rupture Life Modeling and a New Approach to Estimating Frequency of Inservice Inspection of Components at Elevated Temperatures. In *2018 ASME Symposium on Elevated Temperature Applications of Materials for Fossil, Nuclear and Petrochemical Industries*, Seattle, WA, April 3-5, 2018, V001T04A002. DOI: 10.1115/ETAM2018-6711

6. J. T. Fong, P. V. Marcal, R. Rainsberger, L. Ma, N. A. Heckert, and J. J. Filliben. Finite Element Method Solution Uncertainty, Asymptotic Solution, and a New Approach to Accuracy Assessment. In *ASME Verification and Validation Symposium*, Minneapolis, MN, May 16-18, 2018, V001T12A001. DOI: 10.1115/VVS2018-9320

7. J. T. Fong, N. A Heckert, J. J. Filliben, and P. H. Ziel. A Nonlinear Least Squares Logistic Fit Approach to Quantifying Uncertainty in Fatigue Stress-Life Models and an Application to Plain Concrete. In the *ASME 2018 Pressure Vessels and Piping Division Conference*, Prague, Czech Republic, July 15-20, 2018, V06BT06A075. DOI: 10.1115/PVP2018-84739

8. J. T. Fong, N. A. Heckert, J. J. Filliben, and S. R. Doctor. Three Approaches to Quantification of NDE Uncertainty and a Detailed Exposition of the Expert Panel Approach Using the Sheffield Elicitation Framework. In *ASME 2018 Pressure Vessels and Piping Division Conference*, Prague, Czech Republic, July 15-20, 2018, V01AT01A007. DOI: 10.1115/PVP2018-84771

9. A. Greiner-Petter, M. Schubotz, H. S. Cohl, and B. Gipp. MathTools: An Open API for Convenient MathML Handling. In the *Proceedings of the Intelligent Computer Mathematics (CICM 2018)*, Lecture Notes in Computer Science **11006**, Springer. DOI: 10.1007/978-3-319-96812-4_9

10. Z. Ji, Y.-K. Liu, and F. Song. Pseudorandom Quantum States. In *Proceedings of the Advances in Cryptology – CRYPTO 2018*, Lecture Notes in Computer Science **10993** (2018). DOI: 10.1007/978-3-319-96878-0_5

11. K. Krhac, K. Sayrafian, M. Alasti, K. Y. Yazdandoost, and D. Simunic. A Study of Capsule Endoscopy Orientation Estimation Using Received Signal Strength. In *IEEE 29th Annual International Symposium on Personal, Indoor and Mobile Radio Communications (PIMRC)*, Bologna, Italy, September 9-12, 2018, 345-349. DOI: 10.1109/PIMRC.2018.8580786

12. D. R. Kuhn, D. Yaga, R. N. Kacker, Y. Lei, and V. Hu. Pseudo-Exhaustive Verification of Rule Based Systems. In *Proceedings of the 2018 International Conference on Software Engineering and Knowledge Engineering (SEKE 2018)*, 586-591, San Francisco, CA, July 1-3, 2018. DOI: 10.18293/SEKE2018-072

13. P. S. Kuo, J. S. Pelc, C. Langrock, and M. M. Fejer. Using Temperature to Reduce Noise in Quantum Frequency Conversion. In *Proceedings on the Conference on Lasers and Electro-Optics OSA Technical Digest*, San Jose, CA, May 13-18, 2018. DOI: 10.1364/CLEO_SI.2018.SM2D.5

14. P. S. Kuo and B. G. Alberding. Towards Extending Super-Conducting Nanowire Single-Photon Detectors into the Infrared Wavelength Range. In *Proceedings of the Frontiers in Optics/Laser Science OSA Technical Digest*, Washington, DC, September 16-20, 2018. DOI: 10.1364/FIO.2018.JTu3A.62

15. R. J. La. Estimation of Externalities in Interdependent Security: A Case Study of Large Systems. In 2017 *IEEE 56th Annual Conference on Decision and Control (CDC)*, Miami, FL, December 12-15, 2017. DOI: 10.1109/CDC.2017.8264242

16. R. J. La. Identifying Vulnerable Nodes to Cascading Failures: Centrality to the Rescue. In *Complex Networks and Their Applications VII* (L. Aiello, C. Cherifi, H. Cherifi, R. Lambiotte, P. Lió, and L. Rocha, eds.), COMPLEX NETWORKS 2018. *Studies in Computational Intelligence 812*. Springer, Cham, 866-878. DOI: 10.1007/978-3-030-05411-3_69

17. M. H. Lotfi, R. J. La, and N. C. Martins. Bayesian Congestion Game with Traffic Manager: Binary Signal Case. In *Proceedings of the 2018 IEEE Conference on Decision and Control (CDC 18)*, Miami, FL, December 17-19, 2018.

18. L. Ma, O. Slattery, and X. Tang. Ultra-High Spectral Resolution Spectrometer for Single Photon Source Characterization. In *Proceedings of the SPIE 10660, Quantum Information Science, Sensing, and Computation X* **1066006** (2018), Orlando, Florida, April 2018. DOI: 10.1117/12.2303836

19. L. Ma, J. T. Fong, P. V. Mercal, R. Rainsberger, N. A. Heckert, and J. J. Filliben. Uncertainty Quantification of Finite Element Analysis of Uni-Axial Strength Test of Holed Composite Laminates. In *ASME 2018 Pressure Vessels and Piping Conference*, Prague, Czech Republic, July 15-20, 2018, V06BT06A074. DOI: 10.1115/PVP2018-84730

20. V. Marbukh. Network Formation by Contagion Averse Agents: Modeling Bounded Rationality with Logit Learning. In *IEEE/ACM International Conference on Advances in Social Networks Analysis and Mining (ASONAM)*, Barcelona, Spain,

August 28-31, 2018. DOI: 10.1109/ASONAM.2018.8508546

21. V. Marbukh. Towards Efficient Offloading in Fog/Edge Computing by Approximating Effect of Externalities. In *IEEE INFOCOM 2018 - IEEE Conference on Computer Communications Workshops (INFOCOM WKSHPS)*, Honolulu, HI, April 15-19,2018. DOI: 10.1109/INFCOMW.2018.8406835
22. V. Marbukh. On Mitigation Inefficiency of Selfish Investment in Network Recovery from High Loss SIS Infection**.** In *2018 17th IEEE International Conference on Trust, Security and Privacy in Computing and Communications / 12th IEEE International Conference on Big Data Science and Engineering (TrustCom/BigDataSE)*, New York, NY, August 1-3, 2018. DOI: 10.1109/TrustCom/BigDataSE.2018.00293
23. V. Marbukh. Dynamic Job Replication for Balancing Fault Tolerance, Latency, and Economic Efficiency: Work in Progress. In *2018 IEEE International Conference on Services Computing (SCC)*, San Francisco, CA, July 2-7, 2018. DOI: 10.1109/SCC.2018.00043
24. V. Marbukh. Towards Managing Age of Network State Information in Challenged Networks. In *IEEE INFOCOM 2018 - IEEE Conference on Computer Communications Workshops (INFOCOM WKSHPS)*, Honolulu, HI, April 15-18, 2018. DOI: 10.1109/INFCOMW.2018.8406983
25. V. Marbukh. Economics of Networked Infrastructures at the Edge of Undesirable Contagion: A Case of SIS Infection. In *IEEE INFOCOM 2018 - IEEE Conference on Computer Communications Workshops (INFOCOM WKSHPS)*, Honolulu, HI, April 15-19, 2018. DOI: 10.1109/INFCOMW.2018.8406916
26. B. R. Miller. A New Specfun Content Dictionary. In *Proceedings of the 29th OpenMath Workshop*, Hagenberg, Austria, August 13, 2018.
27. P. N. Patrone, A. J. Kearsley, and A. Dienstfrey. The Role of Data Analysis in Uncertainty Quantification: Case Studies for Materials Modeling. In *Proceedings of the 2018 American Institute of Aeronautics and Astronautics SciTech Forum (AIAA SciTech 2018)*, Kissimmee, FL, January 8-12, 2018. DOI: 10.2514/6.2018-0927
28. S. Perez-Simbor, K. Krhac, C. Garcia-Pardo, K. Sayarafian, D. Simunic, and N. Cardona. Impact of Measurement Points Distribution on the Parameters of UWB Implant Channel Model. In *2018 IEEE Conference on Standards for Communications and Networking*, Paris, France, October 29-31, 2018. DOI: 10.1109/CSCN.2018.8581808
29. K. Pomian, J. P. Zwolak, E. Sayre, S. Frankin, and M. B. Kustusch. Network Analysis of IMPRESS Summer Program. In *Proceedings of the Physics Education Research Conference 2017*, Cincinnati, OH, July 26-17, 2017. DOI: 10.1119/perc.2017.pr.074
30. D. G. Porter. Introduction to the HAMT and Tcl. In *Proceedings of the 24th Annual Tcl/Tk Conference*, Houston, TX, October 16-20, 2017. URL: https://www.tcl.tk/community/tcl2017/assets/talk92/Paper.pdf
31. R. Rainsberger, J. T. Fong, and P. V. Marcal. Application of an a Priori Jacobian-Based Error Estimation Metric to the Accuracy Assessment of 3D Finite Element Simulations. In the *ASME 2018 Pressure Vessels and Piping Division Conference* **6B**: Materials and Fabrication, Prague, Czech Republic, July 15-20, 2018, V06BT06A076. DOI: 10.1115/PVP2018-84784
32. J. D. Rezac, A. Dienstfrey, N. Vlajic, A. Chijioke, and P. D. Hale. Generalized Source-Conditions and Uncertainty Bounds for Deconvolution Problems. In *Mathematical Tools for Measurements*, Belfast, Northern Ireland, August 2018. Journal of Physics: Conference Series **1065** (2018). DOI: 10.1088/1742-6596/1065/21/212025
33. M. Schubotz, A. Greiner-Petter, P. Scharpf, N. Meuschke, H. S. Cohl, and B. Gipp. Improving the Representation and Conversion of Mathematical Formulae by Considering their Textual Context. In *Proceedings of the 18th ACM/IEEE Joint Conference on Digital Libraries (JCDL'18)*, Fort Worth, TX, June 3-6, 2018, 233-242. DOI: 10.1145/3197026.3197058
34. E. Williams, J. P. Zwolak, and E. Brewe. Physics Major Engagement and Persistence: A Phenomenography Interview Study. In *Proceedings of the Physics Education Research Conference 2017*, Cincinnati, OH, July 26-27, 2017. DOI: 10.1119/perc.2017.pr.104
35. A. Youssef and B. Miller. Deep Learning for Math Knowledge Processing. In *Conference on Intelligent Computer Mathematics (CICM 2018)*, Hagenberg, Austria, August 2018. Lecture Notes in Computer Science **11006** (2018), 271-286. DOI: 10.1007/978-3-319-96812-4_23
36. J. P. Zwolak, R. Dou, and E. Brewe. Student Perceptions of the Value of Out-of-Class Interactions: Attitudes vs. Practice. In *Proceedings of the Physics Education Research Conference 2017*, Cincinnati, OH, July 26-17, 2017. DOI: 10.1119/perc.2017.pr.115

Technical Magazine Articles

1. S. P. Jordan and Y.-K. Liu. Quantum Cryptanalysis: Shor, Grover, and Beyond. *IEEE Security & Privacy* **16** (September/October 2018), 14-21. DOI: 10.1109/MSP.2018.3761719

2. B. Saunders. Somebody Else's Dream. *SIAM News* **51**:2 (2018), 5-6. URL: https://sinews.siam.org/Portals/Sinews2/Issue%20Pdfs/sn_March2018.pdf

3. B. I. Schneider and R. Eigenmann. National Strategic Computing Initiative. *Computing in Science and Engineering* **20**:5 (2018), 5. DOI: 10.1109/MCSE.2018.05329810

4. B. I. Schneider, B. R. Miller, and B. V. Saunders. NIST's Digital Library of Mathematical Functions. *Physics Today* **71**:2, (2018), 48. DOI: 10.1063/PT.3.3846

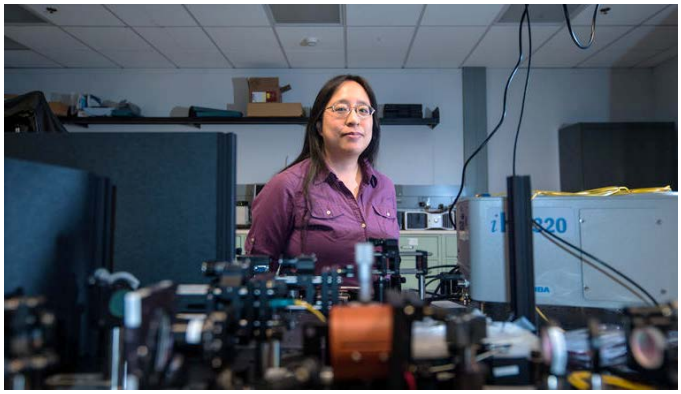

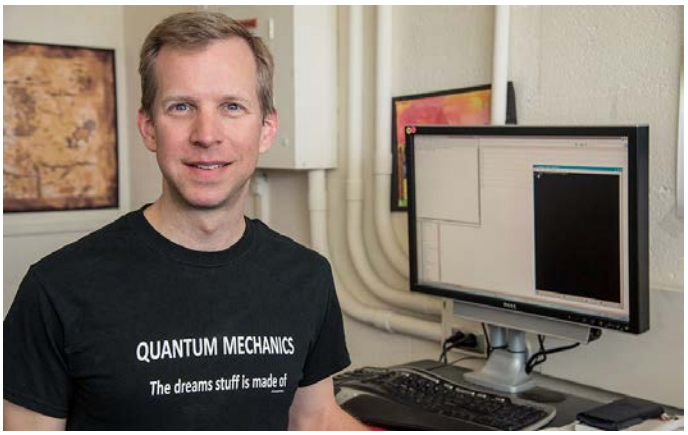

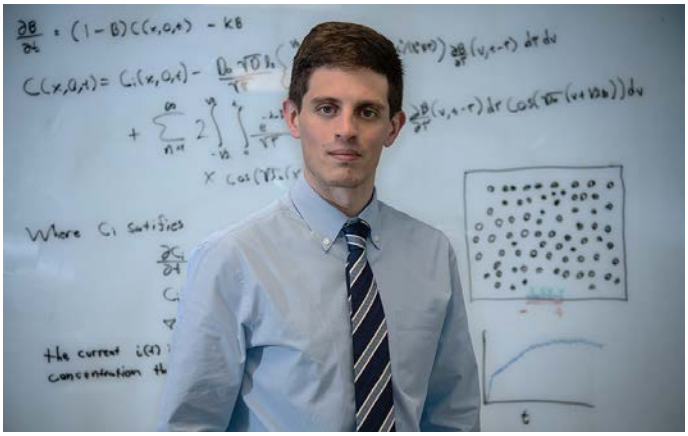

Figure 89. *Three ACMD staff members contributed to the NIST Taking Measure Blog this year. Top to bottom: Paulina Kuo (*It's All Right to Be Wrong in Science). *Scott Glancy (*Bell's Inequality, and T-Shirts: An Entangled Tale). *Ryan Evans (*It All Adds Up: Being a NIST NRC Postdoc in Applied Mathematics).

Technical Reports

1. J. Bernal. Shape Analysis, Lebesque Integration and Absolute Continuity Connections. NISTIR 8217, July 2018. DOI: 10.6028/NIST.IR.8217

2. R. F. Boisvert (ed.), Applied and Computational Mathematics Division, Summary of Activities for Fiscal Year 2017, NISTIR 8208, April 2018, 143 pages. DOI: 10.6028/NIST.IR.8208

3. M. Boss, A. Dienstfrey, Z. Gimbutas, K. Keenan, J. Splett, K. Stupic, and S. Russek. Magnetic Resonance Imaging Biomarker Calibration Service: Proton Spin Relaxation Times. NISTSP-250-97, May 2018. DOI: 10.6028/NIST.SP.250-97

4. E. Knill, Y. Zhang, and P. Bierhorst. Quantum Randomness Generation by Probability Estimation with Classical Side Information. arXiv: 1709.06159, 2017.

5. E. Knill, Y. Zhang, and H. Fu. Quantum Randomness Generation by Quantum Probability Estimation with Quantum Side Information. arXiv: 1806.04553, 2018.

6. M. Kovarek, L. Amatucci, K. A. Gillis, F. A. Potra, J. Ratino, M. Levitan, and D. H. Yeo. Calibration of Dynamic Pressure in a Tubing System and Optimized Design of Tube Configuration: A Numerical and Experimental Study. NIST Technical Note 1994, 2018. DOI: 10.6028/NIST.TN.1994

7. P. Lee, H. Guan, A. Dienstfrey, M. Theofanos, B. Stanton, and M. Schwarz. Forensic Latent Fingerprint Preprocessing Assessment. NISTIR 8215, June 2018. DOI: 10.6028/NIST.IR.8215

8. T. Ndousse-Fetter, W. Grice, P. Kumar, J. Dubois, S. Guha, D. Kilper, P. Kuo, G. Li, L. Ma, I. Monga, A. Nomerotski, N. Peters, O. Slattery, S. Soh, and X. Tang. Report on Roundtable Discussion on Quantum Networks for Open Science, Department of Energy, December 4, 2017. URL: https://www.orau.gov/quantumnetworks2018/Quantum-Networks-Roundtable-Report-Final-2018-02-05.pdf

9. A. Olivas, C. F. Ferraris, N. S. Martys, W. L. George, E. J. Garboczi, and B. Toman. Certification of SRM 2493: Standard Reference Mortar for Rheological Measurements. NISTSP 260-186, October 2017. DOI: 10.6028/NIST.SP.260-187

NIST Blog Posts

1. R. M. Evans. It All Adds Up: Being a NIST NRC Postdoc in Applied Mathematics. Taking Measure Blog, NIST Public Affairs Office, September 4, 2018. URL: https://www.nist.gov/blogs/taking-measure/it-all-adds-being-nist-nrc-postdoc-applied-mathematics
2. S. Glancy. Local Realism, Bell's Inequality, and T-Shirts: An Entangled Tale. Taking Measure Blog, NIST Public Affairs Office, April 30, 2018. URL: https://www.nist.gov/blogs/taking-measure/local-realism-bells-inequality-and-t-shirts-entangled-tale
3. P. Kuo. It's All Right to Be Wrong in Science. Taking Measure Blog, NIST Public Affairs Office, March 12, 2018. URL: https://www.nist.gov/blogs/taking-measure/its-all-right-be-wrong-science

Accepted

1. R. G. Brinson, J. P. Marino, F. Delaglio, L. W. Arbogast, R. M. Evans, A. J. Kearsley, G. Gingras, H. Ghasriani, Y. Aubin, G. K. Pierens, X. Jia, M. Mobli, H. G. Grant, D. W. Keizer, K. Schweimer, J. Ståhle, G. Widmalm, E. R. Zartler, C. W. Lawrence, P. N. Reardon, J. R. Cort, P. Xu, F. Ni, S. Yanaka, K. Kato, S. R. Parnham, D. Tsao, A. Blomgren, T. Rundlöf, N. Trieloff, P. Schmieder, A. Ross, K. Skidmore, K. Chen, D. Keire, D. I. Freedberg, T. Suter-Stahel, G. Wider, G. Ilc, J. Plavec, S. A. Bradley, D. M. Baldisseri, M. L. Sforca, A. C. de Mattos Zeri, J. Y. Wei, C. M. Szabo, C. A. Amezcue, J. B. Jordan, and M. Wikström. Enabling Adoption of 2D-NMR for the Higher Order Structure Assessment of Monoclonal Antibody Therapeutics. *mAbs*.
2. H. S. Cohl, R. S. Costas-Santos, and T. V. Wakhare. On a Generalization of the Rogers Generating Function. *Journal of Mathematical Analysis and Applications.*
3. D. G. Porter and M. J. Donahue. Standard Problems in Micromagnetics. In *Electrostatic and Magnetic Phenomena: Particles, Macromolecules, Nanomagnetics* (M. J. Donahue, ed.), World Scientific Publishing.
4. J. T. Fong, J. J. Filliben, N. A. Heckert, D. D. Leber, P. A. Berkman, and R. E. Chapman. Uncertainty Quantification of Failure Probability and a Dynamic Risk Analysis of Decision Making for Maintenance of Ageing Infrastructure. *Risk Based Approaches to Complex Systems.*
5. A. Greiner-Petter, H. S. Cohl, M. Schubotz, and B. Gipp. Semantic Preserving Bijective Mappings for Representations of Special Functions Between Computer Algebra Systems and Word Processors. *Aslib Journal of Information Management.*
6. S. S. Kalantre. J. P. Zwolak, S. Ragole, X. Wu, N. M. Zimmerman, M. D. Stewart, and J. M. Taylor. Machine Learning Techniques for State Recognition and Auto-Tuning in Quantum Dots. *NPJ Quantum Information.*
7. J. A. Kauffman, W. L. George, and J. S. Pitt. An Overset Mesh Framework for an Isentropic ALE Navier-Stokes HDG Formulation. *2019 Aerospace Sciences Meeting*.
8. A. Keith, C. Baldwin, S. Glancy, and E. Knill. Joint Quantum State and Measurement Tomography with Incomplete Measurements. *Physical Review A.*
9. L. Kocia and P. Love. The Non-Disjoint Ontic States of the Grassmann Ontological Model, Transformation Contextuality, and the Single Qubit Stabilizer Subtheory. arXiv: 1805.09514. *Journal of Physics A.*
10. R. J. La. Influence of Clustering on Cascading Failures in Interdependent Systems, *IEEE Transactions on Network Science and Engineering.*
11. S. Perez-Simbor, K. Krhac, C. Garcia-Pardo, K. Sayrafian, D. Simunic, and N. Cardona. Impact of Measurement Points Distribution on the Parameters of UWB Implant Channel Model. In *Proceedings of the 2018 IEEE Conference on Standards for Communications & Networking (CSCN) 2018*, Paris, France, October 2018.
12. S. Ressler. Standards, the Glue for Innovation. *Standards Engineering – The Journal of SES- The Society for Standards Professionals.*
13. R. Rhorer, S. Mates, E. Whitenton, and T. Burns. History Note: Machining, Strain Gages, and a Pulse-Heated Kolsky Bar. In *Proceedings of the 2018 Annual Conference on Experimental and Applied Mechanics*, Greenville, SC, June 4-7, 2018.
14. D. R. Schultz, H. Gharibnejad, T. E. Cravens, and S. J. Houston. Data for Secondary Electron Production from Ion Precipitation at Jupiter, II: Simultaneous and Non-Simultaneous Target and Projectile Processes in Collision of $O^{q+} + H_2 (q = 0 - 8)$. *Atomic Data and Nuclear Data Tables.* Oct. 2018, DOI: 10.1016/j.adt.2018.08.002

In Review

1. D. A. Anderson, J. D. Benson, and A. J. Kearsley. Foundations of Modeling in Cryobiology – II: Heat and Mass Transport in Bulk and Cell Membrane and Ice-Liquid Interfaces.

2. D. A. Anderson, J. D. Benson, and A. J. Kearsley. Foundations of Modeling in Cryobiology – III: Inward Solidification of a Ternary Solution Towards a Permeable Spherical Cell in the Dilute Limit.
3. F. Ahmadi, Y. Sozer, M. J. Donahue, and I. Tsukerman. A Novel Low Loss and Lightweight Magnetic Material for Electrical Machinery.
4. T. J. Burns and B. W. Rust. Closed-Form Projection Method for Regularizing a Function Defined by a Discrete Set of Noisy Data and for Estimating its Derivative and Fractional Derivative. arXiv:1805.09849.
5. B. Cloteaux. Forced Edges and Graph Structure.
6. B. Cloteaux. One-Pass Graphic Approximation of Integer Sequences.
7. H. S. Cohl, R. S. Costas-Santos, P. R. Hwang, and T. V. Wakhare. Generalizations of Generating Functions for Basic Hypergeometric Orthogonal Polynomials.
8. H. S. Cohl, R. S. Costas-Santos, and J. Zhao. Generalizations of Linearization Formulae for Continuous Hypergeometric Orthogonal Polynomials.
9. G. A. Cooksey, P. Patrone, J. R. Hands, S. E. Meek, and A. J. Kearsley. Dynamic Measurement of Nanoflows: Realization of a Multidecadal Optofluidic Flow Meter to the Nanoliter per Minute Scale.
10. V. Dunjko, Y.-K. Liu, X. Wu, and J. M. Taylor. Super-Polynomial Separations for Quantum-Enhanced Reinforcement Learning.
11. R. M. Evans, A. Balijepalli, and A. J. Kearsley. Diffusion-Limited Reaction in Nanoscale Electronics.
12. J. T. Fong, N. A Heckert, J. J. Filliben, P. V. Marcal, and S. W. Freiman. A Composite Goodness-of-Fit Approach to Selecting the Best Distribution for Estimating the Minimum Strength of a Full-Scale Component or Structure from Laboratory Test Data.
13. H. Gharibnejad, B. I. Schneider, M. Leadingham, and H. J. Schmale. A Comparison of Numerical Approaches to the Solution of Time-Dependent Schrödinger Equation in One Dimension. arXiv: 1809.09164.
14. L. Kocia and P. Love. Stationary Phase Method in Discrete Wigner Functions and Classical Simulation of Quantum Circuits. arXiv: 1810.03622.
15. J. Lawrence and J. Bernal. A Purely Algebraic Justification of the Solution by Singular Value Decomposition to the Constrained Orthogonal Procrustes Problem.
16. G. Lesaja and F. A. Potra. Adaptive Full Newton-Step Infeasible Interior-Point Method for Sufficient Horizontal LCP.
17. L. Ma, O. Slattery, and X. Tang. Optical Quantum Memory and its Applications in Quantum Communication Systems.
18. K. Mayer, and E. Knill. Bounding the Quantum Process Fidelity with a Minimal Set of Input States.
19. W. F. Mitchell and J. S. Villarrubia. An *A Posteriori* Error Estimate for Scanning Electron Microscope Simulation with Adaptive Mesh Refinement.
20. P. N. Patrone, G. Cooksey, and A. J. Kearsley. Dynamic Measurement of Nanoflows: Analysis and Theory of an Optofluidic Flowmeter.
21. P. N. Patrone, P. Brant, J. Younker, D. J. Crowther, C. J. Ruff, M. K. Ng, M. Vadlamudi, and J. E. Lee. Revisiting Fox-Flory: Detailed Study of the Glass-Transition Temperature for Polypropylene Systems.
22. P. N. Patrone, A. Dienstfrey, and G. B. McFadden. Towards a Priori Uncertainty Quantification in Coarse-Grained Molecular Dynamics: Generalized Multipole Potentials.
23. K. Sayrafian and S. Ambroziak. IoT-Health (book chapter).
24. O. Slattery, L. Ma, K. Zong, and X. Tang. Background and Review of Cavity Enhanced Spontaneous Parametric Down Conversion.
25. D. G. Porter and M. J. Donahue. Standard Problems in Micromagnetics.
26. P. Wills, E. Knill, K. Coakley, and Y. Zhang. Performance of Test Supermartingale Confidence Intervals for the Success Probability of Bernoulli Trials.
27. J. W. Woodcock, R. Sheridan, R. Beams, S. J. Stranick, W. F. Mitchell, L. C. Brinson, V. Gudapati, D. Hartman, A. Vaidya, J. W. Gilman, and G. A. Holmes. Damage Sensing Using a Mechanophore Crosslinked Epoxy Resin in Single-Fiber Composites.
28. Y. Zhang, E. Knill, and P. Bierhorst. Quantum Randomness Generation by Quantum Probability Estimation with Quantum Side Information.

Inventions

Patents

1. G. Cooksey, P. N. Patrone, and A. J. Kearsley. Optical Flow Meter for Determining a Flow Rate of a Liquid. US15/967,966.
2. L. Ma, O. Slattery, and X. Tang. Direct Absolute Spectrometer for Direct Absolute Spectrometry. US Patent application number: 16/039,391. Date filed: July 19, 2018.

Invention Disclosures

1. J. Taylor, S. Kalantre, J. Zwolak, X. Wu, and S. Ragole. Generating and Using Synthetic Data Sets to Enable Machine Learning-Based Tuning Techniques for Experiments. NIST Invention Disclosure, NIST Docket #18-032, August 15, 2018. [U.S. Provisional Patent Application serial number 62/722,870, November 29, 2018]

Presentations

Note: When multiple presenters are listed, names of co-presenters with a Division affiliation during this reporting period are underlined.

Invited Talks

1. D. A. Anderson, J. D. Benson, and A. J. Kearsley. "Modeling Heat and Mass Transport in Cryobiology." School of Mathematical and Natural Sciences, Arizona State University, November 8, 2018.
2. R. F. Boisvert (panelist). "Managing and Funding Standard Reference Data." NIST Standard Reference Data Workshop. Gaithersburg, MD, October 17, 2017.
3. R. F. Boisvert. "How We Got Here." ACM Workshop on Reproducibility. New York, December 7, 2017.
4. B. Cloteaux. "Graph Generation for Fun and Profit." Computer Science Seminar, The University of Texas at El Paso, October 28, 2016.
5. H. S. Cohl. "Generalizations of Generating Functions for Basic Hypergeometric Orthogonal Polynomials." AMS Special Session on Orthogonal Polynomials and Applications, Joint Mathematics Meetings 2018, San Diego, CA, January 10, 2018.
6. H. S. Cohl. "Semantic Preserving Bijective Mappings of Mathematical Formulae Between Semantic LATEX and Computer Algebra Systems." AMS Special Session on Mathematical Information in the Digital Age of Science, Joint Mathematics Meetings 2018, San Diego, CA, January 12, 2018.
7. H. S. Cohl. "Fundamental Solutions and Gegenbauer Expansions of the Helmholtz Equations of *d*-dimensional Riemannian Spaces of Constant Curvature." Kalnins Fest 2018, Harnessing Hidden Symmetry: Geometry and Superintegrable Systems, Takapuna, Auckland, New Zealand, February 2, 2018.
8. H. S. Cohl. "Fundamental Solutions and Gegenbauer Expansions of the Helmholtz Equations of *d*-Dimensional Riemannian Spaces of Constant Curvature." Analysis Seminar, University of Auckland, Auckland, New Zealand, February 5, 2018.
9. H. S. Cohl. "Generalizations of Linearization Formulae for Continuous Hypergeometric Orthogonal Polynomials." Symbolic Computation Group Seminar, Johann Radon Institute for Computational and Applied Mathematics (RICAM), Linz, Austria, August 9, 2018.
10. H. S. Cohl. "Fundamental Solutions and Gegenbauer Expansions of the Helmholtz Equations on *d*-dimensional Riemannian Spaces of Constant Curvature." CMS Special Session on Asymptotic Analysis and Applications, Winter 2018 Canadian Mathematical Society Meeting, Vancouver, Canada. December 10, 2018.
11. G. Doğan. "Variational Shape Optimization for Image Analysis." Applied Mathematics Seminar, Clemson University, Clemson, SC, April 2, 2018.
12. G. Doğan. "Fast and Robust Boundary Segmentation Using 2nd Order Shape Sensitivity of Variational Models." SIAM Conference on Imaging Science, Bologna, Italy, June 5-8, 2018.
13. R. M. Evans, A. Balijepalli, and A. J. Kearsley. "Transport Phenomena in Field Effect Transistors." Minisymposium: Transport Phenomena in Biological Processes, Society of Mathematical Biology 2018 Annual Meeting, Sydney, New South Wales, Australia, July 11, 2018.
14. R. M. Evans, A. J. Kearsley, A. Balijepalli, L. W. Arbogast, R. G. Brinson, and F. Delaglio. "From Medical Diagnostic Instruments to Therapeutic Proteins." Society for Industrial and Applied Mathematics (SIAM) Student Seminar, University of Delaware, Newark, DE, April 13, 2018.
15. R. M. Evans, A. J. Kearsley, A. Balijepalli, L. W. Arbogast, R. G. Brinson, and F. Delaglio. "From Medical Diagnostic Instruments to Therapeutic Proteins." Applied Mathematics Seminar, U. S. Naval Academy, Annapolis, MD, March 30, 2018.

16. R. M. Evans, A. Balijepalli, and A. J. Kearsley. "Transport Phenomena in Field Effect Transistors." Center for Nonlinear Analysis, Carnegie Mellon University, Pittsburgh, PA, January 23, 2018.
17. R. M. Evans, A. J. Kearsley A. Balijepalli, and D. A. Edwards. "Measuring Reaction Rate Constants with Optical Biosensors." Mathematics Department, Michigan Technological University, November 10, 2017.
18. J. T. Fong. "A Dynamic Risk Analysis of High-Consequence Low-Failure-Probability Systems for Managing Science Policy Choices Including the 'Do-Nothing' Option." Fletcher School of Law and Diplomacy, Tufts University, Medford, MA, October 2, 2017.
19. J. T. Fong. "Finite Element Method (FEM) Uncertainty and a New Approach to Accuracy Assessment." Mechanical Engineering Department, University of Washington, Seattle, WA, March 28, 2018.
20. J. T. Fong. "Managing Uncertainty in Engineering and a Tool-based Approach to Uncertainty Quantification." Boeing 737 Quality Department, Boeing Company, Renton, WA, April 2, 2018.
21. J. T. Fong. "Six Easy-to-Use Tools for Uncertainty Quantification (UQ) with Examples of Application to Engineering Practice and Research." University of Texas-Arlington Research Institute for PPM, Arlington, TX, May 4, 2018.
22. J. T. Fong. "A Proposal to Re-write BPVC-Section-V-2015-Article 14 (Examination System Qualification)." Section V Working Group WG-Ultrasonics, ASME Code Week, Dallas, TX, May 8, 2018.
23. J. T. Fong. "Uncertainty Quantification Tools for Brain Metrology and an Application to the Analysis of the MRI-based Data of the 2015 MIDA Model." NIST Boulder Division 686 Seminar, Boulder, CO, June 28, 2018.
24. J. T. Fong. "Six Easy-to-Use Tools for Uncertainty Quantification (UQ) with Examples of Application to Engineering Practice and Research." Institute Seminar, ABB Research, Zurich, Switzerland, July 10, 2018.
25. J. T. Fong. "Uncertainty Quantification (UQ) Tools for Brain Metrology and an Application to the Analysis of the MRI-based Data of the 2015 MIDA Model." IT'IS Foundation, Swiss Federal Institute of Technology (ETH), Zurich, Switzerland, July 11, 2018.
26. J. T. Fong. "A Proposal to Re-Write BPVC-Section-V-2015-Article 14 (Examination System Qualification)." Section V Working Group WG-General Requirements Meeting, ASME Code Week, Washington, DC, August 1, 2018.
27. S. Glancy. "Experimentally Generated Randomness Certified by the Impossibility of Superluminal Signals." Towards Ultimate Quantum Theory, Linnaeus University, Växjö, Sweden, June 11-14, 2018.
28. R. N. Kacker, "True Value and Uncertainty in the GUM." XXII IMEKO World Congress, Belfast, Northern Ireland, UK, September 3-6, 2018.
29. R. N. Kacker. "True Value, Error and Uncertainty." Measurement Science, Anaheim, CA, March 20-23, 2018.
30. R. N. Kacker, D. R. Kuhn, Y. Lei, and D. E. Simos. "Combinatorial Testing: An Adaptation of Design of Experiments for Testing Software Systems." 2018 International Symposium on Business and Industrial Statistics (ISBIS), International Statistical Institute, Athens, Greece, July 4-6, 2018.
31. A. J. Kearsley. "Survey of PDE Constrained Optimization." Arizona State University, November 7, 2018.
32. E. Knill. "States in Context I." Condensed Matter Summer School, Boulder, CO, July 2, 2018.
33. E. Knill. "States in Context II." Condensed Matter Summer School, Boulder, CO, July 3, 2018.
34. E. Knill. "Statistics in Context." Condensed Matter Summer School, Boulder, CO, July 16, 2018.
35. L. Kocia. "Stationary Phase Approximation in Discrete Wigner Functions and Transformation Contextuality." Bartlett Group Meeting, University of Sydney, August 2018.
36. P. S. Kuo. "Optical Quantum Technologies and Tools." Frontiers in Optics, Washington, DC, September 19, 2018.
37. Y.-K. Liu. "Unconventional Methods for Characterizing Quantum Systems." Kick-Off Meeting for the MURI Project "Scalable Certification of Quantum Devices and Networks," University of California, Berkeley, June 8, 2018.
38. N. Mouha, M. S. Raunak, D. R. Kuhn and R. N. Kacker. "Finding Bugs in Cryptographic Hash Function Implementations." 28th IEEE Software Technology Conference (STC 2017), Gaithersburg, MD, September 25-28, 2017.
39. P. N. Patrone, A. J. Kearsley, and A. Dienstfrey. "The Role of Data Analysis in Uncertainty Quantification: Case Studies for Materials Modeling." American Institute of Aeronautics and Astronautics

SciTech Forum 2018, Kissimmee, FL, January 10, 2018.

40. P. N. Patrone and A. Dienstfrey. "The Role of Data Analysis in Uncertainty Quantification: Examples from Materials Science." The Minerals, Metals, and Materials Society Annual Meeting, Phoenix, AZ, March 14, 2018.

41. P. N. Patrone, G. Cooksey, and A. J. Kearsley. "The Power of Scaling Methods: Measuring Microfluidic Flow-Rates We Can't Model." George Mason University, Fairfax, VA, April 6, 2018.

42. P. N. Patrone, A. Dienstfrey, and G. B. McFadden. "Multipole Coarse-Graining: Analytical Perspective on Transferability." 2018 Atomistic Simulations for Industrial Needs Workshop, Rockville, MD, August 1, 2018.

43. P. N. Patrone. "Uncertainty Quantification of Atomistic Materials Modeling for Composites." Composites and Advanced Materials Expo, Orlando, FL, December 13, 2017.

44. D. G. Porter. "Tcl Core Team Year in Review." 24th Annual Tcl/Tk Conference, Houston, TX, October 18-20, 2018.

45. R. Pozo. "A Network Measure for the Analysis of Large-Scale Graphs," Mathematics and Statistics Department, American University, Washington, DC, October 30, 2018.

46. M. S. Raunak, D. R. Kuhn, and R. N. Kacker. "Trends in Vulnerabilities." 28th IEEE Software Technology Conference (STC 2017), Gaithersburg, MD, September 25-28, 2017.

47. K. Sayrafian. "Body Area Networks and Pervasive Health Monitoring." R&D 100 Conference, Orlando, Florida, November 16, 2017.

48. K. Sayrafian. "RF Propagation Modeling in Body Area Networking." 40th IEEE International Engineering in Medicine and Biology Conference, Honolulu, Hawaii, July 17-21, 2018.

49. K. Sayrafian. "Kinetic-Based Energy-Harvesting for Body Area Networks." Wireless Body Communications in Medicine Workshop, Bologna, Italy, September 9, 2018.

50. D. E. Simos, D. R. Kuhn, Y. Lei, and R. N. Kacker. "Combinatorial Security Testing Course." Symposium on Hot Topics in the Science of Security, Raleigh, North Carolina, April 10-11, 2018.

51. D. E. Simos, D. R. Kuhn, R. N. Kacker, and S. Mekesis. "Combinatorial Coverage Measurement of Test Vectors Used in Cryptographic Algorithm Validation." 28th IEEE Software Technology Conference, Gaithersburg, MD, September 25-28, 2017.

52. J. E. Terrill. "Using Virtual Reality at the NIST Measurement Science Laboratory." Mixed/Augmented/Virtual Reality Conference (MAVRIC), College Park, MD, October 17-18, 2018.

53. W. E. Wong, R. Gao, L. Hu, D. R. Kuhn, and R. N. Kacker. "Automated Test Generation for High MC/DC Using Guided Concolic Testing." 28th IEEE Software Technology Conference, Gaithersburg, MD, September 25-28, 2017.

54. J. P. Zwolak. "Machine Learning for Experimental Quantum Dot Control." Department of Physics, California State Polytechnic University, Pomona, CA, March 8, 2018.

55. J. P. Zwolak. "Machine Learning for Experimental Quantum Dot Control." Condensed Matter Seminar, University of California San Diego, CA, March 12, 2018.

56. J. P. Zwolak, "Educational Commitment and Attitudes: The Social Network Perspective." American Physical Society Meeting, Columbus, OH, April 2018.

57. J. P. Zwolak, "QFlow Lite: A Machine Learning Approach to Understanding the Charge States in Quantum Dot Experiments." 1st International Workshop on Quantum Software and Quantum Machine Learning, Sydney, Australia, July 19, 2018.

58. J. P. Zwolak, "QFlow Lite: A Machine Learning Approach to Understanding the Charge States in Quantum Dot Experiments." Information Engines at the Frontiers of Nanoscale Thermodynamics Workshop, Telluride, CO, July 25, 2018.

59. J. P. Zwolak, "QFlow Lite: A Machine Learning Approach to Understanding the Charge States in Quantum Dot Experiments." Quantum Lunch Seminar, Los Alamos, NM, August 2, 2018.

60. J. P. Zwolak, S. S. Kalantre, X. Wu, S. Ragole, and J. M. Taylor. "QFlow Lite: A Machine Learning Approach to Understanding the Charge States in Quantum Dot Experiments." Correlations and Coherence at Different Scales Conference, Ustroń, Poland, September 9-14, 2018.

61. J. P. Zwolak. "Applying Machine Learning to Quantum-Dot Experiments." Quantum Many-Body Theory Department, Jagiellonian University, Kraków, Poland, September 18, 2018.

62. J. P. Zwolak. "Auto-Tuning and Rays-Based Learning of Quantum Dot Devices." Centre for Quantum Computation and Communication Technology,

Figure 90. *The NIST Information Technology Laboratory has a yearly presence at the ACM Richard Tapia Celebration of Diversity in Computing. Anthony Kearsley (center) represented ACMD in Orlando in September 2018. He is seen here with (from l. to r.) Richard Tapia (Rice University), Kaitlin Boeckl (ITL Computer Secirity Division), Leticia Velasquez (Rice), and Maurice Fabien (Rice).*

University of New South Wales, Sydney, Australia, November 16, 2018.

Conference Presentations

1. T. Burns. "Closed-Form Projection Method for Regularizing a Function Defined by a Discrete Set of Noisy Data and for Estimating its Derivative and Fractional Derivative." SIAM Conference on Applied Linear Algebra, Hong Kong Baptist University, Hong Kong, China, May 4-8, 2018.
2. T. Burns. "Shear Band Formation in Bulk Metallic Glasses." 55th Annual Technical Meeting of the Society of Engineering Science, University Carlos III, Madrid, Spain, October 10-12, 2018.
3. H. S. Cohl. "Automated Symbolic and Numerical Testing of DLMF Formulae Using Computer Algebra Systems." 11th Conference on Intelligent Computer Mathematics, Research Institute for Symbolic Computation (RISC), Johannes Kepler Universität Linz, Hagenberg, Austria, August 15, 2018.
4. G. Doğan. "An Interface-Based Approach for Segmentation of Multiphase Microstructure Images." 13th World Congress on Computational Mechanics, New York, NY, July 22-27, 2018.
5. M. J. Donahue. "Hybrid Fine/Coarse Stray Field Computation for Micromagnetics." Conference on Magnetism and Magnetic Materials, Pittsburgh, PA, November 6-10, 2017.
6. Douguet, B. I. Schneider, and L. Argenti. "Two-Photon Ionization of Helium Using the Complex Kohn Variational Method." 49th Annual Meeting of the APS Division of Atomic, Molecular and Optical Physics, Ft. Lauderdale, FL, May 2018.
7. R. M. Evans, A. Balijepalli, and A. J. Kearsley. "Transport Phenomena in Field Effect Transistors." American Mathematical Society Fall Eastern Sectional Meeting, Newark, DE, September 29, 2018.
8. R. M. Evans, A. Balijepalli, and A. J. Kearsley. "Nonlinear Partial Differential Equations and Precision Medicine." Joint Mathematics Meetings, San Diego, CA, January 13, 2018.
9. R. M. Evans, A. J. Kearsley, R. G. Brinson, L. W. Arbogast, and F. Delaglio. "Classifying Nuclear Magnetic Resonance Spectra of Biologics." Joint Mathematics Meetings, San Diego, CA, January 12, 2018.
10. R. M. Evans, A. J. Kearsley, and A. Balijepalli. "Precision Medicine and Nonlinear Partial Differential Equations." Eastern Pennsylvania and Delaware Fall Mathematical Association of America Sectional Meeting, Shippensburg, PA, November 18, 2017.
11. J. T. Fong. "MRI Birdcage RF Coil Resonance with Uncertainty and Relative Error Convergence Rates." International COMSOL Users' Conference, Boston, MA, October 5, 2017.
12. J. T. Fong. "Uncertainty in Multi-Scale Creep Rupture Life Modeling and a New Approach to Estimating Frequency of Inservice Inspection of Components at Elevated Temperatures." 2018 ASME Conference on Elevated Temperature Applications of Materials for Fossil, Nuclear and Petrochemical Industries, Seattle, WA, April 5, 2018.
13. J. T. Fong. "Finite Element Method Solution Uncertainty, Asymptotic Solution, and a New Approach to Accuracy Assessment." 7th Annual ASME Verification and Validation Symposium, Minneapolis, MN, May 17, 2018.
14. J. T. Fong. "A Nonlinear Least Squares Logistic Fit Approach to Quantifying Uncertainty in Fatigue Stress-Life Models and an Application to Plain Concrete." ASME Pressure Vessel and Piping Division Conference, Prague, Czech Republic, July 16, 2018.

15. J. T. Fong. "Uncertainty Quantification of Finite Element Analysis of Uni-Axial Strength Test of Holed Composite Laminates." ASME Pressure Vessel and Piping Division Conference, Prague, Czech Republic, July 16, 2018.
16. J. T. Fong. "Three Approaches to Quantification of NDE Uncertainty and a Detailed Exposition of the Expert Panel Approach Using the Sheffield Elicitation Framework." ASME Pressure Vessel and Piping Division Conference, Prague, Czech Republic, July 18, 2018.
17. J. T. Fong. "Finite Element Method Solution Uncertainty, Asymptotic Solution, and a New Approach to Accuracy Assessment." World Congress of Computational Mechanics, New York, NY, July 24, 2018.
18. Z. Gimbutas and J. Bremer. "Discretization of Hypersingular Kernels on Surfaces." SIAM Annual Meeting, Portland, OR, July 9, 2018.
19. W. Griffin and P. Armstrong. "VR Cell Microscopy Visualization." Immersive Visualization for Science, Research, and Art Birds of a Feather, ACM SIGGRAPH Conference, August 13, 2018.
20. W. Griffin and P. Armstrong. "VR Cell Microscopy Visualization." Immersive Visualization for Science, Research, and Art Birds of a Feather, ACM SIGGRAPH Conference, August 13, 2018.
21. G. A. Holmes, J. A. Woodcock, W. F. Mitchell, R. J. Sheridan, and J. W. Gilman. "A Critical Look at the Dynamics of Fiber Failure in Fiber Reinforced Composites," 11th International Conference on the Mechanics of Time Dependent Materials, Milan, Italy, September 6, 2018.
22. S. Z. Jones, D. P. Bentz, N. S. Martys, W. L. George, and A. Thomas. "Rheological Control of 3D Printed Cement Paste." Digital Concrete 2018 – The First International Conference on Concrete and Digital Fabrication, Zurich, Switzerland, September 2018.
23. J. A. Kauffman and J. S. Pitt. "An Overset Mesh Framework Applied to the Hybridizable Discontinuous Galerkin Finite Element Method for Dynamic Meshes." 13th World Congress on Computational Mechanics, New York, NY, July 22–27, 2018.
24. J. A. Kauffman, W. L. George, and J. S. Pitt. "An Overset Mesh Framework for the Hybridizable Discontinuous Galerkin Method." 14th Symposium on Overset and Composite Grids and Solution Technology, College Park, MD, October 2–4, 2018.
25. L. Kocia. "Measurement Contextuality and Planck's Constant." APS March Meeting, Los Angeles, CA, March 2018.
26. P. S. Kuo. "Temperature Dependent Noise in Quantum Frequency Conversion." SPIE Photonics Europe, Strasbourg, France, April 22-26, 2018. DOI: 10.1117/12.2305978
27. P. S. Kuo. "Using Temperature to Reduce Noise in Quantum Frequency Conversion." Lasers and Electro-Optics Conference, San Jose, CA, May 13-18, 2018.
28. S. A. Langer. "Meshing Images with OOF3D." 13th World Conference on Computational Mechanics, New York, NY, July 22-27, 2018.
29. Y.-K. Liu. "Quantum Cryptanalysis of Block Ciphers: A Case Study." Dagstuhl Seminar on "Quantum Cryptanalysis," Wadern, Germany, October 2, 2017.
30. L. Ma, O. Slattery, and X. Tang. "Ultra-High Spectral Resolution Spectrometer for Single Photon Source Characterization." Quantum Information Science, Sensing and Computation X, SPIE Commercial and Scientific Sensing and Imaging, Orlando, FL, April 2018.
31. V. Marbukh. "Towards Resilient yet Economically Viable Networked Infrastructures: Quantitative Metrics and Systemic Risk-Aware Design." 1st International Conference on Infrastructure Resilience, Zurich, Switzerland, February 14-16, 2018.
32. V. Marbukh. "Towards Efficient Offloading in Fog/Edge Computing by Approximating Effect of Externalities." 2nd Workshop on Integrating Edge Computing, Caching, and Offloading in Next Generation Network, IEEE International Conference on Computer Communications 2018 (Infocom 2018), Honolulu, HI, April 15-19, 2018.
33. V. Marbukh. "Dynamic Job Replication for Balancing Fault Tolerance, Latency, and Economic Efficiency: Work in Progress." IEEE World Congress on Services 2018, San Francisco, CA, July 2-7, 2018.
34. V. Marbukh. "On Mitigation Inefficiency of Selfish Investment in Network Recovery from High Loss SIS Infection." International Workshop on Cyber-Physical Systems and Applications (IWCPSA18), 17th IEEE International Conference on Trust, Security and Privacy in Computing and Communications 2018 (IEEE TrustCom-18), New Jersey, July 31 – August 3, 2018.
35. V. Marbukh. "Network Formation by Contagion Averse Agents: Modeling Bounded Rationality with Logit Learning." 4th International Workshop on Dynamics on and Of Networks (DYNO 2018), IEEE/ACM International Conference on Advances in Social Networks Analysis and Mining

(ASONAM 2018), Barcelona, Spain, August 28-31, 2018.

36. N. S. Martys, W. L. George, S. G. Satterfield, and C. F. Ferraris. "Modeling and Visualizing the Flow of Standard Reference Materials for the Calibration of Rheometers Used in the Cement and Concrete Industries." 89th Annual Meeting of The Society of Rheology, Denver, CO, October 2017.
37. N. S. Martys, W. L. George, S. G. Satterfield, and S. Z. Jones. "Computational Modeling of Suspension Flows in Pipes: Application to Cement Based Materials." 90th Annual Meeting of The Society of Rheology, Houston, TX, October 2018.
38. D. G. Porter. "Introduction to the HAMT; Opportunity for Tcl." 24th Annual Tcl/Tk Conference, Houston, TX, October 19, 2017.
39. S. Ressler and K. Chen. "Digital Library of Math Functions Meets Virtual Reality." Birds of a Feather, SIGGRAPH Conference, Vancouver, Canada, August 13, 2018.
40. S. Ressler and K. Chen. "NIST Digital Library of Math Functions Meets Virtual Reality." Mixed/Augmented/Virtual Reality Innovation Conference (MAVRIC), College Park, MD, October 18, 2018.
41. B. Saunders. "An Adaptive Curvature and Gradient Based Grid Generation Method." 15th Meeting on Applied Scientific Computing and Tools (MASCOT2018), Rome, Italy, October 5, 2018.
42. B. Saunders. "Adaptive Curvature-Based Grid Generation for 3D Web Graphics." Curves and Surfaces 2018, Arcachon, France, July 3, 2018.
43. B. Saunders. "NIST's Digital Library of Mathematical Functions and the Digital Age." MD-DC-VA Spring Section Meeting, Mathematics Association of America (MAA), Virginia Military Institute/Washington and Lee University, Lexington, VA, April 14, 2018.
44. K. Sayrafian. "Application of Link Adaptation in Body Area Networks." 28th Annual IEEE International Symposium on Personal, Indoor and Mobile Radio Communications (IEEE PIMRC 2017), October 8-13, 2017.
45. K. Sayrafian. "A Study of Capsule Endoscopy Orientation Estimation Using Received Signal Strength." 29th Annual IEEE International Symposium on Personal, Indoor and Mobile Radio Communications (IEEE PIMRC 2018), September 9-12, 2018.
46. K. Sayrafian. "IoT-Health Overview." Workshop on IoT Enabling Technologies in Healthcare, Barcelona, Spain, April 15, 2018.
47. A. Youssef. "Deep Learning for Math Knowledge Processing." 11th Conference on Intelligent Computer Mathematics (CICM 2018), Hagenberg, Austria, August 2018.
48. J. P. Zwolak, S. S. Kalantre, X. Wu, S. Ragole, and J. M. Taylor. "Applying Machine Learning to Quantum-Dot Experiments: Learning from the Data." American Physical Society March Meeting, Los Angeles, CA, March 5-9, 2018.
49. J. P. Zwolak, S. S. Kalantre, X. Wu, and J. M. Taylor. "Rays-Based Learning and Auto-Tuning of Devices in Quantum Dot Experiments." Silicon Quantum Electronics Workshop, Sydney, Australia, November 15, 2018.

Poster Presentations

1. P. Armstrong and W. Griffin. "Virtual Reality for Cell Microscopy." Mixed/Augmented/Virtual Reality Conference (MAVRIC), College Park, MD, October 17-18, 2018.
2. A. Avagyan. "Towards Full Characterization of Photonic Gates with Weak Local Oscillators." Southwest Quantum Information Technology Workshop, Santa Fe, NM, February 22, 2018.
3. J. Bernal, G. Doğan, and C. Hagwood. "Fast Dynamic Programming for Elastic Registration of Curves, Workshop on Applications-Driven Geometric Functional Data Analysis." Florida State University, October 8-11, 2017.
4. J. Biggins and S. Ressler. "Virtual Tours: Experiments in Monoscopic and Stereoscopic Virtual Reality." The Mixed/Augmented/Virtual Reality Innovation Conference (MAVRIC), College Park, MD, October 18, 2018.
5. G. Cooksey, P. N. Patrone, J. R. Hands, S. E. Meek, and A. J. Kearsley. "Dynamic Measurement of Nanoliter per Minute Flow by Scaled Dosage of Fluorescent Solutions." *22nd International Conference on Miniaturized Systems for Chemistry and Life Sciences (MicroTas 2018)*, Kaohsiung, Taiwan, November 11-15, 2018.
6. G. Doğan. "Scikit-Shape: Python Toolbox for Shape Analysis and Segmentation." SIAM Conference on Imaging Science, Bologna, Italy, June 5-8, 2018.
7. N. Douguet, H. Gharibnejad, B. I. Schneider, and L. Argenti. "Time-Dependent Photoionization of Atomic and Molecular Systems Using a Hybrid

Gaussian and Finite-Elements Discrete Variable Representation Basis Set." 49th Annual Meeting of the APS Division of Atomic, Molecular and Optical Physics (DAMOP), Ft. Lauderdale, FL, May 30, 2018.

8. H. Gharibnejad, D. R. Schultz, and T. E. Cravens. "Secondary Electron Production from Ion Precipitation at Jupiter: Simultaneous and Non-Simultaneous Target and Projectile Processes in Collisions of $O^{q^+} + H_2 (q = 0 - 8)$" 49th Annual Meeting of the APS Division of Atomic, Molecular and Optical Physics (DAMOP), Ft. Lauderdale, FL, May 30, 2018.
9. L. Kocia. "Measurement Contextuality and Planck's Constant." 21st Annual Conference on Quantum Information Processing (QIP), Delft, Netherlands, January 16, 2018.
10. L. Kocia. "Measurement Contextuality and Planck's Constant." 21st Annual Southwest Quantum Information and Technology Workshop (SQUINT), Albuquerque, NM, February 2018.
11. L. Kocia. "Measurement Contextuality and Planck's Constant." 13th Conference on the Theory of Quantum Computation (TQC), Sydney, Australia, July 16, 2018.
12. K. Krhac, K. Sayrafian, and W. Griffin. "An Immersive Platform to Study Wireless Communication and Localization for Next Generation Capsule Endoscopy" 2018 mHealth Technology Showcase, National Institutes of Health, Bethesda, MD, June 4, 2018.
13. D. R. Kuhn, M.S. Raunak, and R. Kacker. "What Proportion of Vulnerabilities Can be Attributed to Ordinary Coding Errors." Symposium on Hot Topics in the Science of Security (HoTSoS 2018), Raleigh, NC, April 10-11, 2018.
14. P. S. Kuo and B. G. Alberding. "Towards Extending Super-Conducting Nanowire Single-Photon Detectors into the Infrared Wavelength Range." Frontiers in Optics Conference, Washington, DC, September 16-20, 2018.
15. L. Ma, O. Slattery, and X. Tang. "Noise Spectral Characterization of Narrow Linewidth Single Photon Source." Quantum Communication, Measurement and Computing (QCMC), Baton Rouge, LA, March 2018.
16. G. McFadden. "Computational Study of Magnetohydrodynamic Equilibria with Emphasis on Fragility of Flux Surfaces." 60th Annual Meeting of the APS Division of Plasma Physics, Portland, OR, November 7, 2018.
17. V. Marbukh. "Towards Managing Age of Network State Information in Challenged Networks." The IEEE International Conference on Computer Communications 2018 (Infocom 2018), Honolulu, HI, April 15-19, 2018.
18. V. Marbukh. "Economics of Networked Infrastructures at the Edge of Undesirable Contagion: A Case of SIS Infection." 2018 IEEE International Conference on Computer Communications (Infocom 2018), Honolulu, HI, April 15-19, 2018.
19. V. Marbukh. "Towards Resilient Yet Economically Viable Networked Infrastructures." The International School and Conference on Network Science 2018 (NetSci 2018), Paris, France, June 15-18, 2018.
20. K. Mayer. "Bounding the Quantum Process Fidelity with a Minimal Set of Input States." 21st Annual Southwest Quantum Information Technology Workshop, Albuquerque, NM, February 22, 2018.
21. A.S. Moorthy, A. J. Kearsley, W. E. Wallace, and S. E. Stein. "Demystifying Match Factors." XXII International Mass Spectrometry Conference, Florence, Italy, August 26-31, 2018.
22. A. S. Moorthy, A. J. Kearsley, W. E. Wallace, and S. E. Stein. "Drug Class Identification Using Mass Spectral Library Searching." 66th American Society of Mass Spectrometry Conference on Mass Spectrometry and Allied Topics, San Diego CA, June 3-7, 2018.
23. A. S. Moorthy, W. E. Wallace, G. Mallard, A. J. Kearsley, and S. E. Stein. "Predicting Molecular Weight with the Hybrid Search." 66th American Society of Mass Spectrometry Conference on Mass Spectrometry and Allied Topics, San Diego CA, June 3-7, 2018.
24. H. Vasconcelos. "Quadrature Histograms in Maximum Likelihood Quantum State Tomography." 21st Annual Southwest Quantum Information Technology Workshop, Albuquerque, NM, February 22, 2018.
25. X. Wu, J. P. Zwolak, S. S. Kalantre, A. R. Mills, J. R. Petta, and J. M. Taylor. "Experimental Implementation of Machine Learning Assisted Auto Tuning of Quantum Dot Devices." Silicon Quantum Electronics Workshop, Sydney, Australia, November 15, 2018.

Web Services

Note: ACMD provides a variety of information and services on its website. Below is a list of major services provided that are currently under active maintenance.

1. *Digital Library of Mathematical Functions:* a repository of information on the special functions of applied mathematics.
2. *Digital Repository of Mathematical Formulae*: a repository of information on special function and orthogonal polynomial formulae.
3. *DLMF Standard Reference Tables on Demand*: an online software testing service providing tables of values for special functions, with guaranteed accuracy to high precision.
4. DLMF in VR: Experiments using WebVR to display several or sometimes all DLMF surfaces simultaneously in an environment in which the user can grab, scale and throw the surfaces.
5. *muMAG*: a collection of micromagnetic reference problems and submitted solutions.
6. *NIST Adaptive Mesh Refinement Benchmark Problems*: a collection of benchmark partial differential equations for testing and comparing adaptive mesh refinement algorithms.
7. *NIST VR Scanning Tunneling Microscopy Head*: A WebVR capable simulation of the head of a scanning tunneling microscope which you may explore.
8. *Quantum Algorithm Zoo*: A repository of quantum algorithms.
9. *Quantum Dot Data for Machine Learning*: A Data Set of Simulated Quantum Dot gate configurations for machine learning.
10. *Virtual Tours:* A collection of virtual tours suitable for using WebVR equipment for self-guided tours of NIST Library, NIST Shops and NIST Net Zero House.

Software Released

Note: ACMD distributes a large number of software packages that have been developed in the course of its work. Listed below are particular packages which have seen new releases during the reporting period.

1. *ACTS:* Advanced Combinatorial Testing System. Version 3.1. R. Kacker.
2. *ChebTools*: Computing with Chebyshev expansions. Version 1.0. B. Alpert.
3. *Itcl*: C++ inspired object-oriented commands for Tcl. Version 4.1.1 (12/22/2017) and 4.1.2 (11/16/18). D. G. Porter.
4. *HEV*: High End Visualization. Versions 2.7.0 (3/27/2018) and 2.7.1 (3/30/2018). S. G. Satterfield, T. Griffin, W. Griffin, and J. E. Terrill.
5. *LaTeXML*: A LaTeX to XML converter. Continuous access from svn/git repository. B. R. Miller.
6. *OOF2*: Image-based analysis of materials with complex microstructures. Versions 2.1.16 (10/19/18). S. A. Langer, A. C. E. Reid, and G. Doğan.
7. *OOF3D*: Three-dimensional analysis of materials with complex microstructures. Versions 3.1.2 (3/9/18), 3.2.0 (8/30/18), and 3.2.1 (10/12/18), S. A. Langer, A. C. E. Reid, and G. Doğan.
8. *OOMMF*: The Object Oriented MicroMagnetic Framework. Versions 1.2b2 (9/30/18) and 2.0a1 (9/30/18). M. J. Donahue and D. G. Porter.
9. *PHAML*: Solution of elliptic boundary value and eigenvalue problems, using finite elements, *hp*-adaptive refinement, and multigrid, on distributed memory and shared memory parallel computers. Versions 1.19.0 (06/08/2018), 1.20.0 (8/28/2019). W. Mitchell.
10. *QFlow-lite*: A repository with Python code for manipulating quantum dot data for machine learning. J. Zwolak.
11. *State-meas-tomo*: Joint Quantum State and Measurement Tomography. Version 1.0 (3/24/18). A. C. Keith, C. H. Baldwin, S. Glancy, and E. Knill.
12. *Tcl/Tk*: Extensible scripting language and GUI toolkit. Versions 8.6.8 (12/22/2017) and 8.6.9 (11/16/2018). D. G. Porter.
13. *TDBC*: Database connection commands for Tcl. Version 1.0.6 (12/22/2017) and 1.1.0 (11/16/18). D. G. Porter.
14. *Thread*: Thread management commands for Tcl. Version 2.8.2 (12/22/2017) and 2.8.4 (11/16/18), D. G. Porter.
15. *Scimark*: Java/C benchmark for scientific and numerical computing. Version 4.0 (12/10/2018). R. Pozo.
16. *Sqlite3*: Bindings to the SQLite database engine for Tcl. Versions 3.21.0 (10/27/17), 3.22.0 (1/29/18), 3.23.0 (4/3/18), 3.23.1 (5/9/18), 3.25.3 (11/16/18). D. Porter.

Conferences, Minisymposia, Lecture Series, Courses

ACMD Seminar Series

Wesley Griffin served as Chair of the ACMD Seminar Series. There were 25 talks presented during this period; all talks are listed chronologically.

1. Tony O'Hagan (University of Sheffield, UK). Uncertainty Quantification and Inversion of Large Models. October 10, 2017.
2. George Sherwood (Testcover.co). Embedded Functions in Combinatorial Testing: Progress in Automating Test Design. October 11, 2017.
3. Aron Laszka (University of Houston). Designing Resilient Cyber-Physical Systems. October 25, 2017.
4. Matthew Brown (Virginia Tech). A Statistical Approach for Ill-Posed Inverse Problems. November 3, 2017.
5. Peter Guba (Comenius University, Slovakia). Convective Instabilities During Solidification of Binary and Ternary Alloys. November 15, 2017.
6. Andrew Ray (Radford University). Examining the Latest Resurgence of Interest in Virtual Reality. December 1, 2017.
7. Alathea Jensen (George Mason University). Stochastic Enumeration with Importance Sampling. December 11, 2017.
8. Stephen P. Jordan (ACMD). Quantum Computation: From Philosophy to Technology in One Generation. January 4, 2018.
9. Sebastian Barillaro (National Institute for Industrial Technology, Argentina). Low Power and Wide Area Networks Technologies for Internet of Things. February 16, 2018.
10. Les Hatton (Kingston University, UK). Conservation of Information in Proteins, Software, Music, Texts, the Universe and Chocolate Boxes. March 6, 2018.
11. Amanda Howard (Brown University). Numerical Methods for Studying Particle Dispersion in Non-Homogeneous Suspension Flows. March 9, 2018.
12. Dionisios Margetis (University of Maryland, College Park). Why Are Crystal Facets Mathematically Interesting? A Continuum-Scale Story with a Microscale Touch. April 3, 2018.
13. Udita Katugampola (Florida Polytechnic University). The Intimate Connection Between the Fractional Integrals and the Time-Fractional Porous Medium Equation (fPME). April 19, 2018.
14. Derrick C. Scott (Delaware State University). Utilizing Next Generation Sequencing to Generate Bacterial Genomic Sequences for Evolutionary Analysis. May 3, 2018.
15. Samuel Cogar (University of Delaware). Eigenvalue Problems in Scattering Theory and their Application to Nondestructive Testing of Materials. May 29, 2018.
16. Salvatore Torquato (Princeton University). Disordered Hyperuniform Materials: New States of Amorphous Matter. June 7, 2018.
17. Michael Mascagni (Florida State University and ACMD). The "White Rat" of Numerical Reproducibility. June 19, 2018.
18. Arthur Sherman (Laboratory of Biological Modeling, National Institutes of Health). Modeling the Pathogenesis and Treatment of Diabetes. July 17, 2018.
19. Marilyn Yazmin Vazquez Landrove (George Mason University). A New Density-Based Clustering Algorithm and its Application to Microstructure Image Segmentation. July 24, 2018.
20. Amy Li (Wellesley College). Analysis of Microfluidic Flow Rate Measurements. August 10, 2018.
21. David Laidlaw (Brown University). Virtual Reality Toolsmithing for Science. September 7, 2018.

Figure 91. *ACMD hosts many visitors throughout the year. Here Professors Derrick Scott and LaTia Scott from Delaware State University's Biological Sciences Department discuss research in visualization with Judith Terrill, Leader of ACMD's High Performance Computing and Visualization Group.*

22. Adarsh Kumbhari (University of Sydney, Australia). The Importance of Mitochondrial Fission and Fusion in a Beating Heart Cell. October 18, 2018.
23. Sebastian Barillaro (National Institute for Industrial Technology, Argentina). IoT-LPWAN Testing Facility for Security and Trust in Networks of Sensors. October 23, 2018.
24. Alexey Gorshkov (NIST Physical Measurement Laboratory). Optimal Quantum Sensing. October 30, 2018.
25. Sandip Kundu (Department of Electrical & Computer Engineering, University of Massachusetts Amherst). Securing Physically Unclonable Functions. December 13, 2018.

Shortcourses

1. J. T. Fong, Competency Training for Participating in Monitoring and NDE Expert Panel (MANDEEP) using SHELF (Sheffield Elicitation Framework). ASME Boiler and Pressure Vessel Code Week, Las Vegas, NV, February 4-5, 2018.

Conference Organization

Leadership

1. B. I. Schneider. Lead Organizer, Institute for Theoretical, Atomic, Molecular and Optical Physics (ITAMP) Workshop on Developing Flexible and Robust Software in Computational Atomic and Molecular Physics. Cambridge, MA, May 14-18, 2018.
2. W. Griffin. Co-Chair, Workshop on Analysis of Large-Scale Disparate Data, 2018 IEEE International Conference on Big Data. Seattle, WA, December 10-13, 2018.
3. K. Sayrafian. Track Chair, IEEE International Symposium on Personal, Indoor and Mobile Radio Communications (IEEE PIMRC 2018). Bologna, Italy, September 9-12, 2018.
4. K. Sayrafian. Track Chair, IEEE European Conference on Networks and Communications (IEEE EuCNC 2019). Valencia, Spain, Sept. 18-21, 2019.
5. K. Sayrafian. Lead Organizer and Co-Chair, IoT-Health 2018: Workshop on IoT Enabling Technologies in Healthcare. Barcelona, Spain, April 15, 2018.
6. K. Sayrafian. Lead Organizer and Co-Chair, IoT-Health 2019: Workshop on IoT Enabling Technologies in Healthcare. Istanbul, Turkey, September 8, 2019.
7. K. Sayrafian. Session Chair, Computational Human Models, 40th International Engineering in Medicine and Biology Conference (IEEE EMBC 2018). Honolulu, Hawaii July 17-21, 2018.
8. K. Sayrafian. Lead Demo and Technical Exhibition Co-Chair, 28th Annual IEEE International Symposium on Personal, Indoor and Mobile Radio Communications (IEEE PIMRC 2017). Montreal, PQ, Canada, October 8-13, 2017.
9. A. Youssef. Chair, Systems and Projects, 11th Conference on Intelligent Computer Mathematics (CICM). Hagenberg, Austria, August 13-17, 2018.

Committee Membership

1. S. Glancy. Member, Program Committee, Southwest Quantum Information Technology Workshop. Santa Fe, NM, February 22, 2018.
2. S. Glancy. Member, Program Committee, Towards Ultimate Quantum Theory. Linnaeus University, Växjö, Sweden, June 11-14, 2018.
3. W. Griffin. Member, Program Committee, 2018 Workshop on Analysis of Large-scale Disparate Data. Seattle, WA, December 10-13, 2018.
4. W. Griffin. Member, Program Committee, 2018 In Situ Infrastructures for Enabling Extreme-scale Analysis and Visualization (ISAV 2018). Dallas, TX, November 12, 2018.
5. W. Griffin. Member, Papers Committee, 2018 Software Engineering Architectures for Real-time Interactive Systems (SEARIS 2018). Reutlingen, Germany, March 19, 2018.
6. W. Griffin. Member, Program Committee, 2018 ACM Symposium on Interactive 3D Graphics and Games (I3D 2018). Montreal, Canada, May 15-18, 2018.
7. W. Griffin. Member, Courses Committee, 2017 ACM SIGGRAPH Conference and Exhibition on Computer Graphics and Interactive Techniques in Asia (SIGGRAPH ASIA). Tokyo, Japan, December 4-7, 2018.
8. W. Griffin. Member, Program Committee, 2017 In Situ Infrastructures for Enabling Extreme-scale Analysis and Visualization (ISAV 2017). Denver, CO, November 12, 2017.
9. R. J. La. Member, Program Committee, IEEE International Conference on Computer Communications (INFOCOM 2018). Honolulu, HI, April 15-19, 2018.

10. R. J. La. Member, Program Committee, Twentieth International Symposium on Mobile Ad Hoc Networking and Computing (ACM MobiHoc). Catania, Italy, July 2-5, 2019.
11. Y.-K. Liu. Member, Program Committee, Quantum Information Processing (QIP 2019). University of Colorado, Boulder, January 14-18, 2019.
12. Y.-K. Liu. Member, Steering Committee, International Conference on Quantum Cryptography (QCrypt 2018). Shanghai, China, August 27-31, 2018.
13. Y.-K. Liu. Member, Program Committee, International Conference on Post-Quantum Cryptography (PQCrypto 2018). Fort Lauderdale, Florida, April 9-11, 2018.
14. W. Mitchell. Member, Scientific Committee, 16th International Conference of Numerical Analysis and Applied Mathematics (ICNAAM). Rhodes, Greece, September 13-18, 2018.
15. K. Sayrafian. Member, International Advisory Board, International Symposium on Medical Information and Communication Technology (ISMICT).
16. K. Sayrafian. Member, Program Committee, Wireless Body Communications in Medicine (WIBCOMM) Workshop. Bologna, Italy, September 9, 2018.
17. K. Sayrafian. Member, Jury, Ph.D. Student Thesis Pitch Competition (3MT), IEEE WCNC 2018, Barcelona, Spain, April 2018.
18. K. Sayrafian. Member, Jury, Ph.D. Student Thesis Pitch Competition (3MT), IEEE PIMRC 2018, Bologna, Italy, Sept. 9-11, 2018.

Session Organization

1. G. Doğan. Co-Organizer, Minisymposium 33, Advances in Reconstruction Algorithms for Computed Tomography. SIAM Conference on Imaging Science, Bologna, Italy, June 5-8, 2018.
2. G. Doğan. Co-Organizer, Minisymposium 65, Variational Methods and Optimization for Image and Data Analysis. SIAM Annual Meeting, Pittsburgh, PA, July 10-14, 2017.
3. W. Griffin. Co-Chair, Birds of a Feather Session: Immersive Visualization for Science, Research, and Art. SIGGRAPH, Vancouver, BC, Canada, August 13, 2018.
4. S. Langer. Co-Organizer, Minisymposium 1902, Image-Based Analysis of Microstructures. 13th World Conference on Computational Mechanics, New York, NY, July 22-27, 2018.
5. X. Tang. Member, Program Committee, Quantum Communications and Quantum Imaging XVII. SPIE Optics and Photonics 2018, San Diego, CA, August 19-23, 2018.

Other Professional Activities

Internal

1. B. K. Alpert. Organizer and Lead, Deep Learning Theory Reading Group.
2. R. Boisvert. Member, ITL Diversity Committee.
3. B. Cloteaux. Member, Washington Editorial Review Board.
4. S. Glancy. Member, Quantum SI Committee for NIST's Strategic Vision.
5. S. Glancy. Member, Boulder Summer Undergraduate Research Fellowship Committee.
6. S. Glancy. Member, ITL Diversity Committee.
7. W. Griffin. Chair, ACMD Seminar Series.
8. A. Kearsley. Chair, ITL Awards Committee.
9. P. Kuo. Member, ITL Space Task Force.
10. P. Kuo. Member, NIST Colloquium Organizing Board.
11. S. Ressler. Division Safety Representative, ITL Safety Committee.
12. B. Schneider. Chair, NIST National Strategic Computing Initiative (NSCI) Seminar Series.
13. O. Slattery. Laser Safety Representative, ITL Safety Committee.

External

Editorial

1. I. Beichl. Member, Editorial Board, *IEEE Computing in Science & Engineering*.
2. R. F. Boisvert. Associate Editor, *ACM Transactions on Mathematical Software*.
3. H. S. Cohl. Member, Editorial Board, *The Ramanujan Journal*.
4. H. S. Cohl. Co-Editor, *OP-SF NET*, The Electronic News Bulletin of the SIAM Activity Group on Orthogonal Polynomials and Special Functions.
5. H. S. Cohl. Co-Editor, *OPSF-S6-6th Orthogonal Polynomials and Special Functions Summer School Lecture Notes.*

6. M. J. Donahue. Editor, *Electrostatic and Magnetic Phenomena: Particles, Macromolecules, Nanomagnetics*, World Scientific Publishing.
7. Z. Gimbutas. Editor, *Advances in Computational Mathematics*.
8. R. J. La. Associate Editor, *IEEE Transactions on Information Theory.*
9. R. J. La. Associate Editor, *IEEE/ACM Transactions on Networking.*
10. W. Mitchell. Associate Editor, *Journal of Numerical Analysis, Industrial and Applied Mathematics.*
11. F. A. Potra. Regional Editor for the Americas, *Optimization Methods and Software*.
12. F. A. Potra. Associate Editor, *Journal of Optimization Theory and Applications.*
13. F. A. Potra. Associate Editor, *Numerical Functional Analysis and Optimization.*
14. F. A. Potra. Associate Editor, *Optimization and Engineering.*
15. B. Saunders. Webmaster, SIAM Activity Group on Orthogonal Polynomials and Special Functions.
16. B. Saunders. Moderator, *OP-SF Talk*, SIAM Activity Group on Orthogonal Polynomials and Special Functions.
17. K. Sayrafian. Associate Editor, *International Journal on Wireless Information Networks (IJWIN).*
18. K. Sayrafian. Member, Editorial Board, *IEEE Wireless Communication Magazine*.
19. B. Schneider. Associate Editor in Chief, *Computing in Science & Engineering.*
20. B. Schneider. Specialist Editor, *Computer Physics Communications.*

Boards and Committees

1. R. F. Boisvert. Member, ACM Digital Library Committee.
2. R. F. Boisvert. Member, Working Group 2.5 (Numerical Software), International Federation for Information Processing (IFIP).
3. R. F. Boisvert. Member, External Advisory Council, Department of Computer Science, George Washington University.
4. B. Cloteaux. Member, Advisory Board, Department of Computer Science, New Mexico State University.
5. A. Dienstfrey. Member, Working Group 2.5 (Numerical Software), International Federation for Information Processing (IFIP).
6. J. T. Fong. Member, American Society of Mechanical Engineers (ASME) Boiler and Pressure Vessel Code Committee.
7. S. Glancy. Member, IEEE Working Group on Metrics and Benchmarks for Quantum Computing Devices and Systems.
8. W. Griffin. Co-Chair, Software Engineering and Architectures for Realtime Interactive Systems (SEARIS) Working Group.
9. F. Hunt. Member, SIAM Nominations Committee.
10. F. Hunt. Member, Association for Women in Mathematics (AWM) Strategic Taskforce on Diversity.
11. P. Patrone. Member, Applied Math and Scientific Computing Graduate Committee, University of Maryland, College Park.
12. D. G. Porter. Member, Tcl Core Team.
13. S. Ressler. Member, W3C Immersive Web Working Group.
14. B. Saunders. Secretary, SIAM Activity Group on Geometric Design.
15. B. Saunders. Member, Selection Committee, Gabor Szego Prize, SIAM Activity Group on Orthogonal Polynomials and Special Functions.
16. K. Sayrafian. Co-Chair, IoT-Health Group at COST CA15104, Inclusive Radio Communication Networks for 5G and Beyond (IRACON).
17. B. I. Schneider. Co-Chair, Networking and Information Technology R&D (NITRD) High End Computing Interagency Working Group.
18. B. Schneider. NIST Representative, Joint Program Office, National Strategic Computing Initiative.

Adjunct Academic Appointments

1. S. Glancy. Lecturer, Department of Physics, Colorado University, Boulder, CO.
2. E. Knill. Lecturer, Department of Physics, Colorado University, Boulder, CO.
3. Y. K. Liu. Adjunct Associate Professor, Department of Computer Science, University of Maryland, College Park, MD.
4. K. Sayrafian. Affiliate Associate Professor, Concordia University, Montreal, Canada.
5. X. Tang. Adjunct Professor, University of Limerick, Ireland.

Thesis Direction

1. I. Beichl. Ph.D. Co-Advisor, George Mason University: A. Jensen.
2. G. Doğan. Member, Ph.D. Thesis Committee, George Mason University: M. Vazquez.
3. Z. Gimbutas. Member, Ph.D. Thesis Committee, University of Colorado Boulder: X. Yang.
4. A. Kearsley. Member, Ph.D. Thesis Committee, Drexel University: A. Chen.
5. F. A. Potra. Ph.D. Advisor, University of Maryland Baltimore County: C. Lai.
6. K. Sayrafian. Ph.D. Co-Advisor, University of Zagreb, Zagreb, Croatia: K. Krhac.

Community Outreach

1. B. Alpert. Member, Computer Science Advisory Committee, Boulder Valley School District, Boulder, CO.
2. S. Colbert-Kelly. Lecturer, Department of Mathematics and Statistics, University of Maryland, Baltimore County, MD.
3. A. Kearsley. ITL Representative, ACM Richard Tapia Celebration of Diversity in Computing, Orlando, FL, September 19-22, 2018.
4. S. Ressler. "3D on the Web," Computer Club, Glenelg High School, Glenelg, MD, October 23, 2018.
5. S. Ressler. "Demonstrations of Virtual Reality," Take your Sons and Daughters to Work Day, NIST, Gaithersburg, MD, April 26, 2018.
6. B. Saunders. Judge (Mathematics), Siemens Competition in Math, Science and Technology, Discovery Communications, Silver Spring, MD, October 6-8, 2017.
7. B. Saunders. Organizer, Virginia Standards of Learning Tutoring Program, Northern Virginia Chapter (NoVAC), Delta Sigma Theta Sorority, Inc. and the Dunbar Alexandria-Olympic Branch of the Boys and Girls Clubs of Greater Washington, January – May 2018.
8. B. Saunders. SIAM Visiting Lecturer, 2018. URL: https://www.siam.org/Students-Education/Programs-Initiatives/SIAM-Visiting-Lecturer-Program
9. B. Saunders. ITL Representative, Grace Hopper Celebration of Women in Computing, Houston, TX, September 26 – 28, 2018.

Awards and Recognition

1. M. Donahue and D. Porter. Outstanding Technology Transfer Award, NIST Information Technology Laboratory, August 2018.
2. M. Donahue and D. Porter. Jacob Rainbow Applied Research Award, NIST, December 2018.
3. F. Hunt. Fellow, American Mathematical Society, November 2018.
4. F. Hunt. Fellow, Outstanding Contribution to Diversity Award, NIST Information Technology Laboratory, August 2018.
5. F. Hunt. Honoree, Celebrating Women in Mathematics, American Mathematics Society. URL: https://www.ams.org/images/celebrating-women-for-web.jpg
6. G. McFadden. Outstanding Reviewer Award, Acta Materialia, April 2018.
7. P. Patrone and A. Dienstfrey. Outstanding Journal Publication Award, NIST Informational Technology Laboratory, August 2018.
8. S. Ressler. 2nd Place, World Standards Day Essay Contest, Society for Standards Professionals, October 2018.
9. B. Saunders. Black History Month Honoree, Mathematically Gifted & Black, 2018. URL: http://mathematicallygiftedandblack.com/honorees/bonita-v-saunders/
10. K. Sayrafian, S. Perez-Simbor, K. Krhac, C. Garcia Pardo, D. Simunic, and N. Cardona. Best Paper Award, IEEE Conference on Standards for Communications and Networking, October 2018.
11. F. Sullivan. NIST Portrait Gallery of Distinguished Scientists, Engineers and Administrators, October 27, 2017.
12. J. P. Zwolak. Scholarship Award, Information Engines at the Frontiers of Nanoscale Thermodynamics Workshop, Telluride, CO, July 19-27, 2018.

Grants Received

External

1. M. Donahue. NIST Support for DARPA Magnetic Miniaturized and Monolithically Integrated Component (M3IC) Program, DARPA: *$127,000.*

Internal

1. B. Alpert. Information Theory in Deep Learning. 2018 ITL Building the Future Program, *$50,000*.

2. C. L. Dennis, T. P. Moffat, A. J. Biacchi, A. R. Hight Walker, S. I Woods, W. L. Tew, and M. J. Donahue. Thermal MagIC: An SI-Traceable Method for 3D Thermal Magnetic Imaging and Control. 2019 NIST Innovations in Measurement Science: *$1.45M*.
3. A. Dienstfrey, S. Russek, K. Stupic, K. Keenan, Z. Gimbutas, and W. Keyrouz. Deep Learning for MRI Reconstruction and Analysis. 2019 Fundamental and Applied Research for AI Program: *$145,000*.
4. S. Glancy. Neural Networks for Quantum Tomography. 2018 ITL Building the Future Program: *$95,000*.
5. S. Glancy and E. Knill (Co-PIs). Metrology with Interacting Photons. NIST Innovations in Measurement Science (IMS) Program, *$130,000*.
6. W. Griffin and J. Terrill. In Situ Machine Learning for Large-scale Simulation Analysis. 2018 ITL Building the Future Program, *$134,000*.
7. W. Griffin, J. Zwolak, and J. Terrill. In Situ Machine Learning for Large-scale Simulation Analysis. 2018 ITL Building the Future Program, *$100,000*.
8. E. Knill, S. Glancy, and P. Bierhorst. Statistical Theory for Quantum Metrology Experiments. 2018 ITL Building the Future Program, *$30,000*.
9. P. Kuo. Dual-Polarization Quantum Frequency Converter. 2019 ITL Building the Future Program: *$30,000*.
10. A. S. Moorthy and A. J. Kearsley. Artificial Intelligence Forensic Compound Identifications. 2018 ITL AI Competition: *$97,000*.
11. P. Patrone and A. Dienstfrey. Fundamentals and Uncertainty Quantification of Coarse Graining II. 2018 ITL Building the Future Program, *$100,000*.
12. P. N. Patrone, A. Dienstfrey, and G. B. McFadden. Fundamentals and Uncertainty Quantification of Coarse Grained Simulations III. 2019 ITL Building the Future Program: *$150,000*.
13. R. Boisvert, B. Schneider, M. Brady, M. Garris, W. Keyrouz, T. Blattner, D. Juba, R. Hanisch, E. Lin, J. Warren, T. Allison, A. Reid, D. Audus, C. Gonzalez, C. Spangler, J. Fowler, A. Liddle, and C. Hacker. Research Computing Infrastructure for AI and Data-Intensive Science. NIST Associate Director for Laboratory Programs: *$2,000,000*.
14. B. I. Schneider, T. Allison, A. J. Kearsley, W. Keyrouz and B. Wallace. Applying Deep Learning and AI to Computational Chemistry. 2019 ITL Building the Future Program*: $150,000*.
15. V. Stanford, O. Aulov, Y.-K. Liu, A. Mink, and P. J. Phillips. Building Blocks of Practical AI: Emerging Processors, Algorithms and Frameworks. 2018 ITL Building the Future Program: *$227,000*.
16. A. Youssef and B. Miller. Deep Learning Neural Networks for Math and Science Knowledge Processing. 2018 ITL Building the Futures Program: *$100,000*.

Grants Awarded

ACMD awards a small amount of funding through the NIST Measurement Science Grants Program for projects that make direct contributions to its research programs. Often such grants support direct cooperation between an external awardee and ACMD. This year the following new cooperative agreements were funded.

1. Concordia University: *Energy Harvesting Optimization for IoT-Health Devices*, $34,263.
2. Theiss Research: *Exploiting Alternate Computing Technologies*, $88,823.10. PI: Alan Mink.
3. Theiss Research: *Algorithms for Image and Shape Analysis in 3D*, $192,783.31. PI: Günay Doğan.
4. The Ohio State University: *Understanding Immersive Metrology Datasets; Scientific and Information Visualization Integration and Hybrid Input*, $81,022.34. PI: Jian Chen.
5. University of Maryland: *New Theory and Resilience Metrics for Systems-of-Systems*, $155,959. PIs: R. La and A. Gueye.
6. University of Maryland: *Joint Center for Quantum Information and Computer Science (QuICS)*, $337,511. PI: A. Childs.
7. University of Texas at Arlington: *SENTINEL: Security Interaction Testing for IoT Systems and Blockchains*, $93,455. PI: Y. Lei.

External Contacts

ACMD staff members interact with a wide variety of organizations in the course of their work. Examples of these follow.

Industrial Labs

Amgen Inc.
BAE Systems
Baxter Healthcare
Biogen Inc.
The Boeing Company
Bruker Inc.
Centre Suisse d'Electronique et Microtechnique (Switzerland)

Deltares (The Netherlands)
Eli Lily and Company
EXL Healthcare
Exxon Mobil
Genentech
Gener8
General Electric Global Research Center
Google
Health Canada (Canada)
HC-Photonics Corp. (Taiwan)
IBM Research
Intel Corp.
John Crane (UK)
Massachusetts General Hospital
Momenta Pharmaceuticals
NTT Corporation (Japan)
Pfizer Essential Health
Raytheon
Roche Pharmaceutical Research & Development (Switzerland)
Siemens
SINTEF (Norway)
Schrodinger LLC

Government/Non-profit Organizations

Air Force Office of Scientific Research
American Society of Mechanical Engineers
American Telemedicine Association
Argonne National Laboratory
Army Research Laboratory
Association for Computing Machinery
Computing Research Association
CSIRO (Australia)
Department of Energy
Food and Drug Administration
Fraunhofer Institute for Mechanics of Materials (Germany)
IDA Center for Computing Sciences
IEEE Computer Society
Italian National Research Council (Italy)
Inst. of Molecular Biology & Biophysics (Switzerland)
Laser Interferometer Gravitational-Wave Observatory (LIGO)
Leibniz-Forschungsinstitut für Molekulare (Germany)
Pacific Northwest National Laboratory
Mayo Clinic
Nanohub.org
NASA Glenn Research Center
NASA Jet Propulsion Laboratory
National Institute of Allergy and Infectious Disease
National Institute of Biomedical Imaging and Bioengineering
Slovenian NMR Centre (Slovenia)
National Institutes of Natural Sciences (Japan)
National Institutes of Health
National Physical Laboratory (UK)
National Research Council (Canada)
National Science Foundation
Oak Ridge National Laboratory
Open Math Society
Pacific Northwest National Laboratory
Patent and Trademark Office
Princeton Plasma Physics Laboratory
Sandia National Laboratories
Santa Fe Institute
Society for Industrial and Applied Mathematics
Society for Science
Swedish Medical Products Agency (Sweden)
Synchrotron Light Laboratory (Brazil)
Theiss Research
World Wide Web Consortium

Universities

Aalto University (Finland)
Aarhus University (Sweden)
Arizona State University
Brown University
Clemson University
Columbia University
Concordia University (Canada)
Courant Institute of Mathematical Sciences
Dartmouth College
Drexel University
Duke University
Ecole Polytechnique de Montreal (Canada)
ETH Zurich (Switzerland)
European University (Cyprus)
Federal University of Ceara (Brazil)
Florida Institute of Technology
Florida Polytechnic University
Florida State University
Free University of Berlin (Germany)
Friedrich-Alexander Universitat (Germany)
George Mason University
Georgetown University
George Washington University
Gdansk University of Technology (Poland)
Harvard University
Hong Kong Polytechnic University (Hong Kong)
Imperial College London (UK)
Indian Institute of Engineering Science and Technology, Shibpur (India)
Indian Institute of Technology, Kanpur & Mandi (India)
Indiana University
Institute for Bioscience and Biotechnology Research
Jacobs University Bremen (Germany)
Jönköping University (Sweden)
Kansas State University
Keene State College
Khallikote College (India)
Linnaeus University (Sweden)

Lund University (Sweden)
McMaster University (Canada)
Medical University of South Carolina
Mepco Schlenk Engineering College
New Mexico State University
New York University
Ohio State University
Polytechnic University of Valencia (Spain)
Princeton University
Purdue University
Quantum Chemistry Research Institute (Japan)
Rice University
Stanford University
Shippensburg University
Stockholm University (Sweden)
Tampere University of Technology (Finland)
Technion, Israel institute of Technology (Israel)
Texas A&M University
Texas Tech University
Tufts University
Universidad de Alcalá (Spain)
Universidad de Porto (Portugal)
University of Akron
University of Amsterdam (The Netherlands)
University of Antwerp (Belgium)
University of Bayreuth (Germany)
University of Bergamo (Italy)
University of Bologna (Italy)
University of California, Berkeley
University of Central Florida
University of Colorado, Boulder
University of Delaware
University of Edinburgh (UK)
University of Erlangen-Nuremberg (Germany)
University of Essex (United Kingdom)
University of Guelph (Canada)
University of Ibague (Colombia)
University of Illinois, Chicago
University of Limerick (Ireland)
University of Lisbon (Portugal)
University of Maryland, Baltimore County
University of Maryland, College Park
University of Melbourne (Australia)
University of Michigan
University of New Mexico
University of New South Wales (Australia)
University of North Carolina, Charlotte
University of Northern Arizona
University of Oregon
University of Oulu (Finland)
University of Queensland (Australia)
University of Sheffield (UK)
University of South Carolina
University of Southern California
University of Sydney (Australia)
University of Tennessee at Knoxville
University of Texas at Arlington
University of Turin (Italy)
University of Venice (Italy)
University of Washington
University of Western Ontario (Canada)
University of Wisconsin−Madison
University of Wisconsin−Milwaukee
University of Zagreb (Croatia)
Virginia Polytechnic Institute
Worcester Polytechnic University
Yale University

Part V

Appendix

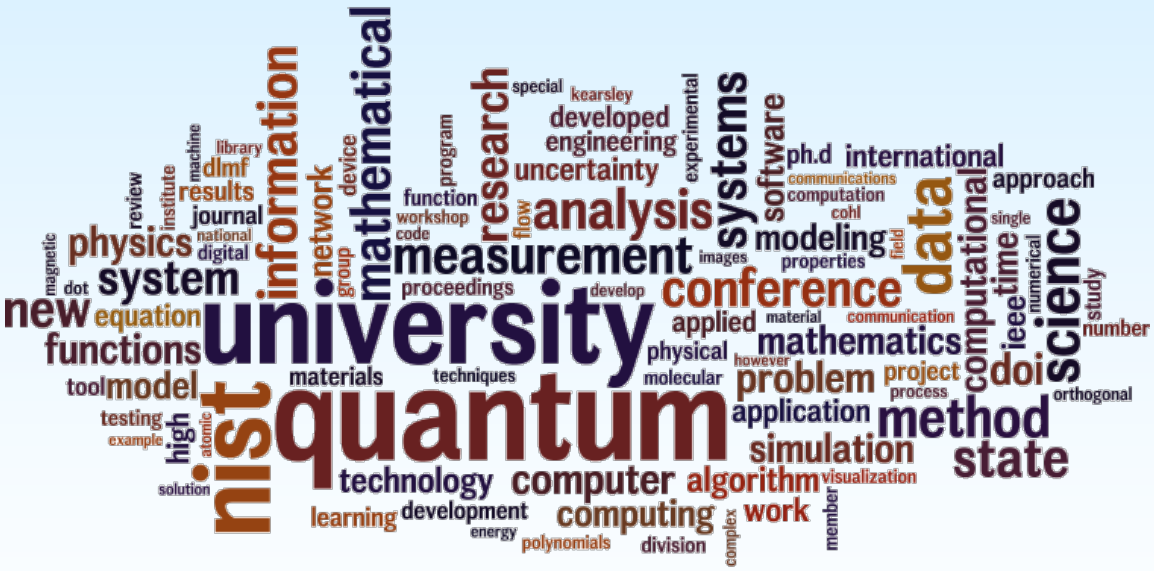

Staff

ACMD consists of full time permanent staff located at NIST laboratories in Gaithersburg, MD and Boulder, CO. This full-time staff is supplemented with a variety of special appointments. The following list reflects all non-student appointments held during any portion of the reporting period (October 2017 – December 2018). Students and interns are listed in Table 3 below. * Denotes staff at NIST Boulder.

Division Staff

Ronald Boisvert, *Chief*, Ph.D. (Computer Science), Purdue University, 1979
Catherine Graham, *Secretary*
Lochi Orr, *Administrative Assistant*, A.A. (Criminal Justice), Grantham University, 2009
Alfred Carasso, Ph.D. (Mathematics), University of Wisconsin, 1968
Roldan Pozo, Ph.D. (Computer Science), University of Colorado at Boulder, 1991
Kamran Sayrafian-Pour, Ph.D. (Electrical and Computer Engineering), University of Maryland, 1999
Christopher Schanzle, B.S. (Computer Science), University of Maryland Baltimore County, 1989

Mathematical Analysis and Modeling Group

Timothy Burns, *Leader*, Ph.D. (Mathematics), University of New Mexico, 1977
*Bradley Alpert, Ph.D. (Computer Science), Yale University, 1990
Sean Colbert-Kelly, Ph.D. (Mathematics), Purdue University, 2012
*Andrew Dienstfrey, Ph.D. (Mathematics), New York University, 1998
Ryan Evans, Ph.D. (Applied Mathematics), University of Delaware, 2016
Jeffrey Fong, Ph. D. (Applied Mechanics and Mathematics), Stanford University, 1966
*Zydrunas Gimbutas, Ph.D. (Applied Mathematics), Yale University, 1999
Fern Hunt, Ph.D. (Mathematics), New York University, 1978
Raghu Kacker, Ph.D. (Statistics), Iowa State University, 1979
Anthony Kearsley, Ph.D. (Computational and Applied Mathematics), Rice University, 1996
Geoffrey McFadden, *NIST Fellow*, Ph.D. (Mathematics), New York University, 1979
Paul Patrone, Ph.D. (Physics), University of Maryland, 2013

Faculty Appointee (Name, Degree / Home Institution)
Daniel Anderson, Ph.D. / George Mason University
Michael Mascagni, Ph.D. / Florida State University
Florian Potra, Ph.D. / University of Maryland Baltimore County

Guest Researchers (Name, Degree / Home Institution)
Sebastian Barillaro, Ph.D. / Industrial Technology National Institute, Argentina
Charles Bezerra Prado, D.Sc. / Instituto Nacional de Metrology, Brazil
Yu (Jeff) Lei, Ph.D. / University of Texas at Arlington
Christoph Witzgall, Ph.D. / *NIST Scientist Emeritus*

Mathematical Software Group

Michael Donahue, *Leader* Ph.D. (Mathematics), Ohio State University, 1991
Javier Bernal, Ph.D. (Mathematics), Catholic University, 1980
Howard Cohl, Ph.D. (Mathematics), University of Auckland, 2010
Stephen Langer, Ph.D. (Physics), Cornell University, 1989
Daniel Lozier, Ph.D. (Applied Mathematics), University of Maryland, 1979
Marjorie McClain, M.S. (Mathematics), University of Maryland College Park, 1984

Bruce Miller, Ph.D. (Physics), University of Texas at Austin, 1983
William Mitchell, Ph.D. (Computer Science), University of Illinois at Urbana-Champaign, 1988
Donald Porter, D.Sc. (Electrical Engineering), Washington University, 1996
Bonita Saunders, Ph.D. (Mathematics), Old Dominion University, 1985
Barry Schneider, Ph.D. (Physics), University of Chicago, 1969

Faculty Appointees (Name, Degree / Home Institution)
Abdou Youssef, Ph.D. / George Washington University

NRC Postdoctoral Associates
Heman Gharibnejad, Ph.D. (Physics), University of Nevada, 2014

Guest Researchers (Name, Degree / Home Institution)
Günay Doğan, Ph.D. / Theiss Research
Adri Olde Daalhuis, Ph.D. / University of Edinburgh
Deyan Ginev, M.Sc. / Chakra Consulting

Computing and Communications Theory Group

Ronald Boisvert, *Acting Leader*, Ph.D. (Computer Science), Purdue University, 1979
Isabel Beichl, *Project Leader*, Ph.D. (Mathematics), Cornell University, 1981
Brian Cloteaux, Ph.D. (Computer Science), New Mexico State University, 2007
*Scott Glancy, Ph.D. (Physics), University of Notre Dame, 2003
Stephen Jordan, Ph.D. (Physics), Massachusetts Institute of Technology, 2008
*Emanuel Knill, *NIST Fellow*, Ph.D. (Mathematics), University of Colorado at Boulder, 1991
Paulina Kuo, Ph.D. (Physics), Stanford University, 2008
Yi-Kai Liu, Ph.D. (Computer Science), University of California, San Diego, 2007
Lijun Ma, Ph.D. (Precision Instruments and Machinery), Tsinghua University, 2001
Vladimir Marbukh, Ph.D. (Mathematics) Leningrad Polytechnic University, 1986
Oliver Slattery, *Project Leader*, Ph.D. (Physics), University of Limerick, 2015
Xiao Tang, *Project Leader*, Ph.D. (Physics), Chinese Academy of Sciences, 1985

NRC Postdoctoral Associates
Lucas Brady, Ph.D. (Physics), University of California at Santa Barbara, 2018
Lucas Kocia, Ph.D. (Chemistry), Harvard University, 2016

Faculty Appointees (Name, Degree / Home Institution)
James Lawrence, Ph.D. / George Mason University

Guest Researchers (Name, Degree / Home Institution)
*Peter Bierhorst, Ph.D. / University of Colorado
*Hilma De Vasconcelos, Ph.D. / Universidade Federal do Ceará, Brazil
*Bryan Eastin, Ph.D. / Northrup Grumman
Assane Gueye, Ph.D. / University of Maryland
Richard La, Ph.D. / University of Maryland
Alan Mink, Ph.D. / Theiss Research
Francis Sullivan, Ph.D. / IDA Center for Computing Sciences
Justyna Zwolak, Ph.D. / University of Maryland

High Performance Computing and Visualization Group

Judith Terrill, Leader, Ph.D. (Information Technology), George Mason University, 1998
William George, Ph.D. (Computer/Computational Science), Clemson University, 1995
Terence Griffin, B.S. (Mathematics), St. Mary's College of Maryland, 1987
Wesley Griffin, Ph.D. (Computer Science), University of Maryland Baltimore County, 2016

Sandy Ressler, M.F.A. (Visual Arts), Rutgers University, 1980
Steven Satterfield, M.S. (Computer Science), North Carolina State University, 1975
James Sims, Ph.D. (Chemical Physics), Indiana University, 1969

NRC Postdoctoral Associates

Justin Kauffman, Ph.D. (Engineering Science and Mechanics), Penn State University, 2018

Guest Researchers (Name, Degree / Home Institution)

Jian Chen, Ph.D. / The Ohio State University
John Hagedorn, M.S. / NIST, Retired

Figure 92. *The NIST Summer Undergraduate Research Fellowship Program (SURF) provides students with valuable research experience. (left) ACMD staff member Paul Patrone with SURF student Amy Li of Wellesley College. (right) ACMD staff members Ryan Evans and Anthony Kearsley with SURF student Felix Perez of Texas Tech (center).*

Figure 93. *A group of SURF students along with students from the Summer High School Internship Program (SHIP) worked in ACMD's immersive visualization lab. Back Row: James Biggins, Paul Armstrong, SURF; Ryan Cho (NIST NCNR), Kevin Chen, SHIP. Front Row: Joseph Waysack, SURF; Telo Yan (NIST NCNR), SHIP*

Table 3. *Student interns in ACMD.*

Name	From	Program		Mentor	Topic
Avagyan, Arik	U. Colorado Boulder	G	PREP	E. Knill	Quantum information processing
Chou, Diana	U. of Maryland	G	SVP	J. Terrill	360-video based visualizations
Eruslu, Hasan	U. of Delaware	G	FGR	S. Langer	Algorithms 3D Image and Shape Analysis
Jensen, Alathea	George Mason U.	G	DGR	I. Beichl	Stochastic enumeration
Khrac, Katjana	U. Zagreb, Croatia	G	FGR	K. Sayrafian	Positioning metrology in the human body
Li, Shuang	USC	G	FGR	S. Langer	Algorithms 3D Image and Shape Analysis
Mayer, Karl	U. Colorado Boulder	G	PREP	E. Knill	Protocols for quantum optics
Van Meter, James	U. Colorado Boulder	G	PREP	E. Knill	Quantum measurement of space-time
Vazquez Lundrove, Marilyn	George Mason U.	G	FGR	S. Langer	Microstructure image analysis
Wiesing, Tom	Jacobs U. Bremen	G	FGR	B. Miller	Digital Library of Math Functions
Zhao, Henan	UMBC	G	FGR	J. Terrill	Understanding metrology datasets
Armstrong, Paul	U. of Maryland	U	SURF	W. Griffin	Evaluation of Head Mounted Displays for Visualizing Cell Microscopy Data
Biggins, James	U. of Maryland	U	SURF	S. Ressler	Virtual Reality Tours: Public Access to Non-public Spaces
Li, Qing Hai	Wellesley College	U	SURF	A. Kearsley	Optimization of Simulations
Miller, David	U. of Maryland	U	SURF	M. Mascagni	Infrastructure for Parallel Monte Carlo
Perez, Felix	Texas Tech	U	SURF	A. Kearsley	Optimization in Chemometrics
Schmale, Henry	Millersville U.	U	SURF	H. Gharibnejad	Higher order time propagators
Showalter, Samuel	DePauw U.	U	SURF	S. Glancy	
Waysack, Joseph	Millersville U.	U	SURF	J. Terrill	Visualization of Nanostructures
Zong, Kevin	U. of Maryland	U	SURF	O. Slattery	Software for single photon counter inter-facing and data analysis
Chen, Kevin	Poolesville H.S.	H	SHIP	S. Ressler	Towards the use of the Virtual Reality in the Digital Library of Mathl Functions
Durbha, Saketram	Fairview H. S.	H	SVP	B. Alpert	Measuring Optical Properties of Aug-mented Reality Glasses
Muralidharan, Arulvel	Fairview H. S.	H	SVP	B. Alpert	Measuring Optical Properties of Aug-mented Reality Glasses

Legend

G Graduate student
U Undergraduate
H High School

PREP Professional Research Experience Program (Boulder)
FGR Foreign Guest Researcher
SVP Student Volunteer Program
DGR Domestic Guest Researcher
SURF Summer Undergraduate Research Fellowship
SHIP Student High School Intenship Program

Glossary of Acronyms

2D	two-dimensional
2DEG	two-dimensional electron gas
3D	three-dimensional
A&M	atomic and molecular
AAAS	American Association for the Advancement of Science
ACM	Association for Computing Machinery
ACMD	NIST/ITL Applied and Computational Mathematics Division
ACTS	Advanced Combinatorial Testing System
AI	artificial intelligence
API	application programmer's interface
APS	American Physical Society
ASME	American Society of Mechanical Engineering
arXiv	preprint archive housed at Cornell University (http://arxiv.org/)
BMG	bulk metallic glass
BMP	Bateman Manuscript Project
BSM	Bell state measurement
Caltech	California Institute of Technology
CAS	computer algebra system
CAVE	CAVE Automatic Virtual Environment
CCM	Combinatorial Coverage Measurement
CENAM	Center for Metrology of Mexico
CFD	computational fluid dynamics
CG	coarse-grained
CI	configuration interaction
CICM	Conference on Intelligent Computer Mathematics
CMA	University of Antwerp Computational Mathematics Research Group
CNN	convolutional neural network
CNOT	controlled not, a fundamental operation in quantum computing
CNST	NIST Center for Nanoscale Science and Technology
CPA	cryoprotective agents
CPU	central processing unit
CS	component system
CFSF	Continued Fractions for Special Function
CSIRO	Australia's Commonwealth Scientific and Industrial Research Organization
CT	combinatorial testing
CTL	NIST Communications Technology Laboratory
CTMC	classical trajectory Monte Carlo
CY	calendar year
DAG	directed acyclic graph
DARPA	Defense Advanced Research Projects Agency
DDoS	distributed denial of service
DG	discontinuous Galerkin
DLMF	Digital Library of Mathematical Functions
DNA	deoxyribonucleic acid
DNN	deep neural network
DOC	Department of Commerce
DoF	degrees of freedom
DOI	digital object identifier
DRMF	Digital Repository of Mathematical Formulae
eCF	Wolfram Computational Knowledge of Continued Fractions Project
EIT	electromagnetically induced transparency
EL	NIST Engineering Laboratory
EOS	equation of state

ETSI	European Telecommunications Standards Institute
FEM	finite element method
FET	field-effect transitors
FFT	fast Fourier transform
FWM	four wave mixing
FY	fiscal year
GDML	Global Digital Mathematical Library
GI	gastrointestinal
GPU	graphics processing units
GST	gate set tomography
GUI	graphical user interface
HDG	hybridizable discontinuous Galerkin finite element method
HEC	High End Computing
HEV	high end visualization
HMD	head-mounted display
HPCVG	ACMD High Performance Computing and Visualization Group
HTML	hypertext markup language
HVAC	heating, ventilation and air conditioning
HVACSIM+	software package and computing environment for simulating HVAC system
Hy-CI	Hylleraas-Configuration Interaction technique
IBBR	UMD-NIST Institute for Bioscience and Biotechnology Research
ICN	information and communication network
ICPEAC	International Conference on Photonic, Electronic, and Atomic Collisions
ICST	International Conference of Software Testing
IDA	Institute for Defense Analysis
IDE	integro-differential equation
IEEE	Institute of Electronics and Electrical Engineers
IFIP	International Federation for Information Processing
IMACS	International Association for Mathematics and Computers in Simulation
IMKT	International Mathematical Knowledge Trust
IMS	NIST Innovations in Measurement Science program
IoT	Internet of things
ISM	Industrial, Scientific and Medical radio band
ITAMP	Harvard-Smithsonian Institute for Theoretical Atomic and Molecular Physics
ITL	NIST Information Technology Laboratory
IWCT	International Workshop on Combinatorial Testing
iWOG	integrated waveguide optical gyroscope
JMONSEL	simulation code used to model electron scattering in materials
JOOMMF	Jupyter Notebook version of OOMMF
JSON	Javascript Object Notation
KLS	Koekoek, Lesky and Swarttouw
KNL	Knight's Landing
LaTeX	a math-oriented text processing system
LCLS	LINAC Coherent Light Source
LDA	linear discriminant analysis
LINAC	linear accelerator
M3IC	DARPA Magnetic, Miniaturized, and Monolithically Integrated Components program
MAA	Mathematical Association of America
MathML	Mathematical Markup Language (W3C standard)
MCMC	Monte Carlo Markov Chain
MD	molecular dynamics
MEMS	micro-electrical mechanical systems
MERSIVE	ACMD toolkit for immersive scientific visualization
MG	metallic glass
MHD	magneto-hydrodynamics
MICS	Medical Implant Communication Service
ML	machine learning

MLP	mathematical language processing
MML	NIST Material Measurement Laboratory
MOS	Magnus, Oberhettinger, and Soni
MOT	magneto-optical trap
MPI	Message Passing Interface
MRAM	magneto-resistive random access memory
MRI	magnetic resonance imaging
MS	mass spectral
muMAG	Micromagnetic Activity Group
NAG	Numerical Algorithms Group
NASA	National Aeronautics and Space Administration
NBS	National Bureau of Standards
NHS	National Health Service (UK)
NISQ	noisy intermediate-scale quantum
NIST	National Institute of Standards and Technology
NISTIR	NIST Internal Report
NITRD	Networking and Information Technology Research and Development
NMR	nuclear magnetic resonance
NRC	National Research Council
NSF	National Science Foundation
NSTAB	code computing three dimensional equilibria of toroidal plasmas
NVD	National Vulnerabilities Database
NYU	New York University
OCR	optical character recognition
OOF	Object-Oriented Finite Elements (software)
OOF3D	3D version of OOF
OOMMF	Object-Oriented Micromagnetic Modeling Framework (software)
OPSF	orthogonal polynomials and special functions
PCA	principal components analysis
PDE	partial differential equation
PET	polyethylene terephthalate
PHAML	Parallel Hierarchical Adaptive Multi Level (software)
PML	NIST Physical Measurement Laboratory
PoCF	probability of cascading failures
POM	part of math
PQC	post-quantum cryptography
QA	quantum annealing
QAO	quantum adiabatic optimization
QAOA	quantum approximate optimization algorithm
QD	quantum dot
QDPD	Quarternian-based Dissapative Particle Dynamics simulation code
QuICS	UMD-NIST Joint Center for Quantum Information and Computer Science
R&D	research and development
RB	randomized benchmarking
RE	Reynolds number
REFPROP	Reference Fluid Thermodynamic and Transport Properties Database
RF	radio frequency
ROI	regions of interest
SEM	scanning electron microscope
SHM	structural health monitoring
SI	International System of Units
SIS	sequential importance sampling
SIAM	Society for Industrial and Applied Mathematics
SIGGRAPH	ACM Special Interest Group on Graphics
SNSPD	superconducting nanowire single photon detector
SPAM	state preparation and measurement, a class of errors in quantum computing
SPDC	spontaneous parametric down conversion

SPIE	International Society for Optical Engineering
SRM	standard reference material
SNN	spiking neural network
STEM	science, technology, engineering, and mathematics
STM	scanning tunneling microscope
SURF	NIST Student Undergraduate Research Fellowship program
TDE	ThermoData Engine
UMBC	University of Maryland Baltimore County
UMD	University of Maryland
UMIACS	University of Maryland Institute for Advanced Computer Studies
UNLV	University of Nevada Las Vegas
UPGMA	unweighted pair group method with arithmetic mean
UQ	uncertainty quantification
URL	universal resource locator
UWB	ultra wide band
VNA	vector network analyzer
VR	virtual reality
VTK	graphics package
W3C	World Wide Web Consortium
WAS	Washington Academy of Sciences
WBAN	wireless body area network
WCE	wireless capsule endoscopy
WebGL	Web-based Graphics Library
X3D	Extensible 3D
X3DOM	an open-source framework for integrating X3D and HTML5
XML	Extensible Markup Language
XSEDE	NSF eXtreme Science and Engineering Discovery Environment